LA-UR-14-27389
Approved for public release; distribution is unlimited.

Title: Database for Regional Geology, Phase 1– A Tool for Informing Regional Evaluations of Alternative Geologic Media and Decision Making

Author(s): Perry, Frank Vinton
Kelley, Richard E.
Birdsell, Suzanne M.
Lugo, Alexander Bryan
Dobson, Patrick
Houseworth, James

Intended for: Report

Issued: 2014-11-12 (rev.1)

Database for Regional Geology, Phase 1– A Tool for informing Regional Evaluations of Alternative Geologic Media and Decision Making

Fuel Cycle Research & Development

Prepared for
U.S. Department of Energy
Used Fuel Disposition Campaign
Frank V. Perry, Richard E. Kelley,
Alexander B. Lugo, Suzanne M. Birdsell,
Los Alamos National Laboratory
Patrick Dobson, James E. Houseworth
Lawrence Berkeley National Laboratory

September 24, 2014
FCRD-UFD-2014-000067
Los Alamos Unlimited Release LA-UR-14-27389

EXECUTIVE SUMMARY

Phase 1 and 2 Websites for the Regional Geology GIS Database

An informational website was completed that allows users to visualize the information contained in the Regional Geology GIS Database. This information includes the distribution of crystalline rock (including basement depth), and salt and shale formations within the contiguous United States. The website provides visualizations of the relationships between geologic media and selected natural and cultural features pertaining to potential siting guidelines for repository siting. The development of this website was Phase 1 of an effort to create a fully interactive web-based mapping application (Phase 2) that will be competed in FY15. The data elements planned for the fully interactive mapping tools are described in this report.

Terrane Maps of Crystalline Basement Rocks

Siting of a deep borehole disposal or R&D facility requires information about the regional geologic setting and geology of the basement at the national, regional and local scale. We have identified and included a number of state to national-scale basement maps in the GIS database. These will serve as a first step in providing a regional geologic framework for understanding the geologic setting, history and overall lithology of different regions, as well as providing a useful aid in identifying and understanding data at the local scale that will be necessary for comparing specific candidate sites for the purposes of site selection.

Inventory of Shale Formations in the US

This section provides a summary of the distribution, thickness, and depth of selected shale formations found within many of the sedimentary basins in the contiguous US. Clay-rich shale formations have a number of properties, such as low permeability, high cation exchange potential, and the ability to self-seal, which make them candidates for a geologic repository for high-level radioactive waste. The United States has an abundance of thick shale deposits that span a wide range of geologic ages, mineralogic compositions, and geologic environments, some of which might be suitable for hosting repositories to safeguard radioactive waste. The objective of this report is to build upon previous compilations of shale formations within many of the major sedimentary basins in the US by developing GIS data delineating isopach and structural depth maps for many of these units. These data are being incorporated into the Los Alamos National Laboratory (LANL) digital GIS database being developed for determining host rock distribution and depth/thickness parameters consistent with repository design. Additional rock properties, such as total organic carbon (TOC) abundance and thermal maturity, are also included where available.

Rock Properties and In-Situ Conditions for Shale Estimated from Sonic Velocity Measurements

This section extends the development of methods to assess hydrological and geomechanical properties and conditions for shale formations based on sonic velocity measurements as reported in Dobson and Houseworth (2013). In that effort, publically available data sets were identified for shales under investigation for nuclear waste disposal in Europe and from shales of interest for oil exploration and production in the North Sea. These data were used in the development of several correlations which link properties to sonic compressional velocity. The advantage of using correlations based on sonic velocity is that properties can be estimated from geophysical logs. This information is often more readily available than direct property measurements on core that would otherwise be required. Furthermore, geophysical logs typically provide a continuous readout along wells that can be more readily used to characterize spatial variability in properties. In this report additional information is provided on the correlation between clay content and sonic velocity presented in Dobson and Houseworth (2013).

Additional correlations are developed here between the sonic velocity and thermal properties, i.e., thermal conductivity and specific heat. Correlations between sonic velocity and the van Genuchten capillary

strength parameter and the van Genuchten pore-size-distribution index are also presented. These van Genuchten parameters can be used for the computation of two-phase capillary pressure and relative permeability parameter functions of saturation. The correlations developed were then used to assess properties and conditions in several shale formations of interest within the United States which have publically available data on sonic velocity. As in the previous study, some of the correlations were found to be weak or poorly defined, indicating that additional independent measurements are desirable to supplement such estimates. Further verification is also needed for many of the parameter estimates for the US shale formations analyzed; therefore, they should be viewed as initial estimates.

CONTENTS

FIGURES

TABLES

ACRONYMS

BRI	brittleness index
DEM	Digital Elevation Model
DOE	Department of Energy
EIA	Energy Information Administration
FY	Fiscal Year
GIS	Geographic Information Systems
HLW	High-Level Waste
INL	Idaho National Laboratory
LANL	Los Alamos National Laboratory
LBNL	Lawrence Berkeley National Laboratory
md	millidarcies
OCR	overconsolidation ratio
psi	pounds per square inch
R&D	Research and Development
RMSE	root-mean-square error
tcf	trillion cubic feet
TOC	total organic carbon
UCS	uniaxial compressive strength
UFDC	Used Fuel Disposition Campaign
US	United States
USGS	U.S. Geological Survey

USED FUEL DISPOSITION CAMPAIGN

DATABASE FOR REGIONAL GEOLOGY, PHASE 1– A TOOL FOR INFORMING REGIONAL EVALUATIONS OF ALTERNATIVE GEOLOGIC MEDIA AND DECISION MAKING

1. Introduction

The objective of the Used Fuel Disposition Campaign's (UFDC) Regional Geology Work Package is to better understand the geologic options for disposal of HLW by creating a spatially-based GIS database that integrates both geologic data for alternative host-rock formations and information that has been historically used for siting guidelines. These two types of information are fundamental to the eventual siting of a geologic repository for HLW. The GIS database will allow analysis of the relationships between potential siting guidelines and potential host-rock formations, providing information on the options available for HLW disposal in different regions of the US.

New information presented in this Regional Geology milestone report is focused on 1) implementation of an informational website (Phase 1) that presents visualizations of the data contained in the GIS Database, 2) a description of FY15 Plans for a fully interactive web-based mapping tool (Phase 2) that allows manipulation of data contained in the GIS Database, 3) a description of basement terrane maps for Precambrian crystalline basement that has been included in the GIS database, 4) new geologic data for shale formations including their organic content and thermal maturity, and 5) further development of correlations between sonic velocity and the physical properties of shale to estimate properties such as clay content, thermal conductivity and two-phase flow parameters that would be important to repository performance.

For convenience and completeness, previous work completed as part of Regional Geology GIS database development effort is included as Appendix A of this report. The appendix consists of the Level 2 Milestone "Regional Geology: A GIS Database for Alternative Host Rocks and Potential Siting Guidelines" (Perry et al. 2014).

2. Implementation of an Informational Website for the GIS Database

We have completed an informational website that provides examples and visualization of the key information available in the GIS Database (Figure 2-1). The website allows users to visualize the distribution of crystalline rock (including basement depth), salt and shale within the contiguous United States and their relationship to selected natural and cultural features pertaining to potential siting guidelines or site characterization issues that would affect repository development. For example, the location of boreholes for oil and gas exploration and production is a consideration for a repository sited in salt or shale formations, but not for siting within crystalline rocks or crystalline basement. Similarly, consideration of seismic hazard would be a factor in siting a repository in many regions west of the Rocky Mountains but would be less important in siting a repository in most regions to the east of the Rocky Mountains. The maps presented on the website allow a qualitative assessment of the relative importance of several potential siting guidelines on repository development in different regions of the US. This version of the website (Phase 1) is primarily for informational purposes and was not designed as an interactive mapping tool. A fully interactive mapping tool is planned for FY15 (described in Section 3 of this report) that will allow a large amount of user interaction including the ability to selective choose and overlay multiple data layers, adjust layer transparency to better visualize multiple data layers, or to zoom to any region of the US.

Figure 2-1. Home page for the Regional Geology GIS database informational website. The figure showing depth and thickness of a salt formation can be enlarged to include a caption explaining the importance of depth of the host rock to siting a repository. The four menu links at the top of the page lead to a series of map overlays showing the distribution of alternative host rocks and their relationship to selected siting guidelines. The sidebar has links to the home page for DOE Used Fuel Campaign and to the Regional Geology Level 2 milestone of January 2014 which contains the complete reference information for material presented on the website

The home page of the website describes the types of information included in the Regional Geology GIS database and the intended use of this information (Figure 2-1). The home page includes four submenus that lead to a series of map overlays for each of the four alternative media. The complete content of the website is organized as outlined below.

The website home page includes an introduction to the GIS database and menu links to the four disposal alternatives:

1. Crystalline (granitic) rocks; slider frame with map images includes:
    a. Map of granite distribution in US
    b. Map of granite distribution and Quaternary faults
    c. Map of granite distribution and seismic hazard
    d. Map of granite distribution and topographic slope
    e. Map of granite distribution and population distribution
2. Crystalline basement; slider frame with map images includes:
    a. Map of depth to crystalline basement in US
    b. Map of depth to crystalline basement, major basement structures, and 2000 meter basement depth contour
3. Salt; slider frame with map images includes:
    a. Map of distribution of salt formations and depth in the US
    b. Map of salt distribution and seismic hazard
    c. Map of salt distribution and oil and gas drilling activities
    d. Map of salt distribution and population distribution
4. Shale; slider frame with map images includes:
    a. Map of distribution of selected shale formations and depth in the US
    b. Map of shale distribution and oil and gas drilling activities
    c. Map of shale distribution and population distribution

For each disposal option, the web interface displays a map frame (known as an “image slider” in the terminology of web design) that first shows the basic geology of each media (distribution/depth). Each successive frame shows selected information for siting guidelines superimposed on the geologic data.

Examples of the webpages showing maps of granite and salt and information for potential siting guidelines are shown in Figures 2-2 through 2-5. Examples of siting guidelines shown for each of the media are appropriate to each media type. The distribution of granite, for example, is shown in relationship to seismic hazard and salt distribution is shown in relationship to oil and gas drilling activity (Figures 2-3 and 2-5).

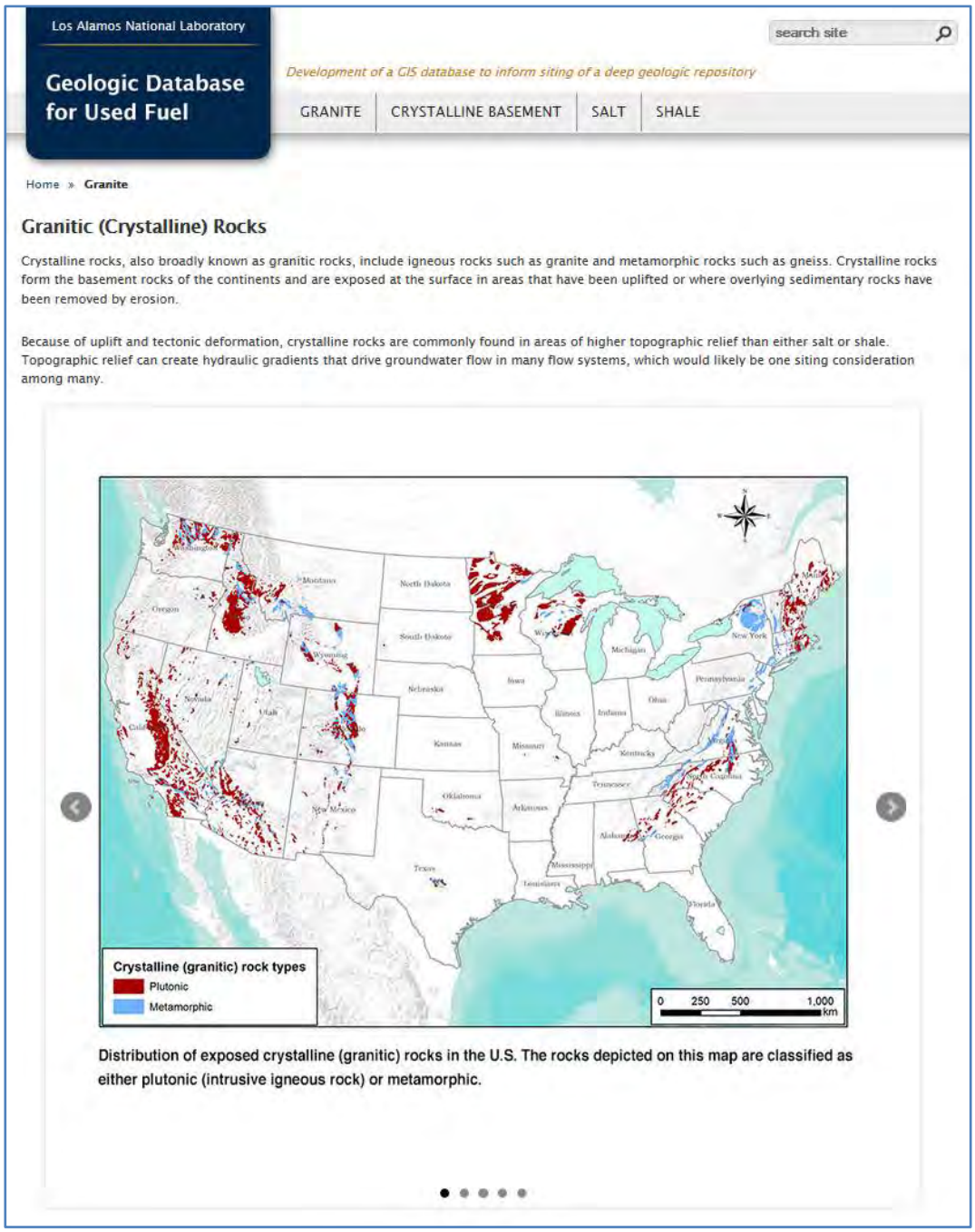

Figure 2-2. Example webpage showing map of the distribution of granitic rocks within a manual fade-in image slider.

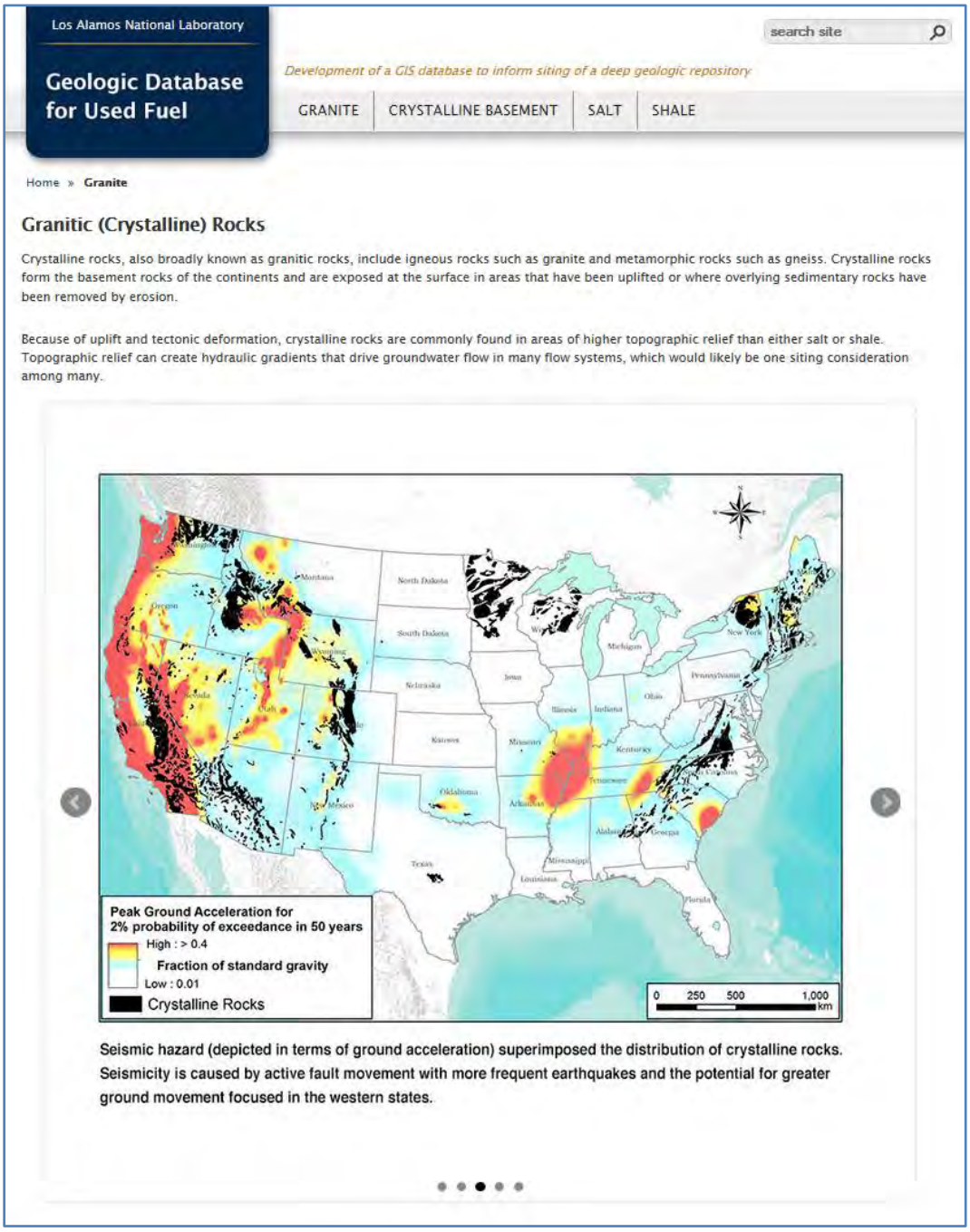

Figure 2-3. Example webpage showing map of the distribution of granitic rocks and relationship to seismic hazard within a manual fade-in image slider.

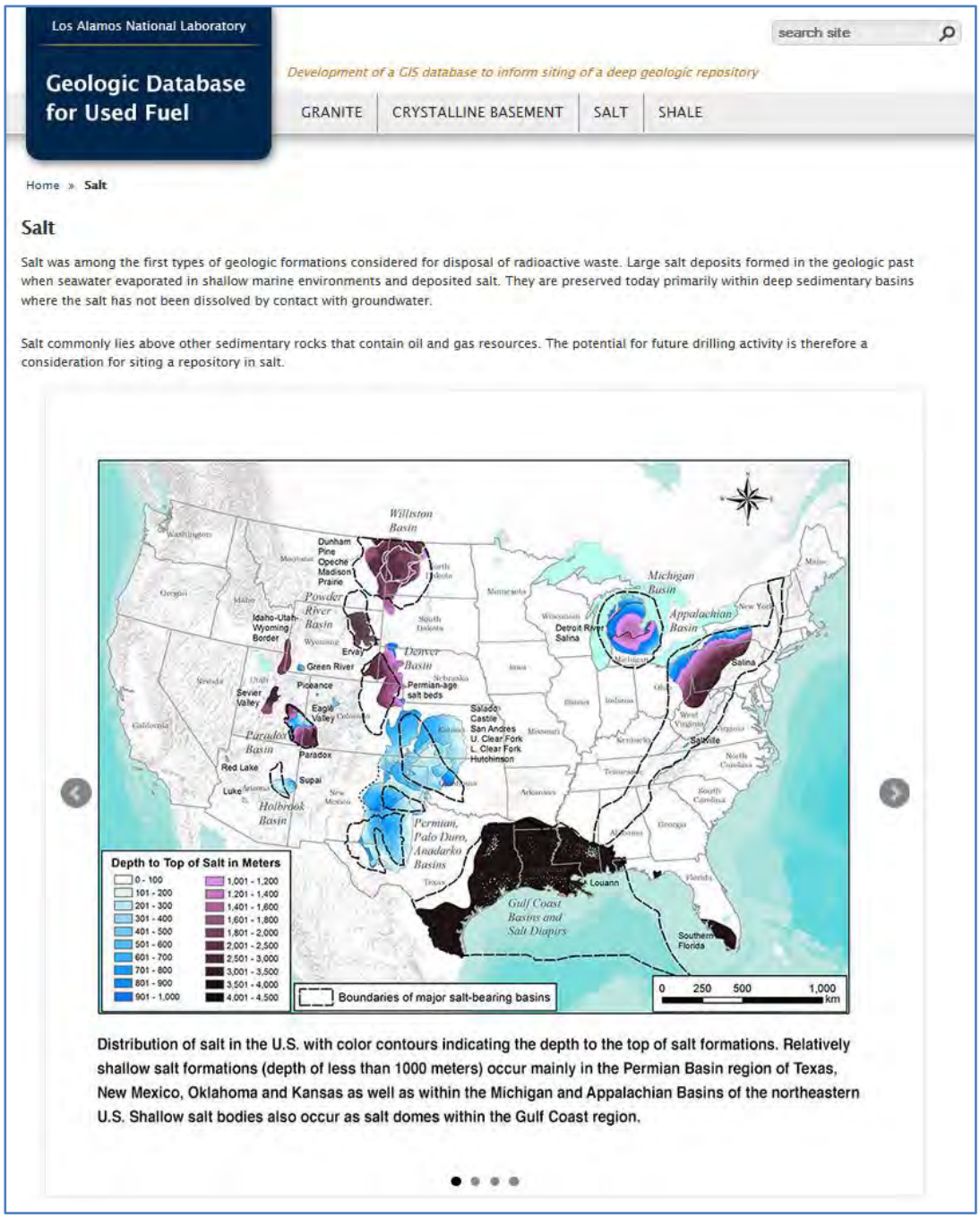

Figure 2-4. Example webpage showing map of the distribution of salt formations within a manual fade-in image slider.

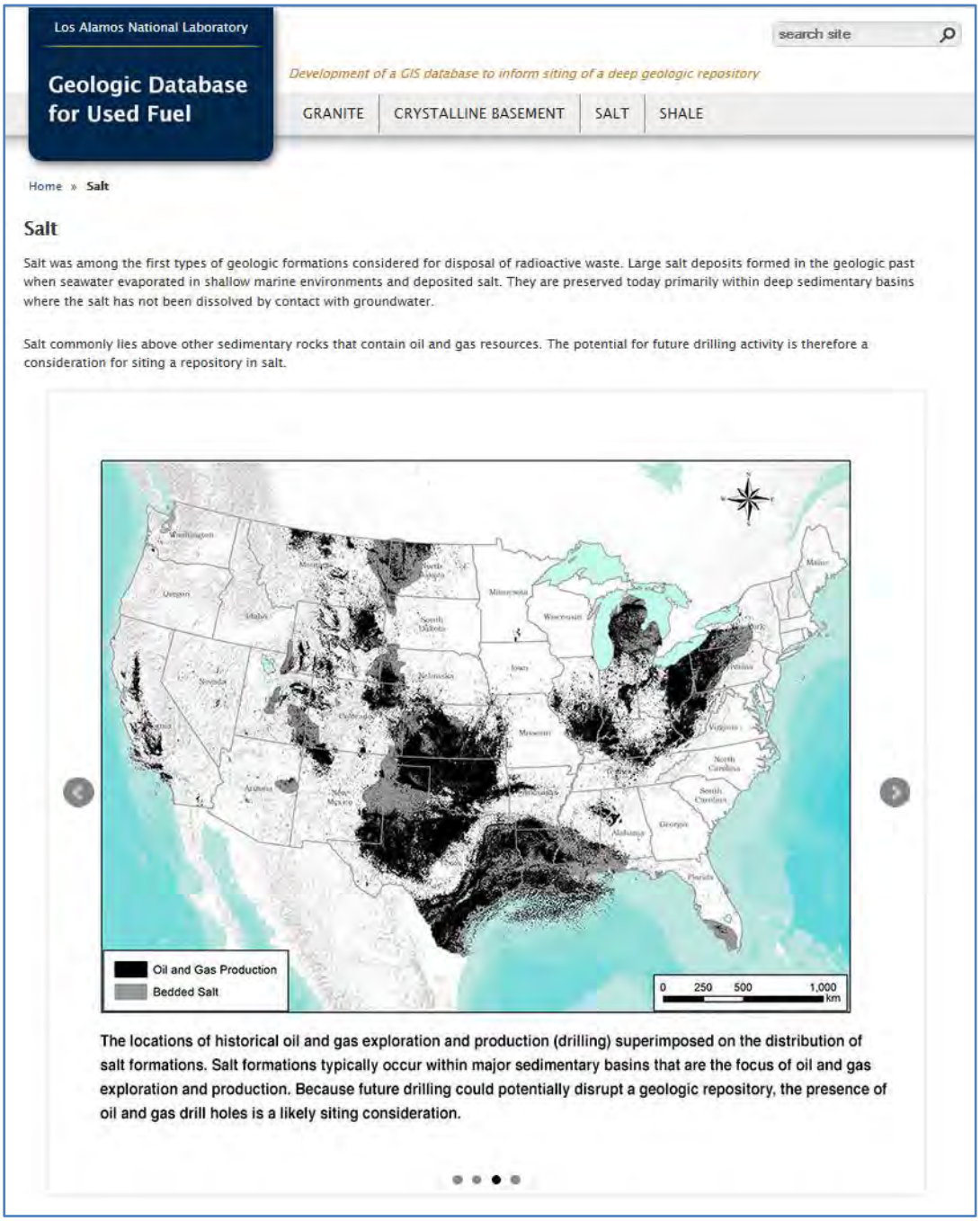

Figure 2-5. Example webpage showing map of the distribution of salt formations and the distribution of oil and gas drilling activities within a manual fade-in image slider.

3. Implementation of an Interactive Web-Based Mapping Application

Planning for Phase 2 of a web-based interface for the GIS Database was completed in FY14 and will be implemented in FY15. In collaboration with INL, we will use ArcGIS Viewer for Flex (http://www.esri.com/software/arcgis/viewer-for-flex) to create the web mapping application. The application will be hosted on INL's existing external GIS server and will take advantage of current GIS application hosting software licenses (ArcGIS Server). The application will build on current customized tools developed by INL for display and query, which will provide a significant reduction in development costs. LANL will provide the geologic data and data pertaining to potential siting guidelines and guidance for how the users will interact with the data.

An example of a fairly simple web application using the ArcGIS Viewer is shown in Figure 3-1. This application was built by the Oregon Department of Geology and Mineral Industries to display geothermal data. Standard functionality built into the ArcGIS Viewer include the ability to pan and zoom, select the data layers to display, adjust layer transparency and display a map legend.

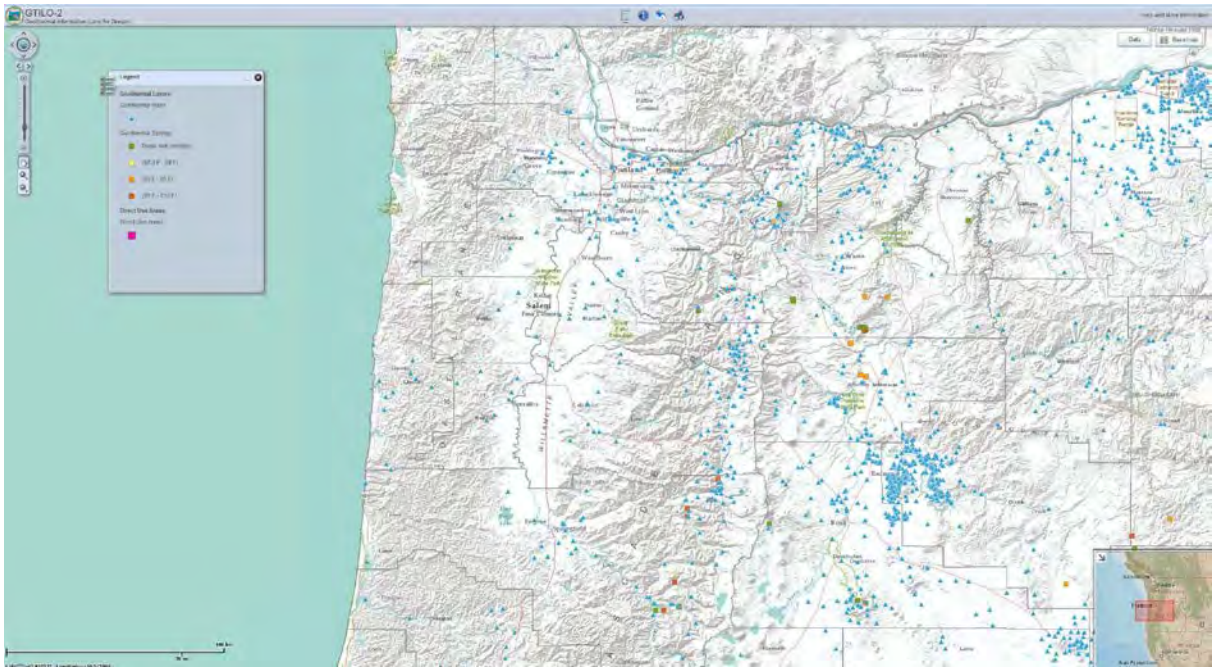

Figure 3-1. Example of a simple interactive mapping application using the ArcGIS Viewer for Flex available at http://www.oregongeology.org/gtilo/index.html. Points on the map are the locations of geothermal wells or the temperatures of geothermal springs.

The mapping application planned for the Regional Geology GIS database will be capable of displaying a large number of data layers and will be customized per project and expected user needs using tools developed by INL. The Data layers planned for inclusion in the mapping application for visualization and/or query include:

- **Geologic Data Layers**
  - Bedded Salt Formations
    - Raster layer(s) for 25 salt formation (depth only)
    - Vector layer (polygon) showing extents of areas of interest (AOI)
    - Vector layer (line) of contours within AOI showing depth intervals
  - Shale Formations
    - Raster layer(s) for 25 salt formation (depth only)
    - Vector layer (polygon) showing extents of areas of interest (AOI)
    - Vector layer (line) of contours within AOI showing depth intervals
  - Crystalline Rock Outcrops
    - Vector Layer (polygon) – Attributes include (age, rock type, area, etc.)
  - Crystalline Basement
    - Raster layer of depth to crystalline basement
  - Sedimentary Basins
    - Vector layer (polygon) of sedimentary basins (USGS)

- **Potential Siting Guideline Data Layers**
  - Population Distribution and Density
    - Raster layer (ORNL – LandScan)
    - Vector layer (polygon) (ORNL – LandScan)
  - Seismic Hazard
    - Raster layer showing peak ground acceleration
    - GeoRSS Feed – USGS Earthquake map service showing active earthquakes at various magnitudes
  - Quaternary Faulting
    - Vector layer (line) showing the distribution of quaternary faults (USGS)
  - Quaternary Volcanism
    - Vector layer (polygon) showing the distribution of quaternary volcanos (USGS)
  - Topography
    - Raster layer showing topographic relief (USGS DEM)
  - Oil and Gas Drilling

        - Vector layer (polygon) 0.5 km polygons showing location of oil and gas drilling (USGS)
    - Major Geologic Structures within Crystalline Basement
        - Raster layer of major structures within crystalline basement interpreted from aeromagnetic data
        - Raster layer of all aeromagnetic results for US
    - Federal Lands
        - Map Service showing land administration for the US – (USGS Protected Areas Database map service)

Specific tools for visualizing and querying map layers will be customized from existing INL tools and, if necessary, developed to accommodate specific requirements. The tools envisioned for this application include:

- Identify
- Layer transparency
- Query by attribute
- Query by location
- Elevation Profile
- Draw/measure
- View shed Analysis
- Select layers from layer list (including metadata links and legends)
- Map tips (“Pop Ups”) showing details of map features

A beta test will be performed on the application by a yet to be determined group of users. The results of the beta test will be compiled into a set of changes, which will be vetted by INL and LANL developers to determine whether they should be implemented. Approved changes will be implemented prior to final release.

4. Terrane Maps of Crystalline Basement Rocks

Siting of a deep borehole disposal or R&D facility requires information about the geology of the basement at the national, regional and local scale. For any potential candidate sites, it would be necessary to identify and document all pertinent geologic data at the local scale in order to compare siting options. Because there are no current candidate sites, we have begun to identify and document data for basement terranes at the national and regional/state scale that will provide a context for understanding the geologic history of different regions and as well as provide a framework and aid in identifying and understanding data at the local scale.

Siting of a deep borehole disposal facility includes consideration of technical factors important to successful completion of the drilling operation and the post-closure safety of the disposal system (Arnold et al., 2013). Basement characteristics that would positively promote these factors include homogeneity of the basement rock, which is more likely in felsic plutonic rocks (granite) and avoidance of major faults and shear zones, which characteristically define the boundaries of large crustal blocks or terranes. Borehole data (including lithologic characterization and geochronology), geophysical data and extrapolation of geologic data from surface exposures of crystalline rock have led to the concept of crustal terranes, which are defined as structurally bound basement blocks with geologic histories that are distinct from adjacent terranes (e.g., McCormick, 2010). Locations of major structures that define the boundaries of basement terranes have been obtained from aeromagnetic data and, to a lesser extent, gravity data (e.g., Sims et al., 2008 and discussion in Section 6.3.9 of Appendix A).

Crystalline basement rocks are the equivalent of exposed granitic crystalline rocks that have been covered by younger sedimentary or volcanic rocks. As such, their lithology includes the same complex assemblages of crystalline igneous and metamorphic rocks that are present in surface exposures. Because they can only be directly observed in borehole samples, lithologic composition and other characteristics of basement rocks can never be understood to the same level of detail as rocks exposed at the surface. Despite these limitations, general patterns of lithologic characteristics and the degree of local variability can be estimated from borehole samples collected within a particular region. Understanding the geometry of basement terranes and the location of terrain boundaries (structures) can assist to better predict the lithology likely to be encountered in a borehole and the relationship of the borehole to potential structural complexity in the basement.

The most recent example of mapping crustal terranes using borehole data and geophysical surveys is by McCormick (2010) for the state of South Dakota (Figure 4-1). The borehole database used in the study consisted of 4830 boreholes that intersected Precambrian basement rock (see Figure 4-1). The most common rock encountered in the crystalline basement was granite. We assume that the boreholes only penetrated the uppermost portion of the crystalline basement and it is therefore possible that the lithology could change in a borehole that penetrates several kilometers of basement rock.

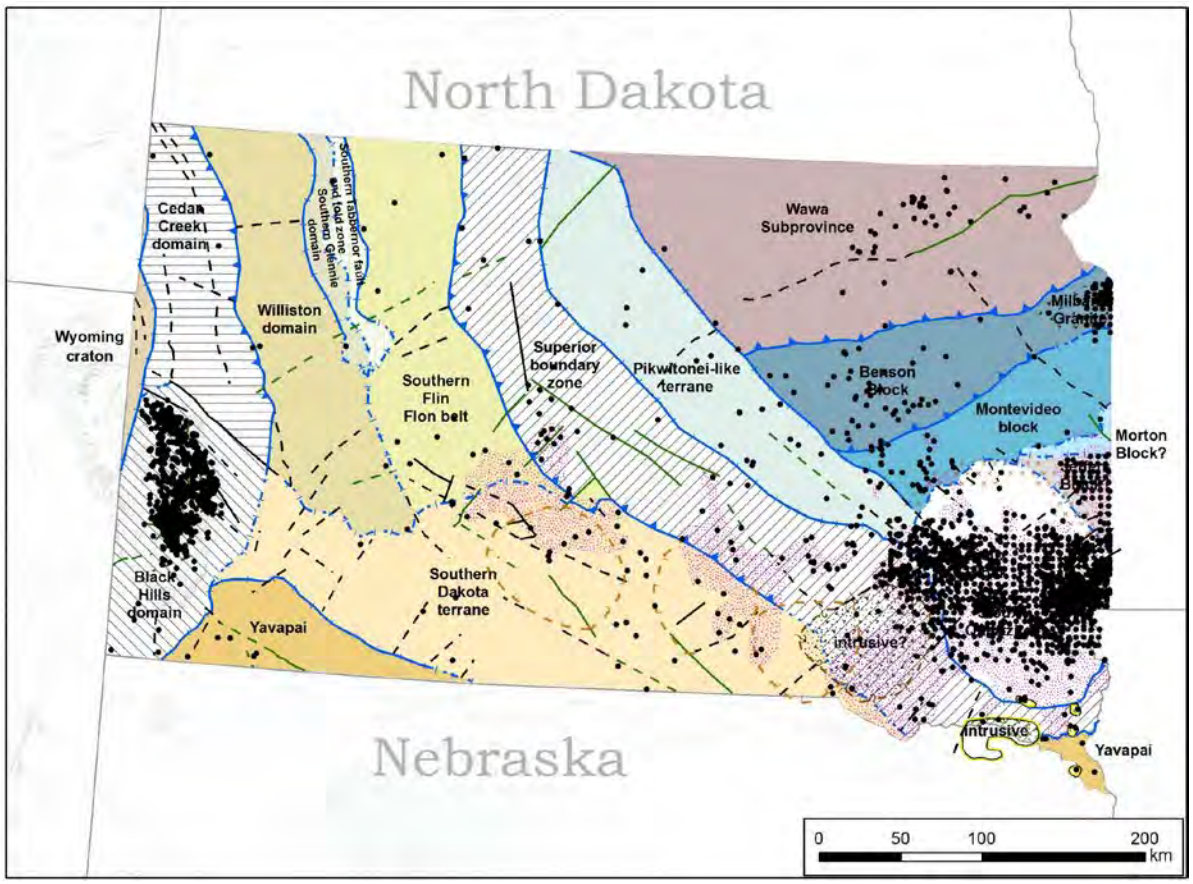

Figure 4-1. Basement terrane map of South Dakota (McCormick, 2010). Solid black circles represent the location of boreholes that penetrated Precambrian basement rocks. Granite was the most common lithology encountered within the crystalline basement.

In addition to South Dakota, several other maps of basement terranes that have been completed at the state and regional scale are included in the GIS database (Figures 4-2 and 4-3). As a whole, the maps at this scale probably provide the best overall balance between broad coverage and useful information about terrane boundaries and terrane lithologies. A potential issue with the state-based data is that interpretations of terrain boundaries and characteristics evolve over time as new data is acquired. Thus terrane mapping may not translate perfectly across state lines where the information for different states was interpreted from data acquired over a number of years or by different investigators.

To compare the location of basement structures compiled at different scales, we overlaid the basement structure map of Sims et al. (2008), which was compiled at the national scale, on the data layers for maps at the state and regional scale (Figure 4-3). In general, the major basement structures depicted at the national scale agree well with terrain boundaries depicted at the state scale, with differences in boundary locations in most cases attributable to new data becoming available and different interpretations of data over the time period that the maps were created (1990-2010).

Local studies based on borehole-based data would provide the best available information for understanding basement characteristics at specific locations being considered for a borehole disposal or demonstration site. In every case, it would be necessary to seek out all available local information when comparing potential candidate sites. A discussion of the uncertainties involved in understanding the

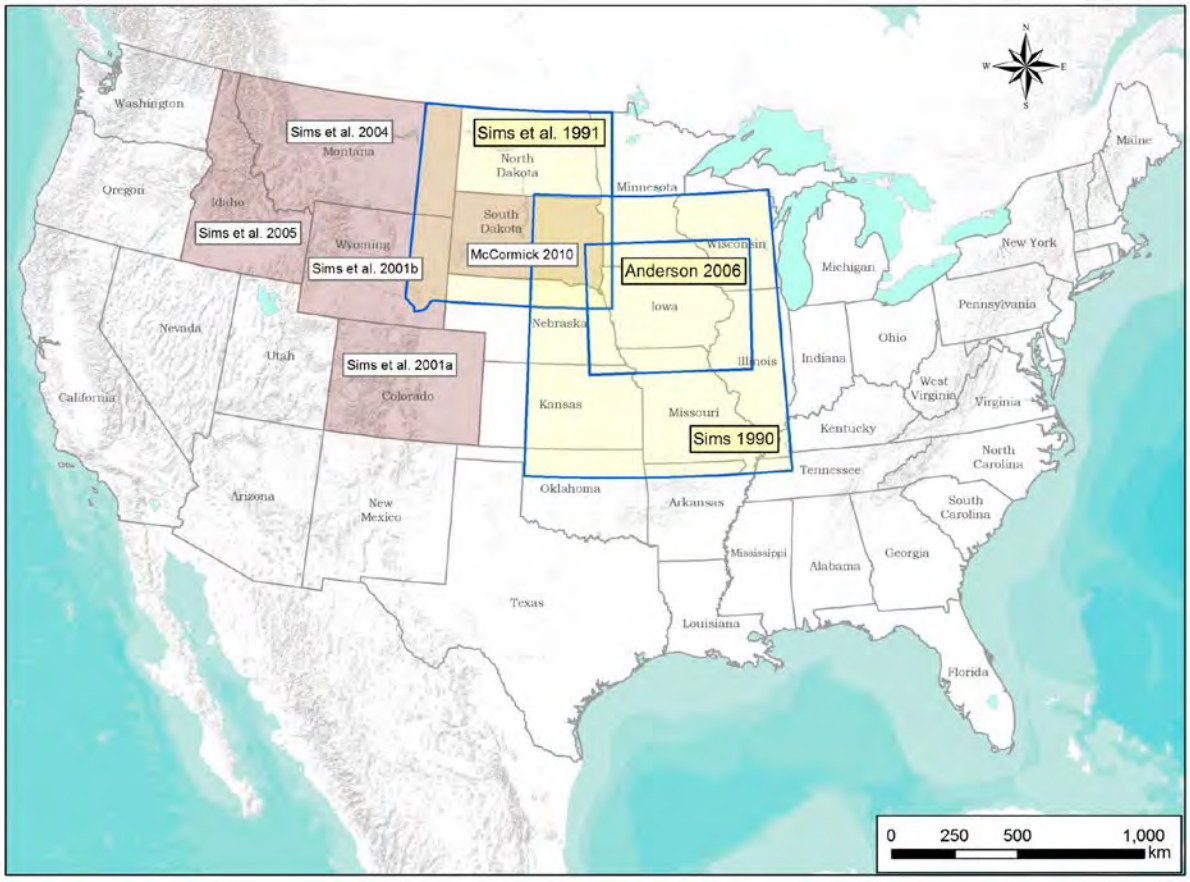

Figure 4-2. Index map showing area coverage and sources for basement terrane maps at the state and regional scale included to date in the GIS database. The map by Sims (1990) of the midcontinent region was digitized for GIS by Dicken et al. (2001).

characteristics of basement rocks at any particular location is presented in Section 2.3.2 of Arnold et al. (2013).

Maps of basement terranes and age provinces (which typically contain multiple individual basement terranes that span a certain age interval) are also available at the national scale. While not providing sufficient detail to compare specific siting alternatives, these maps provide a context for regional comparisons and provide information on the location of terrane boundaries, terrane ages and general information related to terrane lithology. They serve as a starting point for identifying, compiling and understanding data obtained at the more local scale.

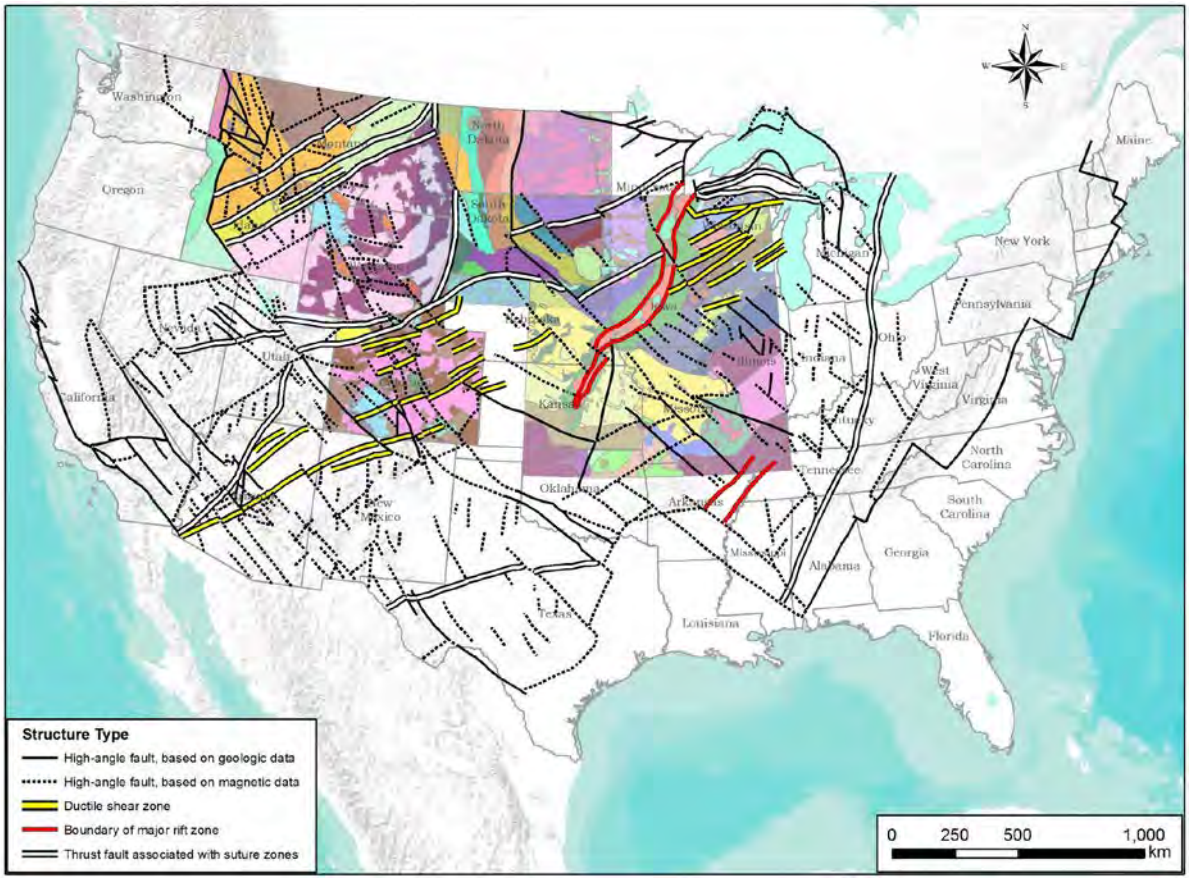

Figure 4-3. Crystalline basement maps for the States of Idaho, Montana, Wyoming, Colorado, and South Dakota, as well as regional maps of the northern midcontinent and the northern Great Plains. The source of each map is shown in Figure 4-1. The basement map by Anderson (2006) centered on Iowa is not shown in this figure because of overlap with the map of the midcontinent region. The structural information overlying the state and regional maps is from Sims et al. (2008). The large number of map units depicted on the map from different sources did not allow inclusion of a legend of the map units for this figure.

A reasonably detailed understanding of the crustal age geometry of the US was known by the 1980s based on a data from a number of radiogenic isotopic systems (e.g., Bennett and DePaolo, 1987 and references therein). We have obtained data for two Precambrian basement maps compiled at the national scale and included them in the GIS database. The first is from Reed et al. (1993) and emphasizes the age and lithology of crustal provinces and terranes (Figure 4-4). The second, from Whitmeyer and Karlstrom (2007), is more detailed in terms of terrane designations, presumably because more data was available for interpretations by 2007. This map emphasizes detailed age distinctions and geometry of accretionary crustal events that formed much of North America during the Proterozoic (Figure 4-5). National-scale depictions of basement terranes and age provinces lack the detail for evaluating specific sites, but can guide acquisition of more local data for purposes of comparing potential sites. They can also aid in identifying regions with favorable basement characteristics, for example, where terranes are composed primarily of granitic intrusions.

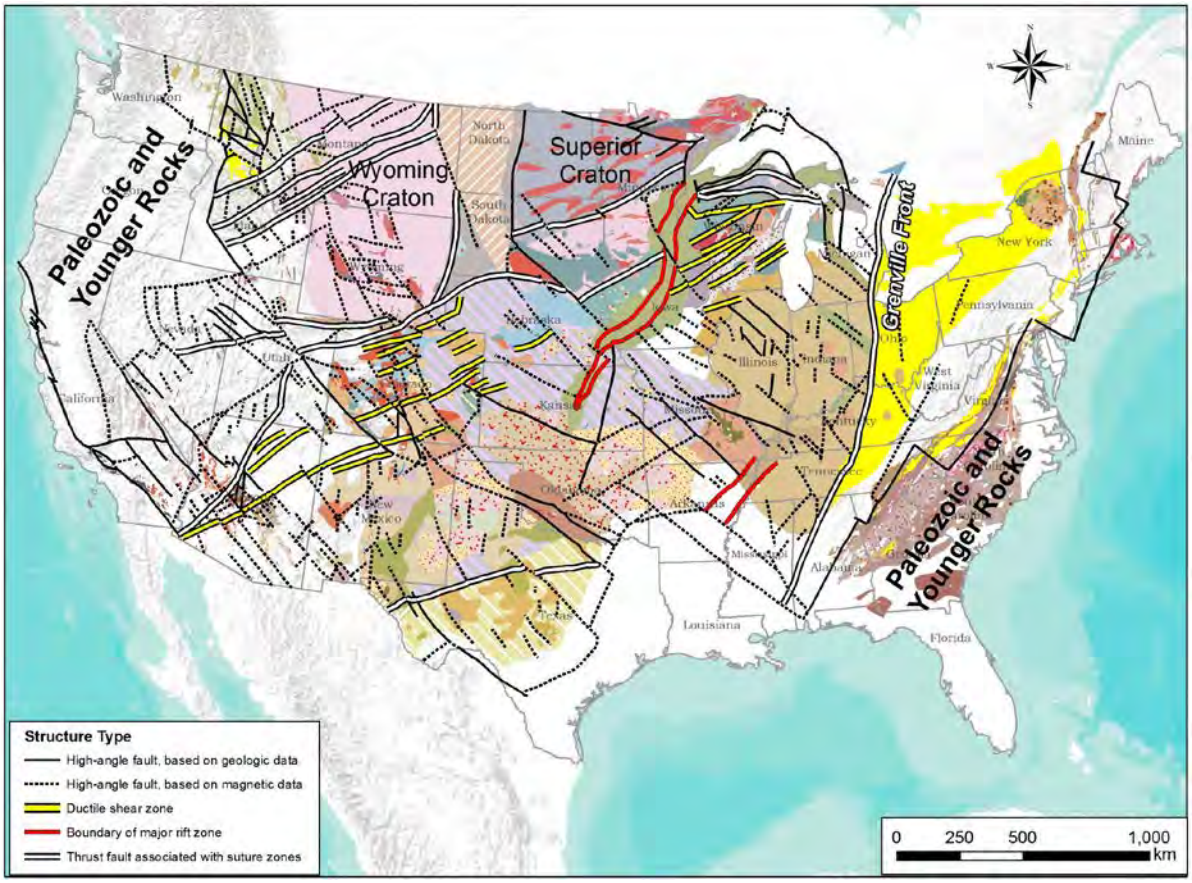

Figure 4-4. Precambrian basement map of Reed et al. (1993) which emphasizes terrane boundaries and the general lithology of each terrane. Structure overlay is from Sims et al. (2008). Note the close correspondence between the lithology and structural boundaries over much of the map area. The large number of map units depicted on the map (>100) did not allow inclusion of a legend of the map units for this figure.

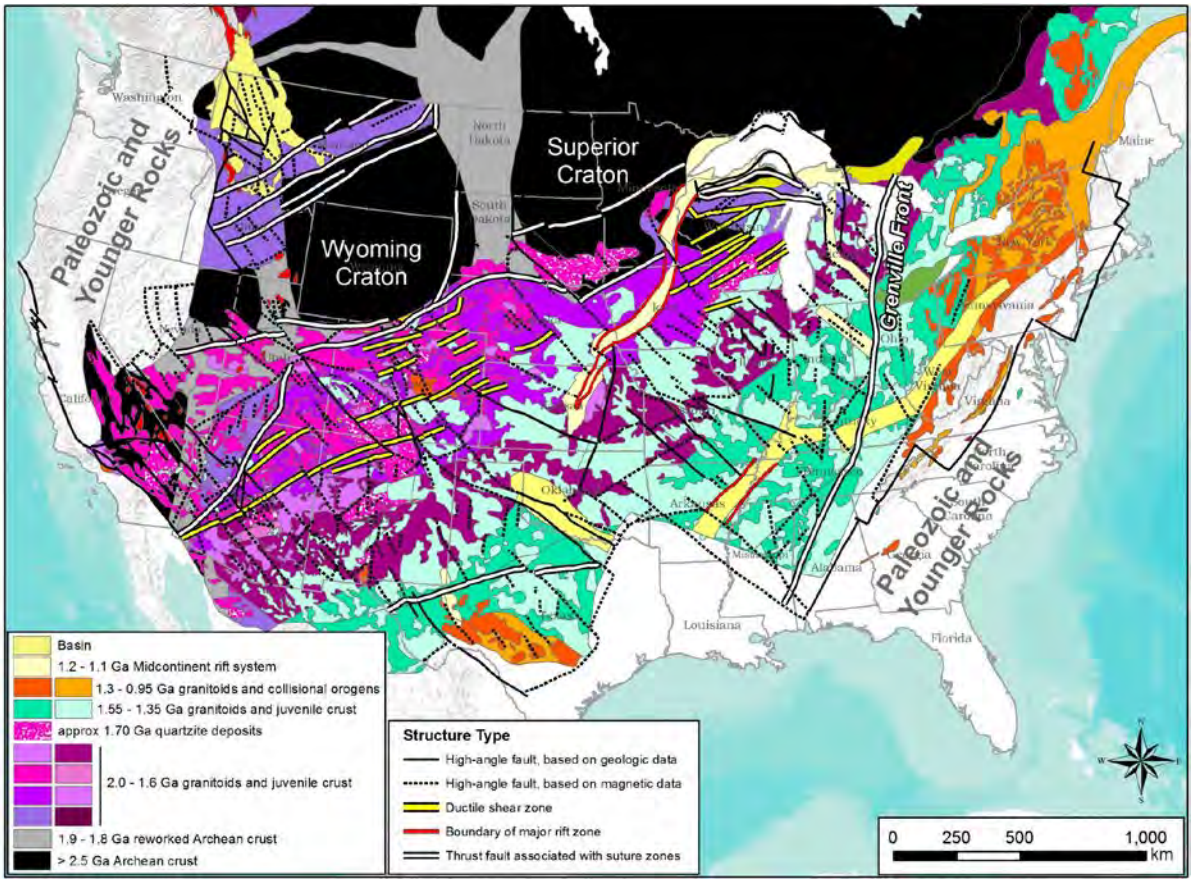

Figure 4-5. Precambrian basement map of Whitmeyer and Karlstrom (2007) with structural overlay from Sims et al. (2008). The map units were color-coded in the GIS software to emphasize major Precambrian time periods: Black indicates Archean (>2.5 Ga); purple shading indicates Paleoproterozoic (2.0-1.6 Ga); green to blue-green shading indicates Mesoproterozoic (1.55-1.35 Ga) and orange shading indicates mid Mesozoic to early Neoproterozoic (1.3-0.95 Ga).

5. Inventory of Shale Formations in the US

The information in this section is reproduced from Dobson and Houseworth (2014).

5.1 INTRODUCTION

This report documents FY14 progress for the work package entitled "Regional Geology R&D – LBNL". The major purpose of this work package is to augment the existing inventory of shale formations in the US in the LANL Geographic Information Systems (GIS) database and to examine physical properties associated with these rocks.

There are two main research tasks for this work package. The first (described in Section 5.2 and 5.3) is to build upon previous work conducted to obtain isopach and structural top data (either from published maps and figures or as GIS shape files) for selected shale units in the US through literature searches and personal contacts, and to include rock property characteristics, such as total organic carbon (TOC) and thermal maturity data, where available. The second task (described in Section 6) is to develop a methodology through the use of sonic velocity logs to estimate hydrologic and geomechanical properties of shales. Publically available field and laboratory data from shale samples have been used to develop correlations between measured sonic velocities and rock properties such as porosity, bulk density, clay content, permeability, uniaxial compressive strength, Young's modulus, and shear modulus.

5.2 INVENTORY OF SHALE FORMATIONS IN THE US

5.2.1 INTRODUCTION

Clay-rich shale formations have a number of properties, such as low permeability, high cation exchange potential, and the ability to self-seal, which make them candidates for a geologic repository for high-level radioactive waste (e.g., Cuadros, 2008). The United States has an abundance of thick shale deposits that span a wide range of geologic ages, mineralogic compositions, and geologic environments, some of which might be suitable for hosting repositories to safeguard radioactive waste. The objective of this report is to build upon previous compilations of shale formations within many of the major sedimentary basins in the US (e.g., Merewether et al., 1973; Gonzales and Johnson, 1985; Dobson, 2011; 2012; Dobson and Houseworth, 2013; Perry et al., 2012; 2013; 2014) by developing GIS data delineating isopach and structural depth maps for many of these units. These data are being incorporated into the LANL digital GIS database developed for determining host rock distribution and depth/thickness parameters consistent with repository design (Perry et al., 2011; 2013; 2014). Three main rock types are being incorporated into this database: salts, shales, and granitic basement rocks. This database can then be utilized for screening and comparison of potential repository sites (e.g., Rechard et al., 2011). This report represents an update of the Dobson and Houseworth (2013) report.

5.2.2 DATA SOURCES

Most of the shale data are from sedimentary basins where oil and gas deposits are present (Figure 5-1). The Energy Information Administration (EIA, 2011b) estimates that around 750 trillion cubic feet of undeveloped technically recoverable shale gas and 24 billion barrels of shale oil resources are in discovered shale plays in the lower 48 states. Formations that have been identified as having at least 20 trillion cubic feet (tcf) of shale gas include the Marcellus Shale (410 tcf), the Antrim Shale (20 tcf), the Haynesville Shale (75 tcf), the Eagle Ford Formation (21 tcf), the Fayetteville Shale (32 tcf), the Barnett and Woodford Shales (97 tcf), and the Mancos Shale (21 tcf). Many of these units are not shales in a strict sense, but may be better described as siliceous mudstones with reduced clay contents; these slightly brittle

rocks can be subjected to successful hydrofracture treatment (Gale and Holder, 2010). While many areas within these sedimentary basins are sites of active and prospective oil and gas exploration and development activities, there may be locations (such as within the shallower basin margins) that could be possible candidates for a repository.

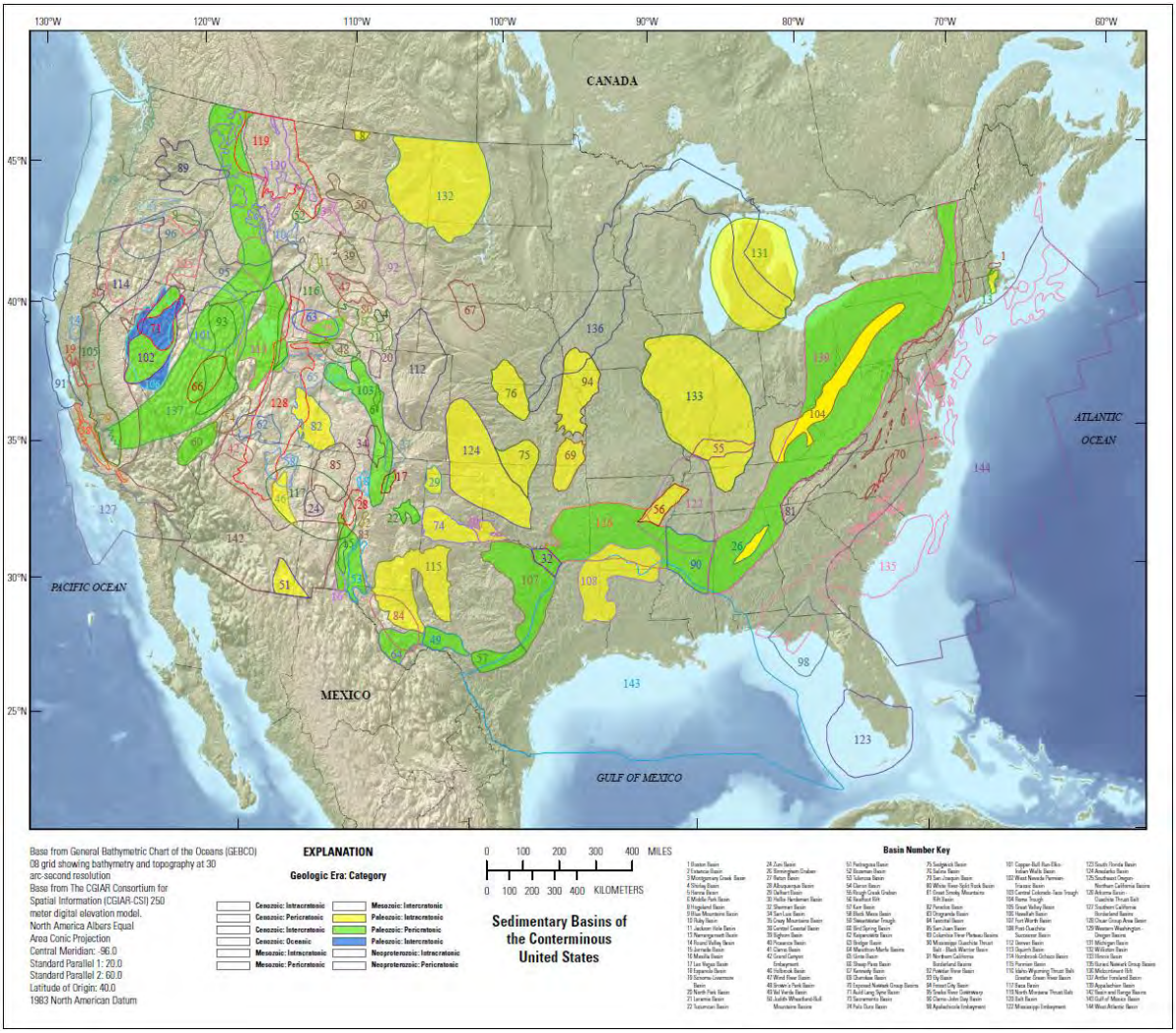

Figure 5-1. Sedimentary basins in the contiguous US. (Coleman and Cahan, 2012)

The data used for this report represent information that was either digitized using ArcGIS from published isopach and structure maps, or was available as GIS shape files that delineate formation isopachs and structural surfaces relative to a known datum, such as sea level or the ground surface. A number of data sources were obtained from the references listed in the discussions in Hovorka et al. (2003) of seal thickness and seal continuity for different saline formations in US sedimentary basins. The U.S. Geological Survey (USGS) Digital Data Series reports on petroleum systems and geologic assessment of oil and gas resources have been another helpful source of information. Numerous state geological survey reports have provided additional detailed information on local basin stratigraphy. Where maps were used to create GIS data layers, a jpeg version of the map was georectified using multiple geographic reference

points (such as country or state boundaries) and the thickness or structure contours were converted to vector format. Where depths are referenced to sea level instead of the ground surface, Digital Elevation Model (DEM) data are used. In the case of GIS data, metadata files were used to ascertain the geodetic reference datum used. In some cases, multiple data sources were used. More details on the methodology used to create the GIS structural top and isopach shape files can be found in Perry et al. (2012).

5.2.3 ISOPACH AND STRUCTURE MAPS

Maps of shale formation extents, thicknesses, and depths were obtained for the following units as organized by sedimentary basin. Table 5-1 summarizes formations for which isopach and/or structural data have been obtained. More comprehensive lists of shale formations can be found in Dobson (2011) and Gonzales and Johnson (1985). Units listed in ***bold italics*** represent formations for which GIS data have been obtained or generated. This report represents the current status of data collection: this is an ongoing process to populate the LANL GIS database.

Table 5-1. Identified data sources for isopach and structural data for shale formations within major sedimentary basins.

Appalachian Basin	
Utica Shale	Patchen et al., 2006 (Plates 1-28 & 2-6) (GIS data obtained from West Virginia Geological and Economic Survey)
Marcellus Shale	Erenpreiss et al., 2011 (GIS data obtained from Ohio Department of Natural Resources)
Olentangy Shale	Gray et al., 1982 (METC/EGSP Series 313, 314, 318, 320)
Ohio Shale	Gray et al., 1982 (METC/EGSP Series 310, 311, 312, 316, 317)
Black Warrior Basin	
Chattanooga Shale	Pashin, 2008 (Figure 6)
Illinois Basin	
Maquoketa Shale	Willman et al., 1975 (Figure O-26); Collinson et al., 1988 (Figure 22); Kolata and Noger, 1990 (Figure 5-13); Bristol and Buschbach, 1973 (Plate 1)
New Albany Shale	Hasenmueller and Comer, 2000 (GIS data obtained from Illinois State Geological Survey)
Michigan Basin	
Eau Claire Formation	Catacosinos and Daniels, 1991 (Figure 6)
Antrim Shale	Wylie and Wood, 2004; 2005; Matthews, 1993 (Figures 4 & 24)
Coldwater Shale	Merewether et al., 1973 (Figures 12 & 13); Gonzales and Johnson, 1985 (Figure 3-20)
Anadarko Basin	
Sylvan Shale	Amsden, 1975 (Plates 7 & 8); Amsden, 1980 (Panel 1)
Woodford Shale	Amsden, 1975 (Plates 3 & 4); Cardott and Lambert, 1985 (Figures 2 & 3); Rottmann, 2000
Kiowa Shale	Macfarlane et al., 1993 (Plates 7 & 8)
Graneros Shale	Macfarlane et al., 1993 (Plates 3 & 4)
Ardmore Basin	
Woodford Shale	Party et al., 2008 (Slides 41 & 43); Cardott, 2012 (Figure 10); Rottmann, 2000
Arkoma Basin	
Sylvan Shale	Amsden, 1980 (Panel 1)
Woodford Shale	Amsden, 1980 (Panel 3); Blackford, 2007 (Plates 12 & 13); Rottmann, 2000

Chattanooga Shale	Li et al., 2010 (Plates 4 & 6)
Fayetteville Shale	Ratchford et al., 2006 (Plates 2 & 3); Li et al., 2010 (Plates 3 & 5)
Gulf Coast Basin	
Wilcox Formation	Pitman, 2008
Eagle Ford Shale	Surles, 1987 (Figures 5, 8, 9, 12, & 14); Pitman, 2008; Harbor, 2011 (Figure 8) (GIS data obtained from US Energy Information Administration)
Haynesville Shale	Hammes et al., 2011 (Figures 7 & 8)
Smackover Formation	Pitman, 2008
Fort Worth Basin	
Barnett Shale	Pollastro et al., 2007 (Figures 6 & 15)
Permian Basin	
Woodford Shale	Broadhead, 2010 (Figures 4 & 12); Comer, 1991 (Plates 1 & 2); Ruppel et al., 2005 (GIS data obtained from University of Texas, Bureau of Economic Geology)
Barnett Shale	Broadhead and Gillard, 2007 (Plates V and VII) (GIS data obtained from New Mexico Bureau of Geology and Mineral Resources)
Williston Basin	
Bakken Shale	LeFever, 2008 (Sheets 1 & 5); LeFever et al., 2012 (GIS data obtained from North Dakota Geological Survey)
Big Snowy Group	Peterson, 1984 (Figure 12)
Pierre (Bearpaw) Shale	Shurr, 1977 (Figures 5 & 6); Carlson, 1982; Smith, 1999; Condon, 2000 (Plates 8 & 23)
Powder River Basin	
Pierre Shale	Shurr, 1977 (Figures 5 & 6); Denson et al., 1993a, b, c, d
Lebo shale member, Fort Union Formation	Lewis and Hotchkiss, 1981 (Plate 3)
Upper Hell Creek confining layer, Lance Formation	Lewis and Hotchkiss, 1981 (Plate 5)
Denver Basin	
Pierre Shale	Shurr, 1977 (Figures 5 & 6); Dechesne et al., 2011 (Plates 4 & 8)
San Juan Basin	
Mancos Shale	Ridgley et al., 2013 (Figures 6 & 10)
Green River Basin	
Green River Formation	Mercier et al., 2010c
Piceance Basin	
Green River Formation	Mercier et al., 2010a; Mercier and Johnson, 2012
Uinta Basin	
Green River Formation	Mercier et al., 2010b; Mercier and Johnson, 2012
Cuyama Basin	
Monterey Formation	Lagoe, 1982 (Plate VI); 1984 (Figure 11); Sweetkind et al., 2013 (GIS data obtained from US Geological Survey)
Santa Maria Basin	
Monterey Formation	Sweetkind et al., 2010 (GIS data obtained from US Geological Survey)
San Joaquin Basin	
Monterey Formation	Hosford Scheirer, 2013 (Figure 7.18)

5.2.3.1 Appalachian Basin

The Appalachian Basin is a composite foreland basin that contains a thick sequence of Paleozoic sedimentary rocks (Ettensohn, 2008). These rocks have been subjected to a number of orogenic events, resulting in faulting and folding. The Marcellus Shale has been the primary focus for numerous geologic studies (e.g., Lash and Engelder, 2011) because of its prolific shale gas resources.

GIS data were obtained for two major shale formations in this basin: the Ordovician Utica Shale and the Devonian Marcellus Shale, both major shale gas targets. The Utica Shale GIS dataset was developed as part of a comprehensive regional stratigraphic study conducted by the Trenton-Black River Research Consortium of the Ordovician Trenton-Black River carbonate system (Patchen et al., 2006). This study generated an interval-thickness map for the Utica Shale and a structural map for the top of the Trenton Limestone, which serves at the base of the Utica Shale. GIS data obtained from the West Virginia Geological and Economic Survey were used to generate isopach and structure maps for the Utica Shale (Figure 5-2).

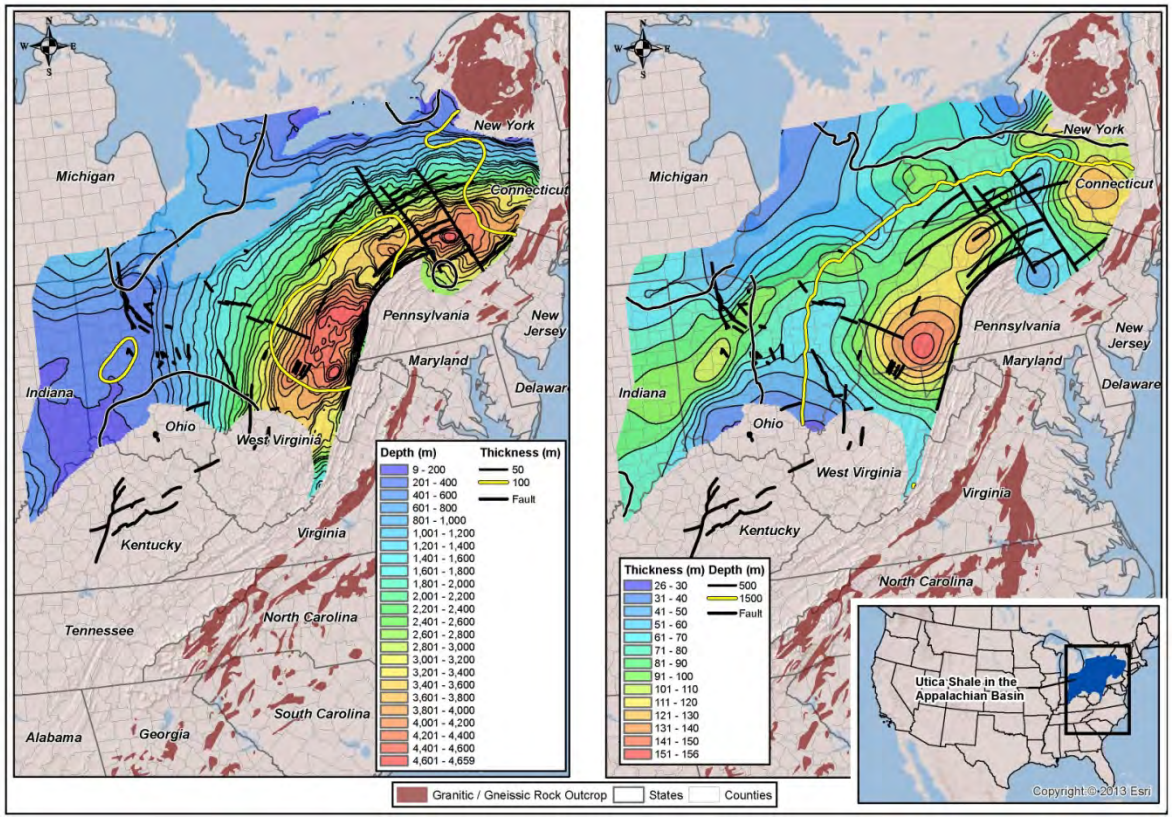

Figure 5-2. Depth and isopach maps of the Utica Shale, Appalachian Basin. Figure produced by LANL from shale data populated into the GIS database.

GIS data obtained from the Ohio Department of Natural Resources were used to generate isopach and structure maps for the Marcellus Shale (Figure 5-3). This unit has a total area of 95,000 square miles (EIA, 2011b). While this unit is very extensive, and is present in Ohio, Pennsylvania, West Virginia, Virginia, western Maryland and New York, there is only a limited area (in eastern Pennsylvania) where the shale thickness is at least 100 m at depths less than 1000 m.

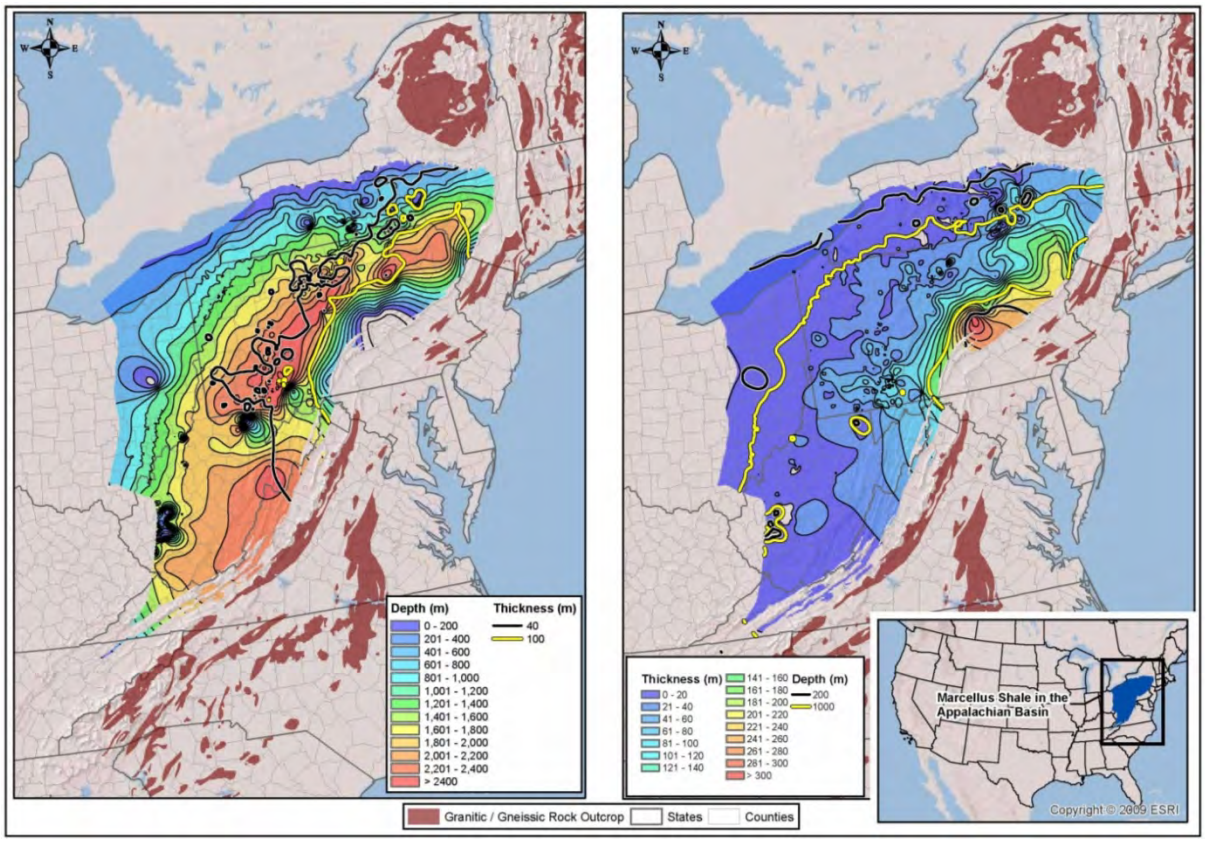

Figure 5-3. Depth and isopach maps of the Marcellus Shale, Appalachian Basin. Figure produced by LANL from shale data populated into the GIS database.

Structural top and isopach maps were also obtained for a number of additional Devonian black shale units in Ohio: the Chagrin, Cleveland and Huron members of the Ohio Shale and the Upper and Lower Olentangy Shales (Gray et al., 1982). The Ohio Shale is equivalent in age to the Chattanooga Shale, the New Albany Shale in the Illinois Basin and the Antrim Shale in the Michigan Basin (Gonzales and Johnson, 1985).

5.2.3.2 Black Warrior Basin

The Black Warrior Basin is a Paleozoic foreland basin located in Alabama and Mississippi (Thomas, 1988). It has three major shale formations: the Devonian Chattanooga Shale, the Mississippian Floyd Shale, and shale layers in the Pennsylvanian Pottsville Formation (Pawlewicz and Hatch, 2007). These shales have been identified as the source rocks for oil and gas deposits in the basin. Pashin (2008) has created an isopach map within the state of Alabama for the Chattanooga Shale (Figure 5-4). Almost all of the mapped section of the Chattanooga in this basin has a thickness less than 30 m.

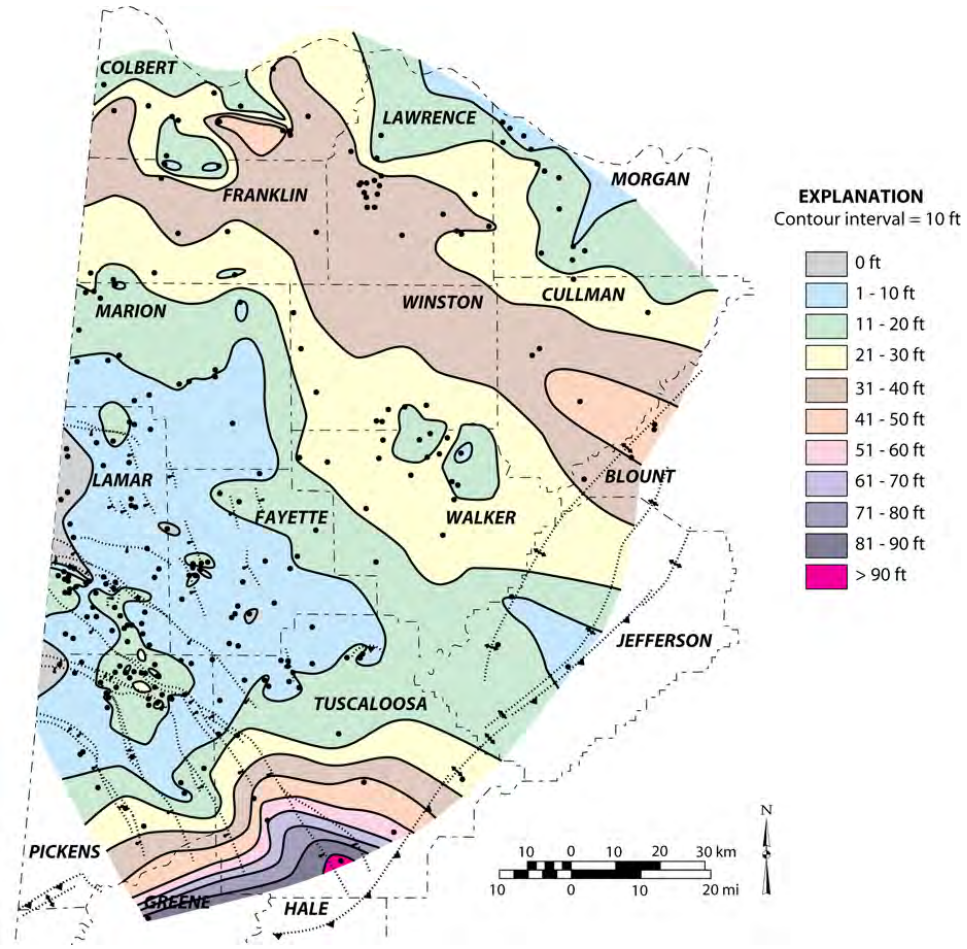

Figure 5-4. Isopach map of the Chattanooga Shale within the Alabama portion of the Black Warrior Basin (Pashin, 2008)

5.2.3.3 Illinois Basin

The Illinois Basin is filled primarily with Paleozoic age rocks, consisting of interbedded siliciclastic and carbonate sediments (Collinson et al., 1988; Swezey, 2009). The Devonian to Mississippian New Albany Shale is the most prominent shale unit in the Illinois Basin, with an areal extent of about 43,500 square miles and a thickness of 100 to 300 ft. (Hasenmueller and Comer, 1994; EIA, 2011b). GIS data for this unit (Figure 5-5) is available over the entire basin (Hasenmueller and Comer, 2000). In the southern portion of the Illinois Basin, there is a small section of this unit with thicknesses greater than 100 m at a depth of less than 1000 m.

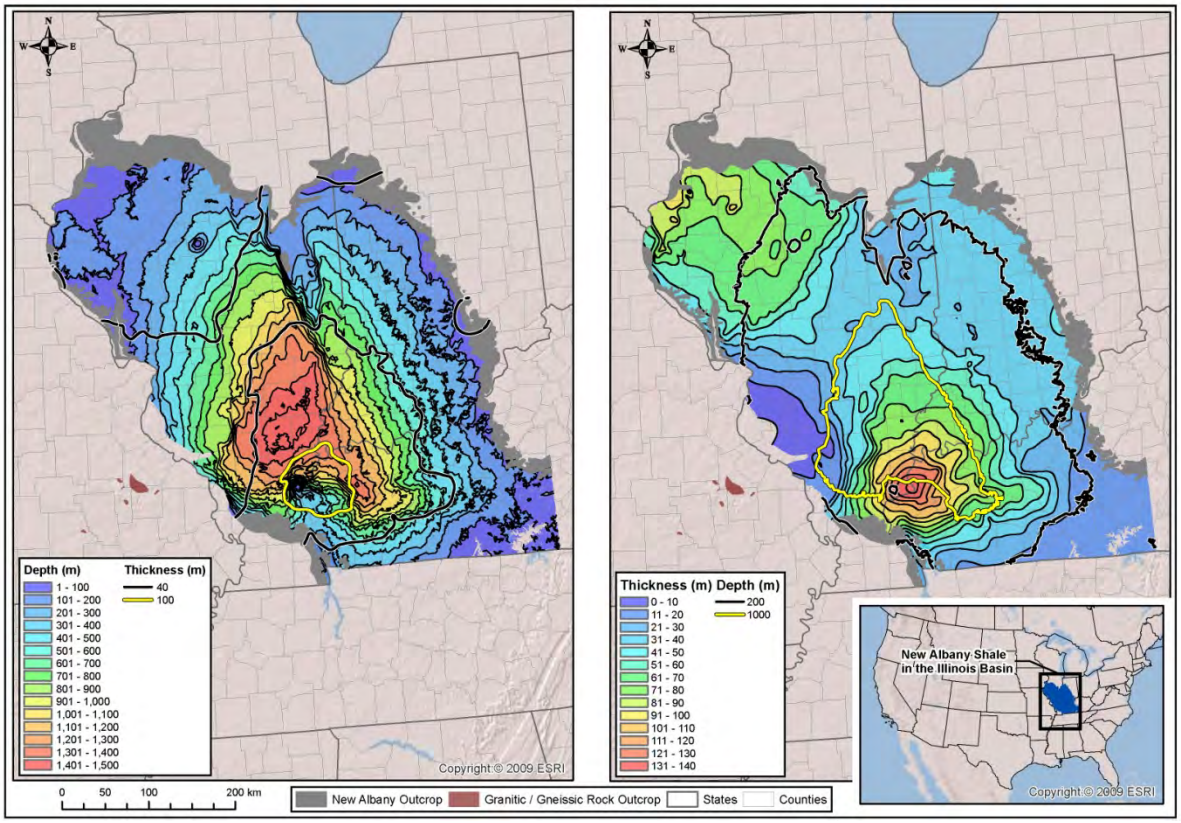

Figure 5-5. Depth and isopach maps of the New Albany Shale, Illinois Basin. Figure produced by LANL from shale data populated into the GIS database.

There are a number of studies with thickness and/or structural depth information on the Ordovician Maquoketa Shale. Bristol and Buschbach (1973) provide a plate depicting the top of the Galena Group, which represents the base of the Maquoketa Shale, for the state of Illinois. Willman et al. (1975) present a figure depicting the thickness of the Maquoketa Group, also restricted to Illinois. Collinson et al. (1988) and Kolata and Noger (1990) provide more regional depictions of the thickness of this unit. Given that this unit is older than the New Albany Shale, it is encountered at greater depths. The Illinois state data (Bristol and Buschbach (1973) and Willman et al. (1975)) were used to generate GIS maps of this unit (Figure 5-6).

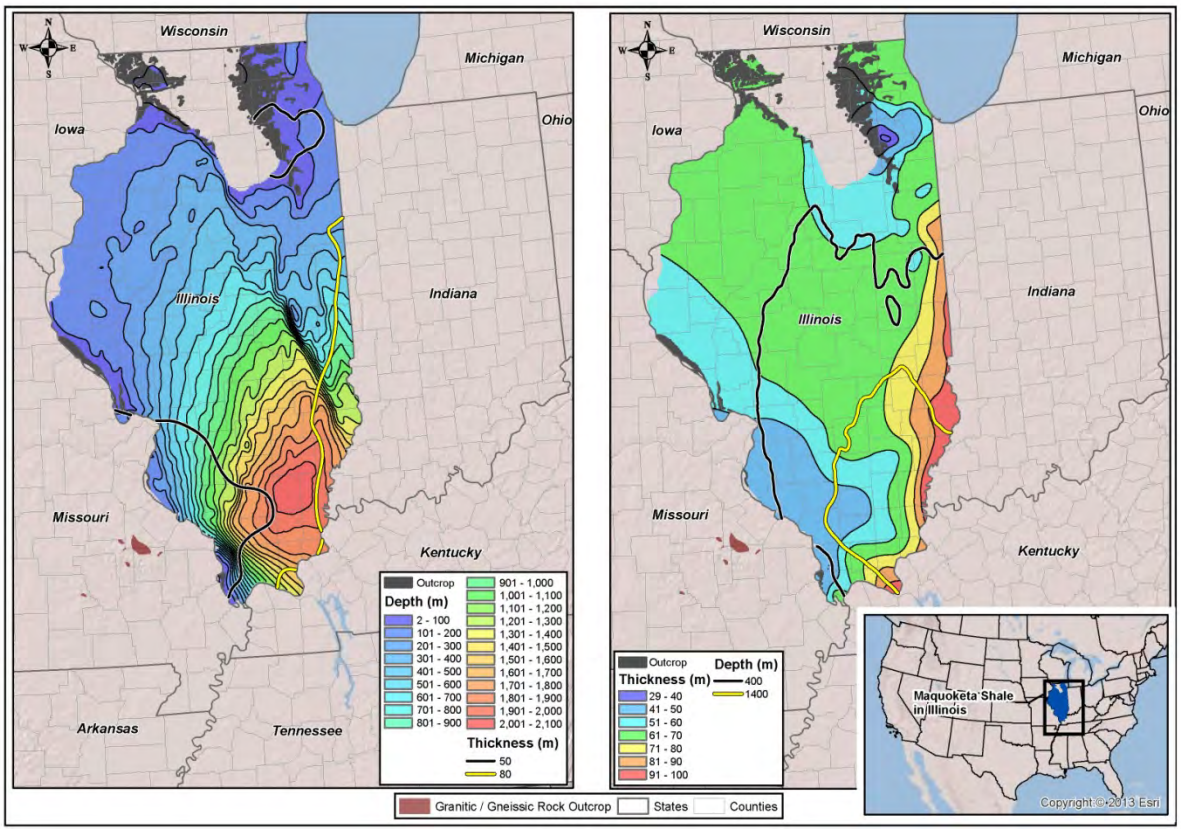

Figure 5-6. Depth and isopach maps of the Maquoketa Shale, Illinois Basin. Figure produced by LANL from shale data populated into the GIS database.

5.2.3.4 Michigan Basin

The Michigan Basin has a thick sequence of Paleozoic evaporites, carbonates, and siliciclastic sedimentary rocks (e.g., Merewether et al., 1973; Catacosinos et al., 1991; Swezey, 2008). Shale formations found in this basin include the Ordovician Utica and Collingwood Shales, the Silurian Cabot Head and Pointe aux Chenes Shales, the Devonian Antrim, Ellsworth, and Bedford Shales and the Mississippian Sunbury and Coldwater Shales. The predominant shale formation in the Michigan Basin is the Antrim Shale, a major producer of natural gas, with estimated recoverable shale gas resources of 20 trillion cubic feet (EIA, 2011b). Wylie and Wood (2004; 2005) and Matthews (1993) generated structure and isopach maps for a number of the hydrocarbon producing units in the Michigan Basin, including the Antrim Shale (Figure 5-7). Agrawal (2009) describes the depositional environment, mineralogy and TOC of the Antrim. GIS data were generated for the Coldwater Shale (Figure 5-8) using the isopach and structure map of Gonzales and Johnson (1985).

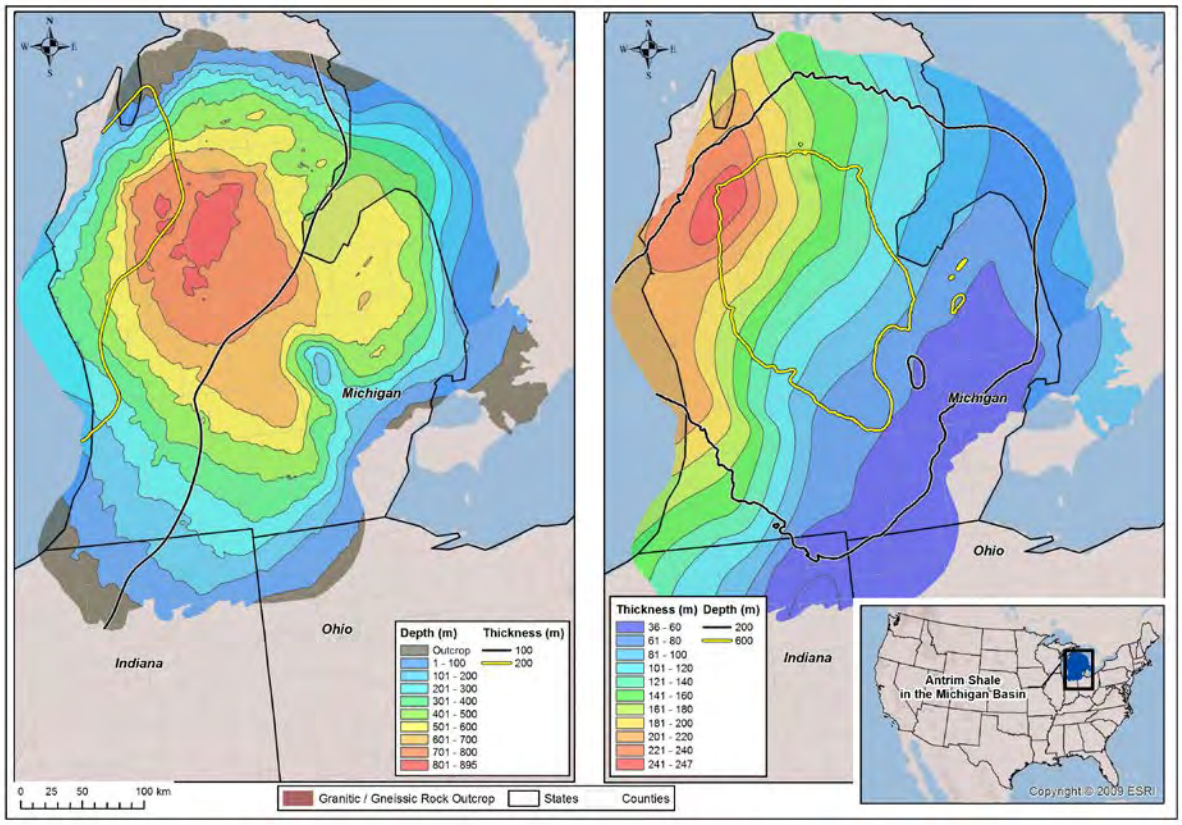

Figure 5-7. Depth and isopach maps of the Antrim Shale, Michigan Basin. Figure produced by LANL from shale data populated into the GIS database.

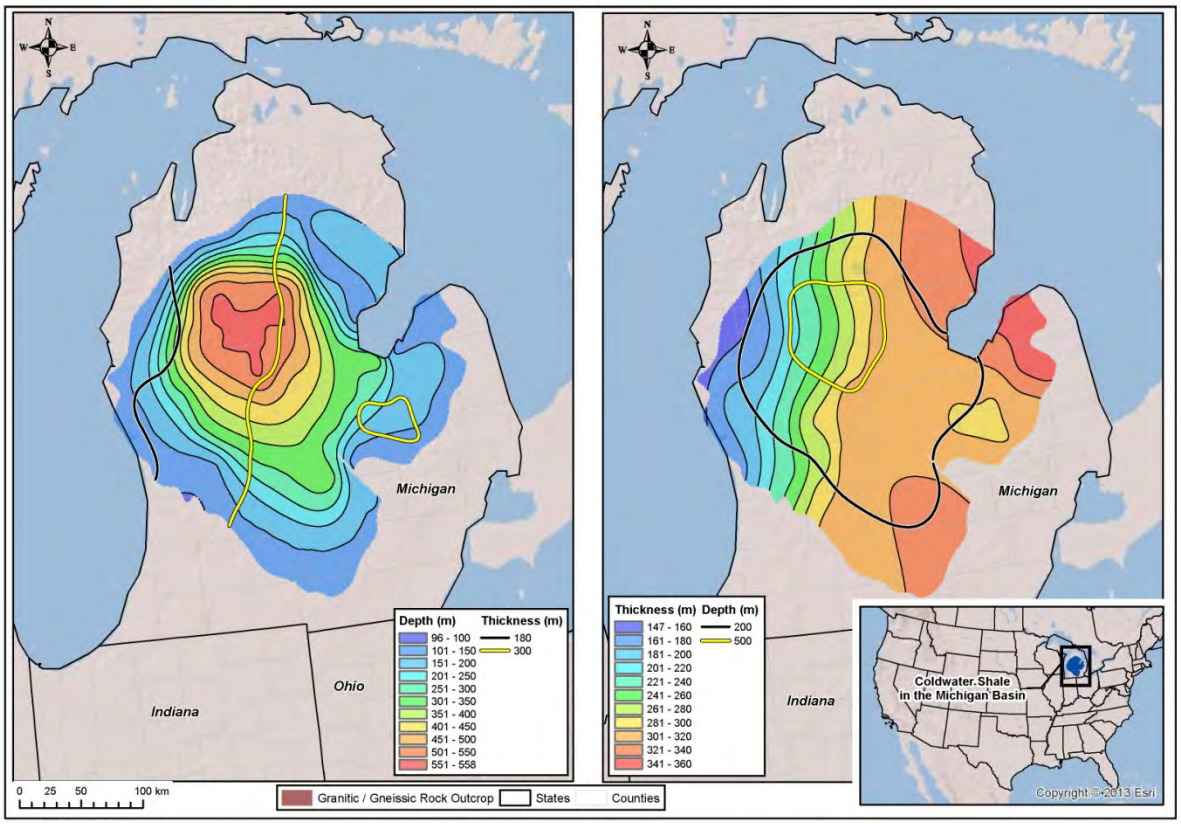

Figure 5-8. Depth and isopach maps of the Coldwater Shale, Michigan Basin. Figure produced by LANL from shale data populated into the GIS database.

5.2.3.5 Anadarko, Ardmore, and Arkoma Basins

The Anadarko, Ardmore, and Arkoma Basins, located in Oklahoma and neighboring states, are a series of fault-bounded sedimentary basins containing abundant hydrocarbon deposits. Detailed structure and isopach maps have been published for a number of the shale-bearing formations in these basins, including the Cretaceous Kiowa Formation and Graneros Shale (Macfarlane et al., 1993), the Mississippian Fayetteville Shale (Ratchford et al., 2006; Li et al., 2010), the upper Devonian/lower Mississippian Woodford Shale (e.g., Amsden, 1975; 1980; Cardott and Lambert, 1985; Rottmann, 2000; Blackford, 2007; Party et al., 2008; Cardott, 2012), the Devonian Chattanooga Shale (Li et al., 2010), and the Ordovician Sylvan Shale (Amsden, 1975).

The Hugoton Embayment of the Anadarko Basin in southwestern Kansas contains a sequence of Paleozoic, Mesozoic, and Cenozoic sedimentary rocks that reaches up to 2900 m in thickness (Macfarlane et al., 1993). In the upper portion of this basin, there are several Cretaceous shale units, including the Kiowa Formation (Figure 5-9) and the Graneros Shale (Figure 5-10), which serve as regional aquitards.

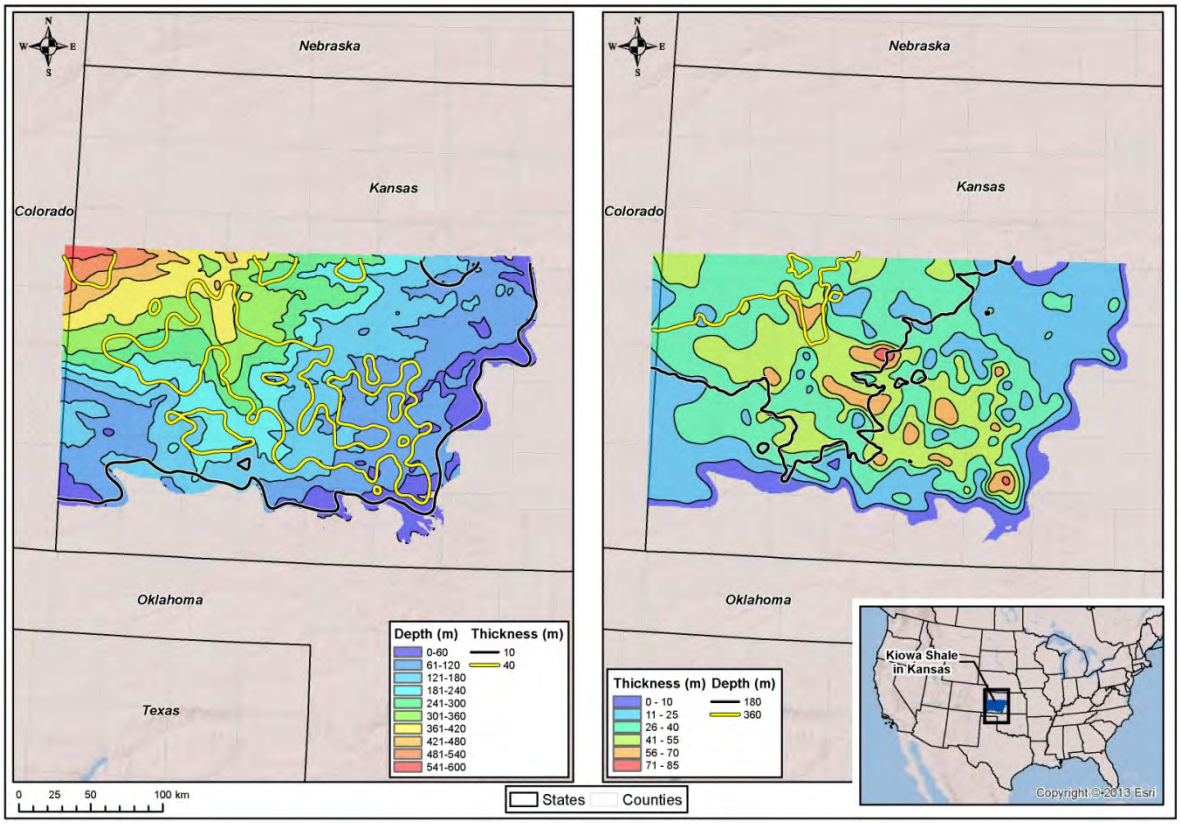

Figure 5-9. Depth and isopach maps of the Kiowa Shale, Anadarko Basin. Figure produced by LANL from shale data populated into the GIS database.

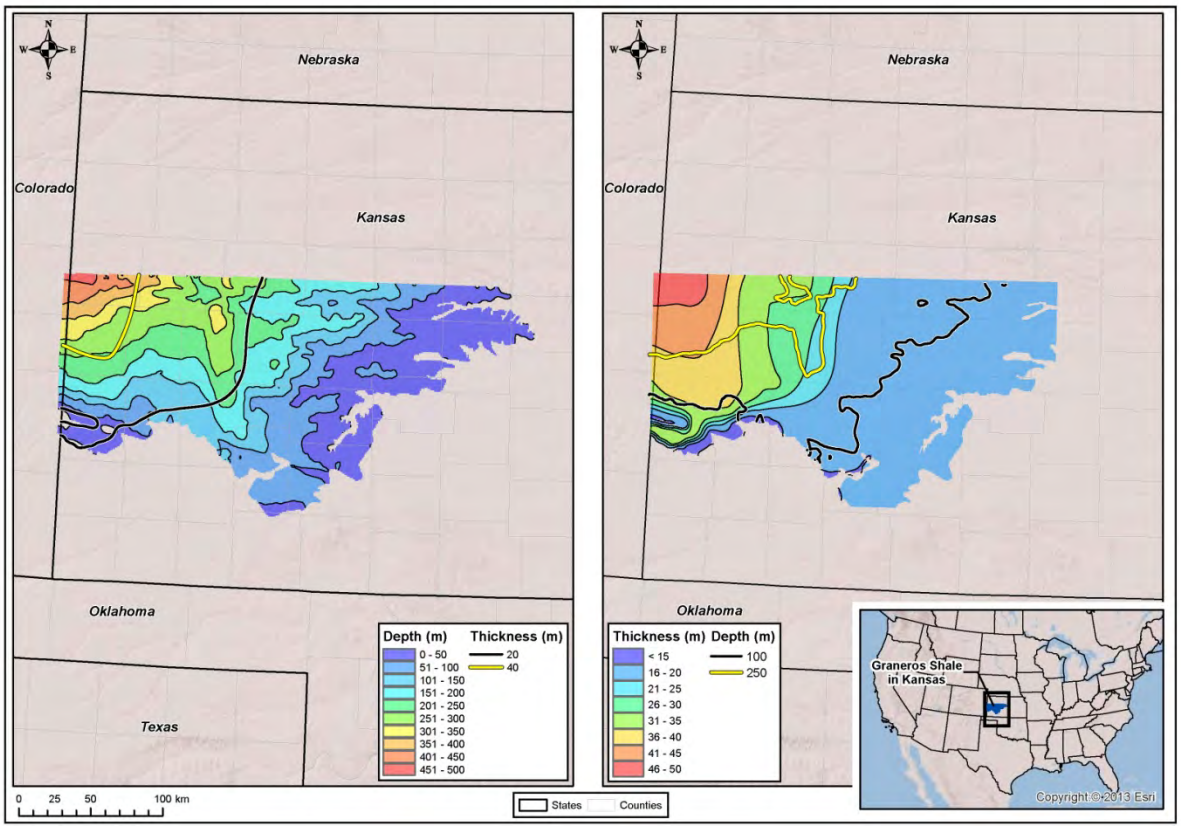

Figure 5-10. Depth and isopach maps of the Graneros Shale, Anadarko Basin. Figure produced by LANL from shale data populated into the GIS database.

Data on the Mississippian Fayetteville Shale and Devonian Chattanooga Shale reported by Ratchford et al. (2006) and Li et al. (2010) were used to construct structure and isopach maps for this unit in the Arkoma Basin in Arkansas (Figures 5-11 and 5-12). These studies also contain extensive geochemical data on the total organic carbon (TOC) and vitrinite reflectance of the shale in this basin.

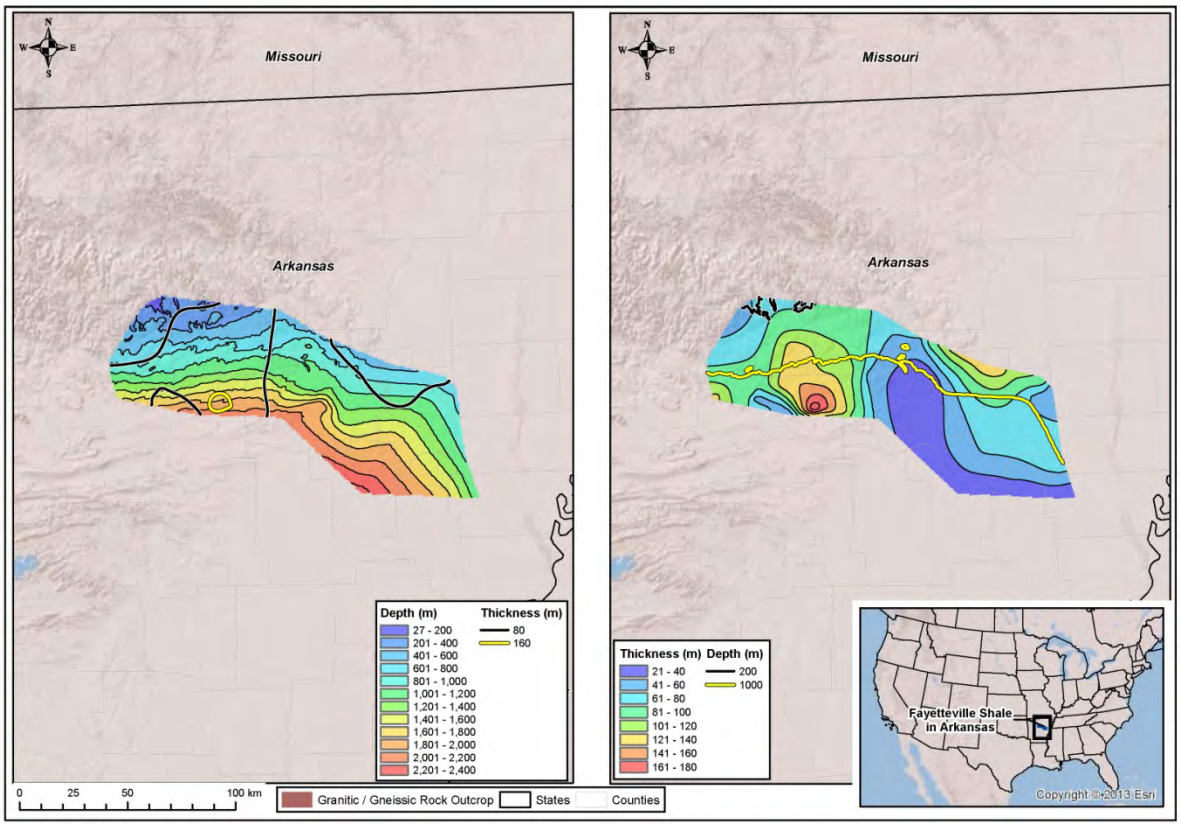

Figure 5-11. Depth and isopach maps of the Fayetteville Shale, Arkoma Basin. Figure produced by LANL from shale data populated into the GIS database.

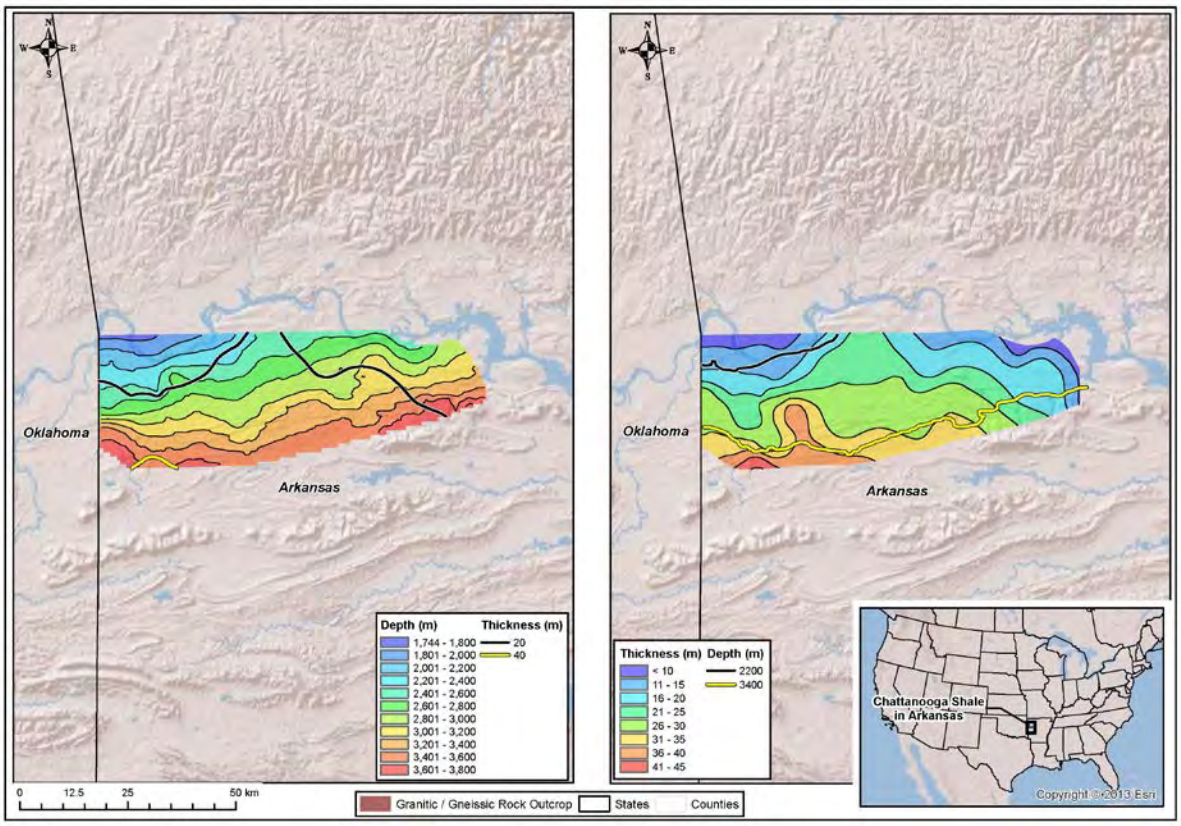

Figure 5-12. Depth and isopach maps of the Chattanooga Shale, Arkoma Basin. Figure produced by LANL from shale data populated into the GIS database.

The Upper Devonian/Lower Mississippian Woodford Shale (e.g., Amsden, 1975; 1980; Cardott and Lambert, 1985; Rottmann, 2000; Blackford, 2007; Party et al., 2008; Cardott, 2012) is a major shale gas play and hydrocarbon source rock in Oklahoma. Agrawal (2009) describes the depositional environment, mineralogy and TOC of the Woodford. GIS data for the Woodford Shale within the Anadarko and Arkoma Basins were generated from Amsden (1975; 1980) (Figure 5-13).

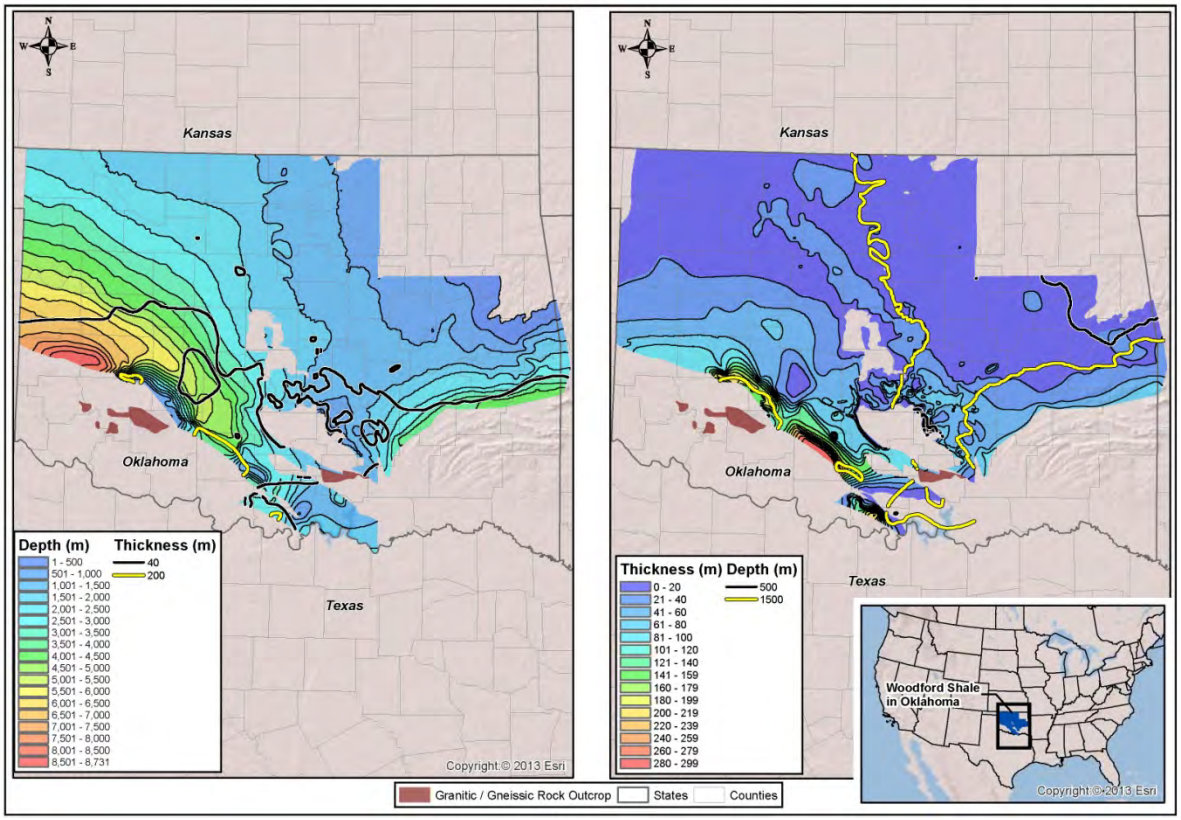

Figure 5-13. Depth and isopach maps of the Woodford Shale, Anadarko and Arkoma Basins. Figure produced by LANL from shale data populated into the GIS database.

5.2.3.6 Gulf of Mexico Basin

The Gulf of Mexico Basin contains extensive sedimentary accumulations both onshore and offshore, many of which host hydrocarbon deposits. Pitman (2008) generated a comprehensive GIS database of petroleum reservoirs and associated source rocks in Gulf of Mexico Basin, including delineation of the Upper Jurassic Smackover Formation, the Upper Cretaceous Eagle Ford Formation, and the Paleocene/Eocene Wilcox Formation. Hammes et al. (2011) presented a detailed description of the regional geology and stratigraphy of the Upper Jurassic Haynesville Shale, including isopach and structure maps of this important shale gas play unit; these maps were digitized to generate GIS data to create depth and isopach maps for this unit (Figure 5-14). Agrawal (2009) describes the depositional environment, mineralogy and TOC of the Haynesville. Surles (1987) constructed isopach maps for the entire Eagle Ford shale and its members, as well as compiled information on the amount of sand and organic matter. Harbor (2011) conducted a detailed study of the lithofacies and stratigraphy of the Eagle Ford Formation. GIS data obtained from the US EIA (EIA, 2010) was used to construct depth and isopach maps for the Eagle Ford Formation (Figure 5-15).

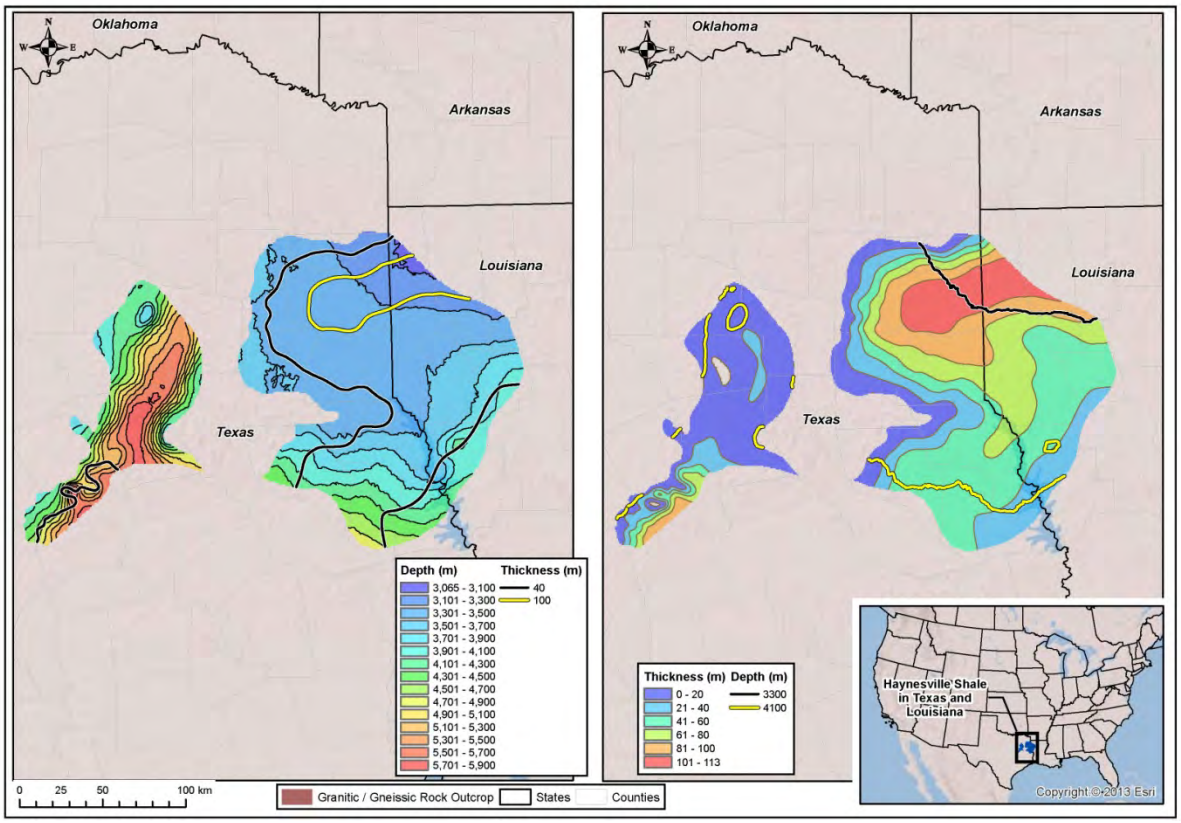

Figure 5-14. Depth and isopach maps of the Haynesville Shale, Gulf of Mexico Basin. Figure produced by LANL from shale data populated into the GIS database.

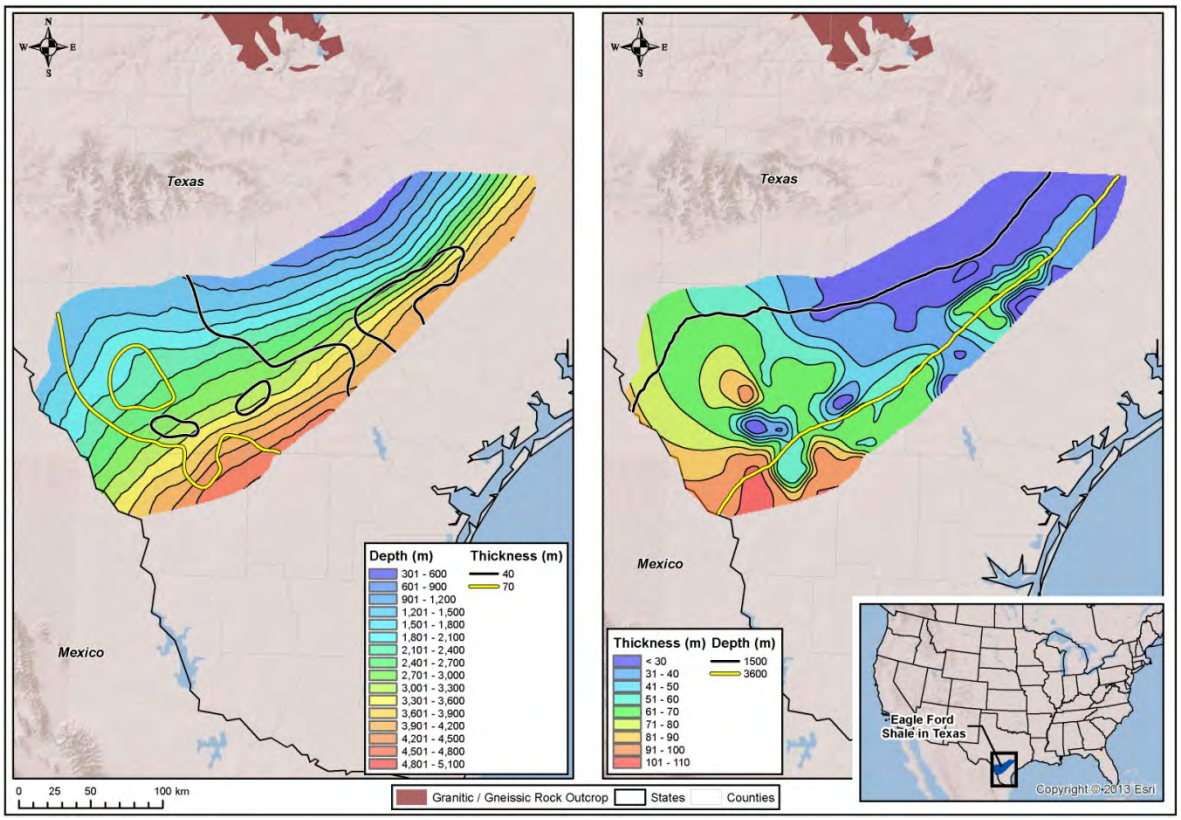

Figure 5-15. Depth and isopach maps of the Eagle Ford Formation, Gulf of Mexico Basin. Figure produced by LANL from shale data populated into the GIS database.

5.2.3.7 Fort Worth Basin

The Mississippian Barnett Shale is a major producer of shale gas in the Fort Worth Basin. Pollastro et al. (2007) conducted a detailed geologic study of this petroleum system, and generated isopach and structure maps for the Barnett Shale; these maps were digitized and integrated into the LANL GIS database (Figure 5-16). Agrawal (2009) describes the depositional environment, mineralogy and TOC of the Barnett.

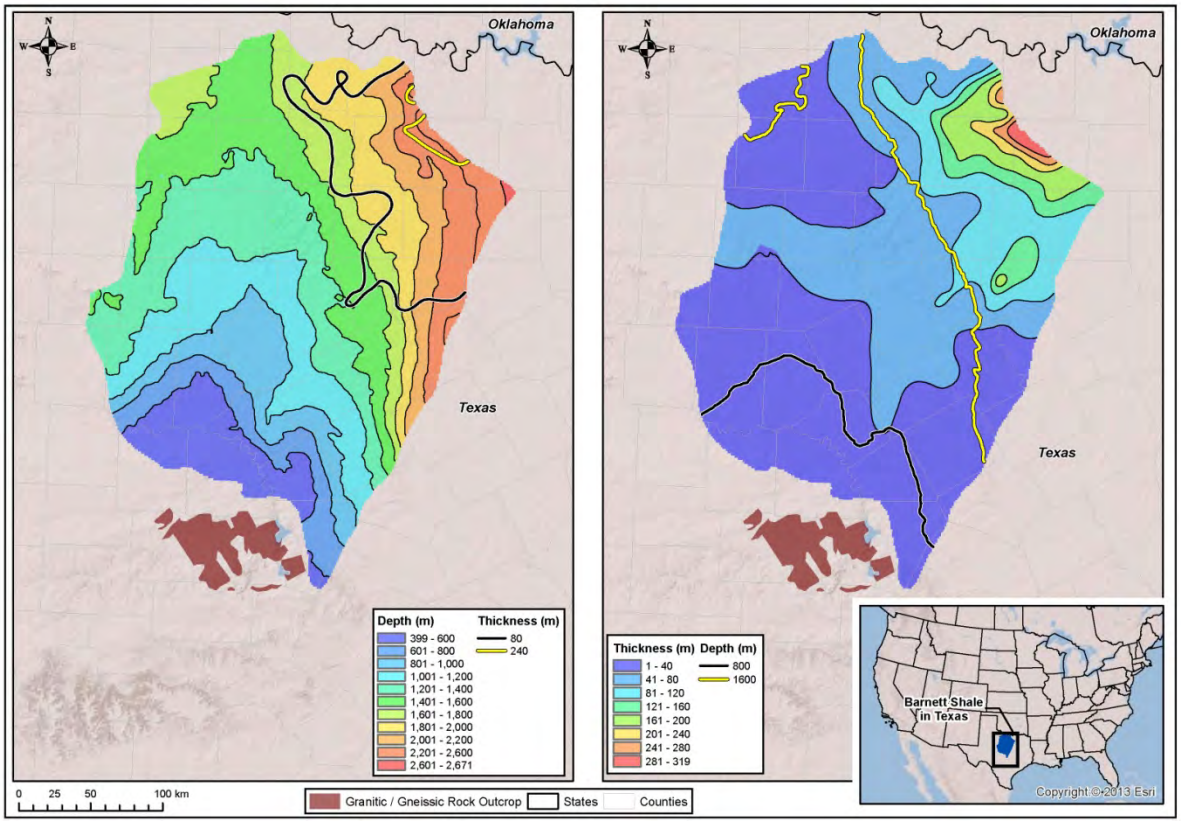

Figure 5-16. Depth and isopach maps of the Barnett Shale, Fort Worth Basin. Figure produced by LANL from shale data populated into the GIS database.

5.2.3.8 Permian Basin

While the Permian Basin is dominated by carbonate and evaporite sequences, it also hosts some siliciclastic units, such as the Woodford Shale. Broadhead (2010) conducted a detailed study of the distribution and source rock characteristics of the Woodford Shale located within the New Mexico portion of the Permian Basin. Structure and isopach maps for the Woodford Shale (Comer, 1991) were converted into GIS surfaces by Ruppel et al. (2005), and are depicted in Figure 5-17.

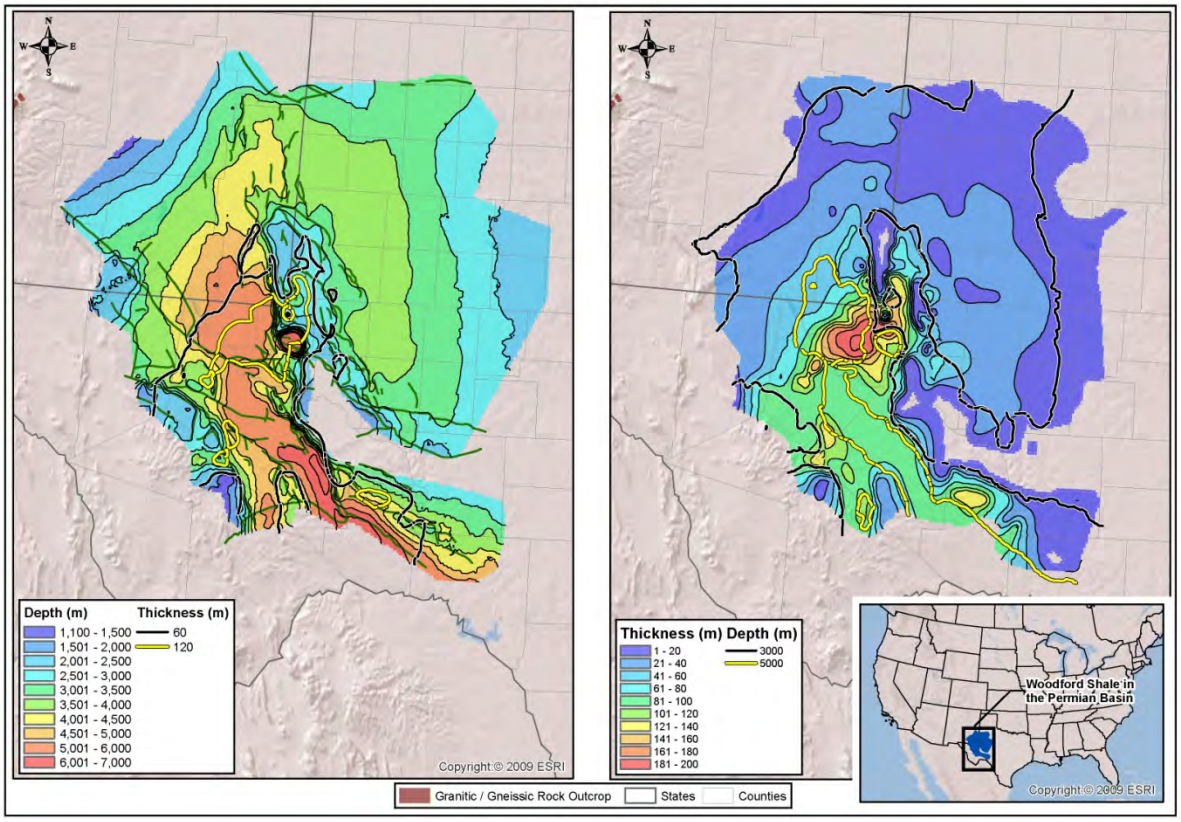

Figure 5-17. Depth and isopach maps of the Woodford Shale, Permian Basin. Figure produced by LANL from shale data populated into the GIS database.

Another major shale unit in the Permian Basin is the Mississippian Barnett Shale. Broadhead and Gillard (2007) provide detailed information on the stratigraphy, structure, and petroleum source rock characteristics, including TOC content and Rock-Eval pyrolysis data (to characterize the organic matter in the rock). Figure 5-18 depicts structural and isopach maps for the Barnett Shale in southeastern New Mexico (Broadhead and Gillard, 2007).

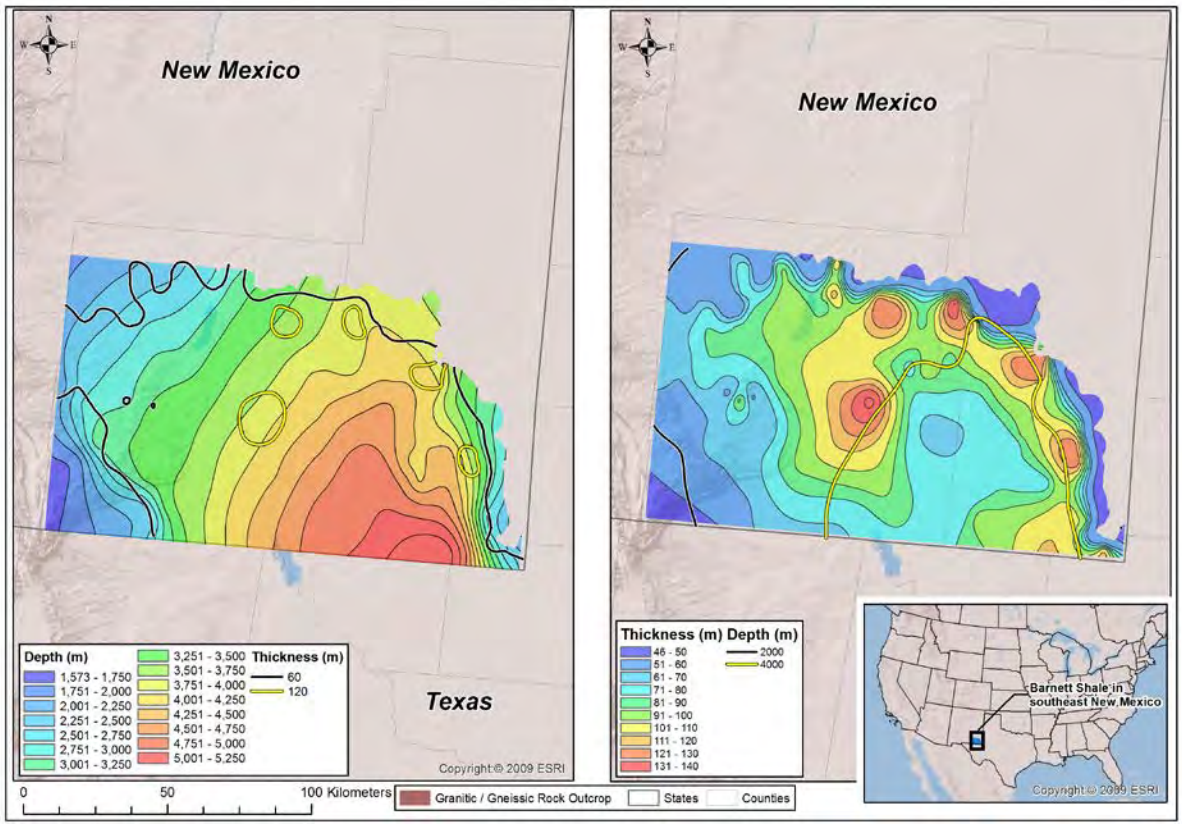

Figure 5-18. Depth and isopach maps of the Barnett Shale, Permian Basin. Figure produced by LANL from shale data populated into the GIS database.

5.2.3.9 Williston Basin

The Williston Basin is an intracratonic basin centered in North Dakota with sedimentary rocks consisting of carbonates, evaporites, sandstones, and shales. These rocks range in age from Precambrian to Tertiary (Gerhard et al., 1982). Shale-bearing units within the Paleozoic section include the Ordovician Ice Box Formation and the Mississippian Bakken and Otter Formations. The Bakken Formation has upper and lower shale members and a middle sandstone member (Pollastro et al., 2008) and contains significant (3.59 billion barrels) reserves of oil shale (EIA, 2011b). GIS data for the Bakken (Figure 5-19) are based on constraints provided by LeFever (2008) and LeFever et al. (2012).

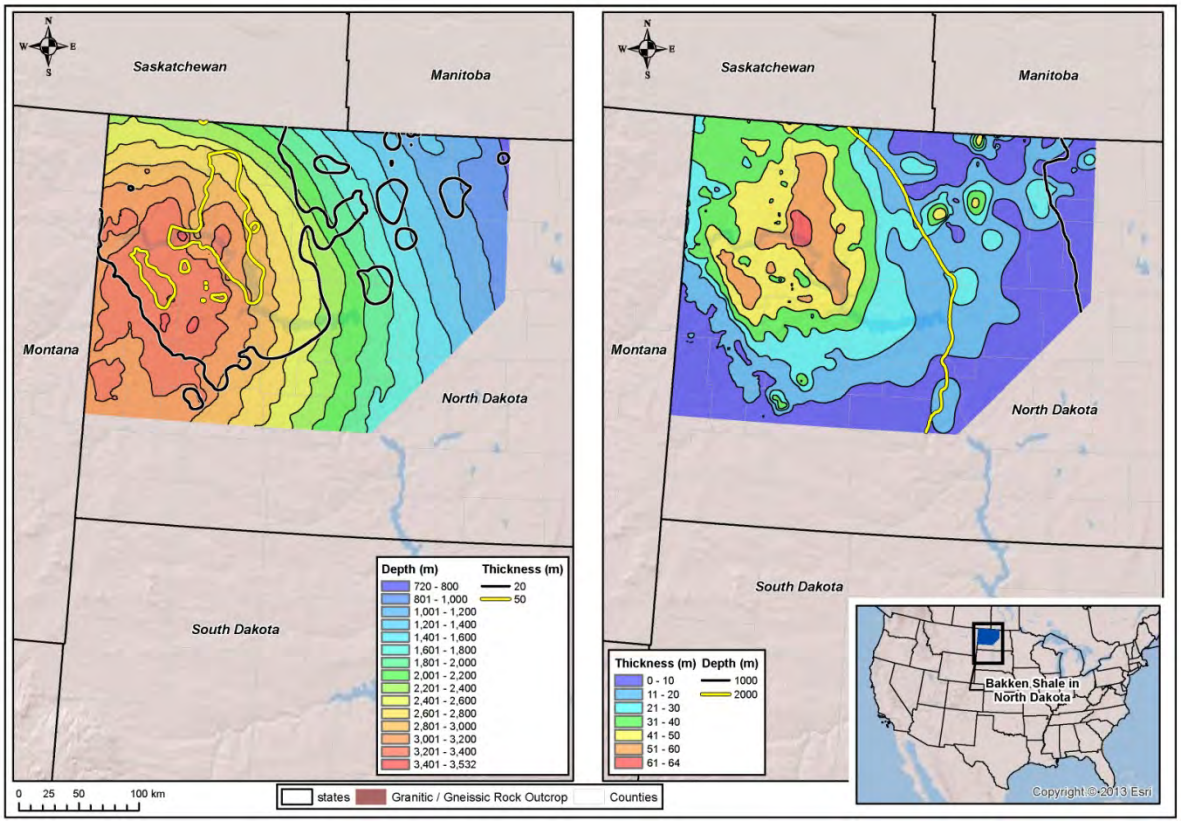

Figure 5-19. Depth and isopach maps of the Bakken Formation, Williston Basin. Figure produced by LANL from shale data populated into the GIS database.

The Williston Basin also contains a sequence of Cretaceous shales, including the Skull Creek, Mowry, Belle Fourche, Carlile, and Pierre (Bearpaw) Shales. There are a number of published isopach and structural maps of the Pierre Shale and its correlative unit, the Bearpaw, for this region (Shurr, 1977; Carlson, 1982; Smith, 1999; Condon, 2000); data from Condon (2000) for eastern Montana were used to generate GIS data for the Bearpaw (Figure 5-20).

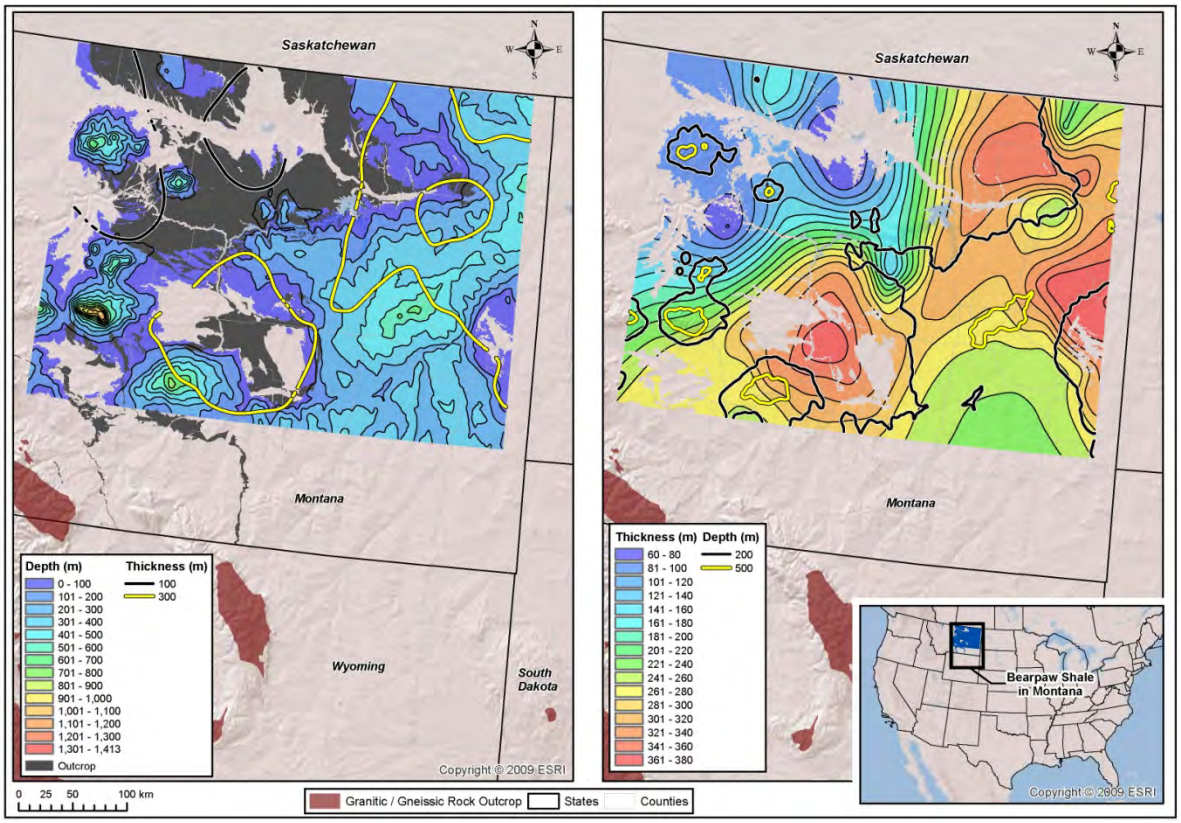

Figure 5-20. Depth and isopach maps of the Bearpaw Shale, Williston Basin. Figure produced by LANL from shale data populated into the GIS database.

5.2.3.10 Powder River Basin

The Powder River Basin contains a thick sequence of Paleozoic, Cretaceous, and Tertiary sediments (Anna, 2009), and is best known for its vast coal resources, consisting of thick deposits of subbituminous or lignite coal occurring at shallow depths. The Pierre Shale (Figure 5-21) forms part of the thick Cretaceous section of sediments (Denson et al., 1993a, b, c, d). As part of a hydrogeologic study of this basin, Lewis and Hotchkiss (1981) generated isopach and structure maps for the Lebo Shale member of the Paleocene Ft. Union Formation (Figure 5-22) and the Upper Hell Creek (or Lance) Formation, which is Upper Cretaceous in age.

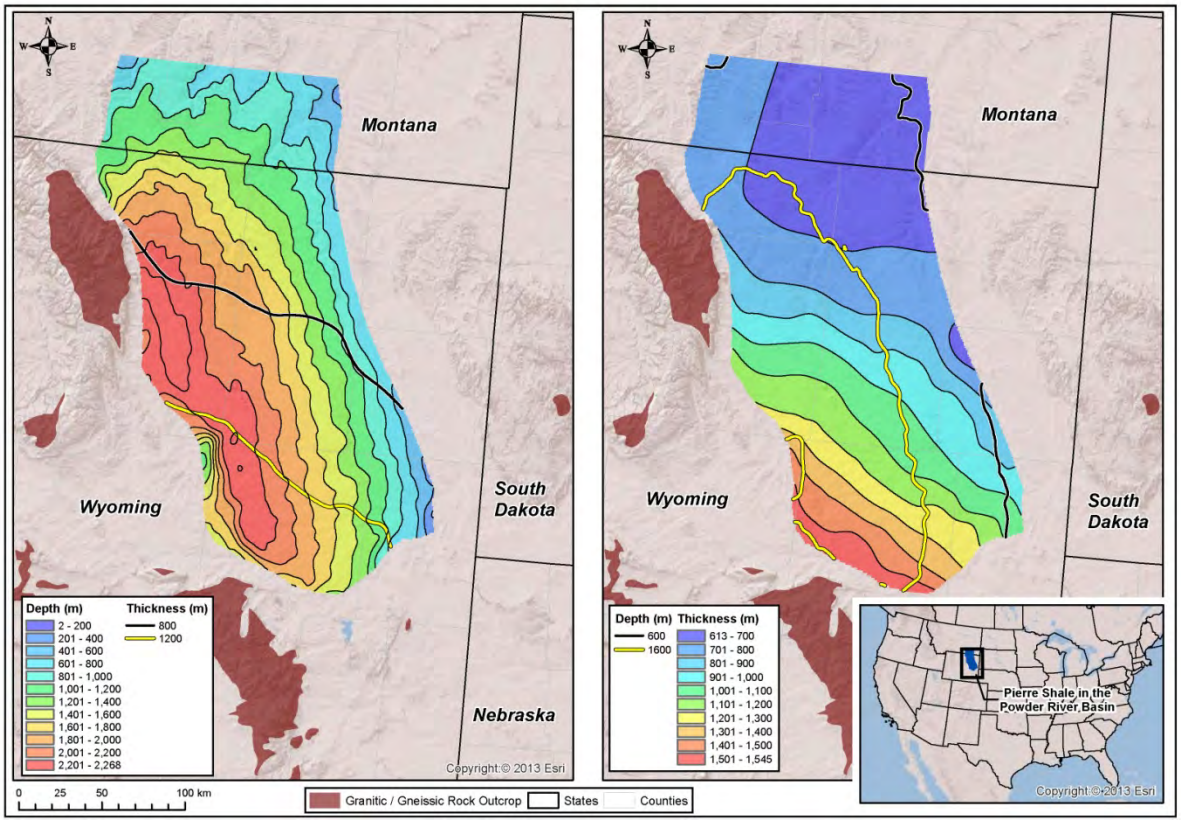

Figure 5-21. Depth and isopach maps of the Pierre Shale, Powder River Basin. Figure produced by LANL from shale data populated into the GIS database.

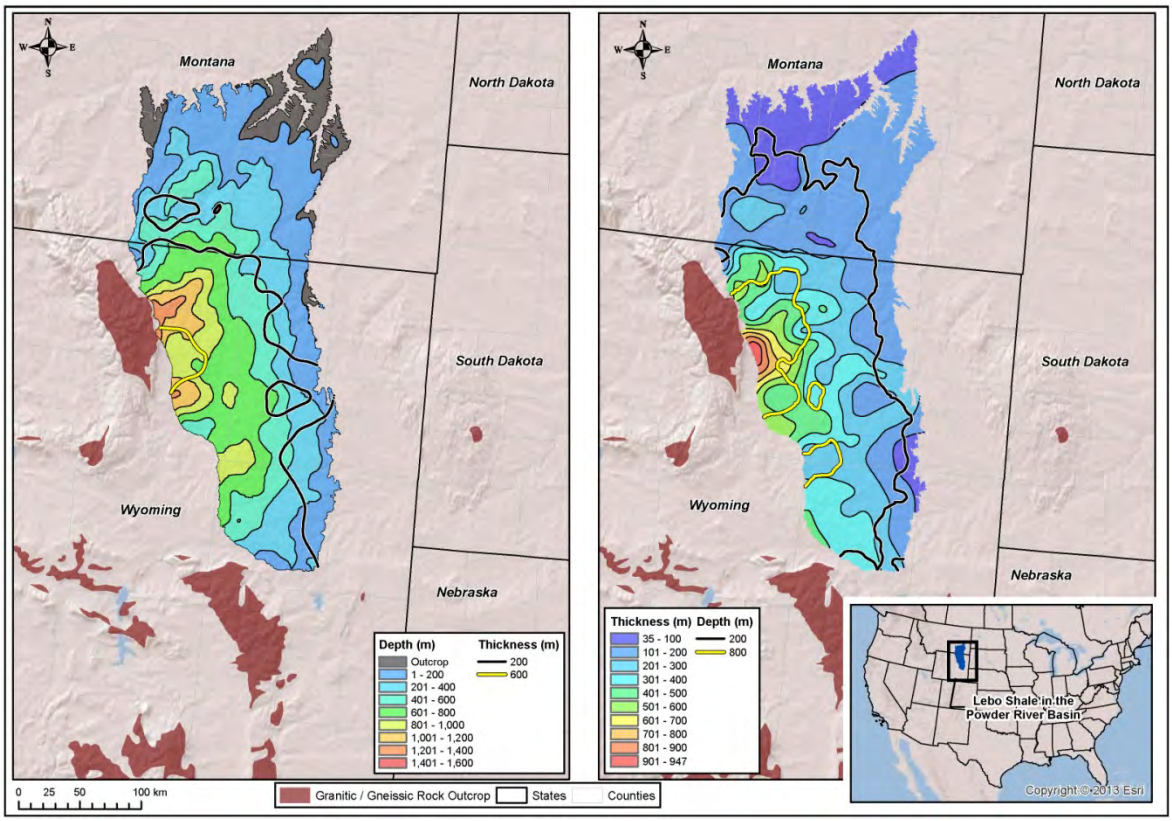

Figure 5-22. Depth and isopach maps of the Lebo Shale, Powder River Basin. Figure produced by LANL from shale data populated into the GIS database.

5.2.3.11 Denver Basin

The Denver Basin is a foreland structural basin bounded to the west by the Rocky Mountains. Most of the sediments in the basin are Cretaceous sandstones, shales, and carbonates (Higley and Cox, 2007); the shale units include the Skull Creek, Mowry, Graneros, Carlile, Niobrara (Smoky Hills Shale Member), and Pierre. The Pierre Shale is the most prominent of these units, and its distribution and thickness (Figure 5-23) has been characterized by Shurr (1977), who conducted an extensive study of this unit as a possible host for radioactive waste, and Dechesne et al. (2011).

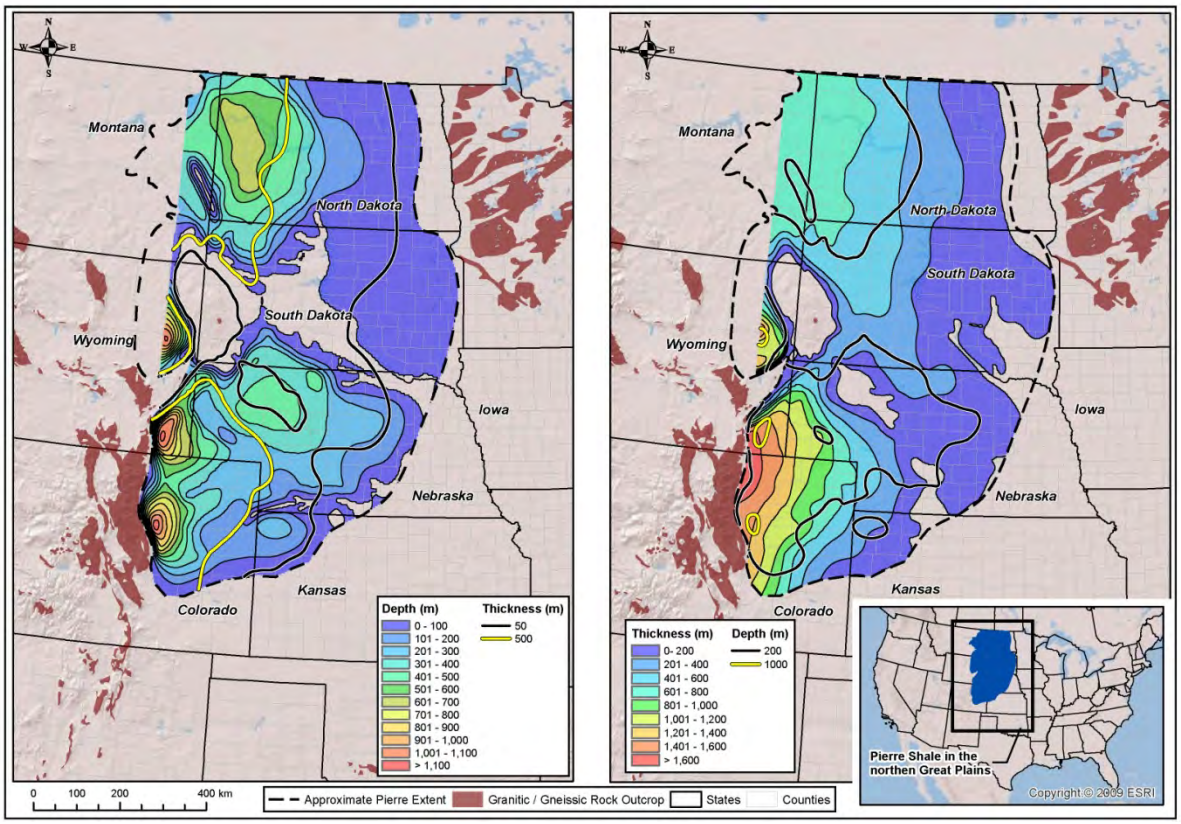

Figure 5-23. Depth and isopach maps of the Pierre Shale in the Williston and Denver Basins. Figure produced by LANL from shale data populated into the GIS database.

5.2.3.12 San Juan Basin

The San Juan Basin is located in southwestern Colorado and northwestern New Mexico. It contains a thick section of Jurassic and Cretaceous sands and shales, including the Upper Cretaceous Mancos Shale (Ridgley et al., 2013). This unit ranges in thickness from less than 30 m up to more than 600 m within the San Juan Basin, and is a source rock for hydrocarbon production in the basin. Isopach and structure maps from Ridgley et al. (2013) were used to develop GIS data for the Mancos in this basin (Figure 5-24).

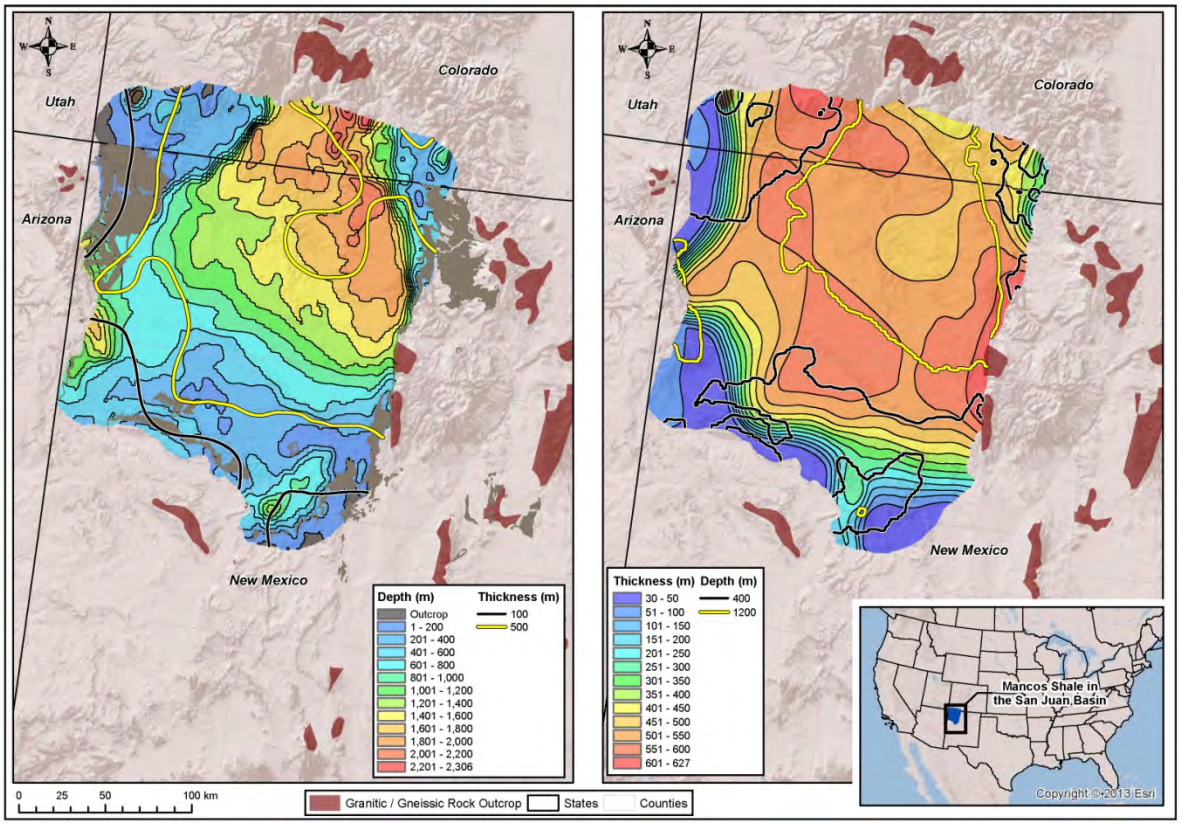

Figure 5-24. Depth and isopach maps of the Mancos Shale in the San Juan Basin. Figure produced by LANL from shale data populated into the GIS database.

5.2.3.13 Green River, Piceance, and Uinta Basins

The Greater Green River, Piceance, and Uinta Basins are located in Wyoming, Utah and Colorado. These basins contain major shale-bearing intervals (USGS Southwestern Wyoming Province Assessment Team, 2005; Dubiel, 2003; Johnson, 2003; Kirshbaum, 2003; USGS Uinta-Piceance Assessment Team, 2003; Johnson et al., 2010). The oldest of these units is the Permian Phosphoria Formation, which contains organic-rich mudstones. These basins also contain a number of shales that are Cretaceous in age, including the Baxter, Hillard, Steele, Lewis, Mancos and Mowry Shales. Present in all three of these basins is the Eocene Green River Formation, which contains the world's largest oil-shale deposit, with about 1.2 trillion barrels of oil in place (Dubiel, 2003). The Green River Formation consists of interbedded oil shales (such as the Parachute Creek Member), organic shales, evaporites, siltstones, sandstones, and mudstones. The Greater Green River Basin contains a number of sub-basins, including the Hoback Basin, the Green River Basin, the Great Divide Basin, the Washakie Basin, and the Sand Wash Basin (Self et al., 2011). The USGS has generated GIS data (Figure 5-25) that maps the thickness and structure of different members of the Green River Formation in these three basins as part of an oil shale resource assessment (Mercier et al., 2010a, b, c; Mercier and Johnson, 2012).

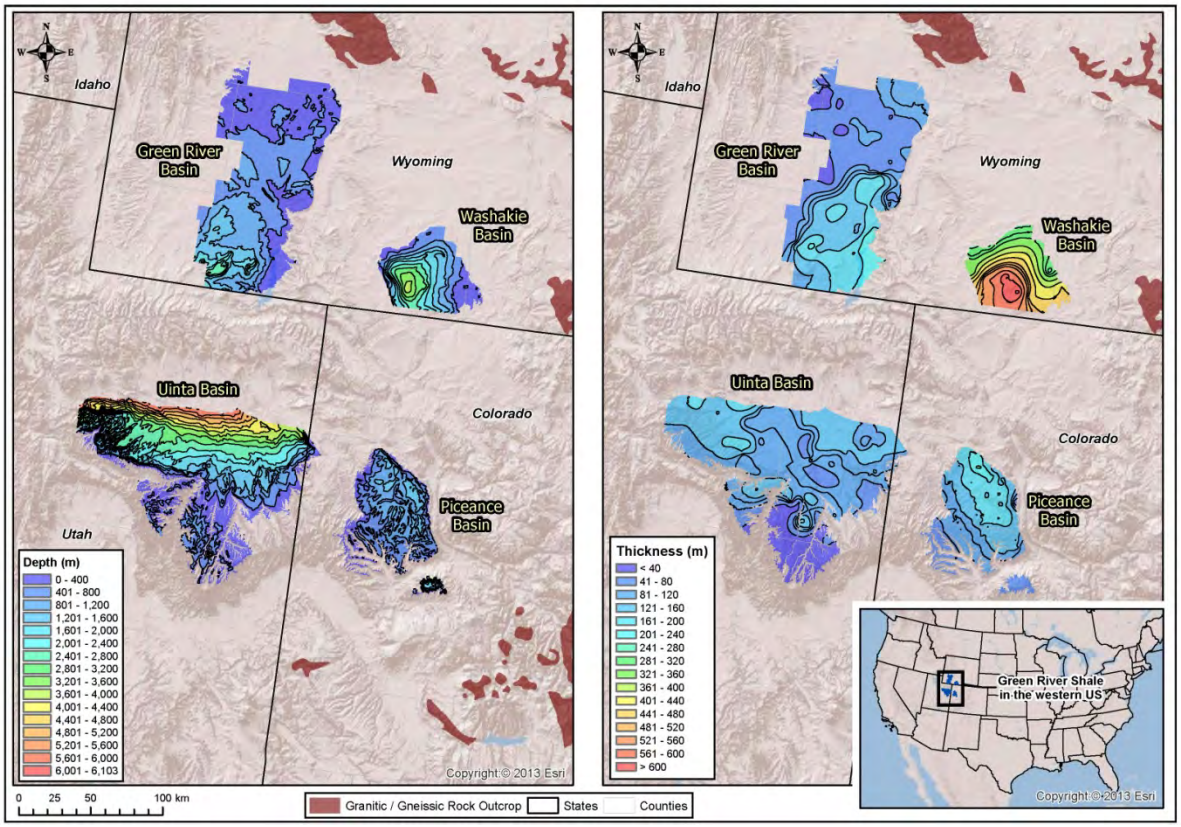

Figure 5-25. Depth and isopach maps of the Green River Shale in the Greater Green River, Uinta, and Piceance Basins. Figure produced by LANL from shale data populated into the GIS database.

5.2.3.14 San Joaquin, Santa Maria, and Cuyama Basins

There are a number of sedimentary basins in central and coastal California which contain thick sequences of siliciclastic rocks; these include the Los Angeles Basin, the San Joaquin Basin, the Ventura Basin, the Santa Maria Basin, and the Cuyama Basin. Most of these sediments are Tertiary in age. The two main

shale-rich sedimentary units (which serve as major hydrocarbon source rocks) in these basins are the Miocene Monterey Formation and the Eocene Kreyenhagen Formation (Magoon et al., 2009). The Monterey Formation has a wide variety of lithologies present (Williams, 1982), including diatomite, porcelanite, siliceous, organic-rich and clay shales, chert, dolomite, calcareous siliceous sediments, and siltstones. Sweetkind et al. (2010; 2013) created digital tabulations of stratigraphic well data for the Santa Maria and Cuyama Basins. Hosford Scheirer (2013) developed a 3-D basin model that includes isopach and structural surface maps of the Monterey Formation for the San Joaquin Basin (Figure 5-26).

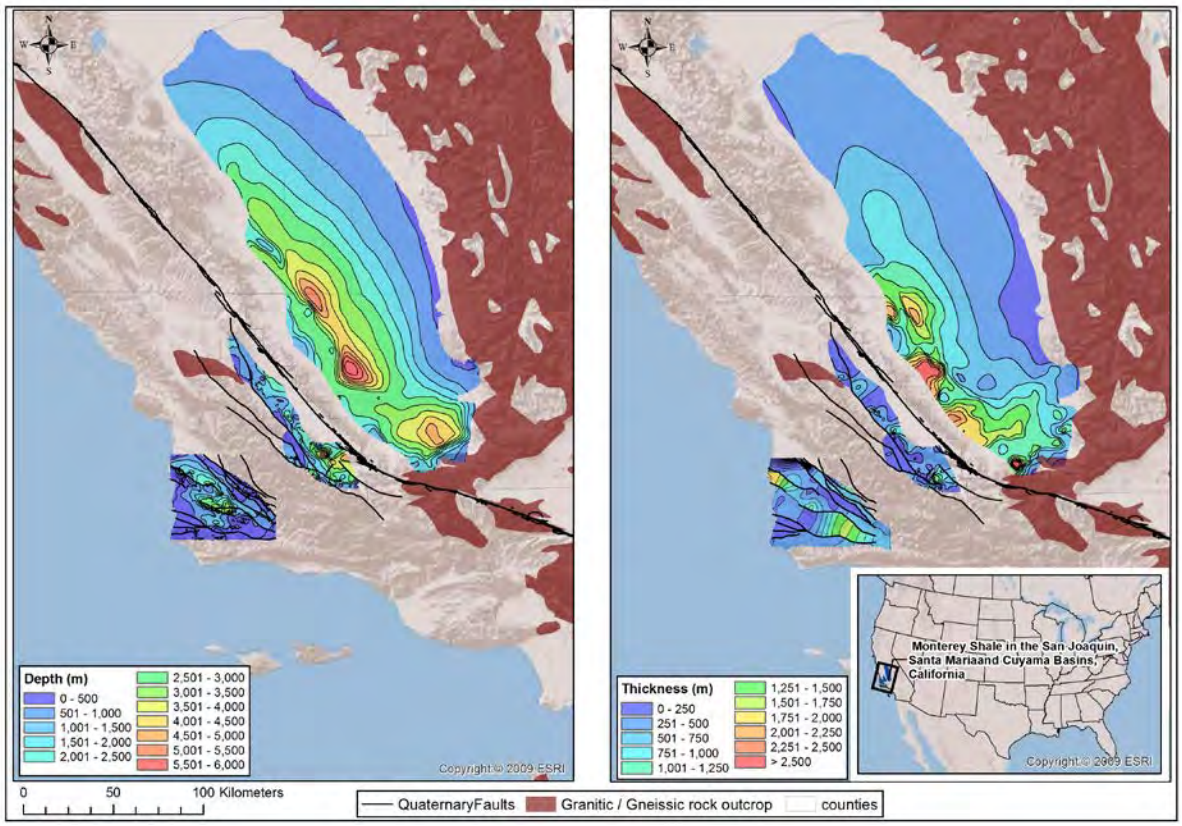

Figure 5-26. Depth and isopach maps of the Monterey Formation in the San Joaquin, Cuyama, and Santa Maria Basins. Figure produced by LANL from shale data populated into the GIS database.

5.2.4 TOTAL ORGANIC CARBON AND THERMAL MATURITY MAPS

The rock properties of shales can impact their viability as a rock barrier for the migration of radionuclides. In many shale sequences, the amount and thermal maturity of organic matter have been studied to determine their viability as potential source and reservoir rocks for the production of oil and gas. The thermal history of shales can also impact their rock properties, as burial diagenesis will result in sediment compaction and mineralogic changes. The integrated thermal history of sedimentary rocks can be evaluated using established techniques such as vitrinite reflectance and changes in conodont color.

Maps depicting lateral variations in total organic carbon (TOC) content and the thermal maturity of shale units were created for the following units as organized by sedimentary basin. Table 5-2 summarizes formations for which TOC and/or thermal maturity data (typically as vitrinite reflectance) have been obtained.

Table 5-2. Identified data sources for TOC and thermal maturity for shale formations within major sedimentary basins.

Appalachian Basin	
Utica Shale	**TOC data**: Engelder, 2011 (Figure 4.12); Patchen et al., 2006 (Figures 7-3, 7-4 & 7-5); Ohio Department of Natural Resources, 2013a **Thermal maturity data**: Repetski et al., 2008 (Figure 6); Patchen et al., 2006 (Figures 7-5 & 7-7); Ohio Department of Natural Resources, 2013b
Illinois Basin	
New Albany Shale	**Thermal maturity data**: Strapoc et al., 2010 (Figure 5); Mastalerz et al., 2013 (Figure 1)
Arkoma Basin	
Chattanooga Shale	**TOC and thermal maturity data:** Li et al., 2010 (Plate 2)
Fayetteville Shale	**TOC and thermal maturity data:** Ratchford et al., 2006 (Plate 23); Li et al., 2010 (Plate 1)
Fort Worth Basin	
Barnett Shale	**Thermal maturity data**: Pollastro et al., 2007 (Figure 12); Montgomery et al., 2005 (Figure 6); Zhao et al., 2007 (Figure 6)
Permian Basin	
Barnett Shale	**TOC and thermal maturity data:** Broadhead and Gillard, 2007 (Plates IX & X) (GIS data obtained from New Mexico Bureau of Geology and Mineral Resources)
San Joaquin Basin	
Monterey Formation	**Thermal maturity data:** Magoon et al., 2009 (Figures 8.9 & 8.14)

The compositions and rock properties of the Utica and Marcellus shales were studied in an analog assessment of their viability as a rock barrier for the migration of radionuclides as part of an evaluation of the proposed Ontario Power Generation Deep Geologic Repository at the Bruce site in Ontario for storage of low and intermediate radioactive waste (Engelder, 2011). High natural gas contents related to the burial and maturation of organic-rich shales can lead to the development of natural hydraulic fractures, which could compromise the integrity of the shales as fluid flow barriers. The Utica Shale has a total organic carbon (TOC) content that varies from 0.28 to 4.26 wt. % (Figure 5-27), with a median value just less than 2% (Ryder et al., 1998). In contrast, the Marcellus has TOC values that generally range from 2 to 12 wt. %, with values typically between 2 and 10% (Bruner and Smosna, 2011). Organic-rich black shales are often characterized by elevated gamma signatures. Agrawal (2009) describes the depositional environment, mineralogy and TOC of the Marcellus.

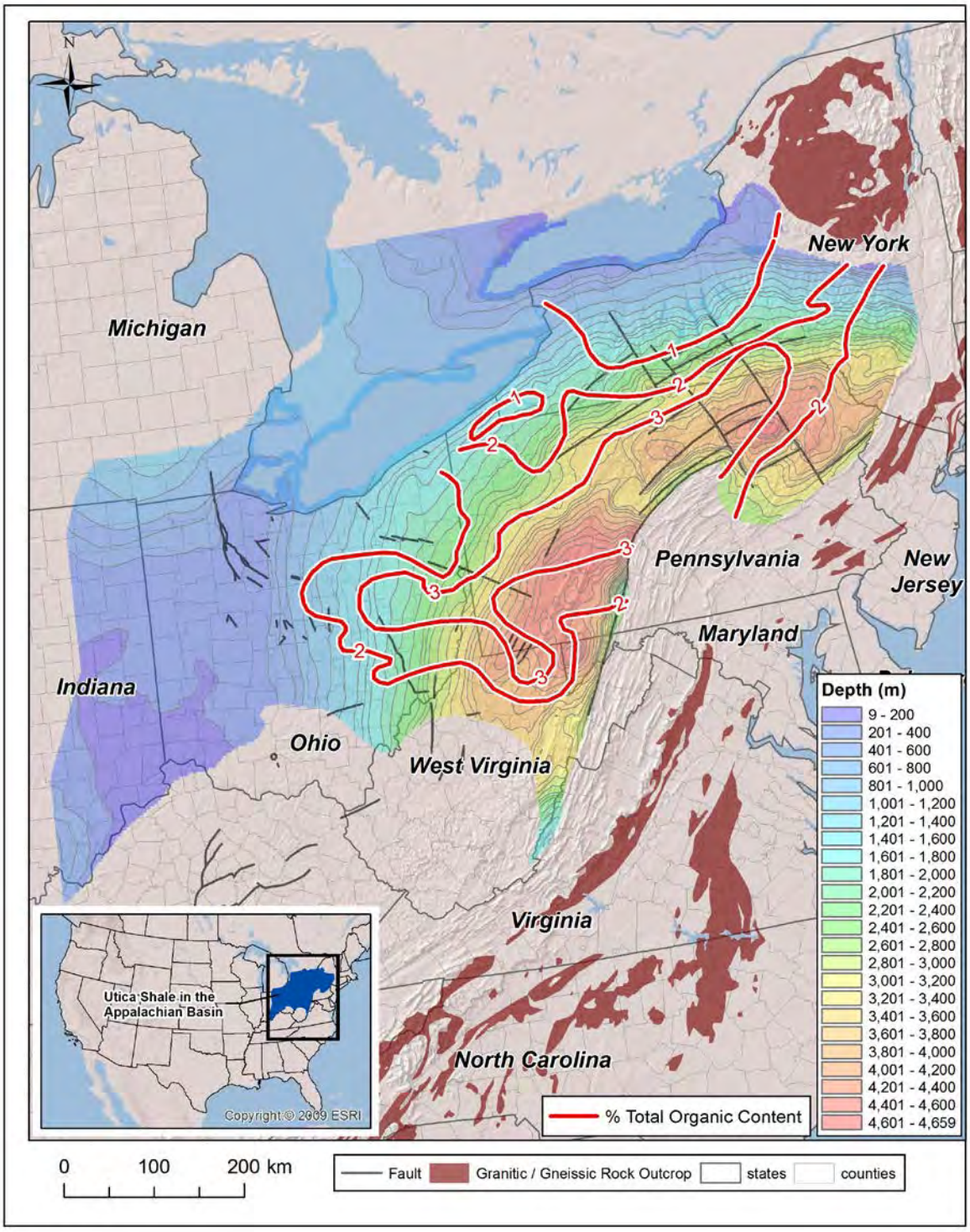

Figure 5-27. Variation in total organic carbon in the Utica Shale, Appalachian Basin. Figure produced by LANL from shale data populated into the GIS database.

Vitrinite reflectance data were used to create thermal maturity maps for the New Albany Shale in the Illinois Basin (Fig. 5-28), the Fayetteville Shale in the Arkoma Basin (Fig. 5-29) (this also has TOC data),

the Barnett Shale in the Fort Worth Basin (Fig. 5-30), and the Monterey Formation in the San Joaquin Basin (Fig. 5-31). As expected, deeper portions of the basins typically have higher % vitrinite reflectance.

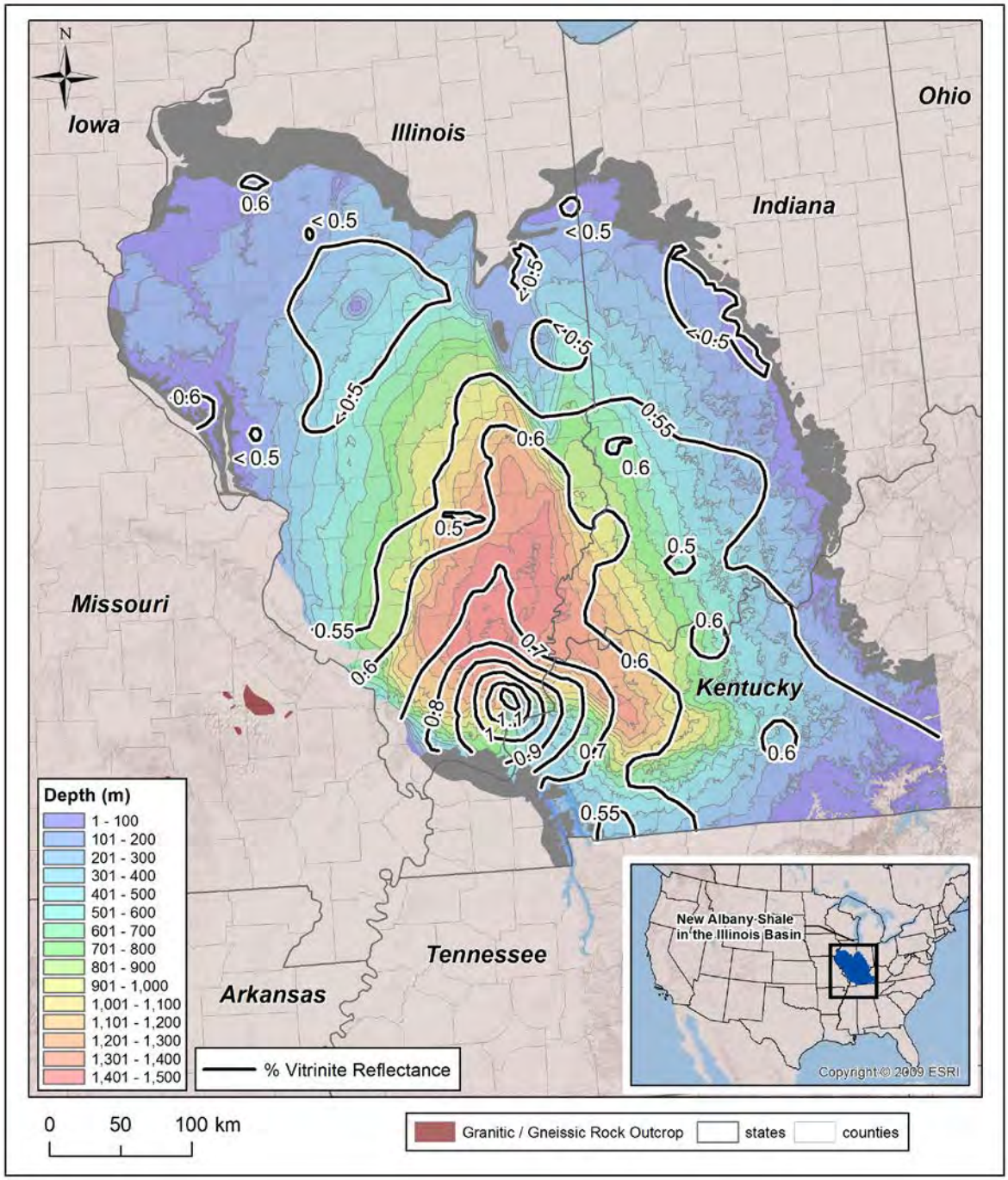

Figure 5-28. Variation in percent vitrinite reflectance in the New Albany Shale, Illinois Basin. Figure produced by LANL from shale data populated into the GIS database.

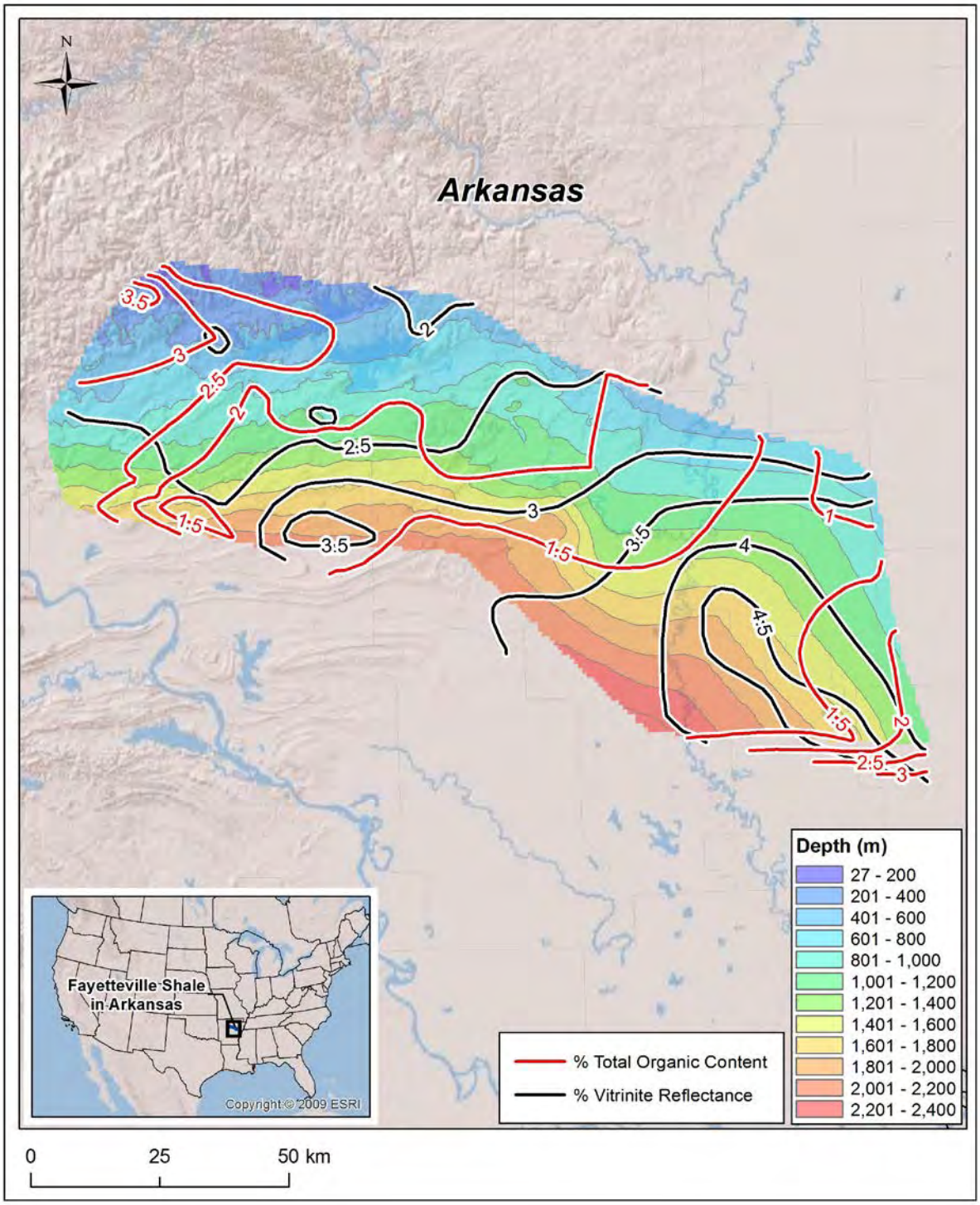

Figure 5-29. Variation in total organic carbon and percent vitrinite reflectance in the Fayetteville Shale, Arkoma Basin. Figure produced by LANL from shale data populated into the GIS database.

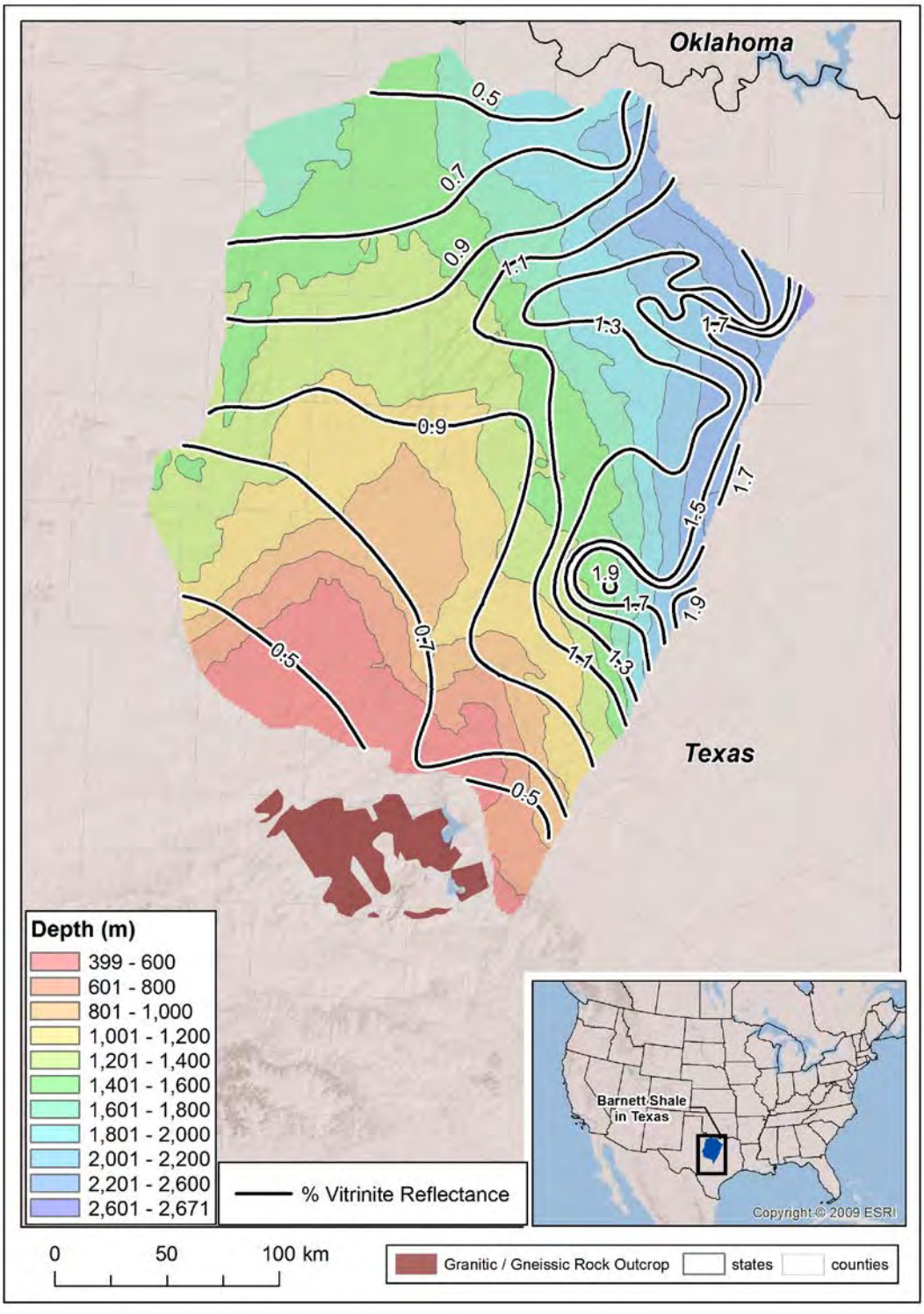

Figure 5-30. Variation in percent vitrinite reflectance in the Barnett Shale, Fort Worth Basin. Figure produced by LANL from shale data populated into the GIS database.

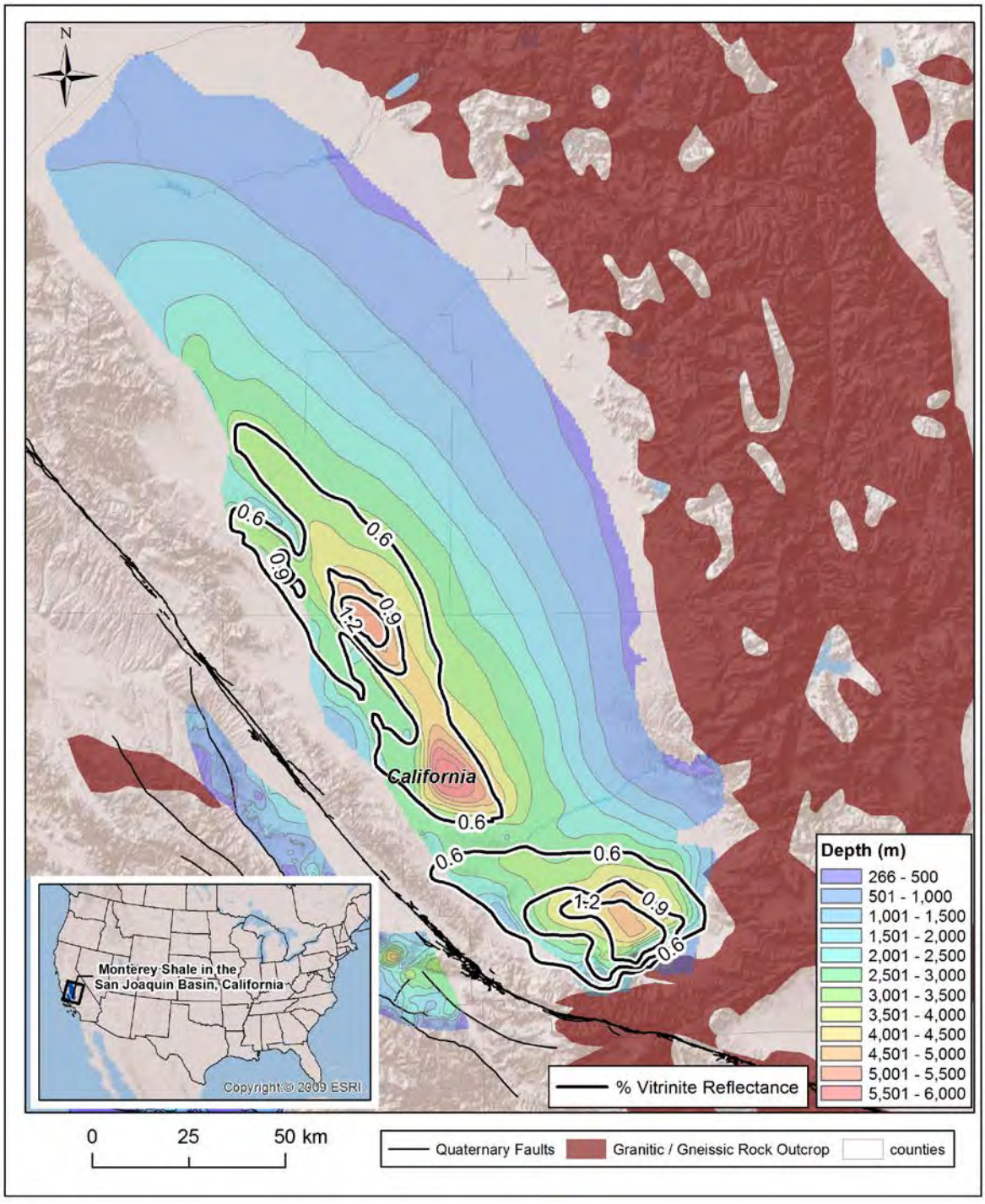

Figure 5-31. Variation in percent vitrinite reflectance in the Monterey Formation, San Joaquin Basin. Figure produced by LANL from shale data populated into the GIS database.

Total organic carbon data were also utilized to create a map for the Barnett Shale in the Permian Basin of SE New Mexico (Fig. 5-32).

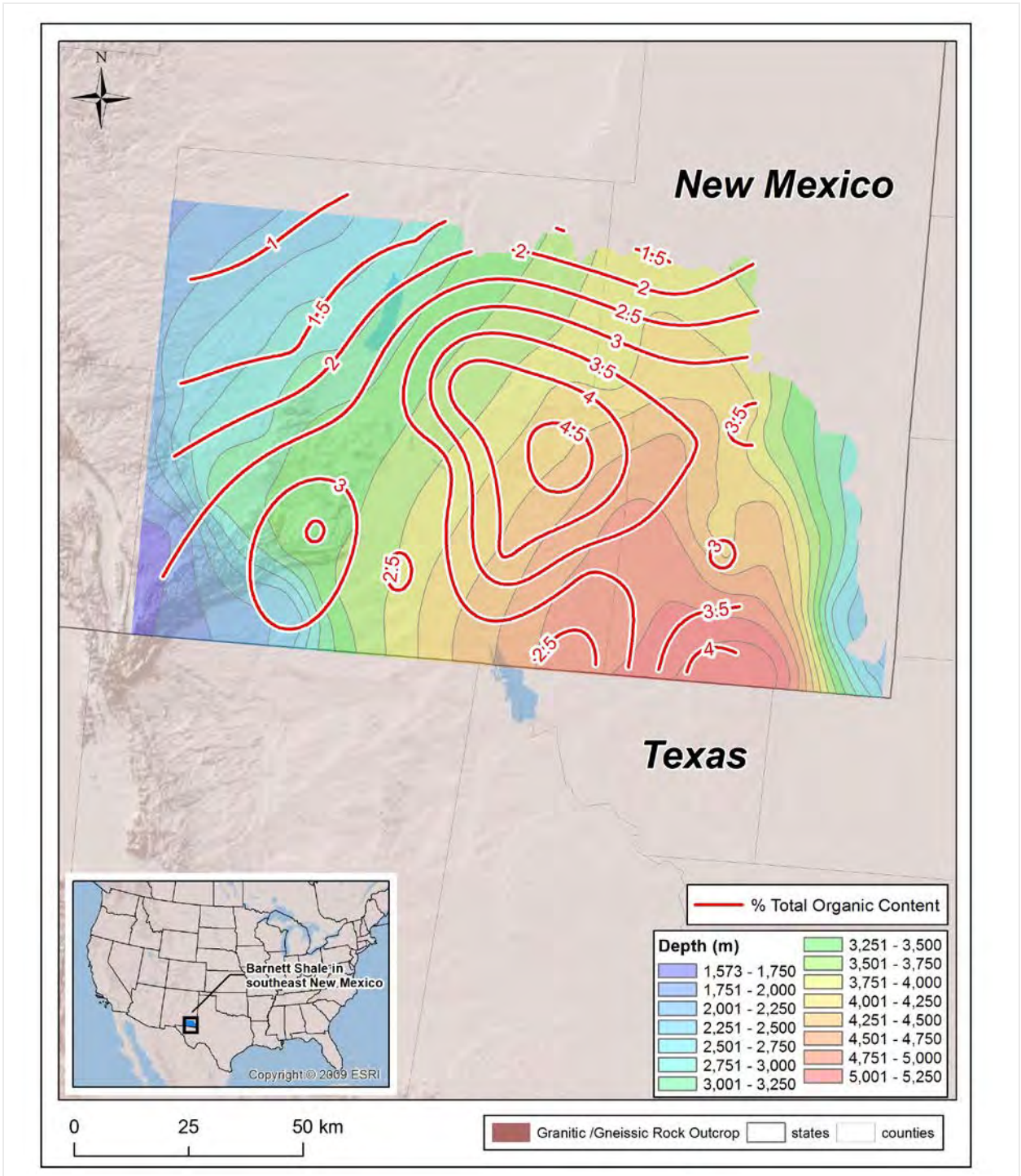

Figure 5-32. Variation in total organic carbon in the Barnett Shale, Permian Basin. Figure produced by LANL from shale data populated into the GIS database.

5.2.5 CONCLUSIONS OF SECTION 5

This report serves as an update relating to the progress of obtaining shale formation extent, thickness and depth data for the LANL geologic database. GIS data have been obtained for many shale formations associated with unconventional shale oil and gas deposits, such as the Marcellus, Utica, Barnett, New Albany, Antrim, Haynesville and Woodford Shales and the Bakken, Eagle Ford, Monterey, and Green River Formations; Figure 5-33 summarizes the shale formations that have been incorporated into the LANL database. Additional GIS data are in the process of being generated through the digitization of published isopach and structure maps. Continued efforts are being made to obtain additional GIS and map data for other shale formations that can be used to augment the GIS database. Associated rock property data such as total organic carbon and thermal maturity data are also being collected and integrated into the GIS database.

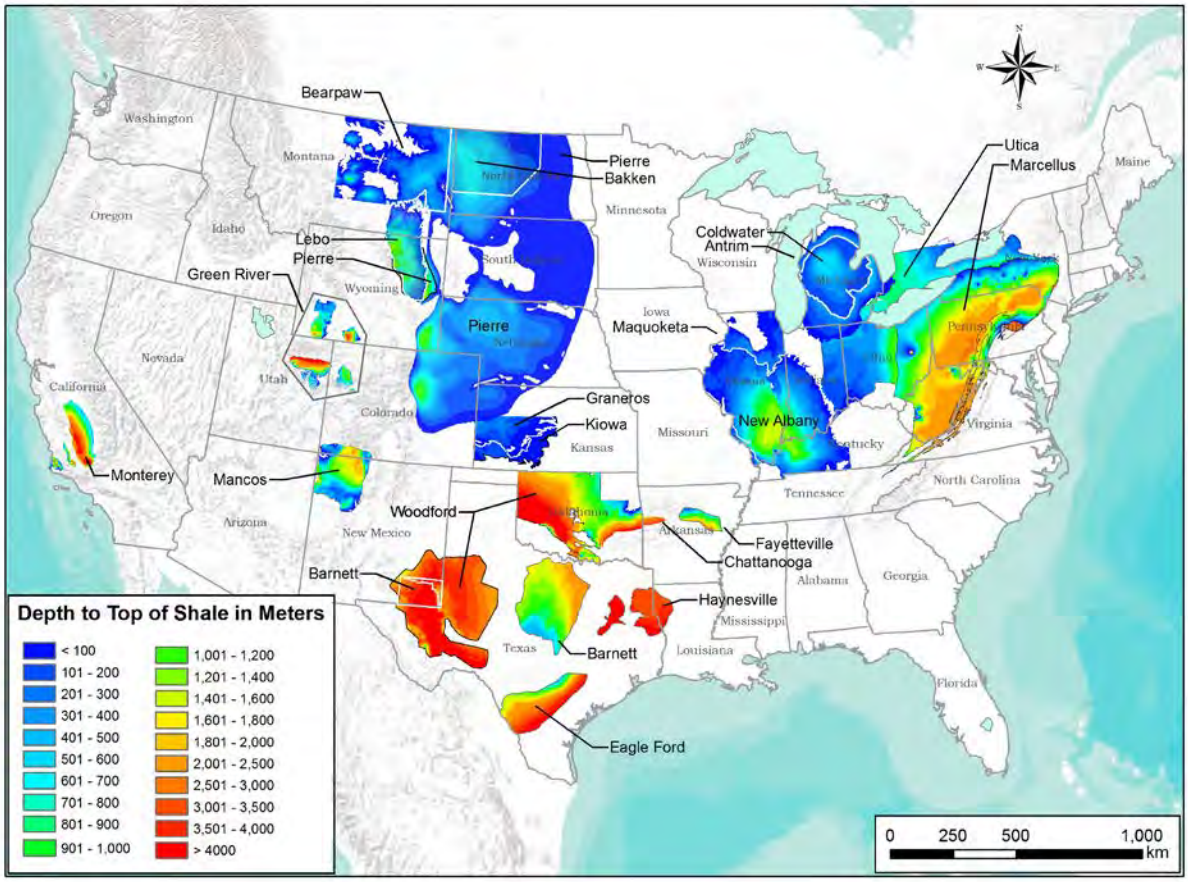

Figure 5-33. Summary of GIS data for depth to top of shale formations within major sedimentary basins in the US currently incorporated in the LANL GIS database. Figure produced by LANL from shale data populated into the GIS database.

6. Rock Properties and In-Situ Conditions for Shale Estimated from Sonic Velocity Measurements

The information in this section is reproduced from Dobson and Houseworth (2014). Previous work on this topic is presented in Section 5 of Appendix A.

6.1 Introduction and Recap of Previous Work

Shale is a sedimentary rock type that is being considered for geologic disposal of high-level radioactive waste. The regional geology task within the UFDC has been tasked to identify shale formations within the United States that should be evaluated as potential "host" formations for this waste disposal activity. Identification and evaluation of shale formations includes description of the formation geometric characteristics (area, depth, and thickness) as well as relevant physical characteristics. Physical characteristics can be measured directly using in-situ measurement methods or on rock samples (core or in some cases drill cuttings) taken during drilling of boreholes into the formation. Although such direct measurements are the most accurate was to determine physical characteristics, they are likely to be prohibitively expensive for initial assessments of possibly numerous shale formations that might need to be evaluated. The alternative pursued here is to estimate various physical characteristics of the formation based on correlations with the compressional (or sonic) velocity of the rock. The advantage of this approach is that sonic velocity is a standard geophysical log that is routinely performed on boreholes and as such is more readily available than direct in-situ or core measurements of properties. If an existing log is not available, it is possible to conduct a log measurement if an existing borehole is available. This can typically be done for less cost than direct in-situ measurements (if such measurements are even possible) or sampling and laboratory measurements on core. Furthermore, a sonic log provides a continuous measure of sonic velocities along the borehole which can be used to evaluate heterogeneities in the formation.

The sonic velocity is used because of the range of properties that have already been identified by other researchers as having a robust correlation with sonic velocity (e.g., porosity, Young's modulus, shear modulus, uniaxial compressive strength) for shale lithologies (Ingram and Urai, 1999; Horsrud, 2001). In a previous report (Dobson and Houseworth, 2013), these correlations were expanded based on additional data available from European investigations of nuclear waste disposal in shale lithologies. Additional correlations with sonic velocity were also developed for bulk density, clay content, Poisson's ratio, cohesive strength, friction angle, and tensile strength. A published correlation relating porosity, clay content, and permeability for mudrock (Yang and Aplin, 2010) was used in combination with the porosity and clay content correlations with sonic velocity to allow estimation of permeability from sonic velocity. The correlation is valid over a wide range of clay content (mass fraction of sub 2 micron particulates), from 12% to 97%, and porosity from 0.04 to 0.78. Similarly, an additional published correlation relating porosity, clay content, and maximum effective stress (Yang and Aplin, 2004) was used in combination with published correlations relating sonic velocity, uniaxial compressive strength and brittleness index (BRI), and the brittleness index with the overconsolidation ratio, to allow an estimate of in-situ pore pressure based on the sonic velocity.

Anisotropic behavior is common for shale and mudrock and is usually found to be a particular type of anisotropy known as *transversely isotropic*. This type of anisotropy is caused by the bedding structure of shales and mudrock. It means that potentially directionally sensitive property values are isotropic for any orientation restricted to be parallel to the bedding plane, but display anisotropy normal to the bedding plane. Anisotropic effects for some of the properties known to be directional such as permeability and Young's modulus were also estimated based on measurements (or estimates) of sonic velocity anisotropy. This was done by using a scaling factor equal to the ratio of sonic velocities parallel and normal to bedding raised to a power (determined empirically). The property value normal to bedding was multiplied

by this scaling factor, A, to obtain a property value parallel to bedding. The anisotropy scaling factor is given by $A = \left(V_{pp}/V_{pn}\right)^{\omega}$, where V_{pn} is the sonic velocity normal to bedding, V_{pp} is the sonic velocity parallel to bedding, and ω is an empirical anisotropy coefficient. To be consistent for properties that do not show directional behavior, the correlations with sonic velocity were conducted using the geometric mean sonic velocity, $V_{pm} = \sqrt{V_{pn}V_{pp}}$, where V_{pn} is the sonic velocity normal to bedding and V_{pp} is the sonic velocity parallel to bedding. Anisotropic property correlations were established by correlating the property normal to bedding with V_{pm}. Then, the property parallel to bedding was established by scaling the same correlation by the anisotropy factor, A.

The correlation between clay content and sonic velocity presented in Dobson and Houseworth (2013) showed a bit more scatter than most of the correlations, which lead to the question as to whether or not it is reasonable to expect a correlation between sonic velocity and clay content. Some additional literature on this subject has been reviewed in Section 6.2 and supports the use of such a correlation. Data that allows the investigation of a correlation between the sonic velocity and thermal properties, i.e., thermal conductivity and specific heat, have been analyzed and correlations have been developed that provide a means to estimate these properties sonic velocities. Additional published correlations that link permeability and air entry pressure along with a correlation between air entry pressure and the van Genuchten capillary strength parameter (α) allow a linkage between sonic velocity and α. An additional relationship from the literature between the air entry pressure and the van Genuchten pore-size-distribution index (m) permits the evaluation of this parameter from the sonic velocity. From these, capillary pressure and relative permeability parameter functions of saturation can be computed.

6.2 Estimating clay content

The clay content of shales was empirically correlated with the geometric mean sonic velocity in Dobson and Houseworth (2013). The clay content is defined as the clay mineral mass fraction. Several authors have reported on the correlation of sonic velocity, porosity, and clay content for more general sandstone rock types with widely varying clay content (Tosaya and Nur, 1982; Kowallis et al., 1984; Castanaga et al., 1985, Han et al., 1986).

Tosaya and Nur present data for sonic velocity, porosity, and clay content. In their data, porosity ranges from 4 to 20 percent and the volume fraction of clay content ranges from 0 to 72 percent. These data are correlated to give the following:

$$V_p = -2.4C - 8.6\phi + 5.8C_v \qquad (6\text{-}1)$$

where V_p is the sonic velocity in km/s, C_v is the volume fraction clay content, and ϕ is the fractional porosity. The relationship indicates the general expected trend of reduced sonic velocities with increased porosity or clay content, with greater sensitivity to changes in porosity, as found by Dobson and Houseworth (2013). Tosaya and Nur (1982) data, shown in Figure 6-1, span different rock types (sandstones, siltstones, and shales) that contain different types of clay (illite, kaolinite, mixed-layer illite-montmorillonite, and illite-chlorite). However, the correlation did not appear to be sensitive to differences in clay mineralogy. Furthermore, the spatial distribution of clay within the samples, observed to vary between pores (authigenic clay) and grain contacts (allogenic clay) did not impact the correlation.

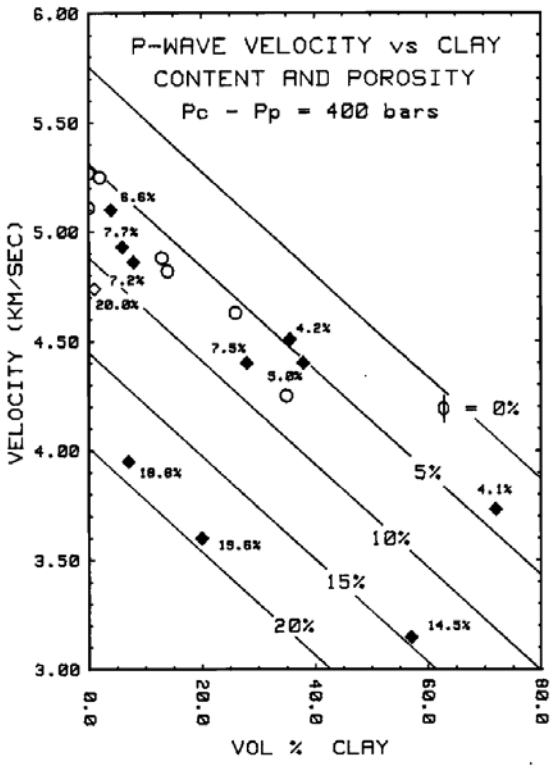

Figure 6-1. Compressional velocity as a function of clay content and porosity at a confining stress of 800 bars and a pore pressure of 400 bars, Tosaya and Nur (1982).

The work of Tosaya and Nur (1982) was extended by Kowallis et al. (1984) to include additional samples that ranged up to 29 percent porosity. A similar linear correlation between sonic velocity, clay content, and porosity was found.

Castanaga et al. (1985) developed correlations for sonic velocity, clay content, and porosity and for shear velocity, clay content, and porosity. Their data also spans sandstones, siltstones, and shales as does Toyasa and Nur (1982), but contain a much larger number of samples. An analysis of the mudrock (shale) samples revealed a unique linear relationship between the sonic (V_p) and shear (V_s) velocities,

$$V_p = 1.16V_s + 1{,}360 \qquad (6\text{-}2)$$

where both velocities are in m/s. The data and correlation line from Castanaga et al., (1985) are shown in Figure 6-2.

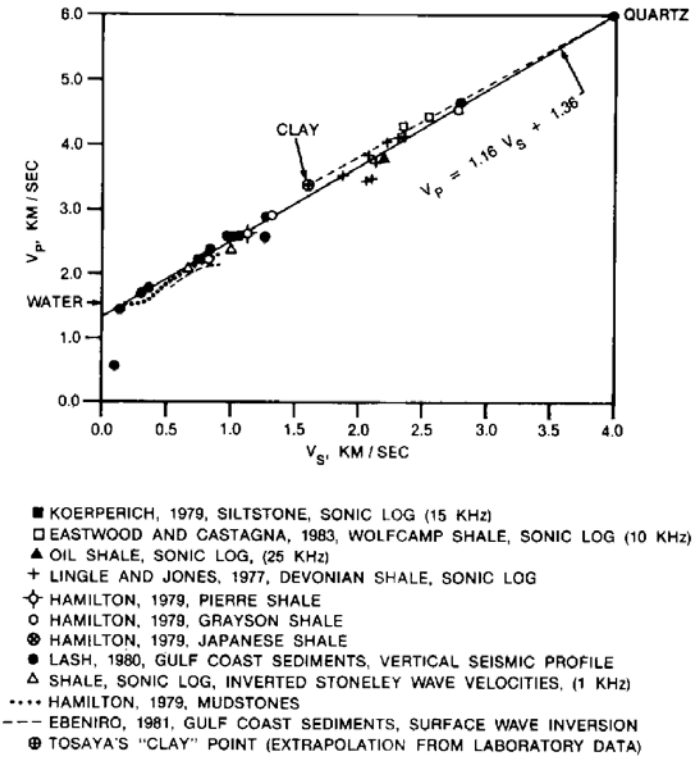

Figure 6-2. In-situ and seismic measurements of sonic and shear wave velocities in mudrocks (Castanaga et al. (1985). Source data listed as Ebeniro (1981) should read Ebeniro (1983).

Castanaga et al. (1985) found that the mudrock line could also be used to approximate the relationship between the sonic and shear velocities for sandstones.

Han et al. (1986) developed independent correlations for sonic and shear velocities as functions of porosity and clay volume fraction for shaly sandstones as shown in Equations (6-3) and (6-4).

$$V_p = 5{,}590 - 6{,}930\phi - 2{,}180C_v \tag{6-3}$$

$$V_s = 3{,}520 - 4{,}910\phi - 1{,}890C_v \tag{6-4}$$

where the velocities are in m/s, ϕ is the porosity (as a fraction), and C_v is the clay volume fraction. In theory, Equations (6-2), (6-3), and (6-4) could be combined to give a relationship between V_p and C_v. However, such a combination does not produce a valid result — C_v is found to be greater than 1 for all reasonable values of V_p.

Shale porosity can be reasonably represented as a function of the sonic velocity alone as shown in Dobson and Houseworth (2013). Therefore, including both velocity and porosity in a correlation for clay content may not improve the correlation. This conclusion was also reached by Cosenza et al. (2014) who analyzed similar correlations for the Callovo-Oxfordian Clay. Instead of clay volume fraction, Cosenza et al. (2014) used the weight fraction of clay, X. Cosenza et al. (2014) investigated several correlation forms including correlations between V_p, X, and ϕ, but found that a simple $V_p - X$ correlation performed as well

as or better than correlations including porosity as an independent variable. Figure 6.3 shows correlations found between X and V_p and X and V_s.

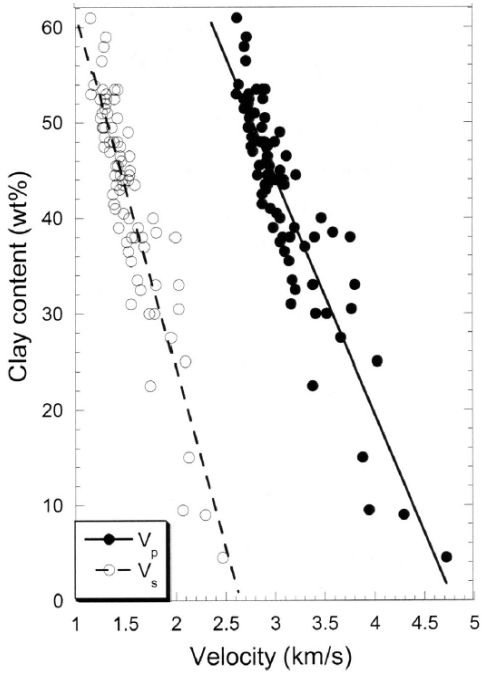

Figure 6-3. Correlation between clay content and sonic and shear velocities for the Callovo-Oxfordian clay. Solid line is for Equations (6-5) (for V_p) and dotted line for (6-6) (for V_s). (Cosenza et al., 2014).

The Cosenza et al. (2014) correlations for X and V_p and X and V_s are:

$$X = 1.186 - 0.000248\, V_p \tag{6-5}$$

$$X = 0.996 - 0.000376\, V_s \tag{6-6}$$

where the velocities are in m/s. Cosenza et al. (2014) does not distinguish between sonic velocity normal or perpendicular to bedding, therefore, these velocities are assumed to represent a mean velocity. Equations (6-5) and (6-6) may be combined to eliminate X to give,

$$V_p = 1.52V_s + 766 \tag{6-7}$$

Equation (6-7) may be compared with the correlation in Equation (6-2). Equation (6-7) gives a relatively low value of $V_p = 766$ m/s at $V_s = 0$ as compared with Equation (6-2), which gives 1,360 m/s. The sonic velocity at a shear velocity of zero may also be compared with the sonic velocity in water (see Figures 6-2 and 6-4). The predicted values of V_p for Equations (6-2) and (6-7) cross over at a shear velocity of 1,650 m/s, and for $V_s \geq 1{,}650$, the predicted values of V_p from Equation (6-7) is greater than the value predicted from Equation (6-2). Although the two correlations are different, within the main middle region (sonic velocities from 2000 to 5000 m/s) the lines are reasonably close as shown in Figure 6-4

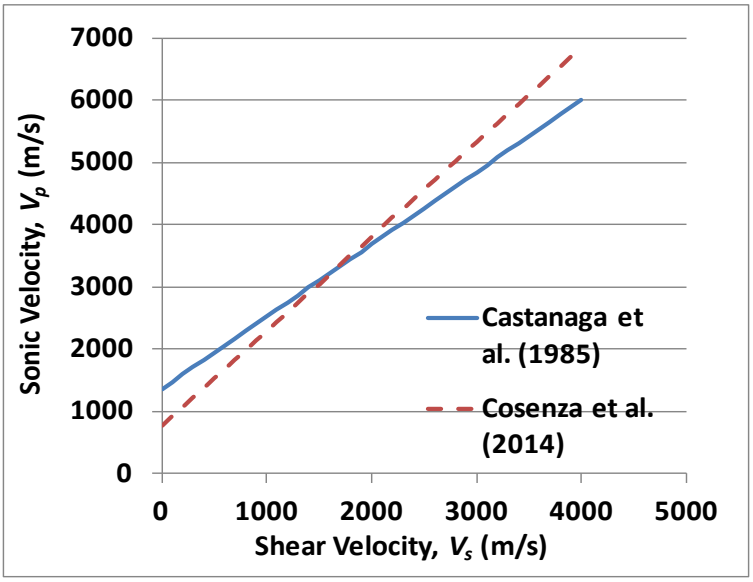

Figure 6-4. Use of Equation (6-5) needs to be truncated at high velocities because $X \leq 0$ for for $V_p \geq 4782$. Therefore, X will be set to zero for $V_p \geq 4782$.

The correlation proposed by Cosenza et al. (2014) is similar to the correlation developed by Dobson and Houseworth (2013) in that clay content is correlated with compressional seismic velocity and found to decrease monotonically with increasing velocity. However, the two correlations are substantially different in terms of quantitative predictions. The correlations are compared in Figure 6-5. The reason for the significant differences, particularly at high velocities, is not understood at this time.

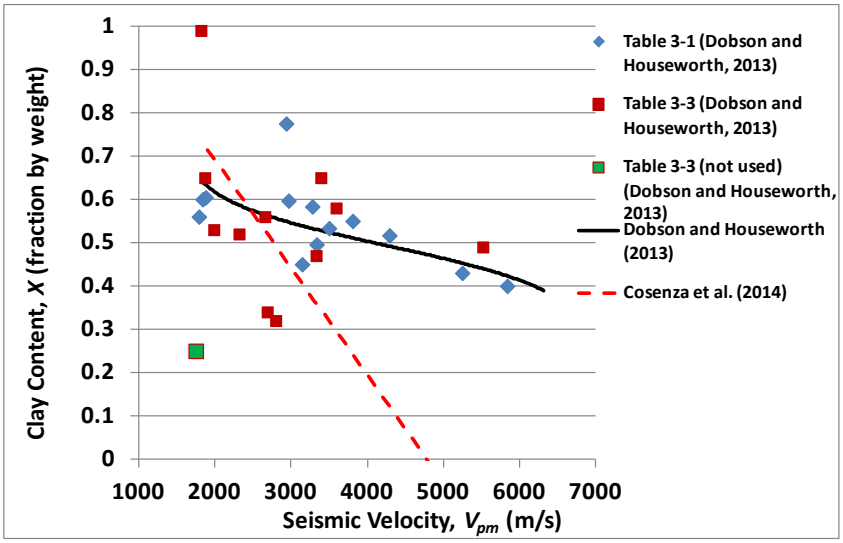

Figure 6-5. Correlation developed by Dobson and Houseworth (2013) compared with the V_p- clay content correlation developed by Cosenza et al. (2014) (also shown in Figure (6-3)).

6.3 Estimating thermal conductivity and specific heat capacity

Data that includes measurements of sonic velocity and thermal conductivity or heat capacity for shales have not been identified. However, sonic velocity has been used as a correlation variable for thermal conductivity of other types of geologic materials (Boulanouar, et al., 2013; Fuchs and Förster, 2013). Goto and Matsubayashi (2009) derived correlations for thermal conductivity and specific heat using porosity as the correlation variable.

6.3.1 Thermal Conductivity

Thermal conductivity measurements in shales, mudrocks, and claystones have been reported by several investigators (Blackwell and Steele, 1989; Midttømme et al., 1997; 1998; Midttømme and Roaldset, 1999; Waples and Tirsgaarde, 2002; Garitte et al., 2012). While none of these have attempted to link thermal conductivity with seismic velocity, Midttømme et al. (1997), Midttømme et al. (1998), and Midttømme and Roaldset (1999) tested arithmetic, geometric, and harmonic mixing-law models as a way to predict thermal conductivity based on porosity and mineral composition. Midttømme et al. (1997) found that there was some dependency seen in the data between thermal conductivity and porosity, however, the relationship between thermal conductivity and mineral composition was found to be weak. In some of these data sets only water content is reported instead of porosity (Midttømme et al., 1997 and Midttømme and Roaldset, 1999). For these cases, the water content was used as a proxy for porosity. The two values can differ when minerals contain waters of hydration as part of the mineral structure, which is counted towards water content but not porosity. Midttømme et al. (1998) measured both for four high-clay-content samples (clay content 44% to 65%); the root-mean-square average difference was about 0.07.

The data for thermal conductivity normal to bedding (K_{thn}) is plotted against porosity (ϕ) for all but the Waples and Tirsgaarde (2002) data (Figure 6-6). Although there is considerable scatter, a trend can be seen between these variables. These data were obtained either from field measurements in boreholes or laboratory measurements using the divided bar method.

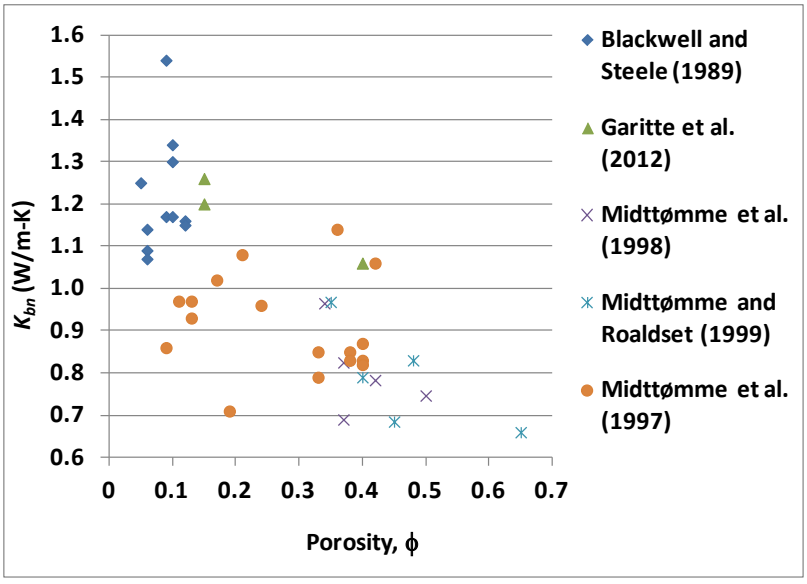

Figure 6-6. Field measurements and lab measurements (divided bar method) for thermal conductivity normal to bedding.

A large data set reported by Waples and Tirsgaarde (2002) is added to the data shown in Figure 6-7. This data was measured in the laboratory using the needle probe method.

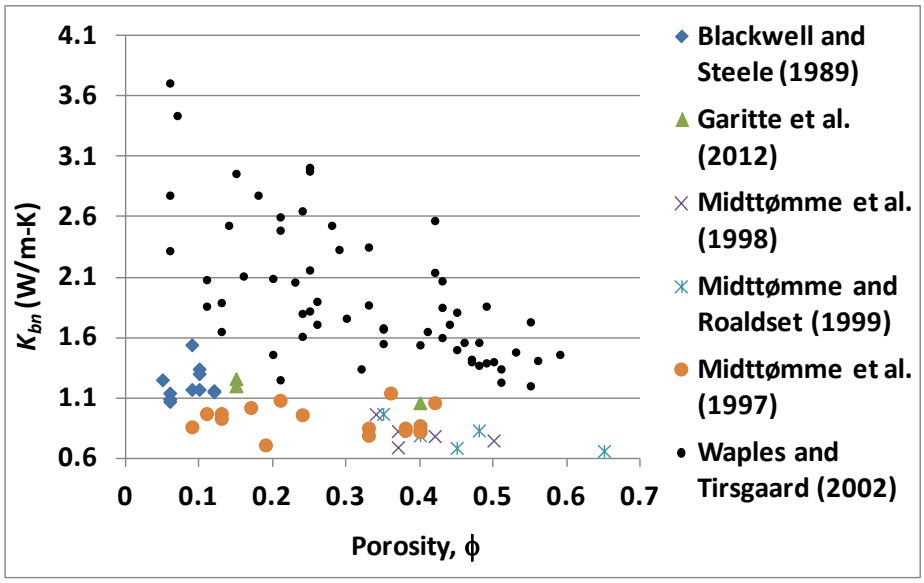

Figure 6-7. Field measurements and lab measurements (both divided bar and needle probe methods) for thermal conductivity normal to bedding.

The clear distinction between the measurements reported by Waples and Tirsgaarde (2002) and the other data sets is apparent. The needle probe measurements give values that are distinctly higher than the field measurements and the divided bar measurements at the same porosity, and lie considerably outside the scatter of these data (Midttømme et al., 1998). This difference caused by measurement methodology was investigated by Midttømme et al. (1999) and similar trends were found comparing needle probe measurements with divided bar measurements. Blackwell and Steele (1989) also comment on discrepancies between laboratory and field measurements of thermal conductivity. Given the differences between the needle probe measurements and other measurement techniques, the data from Waples and Tirsgaarde (2002) are not included in the development of a correlation.

Thermal conductivity studies conducted by Midttømme et al. (1997) found that thermal conductivity showed the strongest relationship with water content (or porosity) and a weaker relationship with mineral content (Midttømme et al., 1997). Three mixing models (arithmetic, geometric, and harmonic) for estimating thermal conductivity were investigated by Midttømme and Roaldset (1999); the best model was found to be the geometric mixing model:

$$K_{bn} = K_w^{\phi} K_g^{1-\phi} \tag{6-8}$$

where, K_{bn} is the bulk saturated rock thermal conductivity normal to bedding, K_w is the thermal conductivity of the pore fluid (water), K_g is the thermal conductivity of the solid, and ϕ is the porosity.

The approach for developing a thermal conductivity correlation is to take the logarithm of Equation (6-8) and average the quantity $\overline{\log(K_s)}$ for the data in Figure 6-6,

$$\overline{\log(K_g)} = \frac{\log(K_{bn}) - \phi \log(K_w)}{1-\phi} \tag{6-9}$$

The value of K_w is taken to be 0.6 W/m-K (Midttømme and Roaldset, 1999). A representative value for the thermal conductivity of the solid is $\overline{K_g} = 10^{\overline{\log(K_g)}}$, and is found to be $\overline{K_g} = 1.1$ W/m-K. Thermal conductivities are then computed from

$$K_{bn} = K_w^{\phi} \overline{K_g}^{1-\phi} \tag{6-10}$$

This correlation is shown in Figure 6-8. By using the correlation between porosity and sonic velocity in Dobson and Houseworth (2013), the thermal conductivity can also be computed from a measurement of the compressional seismic velocity. The root-mean square error (RMSE) for the correlation is 0.154 W/m-K.

The correlation for thermal conductivity parallel to bedding (K_{bp}) is computed using the same methodology for anisotropic materials as describe in Dobson and Houseworth (2013). The thermal conductivity normal to bedding is scaled by the velocity ratio (V_{pr}^{ω}) raised to the power ω. The velocity ratio is given by the sonic velocity parallel to bedding divided by the sonic velocity normal to bedding. If sonic velocity parallel to bedding is not available, a method to estimate this from the normal sonic velocity is described in Dobson and Houseworth (2013). The correlation equation is then,

$$K_{bp} = K_w^{\phi} \overline{K_g}^{1-\phi} V_{pr}^{\omega} \tag{6-11}$$

The power ω is determined by fitting the correlation to the thermal conductivity data parallel to bedding. Doing this gives a value of ω of 2.3.

This fit is shown in Figure 6-9 and has an RMSE of 0.215.

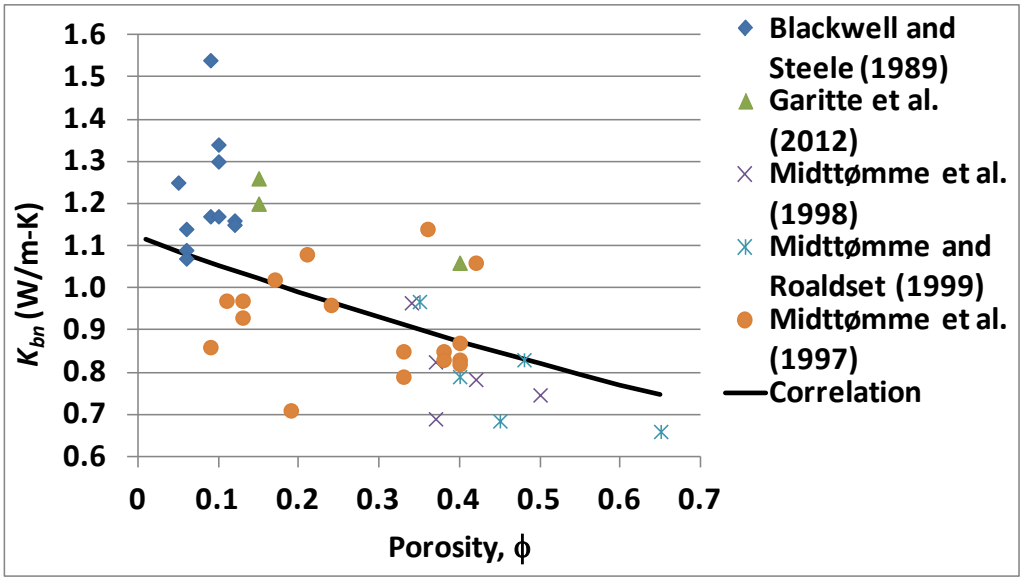

Figure 6-8. Thermal conductivity normal to bedding; data and correlation.

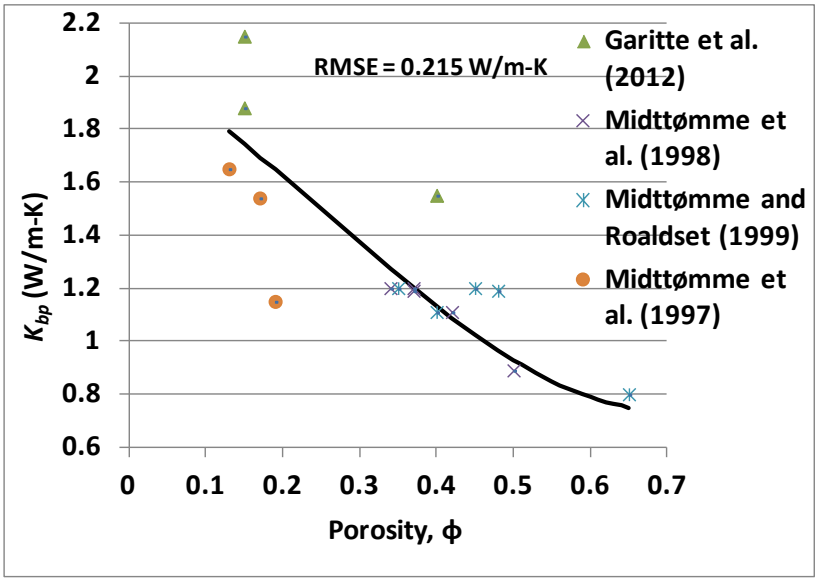

Figure 6-9. Thermal conductivity parallel to bedding; data and correlation.

For unsaturated systems, the thermal conductivity may be estimated from the following logical extensions of Equations (6-10) and (6-11):

$$K_{bn} = K_w^{S_w\phi} K_a^{(1-S_w)\phi} \overline{K_g}^{1-\phi} \tag{6-12}$$

$$K_{bp} = K_w^{S_w\phi} K_a^{(1-S_w)\phi} \overline{K_g}^{1-\phi} V_{pr}^{\omega} \tag{6-13}$$

where the fluid thermal conductivity raised to the power of the porosity, K_w^{ϕ}, has been replaced by the product of the thermal conductivity of water raised to the power of the water content, $K_w^{S_w\phi}$, times the thermal conductivity of air raised to the power of the air content, $K_a^{(1-S_w)\phi}$ in Equation (6-12). This reduces to $K_w^{\phi}$when $S_w = 1$ where the fluid thermal conductivity is for water and reduces to $K_a^{\phi}$when $S_w = 0$. Equation (6-13) is the expression in Equation (6-12) with the anisotropy factor, exactly as Equation (6-11) is formulated relative to Equation (6-10).

6.3.2 Specific Heat

The approach to estimate specific heat follows that of Goto and Matsubayashi (2009) in which the specific heat is computed from an arithmetic average of the rock and fluid components,

$$\rho_b c_b = \phi\rho_w c_w + (1-\phi)\rho_g c_g \tag{6-14}$$

where $\rho_b$is the bulk density of the saturated rock, $\rho_w$is the pore fluid density, and ρ_g is the grain density, $c_b$is the bulk specific heat of the saturated rock, c_w is the specific heat of the pore fluid (water), and c_g is the specific heat of the rock grains. The pore fluid is approximated as water with a density of 1000 kg/m^3 and the pore fluid specific heat is 4126 J/kg-C. As discussed in Section 3.3.1, the previous work of Dobson and Houseworth (2013) has defined a correlation between sonic velocity and porosity (ϕ). A

correlation was also defined for the saturated rock bulk density and sonic velocity. The grain density can then be computed given the porosity, bulk density, and pore fluid density. Therefore, all parameters in Equation (6-14) can be computed given the sonic velocity except for c_b and c_s. However, Waples and Waples (2004) have derived a correlation for the rock grain specific heat as a function of the grain density for low- and moderate-density mineral grains for the range of approximately 2000 to 4000 kg/m^3. This range covers the grain densities encountered in shale and mudrocks. This correlation is given by,

$$\rho_g c_g = 1.0263 \times 10^{-6} \exp\left(0.0002697 \rho_g\right) \tag{6-15}$$

where ρ_g is in kg/m^3 and $\rho_g c_g$ is in J/m^3-K. The data and correlation function plot from Waples and Waples (2004) is given in Figure 6-10.

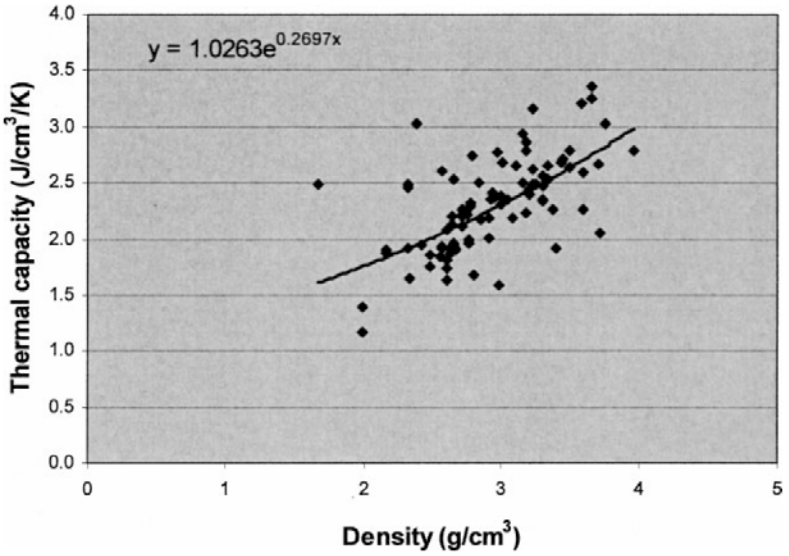

Figure 6-10. Data and correlation between rock grain volumetric specific heat and grain density (Waples and Waples 2004)

Using Equations (6-14) and (6-15) the value of the bulk specific heat of the saturated rock may be computed as a function of porosity. Lab and field measurements of specific heat on clay/shale rocks from the Opalinus Clay (Wileveau and Rothfuchs, 2007), Boom Clay (Li et al., 2007), Callovo-Oxfordian Clay (Delay et al., 2011), and Ypresian Clay (Piña-Diaz, 2011) are shown along with the correlation for specific heat as a function of porosity in Figure 6-11. The correlation is found to have an RMSE relative to the data of 186 J/kg-K. By using the correlation between porosity and sonic velocity in Dobson and Houseworth (2013), the specific heat can also be computed from a measurement of the compressional seismic velocity.

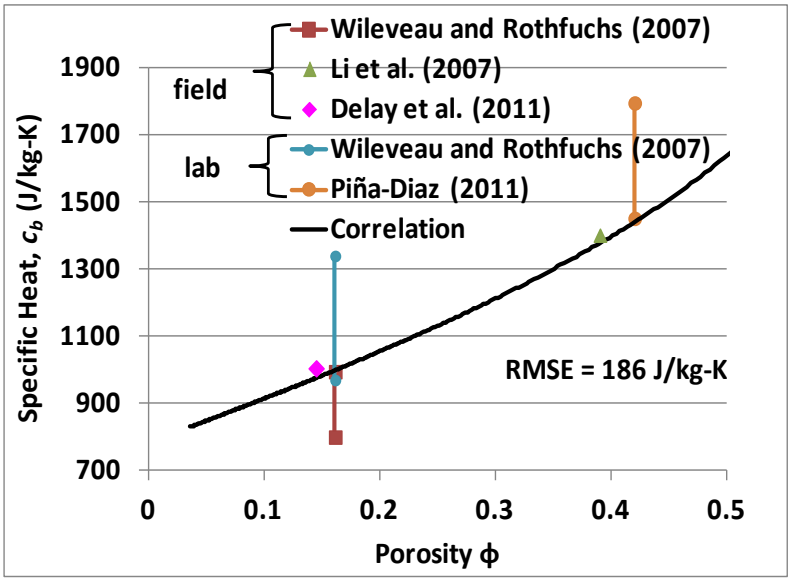

Figure 6-11. Bulk rock specific heat correlation with lab and field data.

The extension of Equation (6-14) for unsaturated conditions is,

$$\rho_b c_b = \phi S_w \rho_w c_w + \phi(1 - S_w)\rho_a c_a + (1 - \phi)\rho_g c_g \tag{6-16}$$

where ρ_w and ρ_a are the water and air mass densities and c_w and c_a are the water and air specific heat capacities.

6.4 Estimating two-phase flow parameters

Two-phase flow processes are of interest for radioactive waste disposal in shale primarily because of the introduction of a gas phase into a water-saturated shale environment during ventilation for repository construction and waste emplacement. Repository heating may also result in the generation of a gaseous phase of H_2O (steam). The introduction of a second immiscible phase results in a phase pressure difference, or capillary pressure, between the gas and liquid phases. Capillary pressure is an additional driving force for flow processes. The presence of two phases also reduces the effective permeability of each phase relative to the intrinsic (phase-saturated) permeability. This reduction is typically represented as a relative permeability, which is the ratio of the effective permeability divided by the intrinsic permeability. Both capillary pressure and relative permeability are functions of phase saturation.

There are a number of models for representing capillary pressure and relative permeability for two-phase systems as functions of saturation. A model that has been widely used for soil systems was developed by van Genuchten (1980). This model uses two independent parameters to describe the capillary pressure parameter function of saturation. The relative permeability parameter function does not introduce any further parameters, as it is derived from the capillary pressure parameter function. The expressions for capillary pressure and relative permeability are:

$$P_c(S_{wn}) = \frac{1}{\alpha}\left\{S_{wn}^{-\frac{1}{m}} - 1\right\}^{1-m} \tag{6-17}$$

$$k_{rw}(S_{wn}) = S_{wn}^{\frac{1}{2}}\left\{1-\left(1-S_{wn}^{\frac{1}{m}}\right)^{m}\right\}^{2} \quad (6\text{-}18)$$

Where P_c is the capillary pressure, S_{wn} is the normalized water saturation, k_{rw} is the dimensionless relative permeability to water, α is a parameter (with units of inverse pressure) referred to as capillary strength, and m is a dimensionless parameter referred to as the pore-size distribution index. The normalized water saturation is given by

$$S_{wn} = \frac{S_w - S_{wr}}{S_{wm} - S_{wr}} \quad (6\text{-}19)$$

where S_{wr} is the residual water saturation at which water ceases to flow, S_{wm} is the maximum water saturation at which gas ceases to flow, and S_w is the physical water saturation (fraction of pore space occupied by water).

The relative permeability parameter function for the gas phase (k_{rg}) also needs to be specified for a two-phase flow model. Charlier et al. (2013) was able to approximate experimental data for gas relative permeability in the Callovo-Oxfordian Clay using the following cubic function (Figure 6-12),

$$k_{rg}(S_{wn}) = (1 - S_{wn})^3 \quad (6\text{-}20)$$

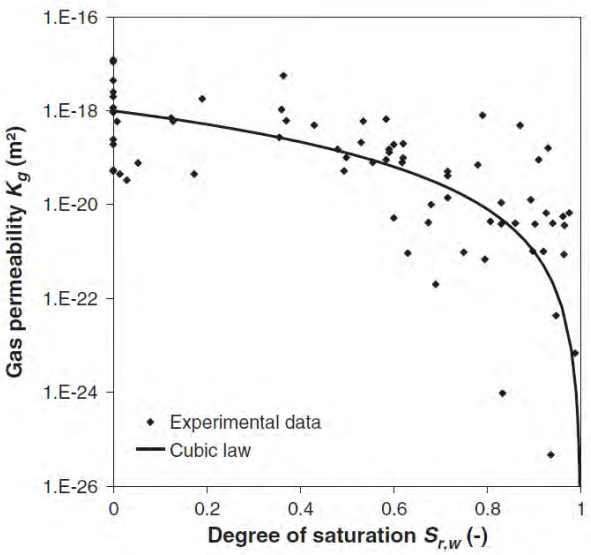

Figure 6-12. Gas relative permeability data and model for the Callovo-Oxfordian Clay (Charlier et al., 2013)

6.4.1 Estimating van Genuchten α

Thomas et al. (1968) investigated the relationship between the threshold (or air entry) pressure and permeability. The air entry pressure is the pressure required for air to enter and start flowing in a water-saturated system. Although the study was not specifically for shale or mudstone, it did involve low-permeability rocks down to microdarcy levels. The correlation is given in Equation (6-21) and shown in Figure 6-13.

$$P_T = 7.37k^{-0.43} \quad (6\text{-}21)$$

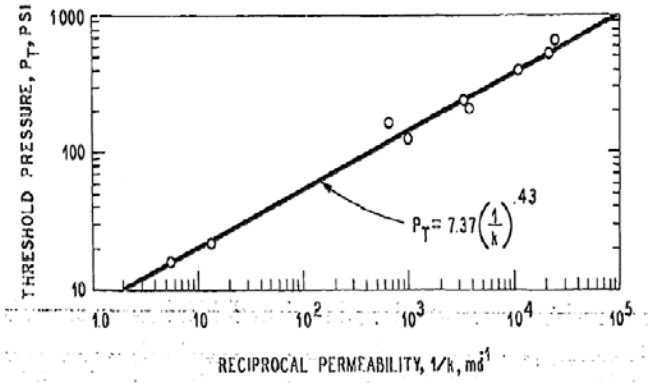

Figure 6-13. Threshold pressure permeability correlation (Thomas et al., 1968)

where P_T is the air entry pressure in pounds per square inch (psi) and k is the intrinsic permeability in millidarcies (md). This relationship is supported by more recent evidence for clay and shale rock types as shown in Figure 6-14. A comparison between Equation (6-21) and the Davies (1991) shale model shown in Figure 6-14 is given in Figure 6-15. The difference in the models is not considered significant in comparison with the data shown in Figure 6-14.

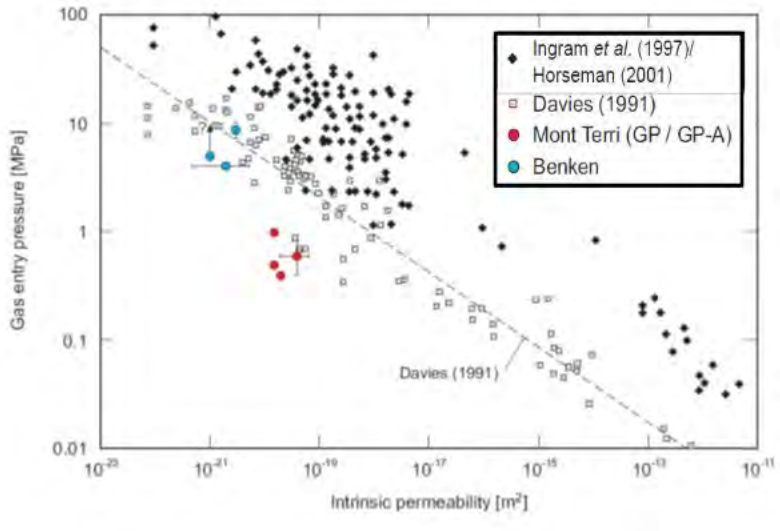

Figure 6-14. Data and correlation between permeability and gas entry pressure (Johnson et al., 2004; Marschall et al., 2005).

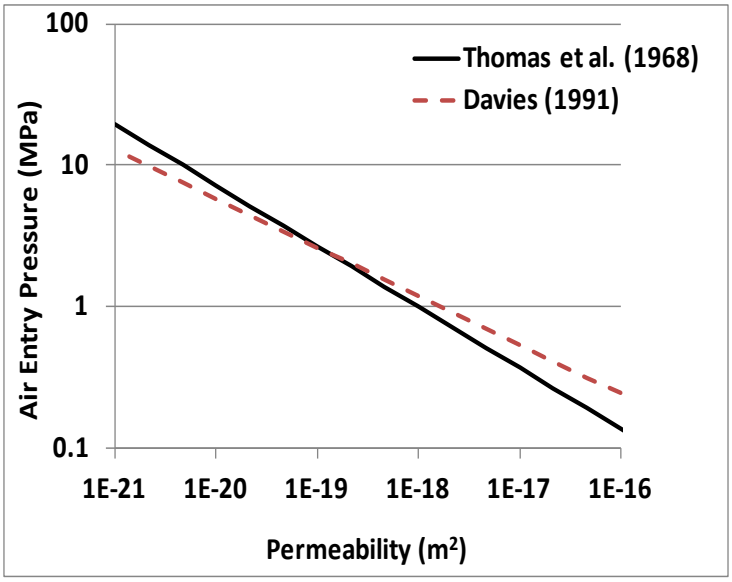

Figure 6-15. Comparison of correlations for air entry pressure as a function of permeability.

A relationship between the air entry pressure and capillary strength was found by Tinjum et al. (1997) to be,

$$\alpha = 0.78 P_T^{-1.26} \tag{6-22}$$

where P_T is expressed in kPa (instead of psi as used for P_T in Equation (6-21)) and α is given in kPa^{-1}. The correlation found by Tinjum et al. (1997) is shown in Figure 6-16.

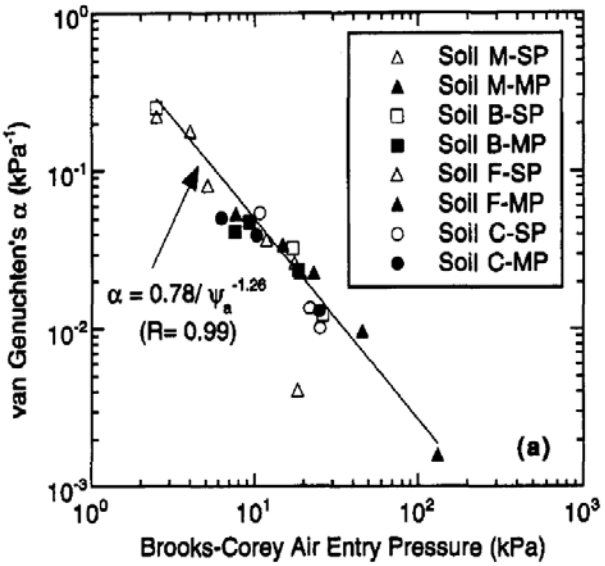

Figure 6-16. Correlation for soils between van Genuchten α and air entry pressure (Tinjum et al., 1997).

The Tinjum et al. (1997) correlation is for soils and does not cover the parameter space for typical claystones and shales investigated here, where air-entry pressures are generally on the order of 1 MPa or more. Therefore, this type of relationship was calibrated to the few clay-shale data points available shown

in Figure 6-17. In this figure, the air-entry pressure was computed from Equation (6-21) using the known permeability and plotted against the van Genuchten α. For anisotropic materials, the geometric mean permeability between bedding normal and bedding parallel permeability values was used.

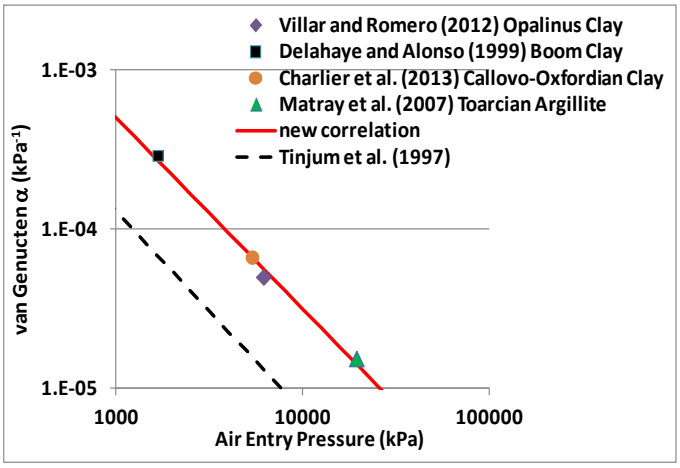

Figure 6-17. Correlation and data for van Genucten α as a function of air-entry pressure for shales and claystones compared with Tinjum et al. (1997) correlation for soils.

The new correlation lies above the Tinjum et al. (1997) correlation with nearly the same slope. The correlation equation is,

$$\alpha = 2.01 P_T^{-1.20} \tag{6-23}$$

where, as for Equation (6-22), P_T is expressed in kPa (instead of psi as used for P_T in Equation (6-21)) and α is given in kPa^{-1}.The correlation has a root-mean square error (RMSE) of 0.034 for $\log(\alpha)$ (in kPa), or a factor of 1.08 on α. Using Equations (6-21) and (6-23), an estimate of capillary strength α can be made given the intrinsic permeability. The intrinsic permeability can be estimated from seismic velocity as described in Dobson and Houseworth (2013). Therefore, α may be estimated from the seismic velocity.

6.4.2 Estimating van Genuchten m

As for van Genuchten α, there is very little data available for the van Genuchten pore-size distribution index m for shales and claystones. The limited data available has been plotted in Figure 6-17 against permeability. These data are for m as used in a drainage (or desaturation) capillary pressure curve. In some cases, measurements found distinctions for the value of m were found for relative permeability and for imbibition processes (see references listed in Figure 6-18). Figure 6-18 shows a trend of decreasing values of m with increasing permeability. The correlation is given in Equation (6-24), which has an RMSE of 0.053. An error function model was used to ensure that m does not go beyond the limits of 0 and 1 at low and high permeabilities, respectively. By using the relationship between the seismic velocity and permeability in Dobson and Houseworth (2013), an estimate of m may be made from the seismic velocity.

$$m = 0.5 - 0.5\mathrm{erf}\left\{\frac{\log(k) + 20.34}{3.94}\right\} \tag{6-24}$$

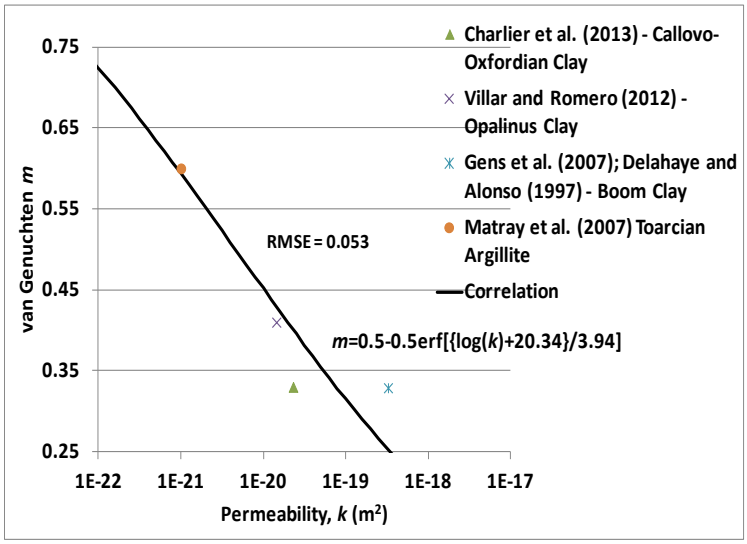

Figure 6-18. Correlation of the van Genucten pore-size distribution index with permeability.

6.4.3 Estimating Residual Saturations

Estimates of the residual saturations (S_{wr} and S_{wm}) are needed for the van Genuchten parameter functions describing capillary pressure and water relative permeability. They are also needed for the Corey parameter function for gas relative permeability. However, very little direct information from shales and mudrocks are available for determining these parameters. A number of relationships relating porosity, permeability and residual water saturation are presented by Alavi et al. (2014). However, these were developed for sandstones and do not give reasonable results for clay/shale rock types. The existence of a residual wetting-phase saturation for a drainage process has been questioned for water-wet materials (such as organic-poor clays and shales) because water maintains hydraulic continuity within the porous material as films on the grain surfaces down to very low water saturations (Dullien et al., 1986). This is particularly true for water-gas fluid systems because gases are typically strongly non-wetting relative to water on mineral surfaces. Therefore, a value of $S_{wr} = 0$ is suggested if no additional site-specific information is available. The maximum wetting phase saturation, S_{wm}, has traditionally been taken to be 1 for the van Genuchten formulation. The maximum wetting-phase saturation corresponds to the residual non-wetting phase saturation for two-phase systems, i.e., $S_{wm} = 1 - S_{gr}$, where S_{gr} is the residual gas saturation. Although a value of $S_{wm} = 1$ (or $S_{gr} = 0$) is true for primary drainage in which gas displaces water from a water-saturated system, this is not the case for imbibition in which water displaces gas. The existence of a residual non-wetting phase saturation for imbibition processes has been well established (e.g., Chatzis et al., 1988). However, because of a lack of data on residual gas saturations for clays and shales, a value of $S_{wm} = 1$ is recommended if site-specific information is not available. For the Opalinus Clay, Marschall et al. (2005) cite the following ranges: $0 \leq S_{wr} \leq 0.5$ and $0 \leq S_{gr} \leq 0.05$.

6.5 Application to US Shale Formations

Given the changes and additions of property estimates introduced here, the application of the correlations to US Shale Formations has been revised from that given in Section 3.3 of Dobson and Houseworth (2013). Figure 6-19 shows the location of formations evaluated.

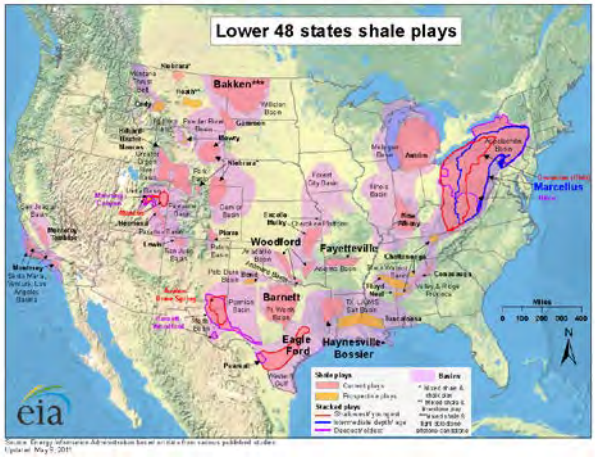

Figure 6-19. Map of U.S. shale gas and shale oil plays (EIA, 2011b).

The correlation inputs are the normal and parallel sonic velocities and an average formation depth. As for the development of correlations described in Section 6.2, if the velocity parallel to bedding is not available, it is estimated using the velocity ratio correlation given by Equation (6-1). Table 6-1 (Dobson and Houseworth, 2013) gives the requisite inputs for the formations, which are the sonic velocity normal to bedding (V_{pn}), the sonic velocity perpendicular to bedding (V_{pp})(where available) and the formation depth (D). The formation water density is also an input, however, for the current analysis, a fresh water density of 1000 kg/m^3 was assumed.

Table 6-1. Inputs for Properties Estimation.

Formation	V_{pn} (m/s)	V_{pp} (m/s)	D (m)
Barnett Shale	4031[(1)]	NA	1000[(2)]
Haynesville Shale	3628[(1)]	NA	3000[(3)]
Pierre Shale (1)	2164[(4)]	2243[(4)]	152[(4)]
Pierre Shale (2)	3140[(5)]	3768[(5)]	1520[(5)]
New Albany Shale	3600[(6)]	4500[(6)]	520[(7)]
Antrim Shale	3174[(8)]	4057[(8)]	328[(8)]
Eagle Ford Shale	4016[(9)]	4083[(9)]	3234[(9)]
Marcellus Shale	3500[(10)]	NA	1920[(10)]
Woodford Shale	4008[(11)]	NA	1220[(11)]
Monterey Shale	4844[(12)]	5310[(12)]	2.7[(12)]

Sources: [(1)] Montaut (2012); [(2)] Bruner and Smosna (2011); [(3)] Nunn (2012); [(4)] McDonal et al. (1958); [(5)] Tosaya (1982); [(6)] Johnston and Christensen (1995); [(7)] CNX/GTI (2008); [(8)] Liu (1997); [(9)] Sondhi (2011); [(10)] Hardage et al. (2013); [(11)] Verma et al. (2013); [(12)] Liu (1994)

6.5.1 Correlations Results

With the sonic velocities from Section 6.3.1, the correlations from Section 6.2 may be used to compute thermal, hydrological, and geomechanical parameters. These results are shown in Table 6-2. Outputs shaded in blue are rock parameters, while outputs shaded in rose are formation conditions (e.g., effective stress, brittleness index, and overconsolidation ratio) that lead to the estimation of pore pressure. The new correlation for this table that supersedes Dobson and Houseworth (2013) is for clay content. New correlations here, beyond those documented in Dobson and Houseworth (2013), are for thermal conductivity (both normal and parallel to bedding), specific heat, and two-phase flow parameters, van Genuchten capillary strength (α) and van Genuchten pore-size distribution index (m).

Table 6-2. Estimated Parameters Using Seismic Velocity Correlations.

Parameters	Barnett Shale	Haynesville Shale	Pierre Shale (1)	Pierre Shale (2)	New Albany Shale
Inputs (from Table 6-1)					
V_{pn} (m/s)	4031	3628	2164	3140	3600
V_{pp} (m/s)	NA	NA	2243	NA	4500
D(m)	1000	3000	152	1524	518
Outputs					
V_{pp} (m/s)	5226	4665	2530	3975	4626
ϕ	0.056	0.087	0.36	0.14	0.094
e	0.060	0.095	0.56	0.16	0.103
ρ_b (kg/m^3)	2640	2590	2220	2520	2580
ρ_{bd} (kg/m^3)	2580	2500	1860	2380	2490
ρ_g (kg/m^3)	2740	2740	2890	2760	2740
X (fraction)	0.48	0.50	0.60	0.52	0.50
k_n(m^2)	6.1E-22	1.3E-21	7.4E-20	3.2E-21	1.4E-21
k_p(m^2)	1.8E-21	3.5E-21	8.6E-20	8.5E-21	3.6E-21
UCS (MPa)	43	31	5.9	21	29
E_n (GPa)	8.1	6.1	0.70	4.1	5.8
E_p (GPa)	23	17	0.81	10.6	14
G (GPa)	3.2	2.5	0.29	1.7	2.4
υ	0.13	0.17	0.39	0.22	0.18
c_n (MPa)	7.9	5.3	0.66	3.2	4.9
c_p (MPa)	20	12.8	0.7	7.4	11
φ (degrees)	24	23	21	23	23
τ_n (MPa)	2.7	1.9	0.24	1.1	1.7
τ_p (MPa)	6.4	4.3	0.27	2.5	3.6
K_{bn} (W/m-K)	0.98	0.96	0.86	0.94	0.96
K_{bp} (W/m-K)	1.78	1.72	0.94	1.62	1.61
c_b (J/kg-K)	856	896	1316	966	905
α (MPa^{-1})	1.47E-02	2.12E-02	1.38E-01	3.40E-02	2.21E-02
m	0.59	0.55	0.33	0.49	0.54
σ'_v (MPa)	47	41	9.3	32	40
σ_{NC} (MPa)	16	47	1.8	23	8.0
UCS$_{NC}$ (MPa)	8.0	23	0.9	11	4.0
BRI	5.3	1.3	6.5	1.8	7.3
OCR	3.2	1.2	3.7	1.5	4.0
σ_{pd} (MPa)	15	33	2.5	21	10
p (MPa)	11	43	0.79	17	3
p_{hs} (MPa)	9.8	29	1.5	15	5.1
p_{op} (MPa)	1.41	13	-0.70	1.9	-1.8

Table 6-2 (continued). Estimated Parameters Using Seismic Velocity Correlations.

Parameters	Antrim Shale	Eagle Ford Shale	Marcellus Shale	Woodford Shale	Monterey Shale
Inputs (from Table 6-1)					
V_{pn} (m/s)	3174	4016	3500	4008	4844
V_{pp} (m/s)	4057	4843	NA	NA	5310
D(m)	328	3234	1920	1219	2.7
Outputs					
V_{pp} (m/s)	4024	5206	4485	5195	6339
ϕ	0.13	0.067	0.10	0.058	0.033
e	0.15	0.071	0.11	0.061	0.035
ρ_b (kg/m^3)	2530	2620	2570	2640	2680
ρ_{bd} (kg/m^3)	2390	2550	2470	2580	2650
ρ_g (kg/m^3)	2760	2740	2740	2740	2740
X (fraction)	0.52	0.49	0.50	0.48	0.46
k_n(m^2)	2.9E-21	8.0E-22	1.6E-21	6.3E-22	3.0E-22
k_p(m^2)	8.1E-21	1.7E-21	4.4E-21	1.8E-21	4.4E-22
UCS (MPa)	22	38	28	42	60
E_n (GPa)	4.3	7.3	5.6	7.9	10.4
E_p (GPa)	11	15	15	22	15
G (GPa)	1.8	2.9	2.3	3.1	3.9
υ	0.22	0.14	0.18	0.13	0.094
c_n (MPa)	3.4	6.8	4.7	7.7	12
c_p (MPa)	8.0	13	11.1	19	17
φ (degrees)	23	23	23	24	24
τ_n (MPa)	1.2	2.4	1.6	2.7	4.1
τ_p (MPa)	2.7	4.4	3.7	6.3	5.6
K_{bn} (W/m-K)	0.95	0.97	0.96	0.98	0.99
K_{bp} (W/m-K)	1.66	1.50	1.70	1.77	1.22
c_b (J/kg-K)	958	870	912	858	826
α (MPa^{-1})	3.27E-02	1.57E-02	2.39E-02	1.50E-02	8.54E-03
m	0.50	0.58	0.53	0.59	0.65
σ'_v (MPa)	33	45	39	47	53
σ_{NC} (MPa)	4.9	51	30	20	0.045
UCS_{NC} (MPa)	2.5	26	15	9.8	0.023
BRI	8.9	1.5	1.9	4.3	2700
OCR	4.6	1.3	1.6	2.8	250.0
σ_{pd} (MPa)	7	34	25	17	0.21
p (MPa)	1.01	49	24	15	-0.14
p_{hs} (MPa)	3.2	32	19	12	0.027
p_{op} (MPa)	-2.2	17	5.0	2.6	-0.17

V_{pn} : compressional sonic velocity normal to bedding; V_{pp} : compressional sonic velocity parallel to bedding; D: present-day formation depth; ϕ: porosity; e: void ratio; ρ_b: brine-saturated bulk density; ρ_{bd}: dry bulk density; ρ_g: grain density; X: mass

fraction of clay minerals; k_n: brine permeability normal to bedding; k_p: brine permeability parallel to bedding; UCS: uniaxial compressive strength normal to bedding; E_n: Young's modulus normal to bedding; E_p: Young's modulus parallel to bedding; G: shear modulus normal to bedding; υ: Poisson's ratio (isotropic); c_n: cohesive strength normal to bedding; c_p: cohesive strength parallel to bedding; φ: friction angle (isotropic); τ_n: tensile strength normal to bedding; τ_p: tensile strength parallel to bedding; K_{bn}: thermal conductivity of water-saturated rock normal to bedding; K_{bp}: thermal conductivity of water-saturated rock parallel to bedding; c_b: specific heat capacity of water-saturated rock; α: van Genuchten capillary strength parameter for capillary pressure parameter function; m: van Genuchten pore-size distribution index for capillary pressure and relative permeability parameter functions; σ_v': maximum effective stress experienced by the formation; σ_{NC}: effective stress at the present-day depth for normal consolidation at hydrostatic pore pressure; $\mathrm{UCS_{NC}}$: uniaxial compressive strength for normal consolidation at present-day depth; BRI: brittleness index; OCR: overconsolidation ratio; σ_{pd}: present-day effective stress; p: present-day pore-fluid pressure; p_{hs}: hydrostatic pressure at present-day depth; p_{op}: pore-fluid overpressure (or underpressure if negative) $(p - p_{hs})$.

6.6 Conclusions of Section 6

Correlations for estimating hydrological and geomechanical formation properties and in-situ conditions from sonic velocities have been developed from data on shale formations that lie outside the United States. These correlations have been applied to estimate properties for several large shale formations in the United States. The advantage of using correlations based on sonic velocity is that properties can be estimated from geophysical logs. This information is often more readily available and in greater quantity than direct property measurements on core that would otherwise be required. Furthermore, geophysical logs provide a continuous readout along wells that can be more readily used to characterize spatial variability in properties.

Previous work (Dobson and Houseworth, 2013) found that several properties (porosity, bulk density, clay content, permeability, uniaxial compressive strength, Young's modulus, shear modulus, Poisson's ratio, cohesive strength, friction angle, and tensile strength) could be correlated with the compressive seismic velocity. In addition, the in-situ conditions for effective stress, overconsolidation ratio, and pore pressure could also be linked to the compressive seismic velocity. The work presented here extends and enhances the correlations developed in Dobson and Houseworth (2013). A study reported by Cosenza et al. (2014) for the Callovo-Oxfordian Clay lends support to the use of seismic velocity correlations for estimating clay content. However the correlations developed by Dobson and Houseworth (2013) differ significantly from the correlation proposed by Cosenza et al. (2014) in terms of quantitative estimates of clay content. These differences remain unresolved.

Correlations for thermal conductivity (including anisotropic effects) and specific heat have been developed based on traditional models representing mixtures of rock grains and pore fluids. The mixing models are based on geometric averaging for thermal conductivity and arithmetic averaging for specific heat. The literature on thermal conductivity measurements indicates that some measurement bias may be present in certain types of thermal conductivity measurements. The data that best represent the physical system have been evaluated and selected for use in the development of the correlation.

Correlations for two-phase flow properties have been developed in terms of the van Genuchten two-phase flow parameters for capillary strength (α) and pore-size distribution index (m). The correlation for van Genuchten capillary strength is based on data that relate permeability to air entry pressure along with data linking air-entry pressure to the capillary strength parameter. Similar correlations have been commonly used for applications to soils and have been extended here for claystones and shales. A similar approach has been used for the pore-size distribution index in that the parameter is correlated with permeability.

The correlations require additional development and verification. In particular, the correlations for the van Genuchten two-phase flow parameters require additional data. Further verification is also needed for many of the parameter estimates in Table 6-2; therefore, they should be viewed as initial estimates.

7. ACKNOWLEDGMENTS

Funding for this work was provided by the Used Fuel Disposition Campaign, Office of Nuclear Energy, of the U.S. Department of Energy.

From Los Alamos National Laboratory, Florie Caporuscio reviewed this report and his comments were greatly appreciated. Tina Thaxton is greatly appreciated for designing the website that describes the GIS database.

From Lawrence Berkeley National Laboratory, Curt Oldenburg reviewed this report and his feedback was greatly appreciated. Editorial assistance was also provided by Helen Prieto and Peter Persoff.

In addition, many individuals generously shared their knowledge and data to help populate the GIS database described in Section 2. Steve Ruppel and Cari Breton of the University of Texas, Bureau of Economic Geology, provided us with their GIS dataset for the Woodford Shale in the Permian Basin. John Bocan, with the West Virginia Geological and Economic Survey, provided us with GIS data for the Utica Shale that had been developed by the Trenton-Black River Research Consortium. Jim McDonald of the Ohio Department of Natural Resources shared with us a regional GIS dataset for the Marcellus Shale. Christopher Korose of the Illinois State Geological Survey provided us with GIS data for the New Albany Shale that was developed by the Illinois Basin Consortium. Jeff Zimmerman of the Susquehanna River Basin Commission provided us with some USGS GIS data for the Utica and Marcellus Shales. David Effert of the Louisiana Department of Natural Resources gave us access to GIS data for the Haynesville Shale. Brian Cardott of the Oklahoma Geological Survey provided us with additional references on the Woodford Shale and Sue Palmer (also of the Oklahoma Geological Survey) provided us with pdf copies of plates depicting the thickness and depth of the Woodford Shale in the Anadarko Basin. Sue Hovorka of the University of Texas, Bureau of Economic Geology, pointed us towards a study conducted by the Gulf Coast Carbon Center, which contains abundant information regarding seals (i.e., shales) in many sedimentary basins in the US. Prof. James Wood (Michigan Tech) provided us with a copy of his digital dataset for the Antrim Shale in the Michigan Basin. Julie LeFever (North Dakota Geological Survey) shared her GIS data for the Bakken Formation. Sam Limerick helped us track down the source files for the EIA shale play maps, and Jack Perrin and Meg Coleman (US EIA) generously provided us with the associated GIS data. Don Sweetkind (USGS) shared the GIS data associated with his reports on the Monterey Formation in the Cuyama and Santa Maria Basins. Many thanks for all of their contributions.

8. REFERENCES

Agrawal, A., 2009. A technical and economic study of completion techniques in five emerging U.S. gas shale plays. M.S. thesis, Texas A&M University, 135 p.

Alavi, M.F., Alavi, M.F., Alavi, M.F., 2014. Determination of Relative Permeability Based on Irreducible Water Saturation and Porosity from Log Data and Flow Zone Indicator (FZI) from Core Data, International Petroleum Technology Conference, Doha, Qatar, January 20-22, 2014, 18 p.

Amsden, T.W., 1975. Hunton Group (Late Ordovician, Silurian, and Early Devonian) in the Anadarko Basin of Oklahoma. Oklahoma Geological Survey Bulletin 121, 214 p.

Amsden, T.W., 1980. Hunton Group (Late Ordovician, Silurian, and Early Devonian) in the Arkoma Basin of Oklahoma. Oklahoma Geological Survey Bulletin 129, 136 p.

Anderson, R.R., 2006, Geology of the Precambrian Surface of Iowa and Surrounding Area, Open File Map OFM-06-7, Iowa Geological Survey.

Anna, L.O., 2009. Geologic assessment of undiscovered oil and gas in the Powder River Basin Province: U.S. Geological Survey Digital Data Series DDS-69-U, 93 p.

Arnold B.W., Brady, P., Altman, S., Vaughn, P., Nielson, D., Lee, J., Gibb, F., Mariner, P., Travis, K., Halsey, W., Beswick, J., and J. Tillman, 2013. Deep Borehole Disposal Research: Demonstration Site Selection Guidelines, Borehole Seals Design, and RD&D Needs. FCRD-USED-2013-000409.

Bennett, V.C. and DePaolo, D.J.,1987, Proterozoic crustal history of the western United States as determined by neodymiom isotopic mapping. Geological Society of America Bulletin, 99, 674–685.

Blackford, M.A., 2007. Electrostratigraphy, thickness, and petrophysical evaluation of the Woodford Shale, Arkoma Basin, Oklahoma. Master's thesis, Oklahoma State University, 84 p.

Blackwell, D.D., Steele, J.L., 1989. Heat Flow and Geothermal Potential of Kansas, in Geophysics in Kansas: Kansas Geological Survey, Bulletin 226, Steeples, D.W. (ed), pp. 267-295.

Boulanouar, A., Rahmouni, A., Boukalouch, M., Samaouali, A., Géraud, Y., Harnafi, M., Sebbani, J., 2013. Determination of Thermal Conductivity and Porosity of Building Stone from Ultrasonic Velocity Measurements, Geomaterials, 2013, 3, pp. 138-144.

Bristol, H.M., and Buschbach, T.C., 1973. Ordovician Galena Group (Trenton) of Illinois - Structure and oil fields. Illinois State Geological Survey, Illinois Petroleum 99, 38 p.

Broadhead, R.F., 2010. The Woodford Shale in southeastern New Mexico: distribution and source rock characteristics. New Mexico Geology, v. 32, pp. 79-90.

Broadhead, R.F., and Gillard, L., 2007. The Barnett shale in southeastern New Mexico: Distribution, thickness, and source rock characterization. New Mexico Bureau of Geology and Mineral Resources, Open-File Report 502, 56 p.

Bruner, K.R., and Smosna, R., 2011. A comparative study of the Mississippian Barnett Shale, Fort Worth Basin, and Devonian Marcellus Shale, Appalachian Basin. National Energy Technology Laboratory Report, DOE/NETL-2011/1478.

Cardott, B.J., 2012. Thermal maturity of Woodford Shale gas and oil plays, Oklahoma, USA, International Journal of Coal Geology, doi:10.1016/j.coal.2012.06.004

Cardott, B.J., and Lambert, M.W., 1985. Thermal maturation by vitrinite reflectance of Woodford Shale, Anadarko Basin, Oklahoma. American Association of Petroleum Geologists Bulletin, v. 69, pp. 1982-1998.

Carlson, C.G., 1982. Structure map on top of the Cretaceous Pierre Formation in North Dakota. North Dakota Geological Survey, Miscellaneous Map No. 23.

Castagna, J.P., Batzle, M.L., Eastwood, R.L., 1985. Relationships Between Compressional-Wave and Shear-Wave Velocities in Elastic Silicate Rocks, Geophysics Vol. 50, No. 4, pp. 571-581.

Catacosinos, P.A., and Daniels, P.A., Jr., 1991, Stratigraphy of middle Proterozoic to Middle Ordovician formations of the Michigan basin. Geological Society of America Special Paper 256, pp. 53-72.

Catacosinos, P.A., Harrison, W.B., III, and Daniels, P.A., Jr., 1991. Structure, stratigraphy, and petroleum geology of the Michigan Basin, Chapter 30, in Leighton, M.W., Kolata D.R., Oltz, D.F., and Eidel, J.J., eds., Interior cratonic basins: American Association of Petroleum Geologists Memoir 51, pp. 561-601.

Charlier, R., Collin, F., Pardoen, B., Talandier, J., Radu J.-P., Gerard, P., 2013. An Unsaturated Hydro-Mechanical Modelling of Two In-Situ Experiments in Callovo-Oxfordian Argillite, Engineering Geology, 165, pp. 46–63.

Chatzis, I., Kuntamukkula, M.S., Morrow, N.R., 1988. Effect of Capillary Number on the Microstructure of Residual Oil in Strongly Water-Wet Sandstones, SPE Reservoir Engineering, pp. 902-912.

CNX/GTI, 2008. New Albany Shale RVSP, New Albany Shale Gas Project, RVSP Seismic Project Report.

Coleman, J.L, Jr., and Cahan, S.M., 2012. Preliminary catalog of the sedimentary basins of the United States. U.S. Geological Survey Open-File Report 2012-1111, 27 p.

Collinson, C., Sargent, M. L., and Jennings, J. R., 1988, Chapter 14: Illinois Basin region, in Sloss, L. L., ed., The Geology of North America, v. D-2, Sedimentary Cover-North American Craton: U.S.: Decade of North American Geology: Geological Society of America, pp. 383-426.

Comer, J.B., 1991. Stratigraphic analysis of the Upper Devonian Woodford Formation Permian Basin West Texas and Southeastern New Mexico. The University of Texas at Austin, Bureau of Economic Geology Report of Investigations No. 201, 63 p.

Condon, S.M., 2000. Stratigraphic framework of Lower and Upper Cretaceous rocks in central and eastern Montana. U.S Geological Survey Digital Data Series DDS-57, 12 p, 23 plates.

Cosenza, P., Robinet, J.C., Prêt, D., Huret, E., Fleury, M., Géraud, Y., Lebon, P., Villiéras, F., Zamora, M., 2014. Indirect Estimation of the Clay Content of Clay-Rocks Using Acoustic Measurements: New Insights from the Montiers-Sur-Saulx Deep Borehole (Meuse, France), Marine and Petroleum Geology, 53, pp. 117-132.

Cuadros, J., 2008. Clay as sealing material in nuclear waste repositories. Geology Today, v. 24, p. 99-103.

Davies, P.B., 1991. Evaluation of the Role of Threshold Pressure in Controlling Flow of Waste-Generated Gas into Bedded Salt at the Waste Isolation Pilot Plant, Sandia Report, SAND90–3246, UC–721, 44 p.

Dechesne, M., Raynolds, R.G., Barkmann, P.E., and Johnson, K.R., 2011. Notes on the Denver Basin geologic maps: Bedrock geology, structure, and isopach maps of the Upper Cretaceous to Paleogene strata between Greeley and Colorado Springs, Colorado. Colorado Geological Survey, 35 p.

Delahaye, C.H., Alonso, E.E., 1999. Modeling of Gas Migration in Clay, MECOM 99, Mendoza, Mecánica Computacional Volume XIX. Number 3. Solid Mechanics, 12 p.

Delay, J., Conil, N., de La Vaissière, R. Meuse/Haute-Marne, 2011. Underground Research Center – Technologies and Techniques for Studying Gas Flow and Thermal Properties of an Indurated Clay-Rock, i-DUST 2010, 03001, DOI: 10.1051/idust/201103001.

Denson, N.M., Gibson, M.L., and Sims, G.L., 1993a. Geologic and structure map, with contours on top of the Pierre Shale, for the north half of the Powder River Basin, southeastern Montana and northeastern Wyoming. U.S. Geological Survey Miscellaneous Investigations Series Map I-2343-A.

Denson, N.M., Gibson, M.L., and Sims, G.L., 1993b. Geologic and structure map, with contours on top of the Pierre Shale, for the south half of the Powder River Basin, northeastern Wyoming. U.S. Geological Survey Miscellaneous Investigations Series Map I-2343-B.

Denson, N.M., Gibson, M.L., and Sims, G.L., 1993c. Geologic map showing thickness of the Upper Cretaceous Pierre Shale in the north half of the Powder River Basin, southeastern Montana and northeastern Wyoming. U.S. Geological Survey Miscellaneous Investigations Series Map I-2380-A.

Denson, N.M., Gibson, M.L., and Sims, G.L., 1993d. Geologic map showing thickness of the Upper Cretaceous Pierre Shale in the south half of the Powder River Basin, northeastern Wyoming and adjacent areas. U.S. Geological Survey Miscellaneous Investigations Series Map I-2380-B.

Dicken, C.L., Pimley, S.G., and Cannon, W.F., 2001, Precambrian basement map of the northern midcontinent, U.S.A. -- A digital representation of the 1990 P.K. Sims map: U.S. Geological Survey Open-File Report 01-021, available online only.

Dobson, P., 2011. Survey of clay/shale formations in the US. In: FY11 Report on Unsaturated Flow and Transport, FCRD-USED-2011-000296.

Dobson, P., 2012. Status of Shale Geology: Information on Extent, Thickness and Depth of Shale Deposits, FCRD-UFD-2012-000296.

Dobson, P., and Houseworth, J., 2013. Inventory of shale formations in the US including geologic, hydrological, and mechanical characteristics, FCRD-UFD-2014-000513.

Dobson P., and J. Houseworth, 2014, Inventory of Shale Formations in the US, Including Geologic, Geochemical, Hydrological, Mechanical, and Thermal Characteristics, FCRD-UFD-2014-000512.

Dubiel, R.F., 2003. Geology, depositional models, and oil and gas assessment of the Green River Total Petroleum System, Uinta-Piceance Province, Eastern Utah and Western Colorado, Chapter 5 of Petroleum systems and geologic assessment of oil and gas in the Uinta-Piceance Province, Utah and Colorado, USGS Uinta-Piceance Assessment Team, U.S. Geological Survey Digital Data Series DDS-69-B. http://pubs.usgs.gov/dds/dds-069/dds-069-b/REPORTS/Chapter_5.pdf

Dullien, F.A.L., Lai, F.S.Y., Macdonald, I.F., 1986. Hydraulic Continuity of Residual Wetting Phase in Porous Media, Journal of Colloid and Interface Science, Vol. 109, No, 1, pp. 201-218.

Eastwood, R.L., Castagna, J.P.,1983. Basis for Interpretation of Ratios in Complex Lithologies, Sot. Prof. Well Log Analysts 24th Annual Logging Symp.EIA (Energy Information Administration), 2010, Eagle Ford Shale Play, Western Gulf Basin, South Texas. Map date May 29, 2010. http://www.eia.gov/oil_gas/rpd/shaleusa9.pdf

Ebeniro, J., Wilson, C. R., and Dorman, J., 1983. Propagation of dispersed compressional and Rayleigh waves on the Texas coastal plain: Geophysics. 48, 27-35.

EIA (Energy Information Administration), 2010. http://www.eia.gov/oil_gas/rpd/shaleusa9.pdf. Map date: May 29, 2010.

EIA (Energy Information Administration). 2011a. http://www.eia.gov/pub/oil_gas/natural_gas/analysis_publications/maps/maps.htm

EIA (Energy Information Administration), 2011b. Review of Emerging Resources: U.S. Shale Gas and Shale Oil Plays. www.eia.gov/analysis/studies/usshalegas/pdf/usshaleplays.pdf

Engelder, T., 2011. Analogue study of shale cap rock barrier integrity. Report for the Nuclear Waste Management Organization, NWMO DGR-TR-2011-23, 108 p.

Erenpreiss, M.S., Wickstrom, L.H., Perry C.J., Riley, R.A., Martin, D.R., and others, 2011. Regional organic-thickness map of the Marcellus Shale with additional organic-rich shale beds in the Hamilton Group included for New York, Pennsylvania, and West Virginia. Ohio Department of Natural Resources, Division of Geological Survey, scale 1 inch equals 52 miles.

Ettensohn, F.R., 2008. The Appalachian foreland basin in Eastern United States. In: Miall, A.D. (ed.) The Sedimentary Basins of the United States and Canada, Vol. 5, Sedimentary Basins of the World. Elsevier, Amsterdam, pp. 105-179.

Fuchs, S., Förster, A., 2013. Well-Log Based Prediction of Thermal Conductivity of Sedimentary Successions: A Case Study from the North German Basin, Geophys. J. Int., doi: 10.1093/gji/ggt382.

Gale, J.F.W., and Holder, J., 2010. Natural fractures in some US shales and their importance for gas production. In: Vining, B.A., and Pickering, S.C., eds., Petroleum Geology: From Mature Basins to New Frontiers. Proceedings of the 7th Petroleum Geology Conference, pp. 1131-1140.

Garitte, B., Gens, A., Vaunat J., Armand, G., 2012. Thermal Conductivity of Argillaceous Rocks: Determination Methodology Using In Situ Heating Tests, Rock Mech Rock Eng, 47, pp. 111–129.

Gens, A., Vaunat, J., Garitte, B., Wileveau, Y., 2007. In Situ Behaviour of a Stiff Layered Clay Subject to Thermal Loading: Observations and Interpretation, Géotechnique, 57, No. 2, pp. 207–228.

Gerhard, L.C., Anderson, S.B., Lefever, J.A. and Carlson, C.G., 1982. Geological development, origin, and energy mineral resources of Williston Basin, North Dakota. American Association of Petroleum Geologists Bulletin v. 66, pp. 989-1020.

Gonzales, S., and Johnson, K.S., 1985. Shales and other argillaceous strata in the United States. Oak Ridge National Laboratory report 84-64794, 594 p.

Goto, S., Matsubayashi, O., 2009. Relations between the thermal properties and porosity of sediments in the eastern flank of the Juan de Fuca Ridge, Earth Planets Space, 61, pp. 863–870.

Gray, J.D., Struble, R.A., Carlton, R.W., Hodges, D.A., Honeycutt, F.M., Kingsbury, R.H., Knapp, N.F., Majchszak, F.L., and Stith, D.A., 1982. An integrated study of the Devonian-age black shales in eastern Ohio. Technical Information Center, US Department of Energy, DOE/ET/12131-1399.

Hamilton, E.L., 1979. VP/VS and Poisson's Ratios in Marine Sediments and Rocks, J. Acoust. Soc. Am., 66, pp. 1093-I 101.

Hammes, U., Hamlin, H.S., and Ewing, T.E., 2011. Geologic analysis of the Upper Jurassic Haynesville Shale in east Texas and west Louisiana. AAPG Bulletin, v. 95, no. 10, pp. 1643-1666.

Han, D-H, Nur, A., Morgan, D., 1986. Effects of Porosity and Clay Content on Wave Velocities in Sandstones, Geophysics, Vol. 51. No. 11, pp. 2093-2107.

Harbor, R.L., 2011. Facies characterization and stratigraphic architecture of organic-rich Mudrocks, Upper Cretaceous Eagle Ford Formation, South Texas. M.S. Thesis, University of Texas, Austin, 184 p.

Hardage, B.A., Alkin, E., Backus, M.W., DeAngelo, M.V., Sava, D., Wagner, D., Graebner, R.J., 2013. Evaluation of Fracture Systems and Stress Fields Within the Marcellus Shale and Utica Shale and Characterization of Associated Water-Disposal Reservoirs: Appalachian Basin, Final Report to RPSEA, RPSEA Subcontract: 08122-55.

Hasenmueller, N.R., and Comer, J.B., eds., 1994. Gas potential of the New Albany Shale (Devonian and Mississippian) in the Illinois Basin, Gas Research Institute Technical Report GRI-92/0391.

Hasenmueller, N.R., and Comer, J.B., eds., 2000. GIS compilation of gas potential of the New Albany Shale in the Illinois Basin, Gas Research Institute Technical Report GRI-00/0068.

Higley, D.K. and Cox, D.O., 2007. Oil and gas exploration and development along the front range in the Denver Basin of Colorado, Nebraska, and Wyoming, in Higley, D.K., compiler, Petroleum systems and assessment of undiscovered oil and gas in the Denver Basin Province, Colorado, Kansas, Nebraska, South Dakota, and Wyoming-USGS Province 39: U.S. Geological Survey Digital Data Series DDS-69-P, ch. 2, 41 p. http://pubs.usgs.gov/dds/dds-069/dds-069-p/REPORTS/69_P_CH_2.pdf

Horseman, S.T., 2001. Gas Migration through Indurated Clays (Mudrocks). In: Gas Generation and Migration in Radioactive Waste Disposal. Proc. of the NEA Workshop in Reims 2000, France.

Horsrud, P., 2001. Estimating Mechanical Properties of Shale From Empirical Correlations, SPE Drilling & Completion.

Hosford Scheirer, A., 2013. The three-dimensional geologic model used for the 2003 National Oil and Gas Assessment of the San Joaquin Basin Province, California: Chapter 7 in Petroleum systems and geologic assessment of oil and gas in the San Joaquin Basin Province, California, U.S. Geological Survey Professional Paper 1713-7, 81 p.

Hovorka, S.D., Romero, M.L., Warne, A.G., Ambrose, W.A., Tremblay, T.A., Treviño, R.H., and Sasson, D., 2003. Technical summary: Optimal geological environments for carbon dioxide disposal in brine formations (saline aquifers) in the United States. Gulf Coast Carbon Center, University of Texas, Bureau of Economic Geology, http://www.beg.utexas.edu/gccc/finalreport.pdf

Ingram G.M., Urai, J.L. and Naylor, M.A., 1997. Sealing Processes and Top Seal Assessment. In: Hydrocarbon Seals: Importance for Petroleum Exploration and Production (eds. P. Molle-Pedersen and A.G. Koesler) Norwegian Petroleum Society, Special Publication 7, Elsevier, Amsterdam, 165-174.

Ingram, G.W., Urai, J.L., 1999. Top-seal leakage through faults and fractures: the role of mudrock properties, from." Aplin, A. C., Fleet, A. J., Macquaker, J. H. S. (eds) Muds and Mudstones: Physical and Fluid Flow Properties. Geological Society, London, Special Publications, 158, 125-135.

Johnson, E.A., 2003. Geologic assessment of the Phosphoria Total Petroleum System, Uinta-Piceance Province, Utah and Colorado, Chapter 9 of Petroleum systems and geologic assessment of oil and gas in the Uinta-Piceance Province, Utah and Colorado, USGS Uinta-Piceance Assessment Team, U.S. Geological Survey Digital Data Series DDS-69-B, http://pubs.usgs.gov/dds/dds-069/dds-069-b/REPORTS/Chapter_9.pdf

Johnson, L., Marschall, P., Zuidema, P., Gribi, P., 2004. Effects of Post-Disposal Gas Generation in a Repository for Spent Fuel, High-Level Waste and Long-lived Intermediate Level Waste Sited in Opalinus Clay, Nagra, Technical Report 04-06, 184 p.

Johnson, R.C., Mercier, T.J., Brownfield, M.E. and Self, J.G., 2010. Assessment of in-place oil shale resources in the Eocene Green River Formation, Uinta Basin, Utah and Colorado: U.S. Geological Survey Digital Data Series DDS-69-BB, Ch. 1, 153 p. http://pubs.usgs.gov/dds/dds-069/dds-069-bb/REPORTS/69_BB_CH_1.pdf

Johnston, J.E., Christensen, N.I., 1995. Seismic anisotropy of shales, Journal Of Geophysical Research, Vol. 100, No. B4, pp. 5991-6003.

Kirschbaum, M.A., 2003. Geologic assessment of undiscovered oil and gas resources of the Mancos/Mowry Total Petroleum System, Uinta-Piceance Province, Utah and Colorado. Chapter 6 of Petroleum Systems and Geologic Assessment of Oil and Gas in the Uinta-Piceance Province, Utah

and Colorado, USGS Uinta-Piceance Assessment Team, U.S. Geological Survey Digital Data Series DDS-69-B, http://pubs.usgs.gov/dds/dds-069/dds-069-b/REPORTS/Chapter_6.pdf

Koerperich. E. A., 1979. Shear Wave Velocities Determined from Long and Short-Spaced Borehole Acoustic Devices: Sot. Petr. Eng., 8237.

Kolata, D.R., and Noger, M.C., 1990. Chapter 5: Tippecanoe I Subsequence Middle and Upper Ordovician Series. In: Interior Cratonic Basins, M.W. Leighton, D.R. Kolata, D.F. Oltz, and J.J. Eider., eds. American Association of Petroleum Geologists Memoir 51, pp. 89-99.

Kowallis, B.J., Jones, L.E.A., Wang, H.F., 1984. Velocity-Porosity-Clay Content Systematics of Poorly Consolidated Sandstones, Journal of Geophysical Research, Vol. 89, No. B12, pp. 10355-10364.

Lagoe, M.B., 1982. Stratigraphy and paleoenvironments of the Monterey Formation and associated rocks, Cuyama Basin, California. Ph.D. thesis, Stanford University, 216 p.

Lagoe, M.B., 1984. Paleogeography of Monterey Formation, Cuyama Basin, California. American Association of Petroleum Geologists Bulletin, v. 68, pp. 610-627.

Lash, C. E. 1980, Shear waves, multiple reflections, and converted waves found by a deep vertical wave test (vertical seismic profiling): Geophysics, 45, pp. 1373-1411.

Lash, G.G., and Engelder, T., 2011. Thickness trends and sequence stratigraphy of the Middle Devonian Marcellus Formation, Appalachian Basin: Implications for Acadian foreland basin evolution. American Association of Petroleum Geologists Bulletin v. 95, pp. 61-103.

LeFever, J.A., 2008. Structural contour and isopach maps of the Bakken Formation in North Dakota. North Dakota Geological Survey Geologic Investigations No. 59, 5 sheets.

LeFever, J.A., LeFever, R.D., and Nordeng, S.H., 2012. Extending the Bakken. Williston Basin Petroleum Conference.

Lewis, B.D., and Hotchkiss, W.R., 1981. Thickness, percent sand, and configuration of shallow hydrogeologic units in the Powder River Basin, Montana and Wyoming. U.S. Geological Survey Miscellaneous Investigations Series, Map I-1317.

Li, P., Ratchford, M.E., and Jarvie, D.M., 2010. Geochemistry and thermal maturation analysis of the Fayetteville Shale and Chattanooga Shale in the western Arkoma Basin of Arkansas. Arkansas Geological Survey Information Circular 40, 191 p.

Li, X., Bernier, F., Vietor, T., Lebon, P. (2007). TIMODAZ (Contract Number: FI6W-CT-036449), Deliverable (No: 2). European Commission under the Sixth Framework Programme Euratom Research and Training Programme on Nuclear Energy (2002-2006), 104 p.

Lingle, R., Jones, A. H. (1977). Comparison of Log and Laboratory Measured P-Wave and S-Wave Velocities: Trans., Soc. Prof. Well Log Analysts, 18th Annual Logging Symp.

Liu, E. (1997). Crosshole Channel Wave Analysis from Antrim Shale Gas Play, Michigan Basin, EAGE Conference and Technical Exhibition, 59th annual meeting 1997, European Association of Petroleum Geoscientists.

Liu, X. (1994). Nonlinear Elasticity, Seismic Anisotropy, and Petrophysical Properties of Reservoir Rocks, Ph.D. thesis, Stanford University.

Macfarlane, P.A., Combes, J., Turbek, S., and Kirshen, D., 1993. Shallow subsurface bedrock geology and hydrostratigraphy of southwestern Kansas. Kansas Geological Survey, Open-File Report 93-1a. (plates updated in 2010 by J.J. Woods).

Magoon, L.B., Lillis, P.G., and Peters, K.E., 2009. Petroleum systems used to determine the assessment units in the San Joaquin Basin Province, California: Chapter 8 in Petroleum systems and geologic

assessment of oil and gas in the San Joaquin Basin Province, California, U.S. Geological Survey Professional Paper 1713-8, 65 p.

Marschall, P., Horseman, S., Gimmi, T. (2005). Characterisation of Gas Transport Properties of the Opalinus Clay, a Potential Host Rock Formation for Radioactive Waste Disposal, Oil & Gas Science and Technology – Rev. IFP, Vol. 60, No. 1, pp. 121-139.

Mastalerz, M., Schimmelmann, A., Drobniak, A., and Chen, Y., 2013. Porosity of Devonian and Mississippian New Albany Shale across a maturation gradient: Insights from organic petrology, gas adsorption, and mercury intrusion. American Association of Petroleum Geologists Bulletin, v. 97 (10), 1621-1643.

Matray, J.M., Savoye, S., Cabrera, J. (2007). Desaturation and Structure Relationships around Drifts Excavated in the Well-Compacted Tournemire's Argillite (Aveyron, France), Engineering Geology, 90, pp. 1–16.

Matthews, R.D., 1993. Review and Revision of the Devonian-Mississippian Stratigraphy in the Michigan Basin: Chapter D in Petroleum Geology of the Devonian and Mississippian Black Shale of Eastern North America, J.B. Roen and R. C. Kepferle, eds., U.S. Geological Survey Bulletin 1909, D1-D85.

McCormick, K., 2010. Precambrian Basement Terrane of South Dakota, Bulletin 41, Department of Environmental and Natural Resources, University of South Dakota. 37p.

McDonal, F.J., Angona, F.A., Mills, R.I., Sengbush, R.L., Van Nostrand, R.G., White, J.E. (1958). Attenuation Of Shear And Compressional Waves In Pierre Shale, Geophysics, Vol. XXIII, No. 3, pp. 421-439.

Mercier, T.J., and Johnson, R.C., 2012. Isopach and isoresource maps for oil shale deposits in the Eocene Green River Formation for the combined Uinta and Piceance Basins, Utah and Colorado: U.S. Geological Survey Scientific Investigations Report 2012-5076, 85 p., 1 pl., http://pubs.usgs.gov/sir/2012/5076/SIR12-5076.pdf

Mercier, T.J., Gunther, G.L., and Skinner, C.C., 2010a. The GIS project for the geologic assessment of in-place oil shale resources of the Eocene Green River Formation, Greater Green River Basin, Wyoming, Colorado, and Utah, U.S. Geological Survey Oil Shale Assessment Team, U.S. Geological Survey Digital Data Series DDS-69-DD, http://pubs.usgs.gov/dds/dds-069/dds-069-dd/REPORTS/69_DD_CH_3.pdf

Mercier, T.J., Gunther, G.L., and Skinner, C.C., 2010b. The GIS project for the geologic assessment of in-place oil shale resources of the Piceance Basin, Colorado. In: Oil shale and nahcolite resources of the Piceance Basin, Colorado, U.S. Geological Survey Oil Shale Assessment Team, U.S. Geological Survey Digital Data Series DDS-69-Y, http://pubs.usgs.gov/dds/dds-069/dds-069-y/REPORTS/69_Y_CH_4.pdf

Mercier, T.J., Gunther, G.L., and Skinner, C.C., 2010c. The GIS project for the geologic assessment of in-place oil shale resources of the Uinta Basin, Utah and Colorado. In: Oil shale resources of the Uinta Basin, Utah and Colorado, U.S. Geological Survey Oil Shale Assessment Team, U.S. Geological Survey Digital Data Series DDS-69-BB, http://pubs.usgs.gov/dds/dds-069/dds-069-bb/REPORTS/69_BB_CH_4.pdf

Merewether, E.A., Sharps, J.A., Gill, J.R., and Cooley, M.E., 1973. Shale, mudstone, and claystone as potential host rocks for underground emplacement of waste. U.S. Geological Survey Open-File Report 73-184, 44 p.

Midttømme, K., Roaldset, E. (1999). Thermal Conductivity of Sedimentary Rocks: Uncertainties in Measurement and Modelling, in Aplin, A. C., Fleet, A.J., Macquaker, J. H. S. (eds), Muds and

Mudstones: Physical and Fluid Flow Properties, Geological Society, London, Special Publications, 158, pp. 45-60.

Midttømme, K., Roaldset, E., Aagaard, P. (1997). Thermal Conductivities of Argillaceous Sediments, in McCann, D. M., Eddleston, M., Fenning, P. J. & Reeves, G. M. (eds), 1997, Modern Geophysics in Engineering Geology, Geological Society Engineering Geology Special Publication No. 12, pp. 355-363.

Midttømme, K., Roaldset, E., Aagaard, P. (1998). Thermal Conductivity of Selected Claystones and Mudstones from England, Clay Minerals, 33, pp. 131-145.

Montaut, A. 2012. Detection and Quantification of Rock Physics Properties for Improved Hydraulic Fracturing in Hydrocarbon-Bearing Shales, Master of Science in Engineering Thesis, The University of Texas at Austin.

Montgomery, S.L., Jarvie, D.M., Bowker, K.A., and Pollastro, R.M., 2005. Mississippian Barnett Shale, Fort Worth Basin, north-central Texas: Gas-shale play with multi-trillion cubic foot potential. American Association of Petroleum Geologists Bulletin, v. 89 (2), 155-175.

Nunn, J.A. 2012. Burial and Thermal History of the Haynesville Shale: Implications for Overpressure, Gas Generation, and Natural Hydrofracture, GCAGS Journal, v. 1 (2012), p. 81–96.

Ohio Department of Natural Resources, 2013a. Division of Geological Survey, Map of maximum TOC for Upper Ordovician Shales. http://geosurvey.ohiodnr.gov/portals/geosurvey/Energy/Utica/Ordov-Shale_TOC-Max_03-2013.pdf

Ohio Department of Natural Resources, 2013b, Division of Geological Survey, Map of Calculated Ro for Upper Ordovician Shales. http://geosurvey.ohiodnr.gov/portals/geosurvey/Energy/Utica/Ordov-Shale_Ro-Average_03-2013.pdf

Party, J.M., Wipf, R.A., Byl, J.M., Lawton, J., and Hill, J.M., 2008. Woodford Shale, Ardmore Basin, Oklahoma: A developing shale play. Oklahoma Geological Survey, Gas Shales Workshop, 51 slides. http://www.ogs.ou.edu/pdf/GSPartyS.pdf.

Pashin, J.C., 2008. Gas shale potential of Alabama. 2008 International Coalbed and Shale Gas Symposium, Paper 808.

Patchen, D.G., Hickman, J.B., Harris, D.C., Drahovzal, J.A., Lake, P.D., Smith, L.B., Nyahay, R., Schulze, R., Riley, R.A., Baranoski, M.T., Wickstrom, L.H., Laughrey, C.D., Kostelnik, J., Harper, J.A., Avary, K.L., Bocan, J., Hohn, M.E., and McDowell, R., 2006. A Geologic play book for Trenton-Black River Appalachian Basin exploration. DOE Award DE-FC26-03NT41856, http://www.wvgs.wvnet.edu/www/tbr/docs/41856R06.pdf

Pawlewicz, M.J. and Hatch, J.R., 2007. Petroleum assessment of the Chattanooga Shale/Floyd Shale - Paleozoic Total Petroleum System, Black Warrior Basin, Alabama and Mississippi, in Hatch, J.R., and Pawlewicz, J.J., compilers, Geologic assessment of undiscovered oil and gas resources of the Black Warrior Basin Province, Alabama and Mississippi. U.S. Geological Survey Digital Data Series DDS-69-I, chap. 3, 23 p. http://pubs.usgs.gov/dds/dds-069/dds-069-i/REPORTS/69_I_CH_3.pdf

Perry, F., Kelley, R., and Woldegabriel, G., 2011. Regional geology and tectonic hazards - FY 2011 Status Report. FCRD-USED-2012-000002.

Perry, F.V., Dobson, P.F., and Kelley, R.E., 2013. Assessment of alternative host-rock distribution in the U.S. using GIS. Proceedings, International High-Level Waste Management Conference 2013, Albuquerque, N.M., April 28-May 2, 2013, American Nuclear Society, pp. 85-93.

Perry, F.V., Kelley, R., and Dobson, P., 2012. Regional geology: Distribution of alternative host rock formations and description of siting factors that potentially influence siting and site characterization. FCRD-USED-2012-27013.

Perry, F.V., Kelley, R.E., Dobson, P.F., and Houseworth, J.E., 2014. Regional geology: A GIS database for alternative host rocks and potential siting guidelines. FCRD-UFD-2014-000068.

Peterson, J.A., 1984. Geology and hydrology of the Madison Limestone and associated rocks in parts of Montana, Nebraska, North Dakota, South Dakota, and Wyoming. U.S. Geological Survey Professional Paper 1273A, 34 p.

Piña-Diaz, Y.E. (2011). Thermo-Hydro-Mechanical Behaviour of Ypresian Clay, Dept. de Enginyeria del Terreny, Cartogràfica i Geofisica E.T.S. Enginyers de Camins, Canals i Ports, Universitat Politècnica de Catalunya.

Pitman, J.K., 2008. Reservoirs and Petroleum Systems of the Gulf Coast. AAPG Datapages GIS Open-File website. http://www.datapages.com/AssociatedWebsites/GISOpenFiles/ReservoirsandPetroleumSystemsoftheGulfCoast.aspx

Pollastro, R.M., Jarvie, D.M., Hill, R.J., and Adams, C.W., 2007. Geologic framework of the Mississippian Barnett Shale, Barnett-Paleozoic total petroleum system, Bend Arch-Fort Worth Basin, Texas. American Association of Petroleum Geologists Bulletin v. 91, pp. 405-436.

Pollastro, R.M., Roberts, L.N.R., Cook, T.A. and Lewan, M.D., 2008. Assessment of undiscovered technically recoverable oil and gas resources of the Bakken Formation, Williston Basin, Montana and North Dakota, 2008: U.S. Geological Survey Open-File Report 2008-1353, 3 sheets.

Ratchford, M.E., Bridges, L.C., Jordan, D., Dow, W.G., Colbert, A., and Jarvie, D.M., 2006. Organic geochemistry and thermal maturation analysis within the Fayetteville Shale study area - Eastern Arkoma Basin and Mississippi embayment regions, Arkansas. Arkansas Geological Survey Information Circular 37, DFF-OG-FS-EAB/ME 008, 12 p.

Rechard, R.P., Perry, F.V., and Cotton, T.A., 2011. Site selection, characterization, and research and development for spent nuclear fuel and high-level waste disposal. International High-Level Radioactive Waste Management Conference 2001, Albuquerque, NM, April 10-14, 2011, American Nuclear Society, pp. 174-181.

Reed, J.C., 1993, Map of the Precambrian Rocks of the Conterminous United States and Some Adjacent Parts of Canada, in Reed, J.C., and others eds., Precambrian; Conterminous U.S., Geological Society of America, The Geology of North America, The Decade of North American Geology (DNAG), v. C-2, pl. 1.

Repetski, J.E., Ryder, R.T., Weary, D.J., Harris, A.G., and Trippi, M.H., 2008. Thermal maturity patterns (CAI and %Ro) in Upper Ordovician and Devonian rocks of the Appalachian Basin: A major revision of USGS Map I-917-E using new subsurface collections. USGS Scientific Investigations Map 3006.

Ridgley, J.L., Condon, S.M., and Hatch, J.R., 2013. Geology and oil and gas assessment of the Mancos-Menefee Composite Total Petroleum System, San Juan Basin, New Mexico and Colorado, chap. 4 of U.S. Geological Survey San Juan Basin Assessment Team, Total petroleum systems and geologic assessment of undiscovered oil and gas resources in the San Juan Basin Province, exclusive of Paleozoic rocks, New Mexico and Colorado. U.S. Geological Survey Digital Data Series 69-F, p. 1-97.

Rottmann, K., 2000. Isopach map of Woodford Shale in Oklahoma and Texas Panhandle. In: Hunton play in Oklahoma (including northeast Texas panhandle): Oklahoma Geological Survey Special Publication 2000-2, plate 2.

Ruppel, S.C., Jones, R.H., Breton, C.L, and Kane, J.A., 2005. Preparation of maps depicting geothermal gradient and Precambrian structure in the Permian Basin: unpublished contract report prepared for the U. S. Geological Survey, 21 p. plus data CD.

Ryder, R.T., Burruss, R.C. and Hatch, J.R., 1998. Black shale source rocks and oil generation in the Cambrian and Ordovician of the central Appalachian Basin, USA. AAPG Bulletin 82, pp. 412-441.

Self, J.G., Ryder, R.T., Johnson, R.C., Brownfield, M.E., and Mercier, T.J., 2011. Stratigraphic cross sections of the Eocene Green River Formation in the Green River Basin, southwestern Wyoming, northwestern Colorado, and northeastern Utah, in U.S. Geological Survey Oil Shale Assessment Team, ed., Oil shale resources in the Eocene Green River Formation, Greater Green River Basin, Wyoming, Colorado, and Utah. U.S. Geological Survey Digital Data Series DDS-69-DD, chap. 5, 7 p., 24 plates.

Shurr, G.W., 1977. The Pierre Shale, Northern Great Plains; A potential isolation medium for radioactive waste. U.S. Geological Survey Open File Report 77-776, 27 p.

Sims, P.K., 1990. Precambrian basement map of the northern midcontinent, U.S.A. U.S. Geological Survey Miscellaneous Investigations Map I-1853-A, 1:1,000,000, with pamphlet, 9p.

Sims, P.K., Bankey, V., and Finn, C.A., 2001a, Precambrian basement map of Colorado—A geologic interpretation of an aeromagnetic anomaly map: U.S. Geological Survey Open-File Report 01–364, scale 1:1,000,000.

Sims, P.K., Finn, C.A., and Rystrom, V.L., 2001b, Preliminary Precambrian basement map of Wyoming showing geologic-geophysical domains: U.S. Geological Survey, 01–199, scale 1:1,000,000.

Sims, P.K., Lund, K., and E. Anderson, 2005. Precambrian Crystalline Basement Map of Idaho—An Interpretation Of Aeromagnetic Anomalies. Scientific Investigations Map 2884, U.S. Geological Survey.

Sims, P.K., O'Neill, J.M., Bankey, V., and Anderson, E., 2004, Precambrian basement geologic map of Montana—An interpretation of aeromagnetic anomalies: U.S. Geological Survey Scientific Investigations Map, scale 1:1,000,000.

Sims, P.K., Peterman, Z.E., Hildenbrand, T.G., and Mahan, Shannon, 1991, Precambrian basement map of the Trans-Hudson orogen and adjacent terranes, northern Great Plains, U.S.A.: U.S. Geological Survey Miscellaneous Investigations Series Map I-2214, scale 1:1,000,000.

Sims, P.K., Saltus, R.W., and E.D. Anderson, 2008. Precambrian Basement Structure Map of the Continental United States – An Interpretation of Geologic and Aeromagnetic Data. Scientific Investigations Map 3012, U.S. Geological Survey.

Smith, L.N., 1999. Structure contour map on the top of the Upper Cretaceous Pierre (Bearpaw) Shale, east-central Montana. Montana Bureau of Mines and Geology, Montana Ground-Water Assessment Open-File Report 13, Revision 1.1.

Sondhi, N. (2011). Petrophysical Characterization of Eagle Ford Shale, M.S. Thesis, University of Oklahoma.

Strapoc, D., Mastalerz, M., Schimmelmann, A., Drobniak, A., and Hassenmuller, N.R., 2010. Geochemical constraints on the origin and volume of gas in the New Albany Shale (Devonian-Mississippian), eastern Illinois Basin. American Association of Petroleum Geologists Bulletin Bulletin, v. 94 (11), 1713-1740.

Surles, M.A., Jr., 1987. Stratigraphy of the Eagle Ford Group (Upper Cretaceous) and its source-rock potential in the East Texas Basin. Baylor Geological Studies Bulletin No. 45, 57 p.

Sweetkind, D.S., Bova, S.C., Langenheim, V.E., Shumaker, L.E., and Scheirer, D.S., 2013. Digital tabulation of stratigraphic data from oil and gas wells in Cuyama Valley and surrounding areas, central California. U.S. Geological Survey Open-File Report 2013-1084, 44 p.

Sweetkind, D.S., Tennyson, M.E., Langenheim, V.E., and Shumaker, L.E., 2010. Digital tabulation of stratigraphic data from oil and gas wells in the Santa Maria Basin and surrounding areas, central California coast. U.S. Geological Survey Open-File Report 2010-1129, 11 p.

Swezey, C.S., 2008. Regional stratigraphy and petroleum systems of the Michigan Basin, North America. U.S. Geological Survey Scientific Investigations Map 2978, 1 sheet. http://pubs.usgs.gov/sim/2978/sim2978MichChart.pdf

Swezey, C.S., 2009. Regional stratigraphy and petroleum systems of the Illinois Basin, U.S.A. U.S. Geological Survey Scientific Investigations Map 3068, 1 sheet. http://pubs.usgs.gov/sim/3068/illinoisbasin.pdf

Thomas, L.K., Katz, D.L., Tek, M.R. (1968). Threshold Pressure Phenomena in Porous Media, Society of Petroleum Engineers Journal, Transactions, Vol. 243, pp. 174-184.

Thomas, W.A., 1988. The Black Warrior Basin. In: Sloss, L.L., ed., The Geology of North America, v. D-2, Sedimentary Cover-North American Craton: U.S.: Decade of North American Geology: Geological Society of America, pp. 471-492.

Tinjum, J.M., Benson, C.H., Blotz, L.R. (1997). Soil-Water Characteristic Curves for Compacted Clays, Journal of Geotechnical And Geoenvironmental Engineering, pp. 1060-1069.

Tosaya, C., Nur, A. (1982). Effects of Diagenesis and Clays on Compressional Velocities in Rocks, Geophysical Research Letters, Vol. 9, No. 1, pp. 5-8.

Tosaya, C.A. (1982). Acoustical Properties of Clay-Bearing Rocks, Ph.D. Dissertation, Stanford University.

USGS Southwestern Wyoming Province Assessment Team, 2005. The Southwestern Wyoming Province - Introduction to a geologic assessment of undiscovered oil and gas resources, U.S. Geological Survey Digital Data Series DDS-69-D, Chapter 2, 34 p. http://pubs.usgs.gov/dds/dds-069/dds-069-d/REPORTS/69_D_CH_2.pdf

USGS Uinta-Piceance Assessment Team, 2003. Petroleum systems and geologic assessment of oil and gas in the Uinta-Piceance Province, Utah and Colorado: U.S. Geological Survey Digital Data Series DDS-69-B, Ch. 2. http://pubs.usgs.gov/dds/dds-069/dds-069-b/REPORTS/Chapter_2.pdf

van Genuchten, M.T. (1980). A closed-form equation for predicting the hydraulic conductivity of unsaturated soils. Soil Science Society of America Journal, 44, 892-898.

Verma, S., Mutlu, O., Marfurt, K.J. (2013). Seismic modeling evaluation of fault illumination in the Woodford Shale, SEG Houston 2013 Annual Meeting.

Villar, M.V., Romero, F.J. (2012). Water Retention Curves of Opalinus Clay, Informes Técnicos Ciemat 1262, 33 p.

Waples, D.W., Tirsgaard, H. (2002). Changes in Matrix Thermal Conductivity of Clays and Claystones as a Function of Compaction, Petroleum Geoscience, Vol. 8 2002, pp. 365–370.

Waples, D.W., Waples, J.S. (2004). A Review and Evaluation of Specific Heat Capacities of Rocks, Minerals, and Subsurface Fluids. Part 1: Minerals and Nonporous Rocks, Natural Resources Research, Vol. 13, No. 2, pp. 97-122.

Whitmeyer, S.J. and Karlstrom, K.E. 2007. Tectonic model for the Proterozoic growth of North America. Geosphere, 3, p. 220–259, doi: 10.1130/GES00055.1.

Wileveau, Y., Rothfuchs, T. (2007). THM Behaviour of Host Rock (HE-D) Experiment: Study of Thermal Effects on Opalinus Clay, Mont Terri Project, Technical Report 2006-01.

Williams, L.A., 1982. Lithology of the Monterey Formation (Miocene) in the San Joaquin Valley of California. In: Williams, L.A., and Graham, S.A., eds., Monterey Formation and associated coarse clastic rocks, central San Joaquin Basin, California. Pacific Section, Society of Economic Paleontologists and Mineralogists Annual Field Trip Guidebook, pp. 17-35.

Willman, H.B., Atherton, W., Buschbach, T.C., Collinson, C., Frye, J.C., Hopkins, M.E., and Lineback, J.A., 1975. Handbook of Illinois stratigraphy, Illinois Geological Survey Bulletin 95, 261 p.

Wylie, A.S., and Wood, J.R., 2005. Historical production trends suggest remaining upside for E&D in Michigan. Oil and Gas Journal, vol. 103, issue 23.

Wylie, A.S., Jr., and Wood, J.R., 2004. Map views of the producing formations in Michigan, the Michigan Basin, U.S. American Association of Petroleum Geologists Eastern Section Meeting, Columbus, OH, Oct. 3-6, 2004.

Yang, Y., Aplin, A.C. (2004). Definition and practical application of mudstone porosity–effective stress relationships, Petroleum Geoscience, Vol. 10, pp. 153–162.

Yang, Y., Aplin, A.C. (2010). A permeability–porosity relationship for mudstones, Marine and Petroleum Geology, 27, 1692–1697.

Zhao, H., Givens, N.B., and Curtis, B., 2007. Thermal maturity of the Barnett Shale determined from well-log analysis. American Association of Petroleum Geologists Bulletin, 94 (4), 535-549.

Appendix A

Regional Geology: A GIS Database for Alternative Host Rocks and Potential Siting Guidelines

Fuel Cycle Research & Development

Prepared for U.S. Department of Energy
Used Fuel Disposition Campaign
Frank V. Perry
Richard E. Kelley
Suzanne M. Birdsell
Los Alamos National Laboratory
Patrick F. Dobson
James E. Houseworth
Lawrence Berkeley National Laboratory
January 2014
FCRD-UFD-2014-000068
Los Alamos Unlimited Release LA-UR-14-20368

DISCLAIMER

This information was prepared as an account of work sponsored by an agency of the U.S. Government. Neither the U.S. Government nor any agency thereof, nor any of their employees, makes any warranty, expressed or implied, or assumes any legal liability or responsibility for the accuracy, completeness, or usefulness, of any information, apparatus, product, or process disclosed, or represents that its use would not infringe privately owned rights. References herein to any specific commercial product, process, or service by trade name, trade mark, manufacturer, or otherwise, does not necessarily constitute or imply its endorsement, recommendation, or favoring by the U.S. Government or any agency thereof. The views and opinions of authors expressed herein do not necessarily state or reflect those of the U.S. Government or any agency thereof.

CONTENTS

FIGURES

TABLES

ACRONYMS

AEC	Atomic Energy Commission
BRI	Brittleness Index
DEM	Digital Elevation Model
DOE	Department of Energy
EIA	Energy Information Administration
EPRI	Electrical Power Research Institute
FY	Fiscal Year
GAO	General Accounting Office; later named the Government Accountability Office
GIS	Geographic Information System
HLW	High-Level Waste
LANL	Los Alamos National Laboratory
LBNL	Lawrence Berkeley National Laboratory
MIT	Massachusetts Institute of Technology
NOAA	National Oceanic and Atmospheric Administration
NWMO	Nuclear Waste Management Organization (Canada)
NWPA	Nuclear Waste Policy Act
OCR	Overconsolidation Ratio
R&D	Research and Development
RMSE	Root-Mean-Square Error
SMU	Southern Methodist University
tcf	trillion cubic feet
TOC	Total Organic Carbon
UFDC	Used Fuel Disposition Campaign
UK	United Kingdom
UCS	Uniaxial Compressive Strength
UNF	Used Nuclear Fuel
US	United States
USGS	United States Geological Survey
WGS	World Geodetic System

REGIONAL GEOLOGY: A GIS DATABASE FOR ALTERNATIVE HOST ROCKS AND POTENTIAL SITING GUIDELINES

1. Introduction

The objective of this work package is to create a spatial database that integrates both geologic data for alternative host-rock formations and information that has been historically used for siting guidelines, both in the US and other countries. These two types of information are fundamental to the eventual siting of a geologic repository for HLW. The database will allow analysis of the relationships between potential siting guidelines and potential host-rock formations, providing information on the options available for HLW disposal in different regions of the US.

The Used Fuel Disposition Campaign (UFDC) has identified the need to build a spatial database to manage and analyze information concerning regional geology necessary to support the site screening and site evaluation decision points identified in the Used Fuel Disposition Campaign Disposal Research and Development Roadmap (Nutt, 2011). The UFDC is considering three alternative geologic host rocks for mined repositories (granitic, salt and clay-bearing rock) and crystalline (granitic) basement rock for deep borehole disposal (Nutt, 2011). Much of the work completed in FY12 and FY13 was focused on identifying available and suitable spatial data for these alternative host rocks, identifying data for siting factors that would influence siting decisions and exploring spatial analysis methods to visualize and analyze the relationships between geologic host rocks and potential siting guidelines that have been proposed in the past. This work makes no attempt to design a site screening tool to screen specific sites or to suggest a specific set of siting guidelines. Instead, the objective of this work is to create a tool to better understand the distribution of suitable alternative host rocks at the regional scale and the potential siting guidelines that could impact future siting screening and site selection activities and decision points. One of the future goals of this work is to make both the geologic and siting guidelines data available on the internet in an interactive format to provide an educational and outreach tool to communicate siting options within the US.

This report represents a significant update and expansion of Perry et al. (2012) while preserving all the data presented in that report. It completes the population of data into the GIS database for the geometry of salt formations and substantially adds to the population of data included for the geometry of shale formations. It fully incorporates the information provided in Dobson and Houseworth (2013), which is included in this report as Sections 4.3 and 5. These sections describe the geology and geometry of shale formations and the rock properties and in situ conditions of shale estimated from borehole seismic velocities. Finally, this report presents information on a number of potential siting guidelines that have been applied in previous US and other national programs, as well of examples of their relationships to alternative geologic media considered as disposal options in the UFDC (Section 6 of this report).

The primary objective of this report is to document progress in populating a GIS Database with information concerning the distribution of alternative host rock formations in the US, and of potential siting guidelines that could impact site screening and site evaluation. The primary geologic data includes the geometry (elevation variations) of the upper surfaces of formations, thickness variations, and the regional extent of potentially suitable host-rock formations. The depth to suitable host-rock formations is a potential siting guideline in itself. Other siting guidelines discussed in this report include population distribution and density, the distribution of oil and gas resources, topographic variations, seismic hazards and the location of tectonic features, depth to crystalline basement and the distribution of tectonic features within deep crystalline basement.

Data for salt deposits in all of the major sedimentary basins of the US has been obtained and populated into the GIS database. These data are presented in Section 4.2 of this report. Data for salt populated within the GIS database includes every major and most minor salt deposit in the US and are considered complete. The database for salt represents the most comprehensive and accurate compilation of salt formations in the US that has ever been created. Data for the distribution of salt units along the coast of the Gulf of Mexico, including the location and shape of individual salt domes, are included in the GIS database but have not yet been analyzed for depths to the top of individual salt domes. Data for a significant number of shale formations have been included in the GIS database and are presented in Section 4.3 of this report, from information provided by Dobson and Houseworth (2013).

In the two or three decades leading up to the mid-1980s, a large amount of thought and work was devoted to study of a variety of host rocks and geologic environments that could enable safe and practical storage of radioactive waste. A number of characteristics of host rocks and geological environments were generally agreed upon that would be suitable for safe disposal of high-level waste. Johnson and Gonzales (1978) summarized these characteristics with emphasis on disposal in salt, but they apply equally to disposal in shale or other bedded media.

Prefered dimensional and geometric characteristics of the host formations include:

- ***Suitable depth*** to insure isolation from the biosphere while still practicle to mine and construct a repository using feasible technologhy. A depth range of between 300-1000 meters is suggested as optimal with 1500 meters suggested as a practicle limit.
- ***Suitable Thickness and Extent*** to promote isolation of the waste and ability to choose optimal sites within a formation.
- ***Shallow dip of inclination of strata*** to enable design of horizontal tunnels over large subsurface areas. Steep dips or folding also indicate past deformation and complex structures that could compromise repository performance.
- ***Homogeneity of the storage host-rock storage horizon*** to simplify repository construction and fuller understanding of host rock enviroment.

A number of other factors discussed that characterize the regional geologic environment and the siting framework of host-rock formations include:

- ***Nature and extent of adjacent strata***
- ***Faulting and jointing, both regionally and associated with the host formation***
- ***Regional characteristics of seismicity, groundwater and mineral resources***

The goal of this work package is to capture these and other parameters both common and specific to alternative host rocks in an integrated geologic and siting guidelines database that can be used to analyze both primary geologic factors and siting factors that could impact future siting activities.

2. GIS Data Sources and Adequacy

Alternative geologic host rocks for the disposal of HLW have not been studied as part of DOE-sponsored R&D since passage of the Nuclear Waste Policy Act in 1987. Much of the original regional reconnaissance work to understand salt, shale and granitic rocks was conducted before the advent of the widespread use of geographical information systems (GIS). Therefore, the resulting data was not in digital format or stored in computer systems that would allow the types of spatial analysis that can be conducted today. These data (currently in the form of published maps and report figures) can now be recovered, and digitized and converted to an appropriate GIS format for spatial analysis and presentation. In addition, a large quantity of new data for alternative host formations (in particular shale) has become available in the past few years, much of it already in GIS format, that can be directly imported into a GIS database.

A GIS allows visualization and quantitative analysis of data layers and how the features represented by the data layers spatially interact. Data layers can represent any information of interest for repository siting and site characterization, including different types of geologic rock, geologic features and tectonic hazards, as well as cultural and political features including population distribution, transportation infrastructure, land ownership, land use, etc. Data utilized in a GIS may already exist in a digital form that can be readily imported into the GIS, or be in an "analog" format such as printed maps or figures that documented information from earlier disposition studies. These types of data can be digitized and rectified for incorporation into GIS.

A review of data sources indicates that currently available data are probably adequate to represent the distribution of suitable alternative host rock formations at the national and regional scale. A large amount of data has been gathered since at least the early 1960s by the USGS, the DOE and its predecessors, university researchers, state agencies and the oil and gas industry. More modern sources of data are often available as GIS formatted data and are readily imported into the GIS database. Older sources of data, including most of the previous regional survey work of potential host rocks supported by DOE in the 1970s and 1980s are not in GIS format and must be digitized and converted to a suitable GIS format (see Section 3 of this report).

A modern digital map of North America (Garrity and Soller, 2009) is available as a GIS "geodatabase" (http://pubs.usgs.gov/ds/424/) and is readily imported in the GIS to display crystalline plutonic and metamorphic (i.e., granitic) rocks or other potential host rocks exposed at the surface. Digital maps are also available for all states if a greater level of detail is needed at the regional scale (http://tin.er.usgs.gov/geology/state/). In some cases, older geological data, such as depth to crystalline basement rock, has been digitized for use in applications such as geothermal energy R&D and is available by contacting university research groups (http://smu.edu/geothermal/).

We are incorporating individual formation-level data for sedimentary rocks (salt and shale) at the basin scale. Data for salt and shale is inherently more difficult to acquire because it is largely subsurface data. Exposures at the surface are often poor or non-existent (as is always the case for salt, and often the case for shale) and therefore geologic map data has limited use. The challenge with these rocks is to identify formations that have suitable depth and thickness to host a mined repository. Subsurface information on depth and thickness is generally dependent on drilling data that is most often obtained by the oil and gas industry and is generally proprietary. Synthesis of drilling data to determine depth and thickness of formations on broad regional scales has been done in the past by state geological surveys or bureaus of economic geology, or in regional surveys by the USGS. DOE contractors have synthesized data at the regional scale for salt and shale, but these data were published before the advent of widespread use of GIS and are presented as printed figures and maps that require digitization and conversion to appropriate GIS data format (see Section 3.2). New subsurface data on shale formations has become available in the past few years due to increased exploration and production of natural gas from shale. Some of these data are available in GIS format (from sources such as the USGS Energy Resources Program (e.g., National Oil and Gas Assessment Project (http://energy.usgs.gov/OilGas/AssessmentsData/NationalOilGasAssessment.aspx).

Data for natural and cultural features and conditions that could potentially be applied as siting guidelines are generally available in GIS format from well-established government or university sources. These data include seismic hazard data (USGS), natural resources data (USGS, EIA), population (census) data, digital elevation models for topographic analysis, geothermal gradient and land use (federal or protected lands), among others.

One focus of work in FY12 and FY13 was to complete the acquisition and processing of data for salt deposits in the major sedimentary basin of the US. These data are available from various project reports (mostly pre-1990) that can be used to create GIS data. Three reports and map series have presented national compilations of salt data including the basic geometry of salt formations (thickness, structural contours, and formation extent) for the entire US:

1. Pierce and Rich (1962)
2. Johnson and Gonzales (1978)
3. Ege (1985)

These references provide the primary data that has been populated into the GIS database. Data quality and completeness varies among these reports depending on the specific salt body being discussed. It is valuable to compare these sources against one another to choose the most useful data or combination of data for digitization and inclusion in the GIS database.

We have augmented the national data sources discussed above with regional or state-level data sets where appropriate to obtain the best available data for salt bodies.

These sources include:

1. Hovorka (1998) presents detailed geometry of the Salado Formation in the Midland Basin for purposes of cavern storage in salt
2. Rauzi (2000) presents detailed geometry of the Supai Formation in the Holbrook Basin for purposes of cavern storage
3. Presley (1981) presents detailed geometry data for the San Andres Formation in the Palo Duro Basin as part of HLW waste disposal studies
4. The USGS has presented several reports beginning in the late 1950s describing salt in specific sedimentary basins for purposes of HLW disposal (e.g., Baltz, 1957; Sandberg, 1962).

3. Database Creation and Methods

Documentation of data is being implemented through creation of a GIS that will allow management, querying, analysis and display of relevant information that will impact future site screening and site evaluation decision points. GIS datasets are being created for granitic rock distribution, depth and other pertinent features of crystalline basement, and the major occurrences of salt and shale in the US using ArcGIS Desktop, Version 10.

3.1 Database description

GIS datasets for the geologic parameters discussed above are being constructed using the ArcGIS “file geodatabase” format. The file geodatabase uses an efficient data structure that is optimized for performance and storage. This system allows easy importation of spatial and tabular data from many different native formats and allows for easy extraction of data into many formats for future customer use. File geodatabases have no storage size limit. Individual datasets within a file geodatabase, such as a feature class or table, have a size limit of 1 terabyte, allowing for nearly unlimited attribution of data. In addition, both raster and vector data can be stored in the geodatabase. Some of the data obtained to date is already in a digital format that can be loaded into the file geodatabase. These formats included ArcGIS coverages and shapefiles, Microsoft Excel tables, DBF files, and delimited text files. More commonly, if digital data is not available, paper media or published figures are processed by means of digitizing as described below.

3.2 Digitization of Data Sources

Published maps and figures showing various spatial parameters for features important to understanding regional geology and siting guidelines are digitized and incorporated into the GIS database. Geologic features of primary interest for this report are the extent, thickness and depth of salt and shale formations. Paper maps representing these features can be scanned at high resolution, saved as bitmaps (JPEG, TIFF, etc.) and loaded into the GIS software for on-screen digitizing. Figures from published sources can likewise be imported into GIS software for on-screen digitizing (Figure 3-1). If the maps are available in a georectified digital format, they are loaded directly into the GIS software (this is not typically the case). Non-rectified or non-digital maps and figures are rectified into a standard map coordinate system such as WGS 84 latitude and longitude. Intersection points of known latitude and longitude, if present, are used to rectify the image. Otherwise, other known geographic control points such as state, county or township boundary intersections, cities, or other landmarks are used to rectify the map image using the georeferencing tool in ArcGIS 10.1. Once the images are properly rectified, the data (typically contour lines representing the thickness or top surface elevations of a formation) are then digitized using ArcScan, (a sub-program of ArcGIS) into points, lines or polygons and loaded into the file geodatabase as spatially referenced features. The features are assigned attributes and values based on the parameters they represent (e.g., elevation relative to sea level, depth from surface, formation thickness).

An example of part of the process of converting a figure to a useable spatial feature in the GIS database is shown in Figure 3-1 (see figure caption for explanation). The original source map represented in Figure 3-1 is a PDF of Plate 2 in Rauzi (2000), which represents the structure contour map of the top of the evaporite interval relative to sea level. In detail, the structural contour map is drawn on the top of a widespread anhydrite layer within the basin that lies 5-20 feet above the top of the halite. The extent of salt within the basin is equivalent to the extent of the color-contoured area shown in Figure 3-1, which is defined by the zero-isopach line for salt (zero thickness) in Plate 1 of Rauzi (2000).

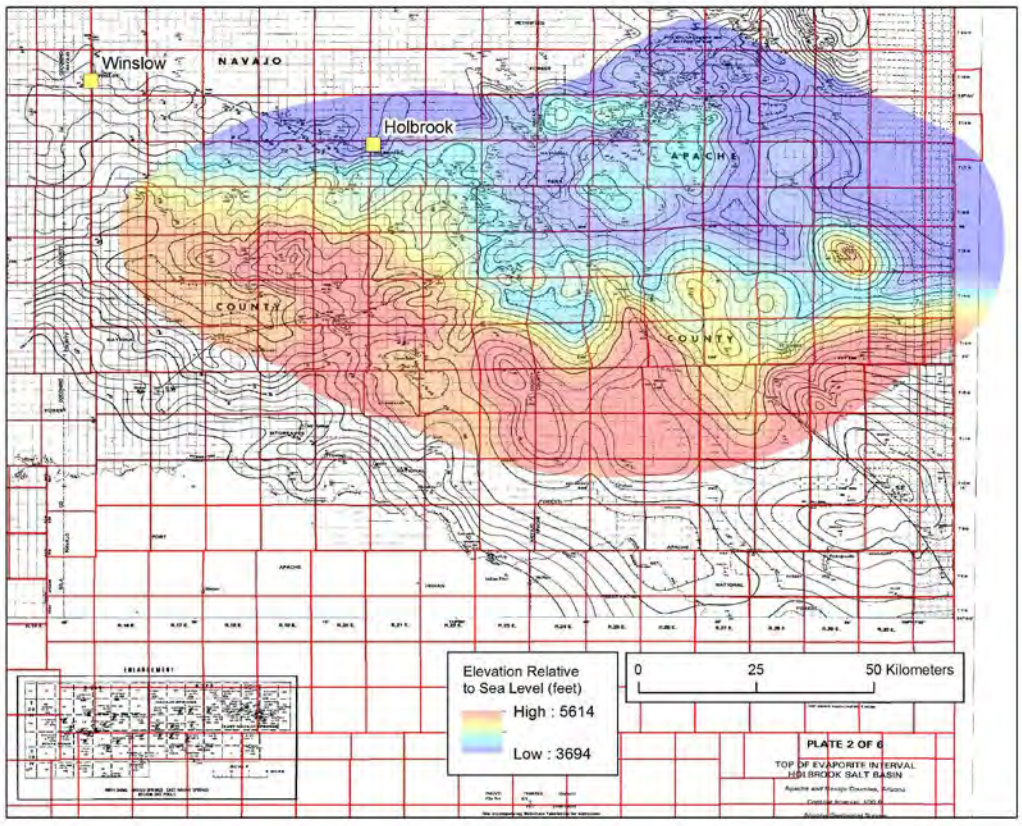

Figure 3-1. An example of geologic source data from Rauzi (2000). The black and white image (Plate 2 of Rauzi, 2000) represents the structure contour map of the top of the evaporite interval within the Holbrook Basin of Arizona. Contour interval is 100 feet and contour values are in elevation relative to sea level. The color-contoured portion of map is a calculated raster surface based on interpolation of the contour lines that were digitized using ArcGIS. The interpolated elevation surface faithfully represents the original contour lines of the image. The calculated elevation surface is converted to meters and then subtracted from a DEM surface of the same area to derive a depth from surface map (see Figure 4-26). The original image was rectified to a standard map coordinate system (WGS 84) using township boundaries (shown in red) as control points. Extent of salt in western New Mexico is only approximate.

3.3 Calculation of Depth to Top of Formation

Formation maps that represent surface relief on the top of salt or shale formations are represented in reports or maps as either depth from the earth's surface or elevation relative to sea level (more commonly). For purposes of repository siting, it is useful to represent the top surfaces of formations as depth in meters, since siting decisions are framed in terms of depth of the repository below the ground surface. If a data source represents the top surface of a formation as depth, the process for populating the data into the GIS database is 1) rectify the image and digitize the contour lines (almost always represented in feet), 2) interpolate the contours to create a depth surface grid with x,y values representing location and z data representing depth in feet, 3) convert the z values of depth in feet to depth in meters, 4) re-contour the depth grid to display map contours in meters. If the top surface of a formation is represented as an elevation surface (e.g., Figure 3-1), an additional step is needed to convert the elevation grid to a depth

grid. The elevation surface is subtracted from a DEM of the earth's surface within the region to represent the depth grid. For example, where a grid point has a formation elevation value of 300 meters and a ground elevation value of 1000 meters, the depth from ground surface value will be 700 meters at that point (compare Figures 3-1 and 4-26).

3.4 Projections

Geologic data and data for siting factors that have been included in the database to date are typically in a geographic coordinates system (i.e., degrees of latitude and longitude) that is straightforward to import into a GIS system. However, some of the datasets obtained are in various projected coordinate systems that are applicable to a continental scale, such as Lambert Conformal or Albers Equal Area. The coordinate system and the projection of the data are not significant as long as they are known and properly defined in the GIS system.

Maps and figures produced from the database are typically projected into a system which best depicts the features of interest over the area in which the features exist. Common map projections include Universal Transverse Mercator (UTM) coordinates for local and regional maps and Lambert Conformal or Albers Equal Area for maps covering larger areas.

4. Geology and Distribution of Alternative Host Rocks

4.1 Overview

A primary goal of this work package is to populate a GIS system with data for the distribution of alternative geologic host media for disposal of HLW. For granitic host rocks, population of the database is relatively straightforward, and involves identifying surface exposures of appropriate rock types documented in geologic databases or maps and importing these data into the GIS. For salt and shale formations, the problem is more difficult as both types of deposits (particularly salt) are largely subsurface features not well exposed at the surface. It is therefore not simply a matter of bringing information from geologic maps into the GIS. These subsurface data are obtained primarily from drilling data and interpretation of geologic relationships within sedimentary basins. Fortunately, instead of having to recover and interpret this primary subsurface data, it is often synthesized in reports that describe subsurface occurrences of salt and shale for purposes of HLW disposal, carbon sequestration, oil and gas exploration and subsurface storage of natural gas or, more recently, compressed air.

For both salt and shale, sedimentary basins provide the framework for identifying suitable formations and their associated data to populate into the GIS database (Figure 4-1). Sedimentary basins preferentially preserve thick and laterally continuous occurrences of salt and shale at depths potentially suitable for hosting of a geologic repository. In FY13 we completed the process of populating GIS data for major salt formations into the Regional Geology database. Likewise, we completed populating GIS data for many shale formations and will continue this effort in FY14.

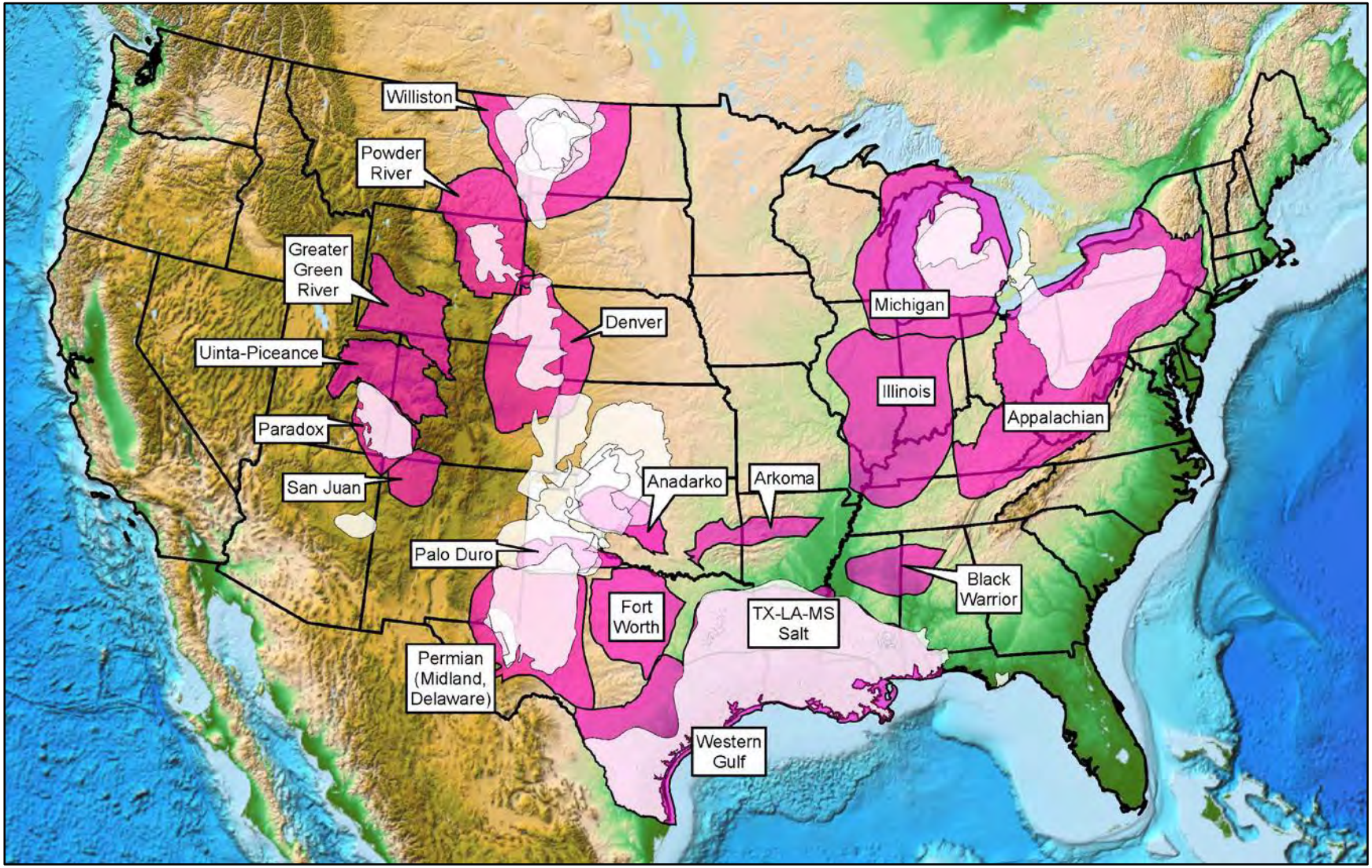

Figure 4-1.Selected major sedimentary basins of the US discussed in this report (EIA, 2011). White-shaded areas indicate extent of major salt formations described in this report and show their relationship to the major shale-bearing sedimentary basins. These basins provide the framework for identifying data for salt and shale for inclusion in a GIS database.

4.2 Salt

4.2.1 Overview

Information on the distribution of salt in the United States for purposes of HLW disposal is described in two major reports by Pierce and Rich (1962) and Johnson and Gonzales (1978) and in a series of map plates in Ege (1985). These sources represent the best current compilations of salt formations at the national scale. A map of areas underlain by salt deposits presented by Johnson and Gonzales (1978) has been used extensively over the years to communicate salt distribution in the US. While useful to readily communicate the overall distribution of salt in the US, it does not provide information about the true extent of salt or the relationship of individual salt formations within major basins. Our goal is to use information provided in available reports such as Johnson and Gonzales (1978) and other publications to document within a common database the extent, depth and thickness of individual formations present within the sedimentary basins of the US.

The distribution of salt in the US is dictated primarily by the location of deep sedimentary basins that inhibit erosion and dissolution of salt bodies over geologic time (Figures 4-1 and 4-2). Depth to the top of salt bodies varies greatly depending on location within basins and from basin to basin with the shallowest salts present on basin margins and the deepest salts present in basin interiors. Nationally, the largest salt bodies that are present within several hundred meters of the surface occur at the margins of the Michigan Basin, the northern margin of the Appalachian Basin and in what is informally termed the Permian Basin of Texas, New Mexico, Oklahoma and Kansas (Figure 4.2). Smaller salt bodies occur at shallow depth within the Paradox and Holbrook Basins of Utah and Arizona and as salt domes along the Gulf Coast of Texas, Louisiana and Mississippi (Figure 4-2). The ages, basin location and area of extent of each salt body are listed in Table 1. Overall, salt at all depths underlies slightly more than 20% of the landmass of the contiguous US.

National screening of salt in the 1960s and 1970s (Pierce and Rich, 1962; Johnson and Gonzales, 1978) resulted in the identification of four regions with salt of appropriate depth and thickness to host a repository (DOE, 1986a). The four regions identified (see Figure 4-2) were:

- Michigan and Appalachian Basins
- Permian Basin of New Mexico/Texas to Kansas
- Paradox Basin
- Salt domes of the Gulf Coast region

After proceeding to the area screening phase, further screening of the Michigan and Appalachian Basins was deferred, in part due to recognition of unfavorable conditions related to high population density and presence of abundant oil and gas resources (DOE, 1986a).

Isopach maps for aggregate salt thickness used in this report (and following the convention used in the salt literature) represent the total summed thickness of salt within a particular geologic formation, not the total thickness of the formation. This is because formations containing salt typically contain interbedded carbonate, anhydrite and siliciclastic beds reflecting cyclical shallow marine and near-shore depositional environments that occur during marine transgressions and regressions (Figure 4-3). Depth maps represent the depth to the top of the uppermost salt, recognizing that a formation or group may contain multiple salt intervals. For maps with frames depicting both depth and thickness (e.g., Figure 4-5), representative thickness or depth reference contours are shown in each frame to provide a better sense of the depth/thickness relationship for each salt body.

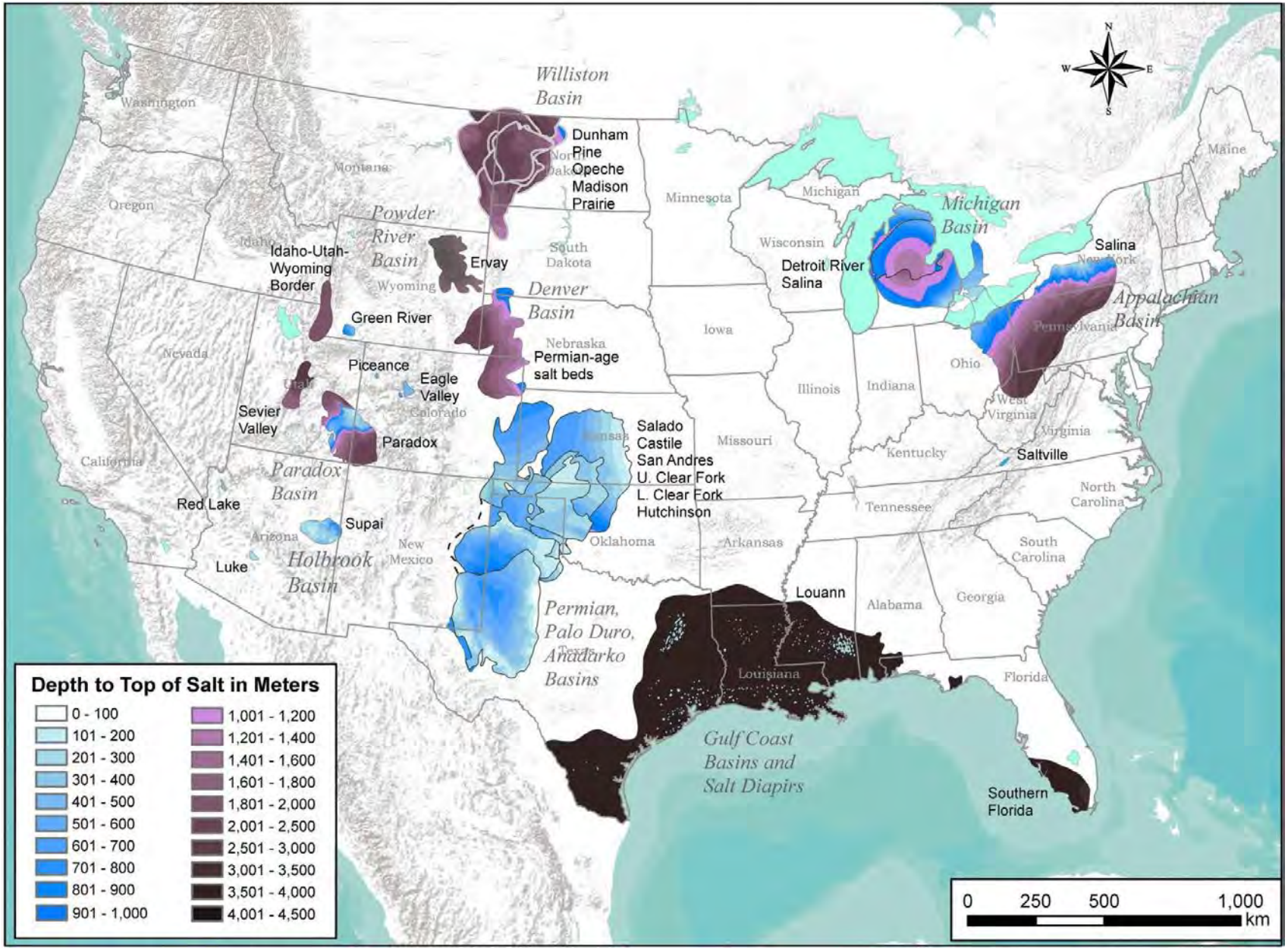

Figure 4-2. Distribution and depth to top of salt formations in major sedimentary basins of the U.S. White to blue shading indicates salt at depth of less than 1000 meters. Light to dark purple shading indicates salt at depth of greater than 1000 meters to as deep as 4500 meters. Salt formations are labeled by name or by common reference and listed in stratigraphic order where more than one salt formation is present in a basin.

Table 4-1. The areal extent (in square kilometers) of Mesozoic and Paleozoic salt units calculated from GIS data (in order of decreasing area)

Salt Unit	Age	Basin	Area (sq. km)
Luann	Jurassic	Gulf Coast Salt Basins	404,249
San Andres	Permian	Palo Duro, Anadarko, Dalhart, shelf areas	153,037
Salina	Silurian	Appalachian	138,195
Hutchinson	Permian	Anadarko, Kansas shelf	113,588
Salado	Permian	Midland, Delaware	107,146
Lower Clear Fork	Permian	Palo Duro, Anadarko, shelf areas	>101,849
Salina	Silurian	Michigan	96,844
Madison	Mississippian	Williston	81,861
Upper Clear Fork	Permian	Palo Duro, Dalhart	>75,980
Ervay-Opeche-San Andres equivalents	Permian	Denver	56,009
Pine	Permo-Triassic	Williston	55,597
Prairie (within US)	Devonian	Williston	40,781
Paradox	Pennsylvanian	Paradox	35,267
Dunham	Jurassic	Williston	28,401
Opeche	Permian	Williston	25,778
Ervay	Permian	Powder River	22,695
Castile	Permian	Delaware	13,576

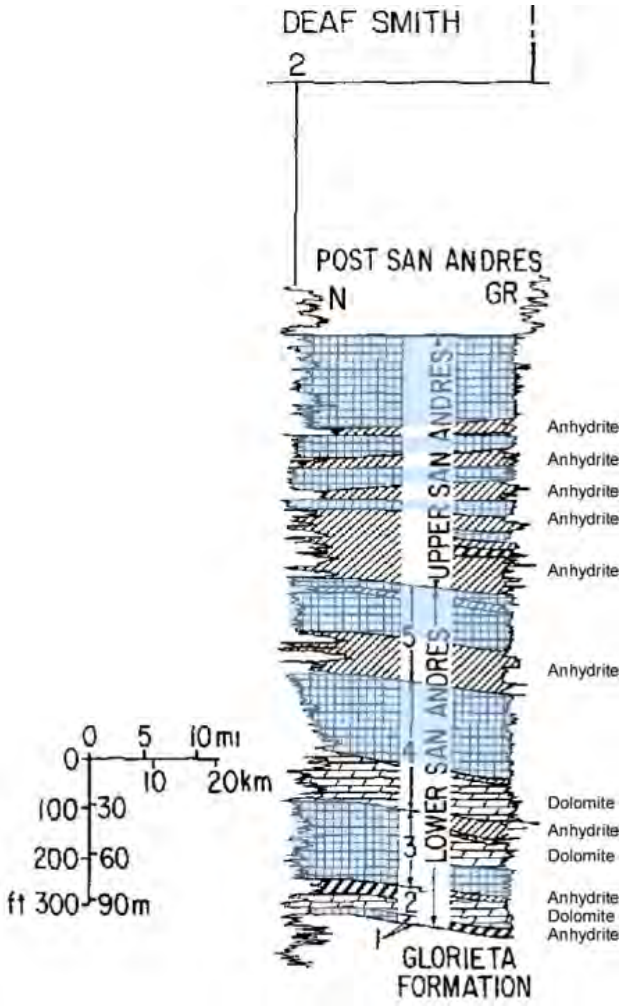

Figure 4-3. Stratigraphic cross section from north (L) to south (R) of the San Andres Formation beneath Deaf Smith County Texas (from Presley, 1981). Blue-shaded units are mixed salt and mudstone (shale) horizons. Other labeled units are interbedded anhydrite and dolomite. Salt in the lower San Andres is relatively pure with low clay and silt content (<5%). The "Cycle 4" salt (~60 meters in thickness) in the lower San Andres was a preferred horizon for high-level radioactive waste disposal at the time of the West Texas Waste Isolation Study.

4.2.2 Michigan Basin

The Michigan Basin is a circular intracratonic structural basin filled with up to 4800 meters of marine Paleozoic carbonates, shale, sandstone and evaporite beds and a small remnant of terrestrial Jurassic sediment in the basin center (Catacosinos et al., 1991). These sediments are overlain by a few hundred meters of Pleistocene glacial drift. The older sediments (Cambrian-Middle Devonian) are dominated by carbonate rocks while the younger sediments (Upper Devonian-Pennsylvanian) are dominated by mudstone, shale and sandstone (Swezey, 2008). The Salina and Detroit River Groups (containing salt) occur within the older carbonate rocks (Figure 4-4). The stratigraphy of the Michigan Basin largely mirrors that of the Appalachian Basin discussed in Section 4.2.3. The Michigan Basin is separated from the Appalachian Basin to the southeast by the Findlay arch in northern Ohio. Sedimentary strata dip gently towards the center of the basin at angles of less than 1 degree (Johnson and Gonzales, 1978).

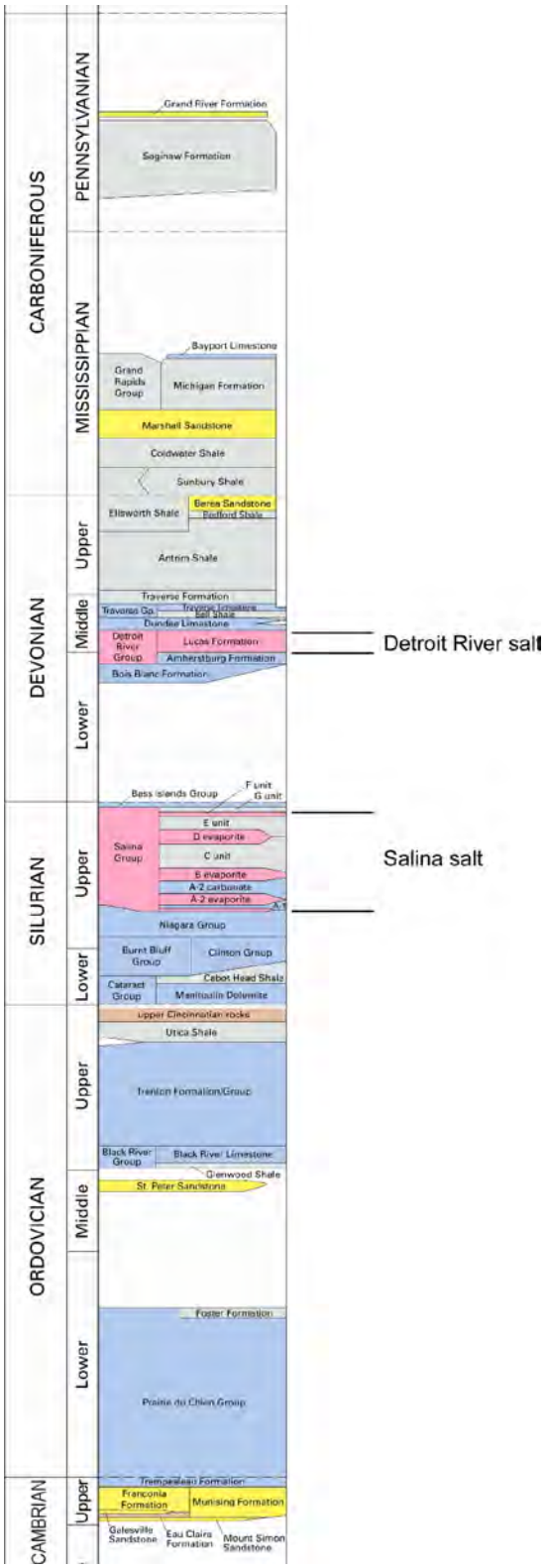

Figure 4-4. Stratigraphy of the central Michigan Basin modified from Swezey (2008). Pink units are salt of the Salina and Detroit River Groups. Basin stratigraphy is similar to that of the Appalachian Basin (older carbonates, younger mudstones/sandstones) with salt of the Detroit River group absent.

The two major salt groups in the Michigan Basin are part of the Salina and Detroit River Groups of Silurian and Devonian age, respectively. Both groups contain many individual salt intervals interbedded with carbonate and anhydrite, and shale in the case of the Salina (Johnson and Gonzales, 1978). Data sources used to create GIS data for the Michigan Basin are listed in Table 4-2.

Table 4-2. GIS data sources for the Michigan Basin

Salt	Reference	Source Features used in GIS Database
Salina	Pierce and Rich (1962)	Elevation and isopach contours, extent of salt
Detroit River	Johnson and Gonzales (1978)	Depth and isopach contours, extent of salt

4.2.2.1 Salt of the Salina Group

The Salina Group contains five major salt units termed, from oldest to youngest, the A-1, A-2, B, D, and F (Johnson and Gonzales, 1978; Figure 4-4). Salina units C and E are dominantly shale. The salt units generally become more interbedded with shale and dolomite and consist of thinner individual salt beds as they become younger (Johnson and Gonzales, 1978).

The A-1 and A-2 salts are separated by dolomite of the Ruff Formation (Catacosinos et al., 2000). Both units are mostly clean massive salt with typical thicknesses of 60-150 meters (A-1) and 100-150 meters (A-2) with the greatest thickness in the central part of the basin (Johnson and Gonzales, 1978). The top of the A-2 unit is at a depth of more than 2000 meters in the center of the basin and between 900 and 1200 meters at the basin margins. The B salt consists of about 50 meters of clean salt in the lower half of the unit and is interbedded with shale and dolomite in the upper half of the unit. The D salt consists of two relatively thin salts (~10 meters) separated by a thin dolomite bed. The F salt consists of numerous beds 2-6 meters thick interbedded with shale, dolomite and anhydrite. The two lowest beds and the uppermost bed are clean massive salt that have a thickness of 10-30 meters ((Johnson and Gonzales, 1978).

The aggregate thickness of salt in the Salina Group is more than 500 meters in the center of the basin and less than 100-200 meters nearer the edges of the basin. The depth to the top of the F salt is more than 1800 meters in the center of the basin and less than 200 meters at the southern and northern edges of the salt extent (Figure 4-5).

4.2.2.2 Salt of the Detroit River Group

The Lucas Formation of the Detroit River Group is dominated by beds of dolomite and anhydrite with lessor amounts of salt, limestone and sandstone (Landes, 1951). The evaporite sequence within the upper part of the Lucas Formation and consists of numerous salt beds interbedded with anhydrite (Johnson and Gonzales, 1978). Salt has a maximum aggregate thickness of about 150 meters with depth ranging from greater than 1200 meters in the center of the basin to a little more than 500 meters at its northernmost extent (Figure 4-6). Individual salt beds vary in thickness from 5 meters to 35 meters for the uppermost bed in the sequence (Johnson and Gonzales, 1978).

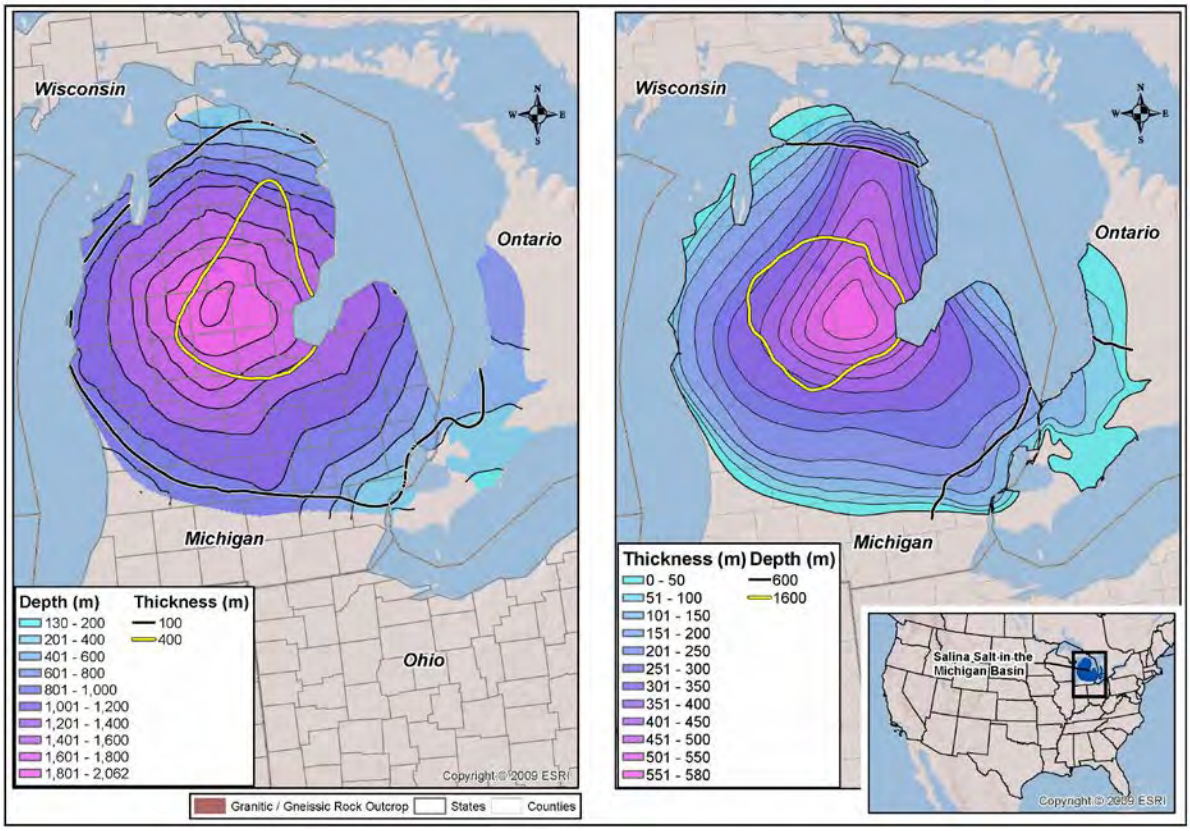

Figure 4-5. Depth to top and aggregate thickness of salt of the Salina Group in the Michigan Basin. Salt beneath Great Lakes is not shown. Depth of salt is depth to top of the F Salt, the youngest unit in the Salina Group.

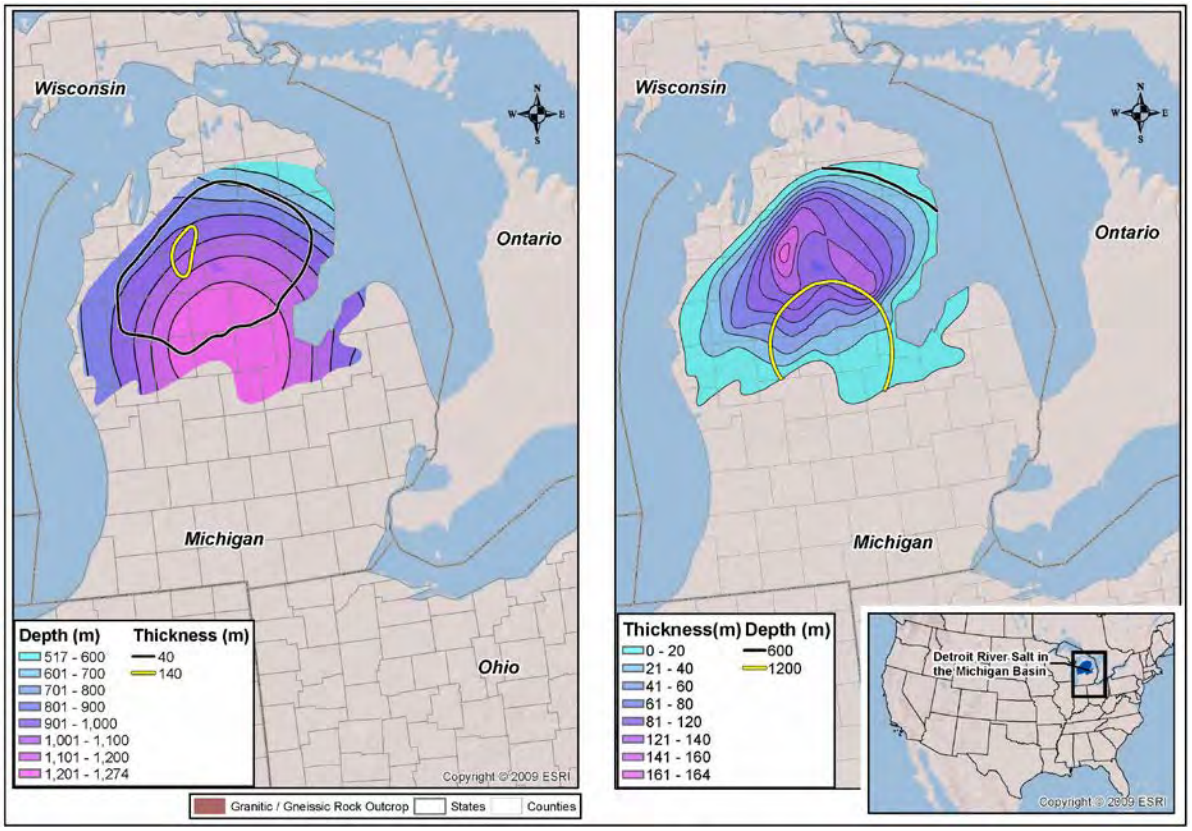

Figure 4-6. Depth to top and aggregate thickness of the Detroit River Group in the Michigan Basin. Salt beneath the Great Lakes is not shown.

4.2.3 Appalachian Basin

The Appalachian Basin is a major foreland basin lying to the northwest of the Appalachian Mountains. The basin is asymmetrical with the basement surface and overlying sediments ramping gently to the southeast to the edge of the Valley and Ridge Province. The sediments are Cambrian to Permian Paleozoic rocks that vary in total thickness from roughly 1000 meters at the northeastern edge of the basin in northern Ohio to 7500 meters near the southeastern edge of the basin in southern Pennsylvania (Ryder et al., 2012). The oldest rocks, Cambrian through middle Devonian, are dominated by carbonate units, while Upper Devonian through Permian age rocks are dominated by shale, mudstone and sandstone. The Upper Silurian Salina Group is the only significant evaporite within the basin and occurs within the upper half of the carbonate-dominated Cambrian to Middle Devonian stratigraphic interval (Swezey, 2002).

Salt of the Salina Group within the Appalachian Basin is present beneath parts of Pennsylvania, New York, Eastern Ohio and northern West Virginia (Figure 4-7). The Salina Group is thinner than in the Michigan Basin, and does not include the thick salts within the A-1 and A-2 units found in the Michigan Basin (Johnson and Gonzales, 1978). The thickest salt occurs in the northeast part of the basin straddling the New York-Pennsylvania state border where it reaches a thickness of about 260 meters (Figure 4-7). The depth to the top of the salt exceeds 3000 meters at the southeast edge of basin along the Valley and Ridge province margin. The top of the salt in the northern margin in New York and the northeast margin in Ohio is at a depth of less than 600 meters. (Figure 4-7).

The B unit is the oldest salt within the Salina Group of the Appalachian Basin. Individual salt beds are 1-6 meters thick with an aggregate thickness of 15-30 meters (Johnson and Gonzales, 1978). Individual beds are separated by shale. Salt beds of the D unit are of similar thickness with an aggregate thickness of up to 40 meters in southern New York (Johnson and Gonzales, 1978). The F unit is the major salt-bearing unit within the Salina Group in the basin and has an aggregate salt thickness of up to 150 meters. Individual salt beds are 3-25 meters thick in eastern Ohio and 20-50 meters thick in southern New York (Johnson and Gonzales, 1978; see also Figure 4-7). The data source used to create GIS data for the Appalachian Basin is listed in Table 4-3.

Table 4-3. GIS data sources for the Appalachian Basin

Salt	Reference	Source Features used in GIS Database
Salina	Pierce and Rich (1962)	Elevation and isopach contours, extent of salt

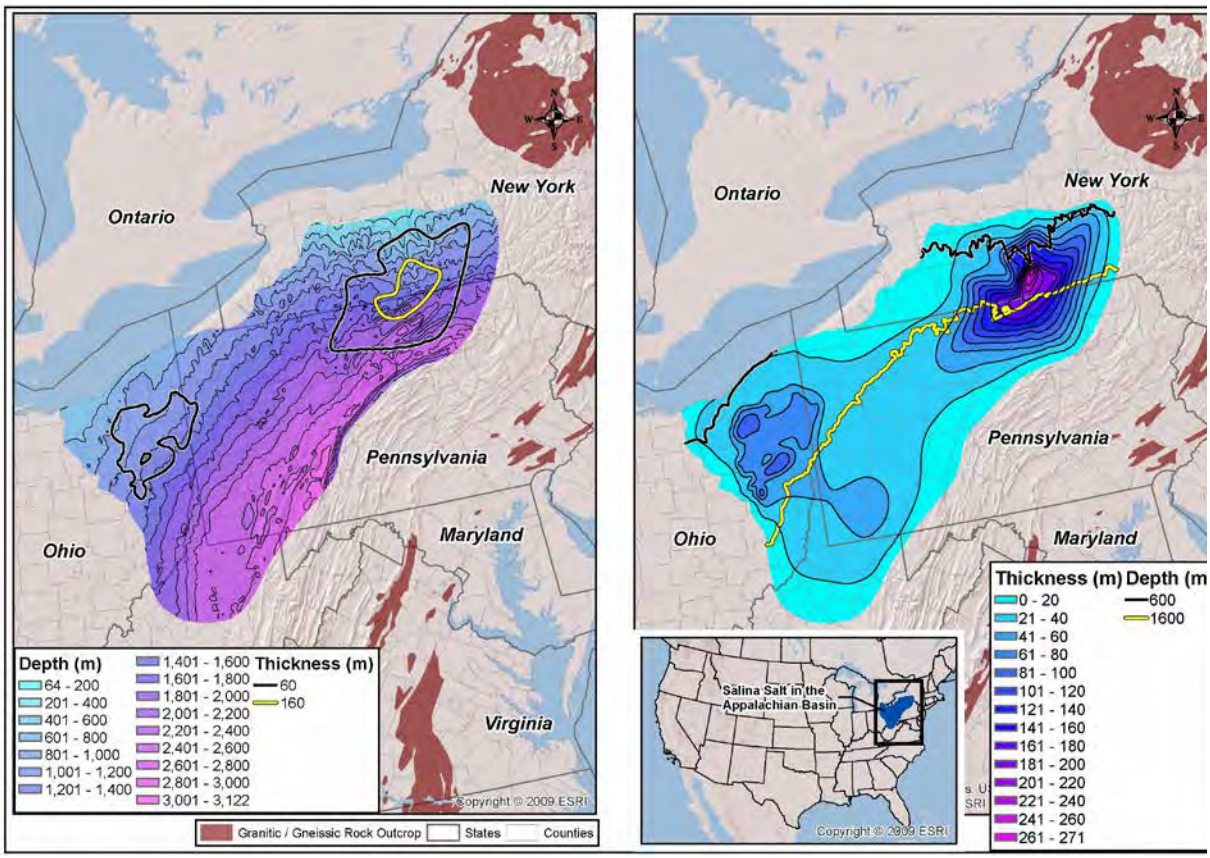

Figure 4-7. Depth to top and aggregate thickness of salt in the Silurian Salina Group in the Appalachian Basin. Depth of salt is depth to top of the F Salt, the youngest unit in the Salina Group.

4.2.4 Paradox Basin

Barbeau (2003) and Trudgill (2011) describe complementary models for the development of the Paradox Basin and of the salt structures within the basin. According to these models, the Paradox Basin formed as a flexural foreland basin in response to the rise of the Uncompahgre uplift during formation of the ancestral Rocky Mountains. The basin was filled by ~30 evaporite cycles representing seawater transgressions and regressions that deposited the ~2500 meters of evaporites. The depositional cycles of the Paradox Formation, each recording a marine transgression and regression, deposited individual sequences (from bottom to top) of anhydrite, black shale, dolomite, anhydrite and halite (Raup and Hite, 1992). Following deposition of the Paradox Member, Permian sediments shed to the southwest off the Uncompahgre uplift differentially loaded and deformed the salt to form the salt-cored anticlines in the northeast part of the basin (Trudgill, 2011; see also Figure 4-9).

In most of the basin the depth to the top of the salt is about 1500 meters but becomes relatively shallow in the area of the salt anticlines (Figure 4-8). However, most of the deformed halite and associated rocks, which vary in thickness from 700 to 4000 m, form the cores of the anticlines. Individual salt beds are 6-240 meters in the central part of the basin (Raup and Hite, 1992).

Data sources used to create GIS data for the Paradox Basin are listed in Table 4-4.

Table 4-4. GIS data sources for the Paradox Basin

Salt	Reference	Source Features used in GIS Database
Paradox	Ege (1985)	Depth and isopach contours; northern extent of Paradox salt
Paradox	Trudgill and Arbuckle (2009)	Location of salt anticlines, southern extent of Paradox salt

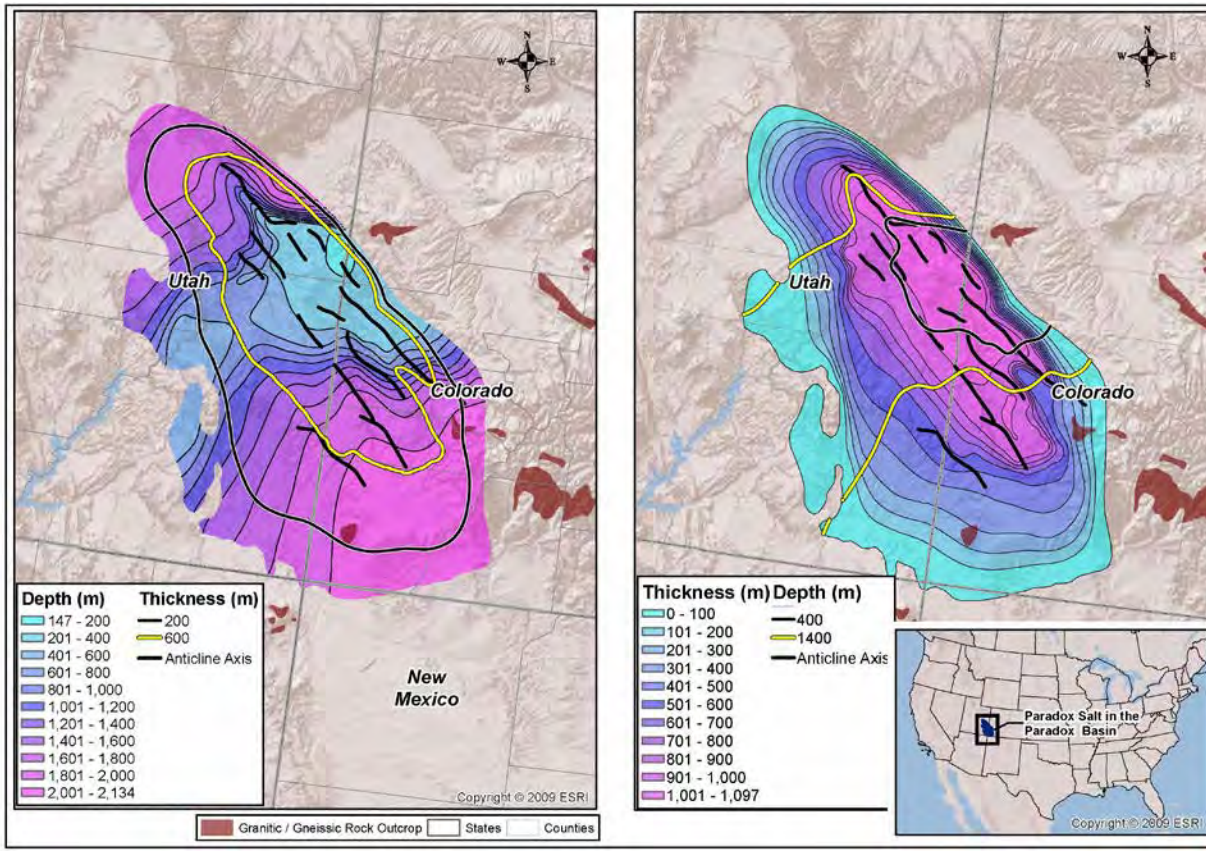

Figure 4-8. Depth to top and aggregate thickness of the Pennsylvanian Paradox Salt in the Paradox Basin. Thickness of salt in salt-cored anticlines may locally exceed 4000 meters. Granitic rocks shown within and near the margins of the Paradox Basin are Late Cretaceous to Early Tertiary diorite to gabbro intrusions. Relationships between the intrusive rocks and intruded salt are undoubtedly complex (Baltz, 1957), and the salt geometry shown in the areas near the intrusive bodies is therefore considered to be greatly simplified.

4.2.5 Williston Basin

The Williston Basin is the northernmost of several major energy-producing basins that extend from north to south through the center of the US (Figures 4-1 and 4-2). These basins, which include the Williston, Powder River, Denver, Anadarko, Palo Duro, Midland and Delaware, are the primary locations of Permian-age salts in the US. These basins are discussed in north to south sequence in the following sections.

The Williston Basin is an intracratonic basin that forms the southeastern extent of the Western Canada Sedimentary Basin (Kent and Christopher, 1994). Sediment thickness is approximately 4900 meters and the rocks range in age from Cambrian through Cretaceous. As documented by Sandberg (1962), the Williston Basin was characterized in the early years of radioactive waste disposal studies for injection of liquid waste into deep sedimentary basins, an option suggested by the National Academy of Sciences in 1957. Rock types suggested as potential host rocks for injection included sandstone, shale and salt (in solution caverns) at depth ranging from a few thousand to more than 10,000 feet.

Salt formations in the Williston Basin range in age from Devonian to the Jurassic, the longest age range for salt within any single basin in the US (Johnson and Gonzales, 1978). Salt units occur within the Devonian Prairie Formation, the Mississippian Madison Group (seven separate salt formations), the Permian Opeche Formation, the Permian-Triassic Pine Salt, and the Jurassic Dunham Salt (Johnson and Gonzales, 1978). The spatial and age/depth relationships of the salts in the Williston Basin are shown in Figure 4-9. The basin underlies a large part of western North Dakota, eastern Montana, northwest South Dakota, and part of southern Canada. The center of salt deposition within the Williston is in western North Dakota (Figure 4-9). The Nesson and Cedar Creek anticlines are major structural features within the basin and are closely associated with oil and gas production. The anticlinal structures are propagated through several of the salt formations and can be seen as changes in the thickness and depth of salt (see for example the northern and southwestern margins of the Pine Salt in Figure 4-13).

Depths to salt bodies in the center of the Williston Basin range from about 2200 meters for the youngest salt to greater than 3600 meters for the oldest salt. At the basin margins, salt is relatively shallow at about 1000 meters depth in two areas – the easternmost margin of the Madison Group Salt and the southernmost margin of the Pine Salt (Figure 4-9).

Data sources used to create the GIS database for salts of the Williston Basin are listed in Table 4-5.

Table 4-5. GIS data sources for salts of the Williston Basin

Salt	Reference	Source Features used in GIS Database
Prairie, Madison, Pine and Dunham	Pierce and Rich (1962)	Elevation and isopach contours, extent of salt
Opeche	Johnson and Gonzales (1978)	Depth contours

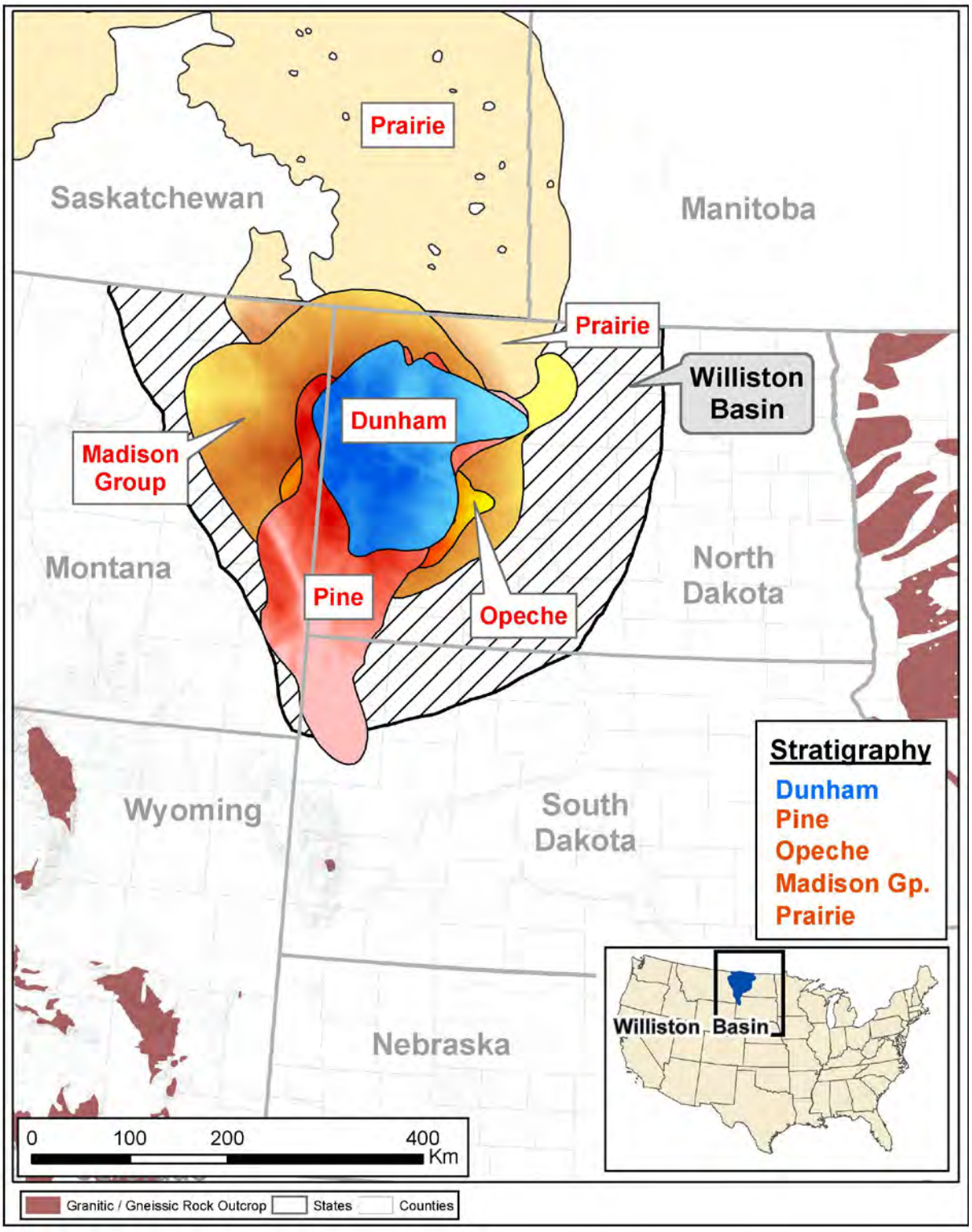

Figure 4-9. Overview of the distribution of major salt-bearing formation and their stratigraphic relationships within the Williston Basin of North Dakota, South Dakota and Montana. Color shading represents relative depth variations for each salt with deeper colors representing greater depth within a given salt. Brownish shades represent Paleozoic salt (Devonian-Permian), blue represents Mesozoic salt (Jurassic). Scale is the same as that of Figure 4-14 for the Permian Basin. Also shown is the extension of the Prairie salt in the Western Canadian Sedimentary Basin of southern Canada (Meijer Drees, 1994). No representation of depth is given for the Canadian portion of the Prairie Formation.

4.2.5.1 Salt of the Prairie Formation

The salt of the Devonian Prairie Formation is the oldest, deepest and thickest salt in the Williston Basin. Thickness ranges from less than 20 meters at the margins of the formation to almost 140 meters in the central part of the formation near the US-Canada border (Figure 4-10). The Prairie salt ranges in depth from about 1700 meters at the eastern basin margin to over 3600 meters at the southern margin of the formation (Figure 4-10). The Prairie salt extends for over 1000 kilometers to the northwest of the Williston Basin as the major evaporite formation in the Western Canada Sedimentary Basin (Meijer Drees, 1994).

4.2.5.2 Salt of the Madison Group

Salt of the Mississippian Madison Group consist of seven salt beds primarily within the Charles Formation, The salts are designated "A" through "F" and "X" from youngest to oldest (Anderson and Hansen, 1957). The aggregate thickness of the seven salt units is slightly over 100 meters in the center of the basin (Figure 4-11). The thickest individual salt is the "A" salt with a thickness of up to 45 meters (Anderson and Hansen, 1957). The "X" salt has a limited extent on the far eastern edge of the Madison group and ranges in thickness from about 3-9 meters. The "X" salt is the oldest salt body in the Madison Group but lies at a relatively shallow depth because of its localized position (shown as a protuberance) near the eastern margin of the Williston Basin (Figure 4-11). Well data indicates a minimum depth for the "X" salt of 1100 meters (Anderson and Hansen, 1957), while elevation contouring by Pierce and Rich (1962) indicates a minimum depth of slightly more than 800 meters, which may represent a discrepancy in the contouring. Aside from the "X" salt, the "D" and "F" salts have the greatest areal extent in the basin and generally define the boundaries of the main body of the Madison salt bodies (Figure 4-11). These two salts have a maximum thickness of 18 and 27 meters, respectively (Anderson and Hansen, 1957).

4.2.5.3 Salt of the Opeche Formation

The Permian Opeche Formation is a red bed sequence of shale, sandstone and anhydrite that in North Dakota contains a salt bed first referred to as the Permian "A" salt by Anderson and Hansen (1957). It reaches a thickness of nearly 50 meters at its depositional center and ranges in depth from greater than 1600 meters at its eastern margin to greater than 2300 meters at its center (Figure 4-12). The salt is impure and lenticular and grades into shale and anhydrite (Johnson and Gonzales, 1978). Nordeng (2009) notes the presence of a "B" salt in the Opeche Formation that is thinner than the "A" salt and much more discontinuous.

4.2.5.4 Pine Salt of the Spearfish Formation

The Permo-Triassic Pine Salt within the Spearfish Formation is a massive and fairly pure salt that reaches a thickness of 100 meters in southwest North Dakota and northeast South Dakota. It is the only Williston Basin salt present in South Dakota (Figure 4-9). The depth to the top of the Pine Salt ranges from more than 2300 meters in the central Williston Basin to as shallow as approximately 1200 meters at its most southern extent at the southern margin of the basin (Figure 4-13).

4.2.5.5 Dunham Salt

The Dunham Salt within the Jurassic Piper Formation is the youngest salt in the Williston Basin (Figure 4-9). The maximum thickness of the Dunham Salt is 30-40 meters based on isopach data (Figure 4-14) from Pierce and Rich (1962). Nordeng (2009) notes a maximum thickness of 57 meters and presents an isopach map of the Dunham Salt that shows an extremely discontinuous body. The boundary shown in Figure 4-14 should therefore be considered a generalized envelope around a discontinuous interior. Depth of the Dunham Salt ranges from about 1400-2300 meters.

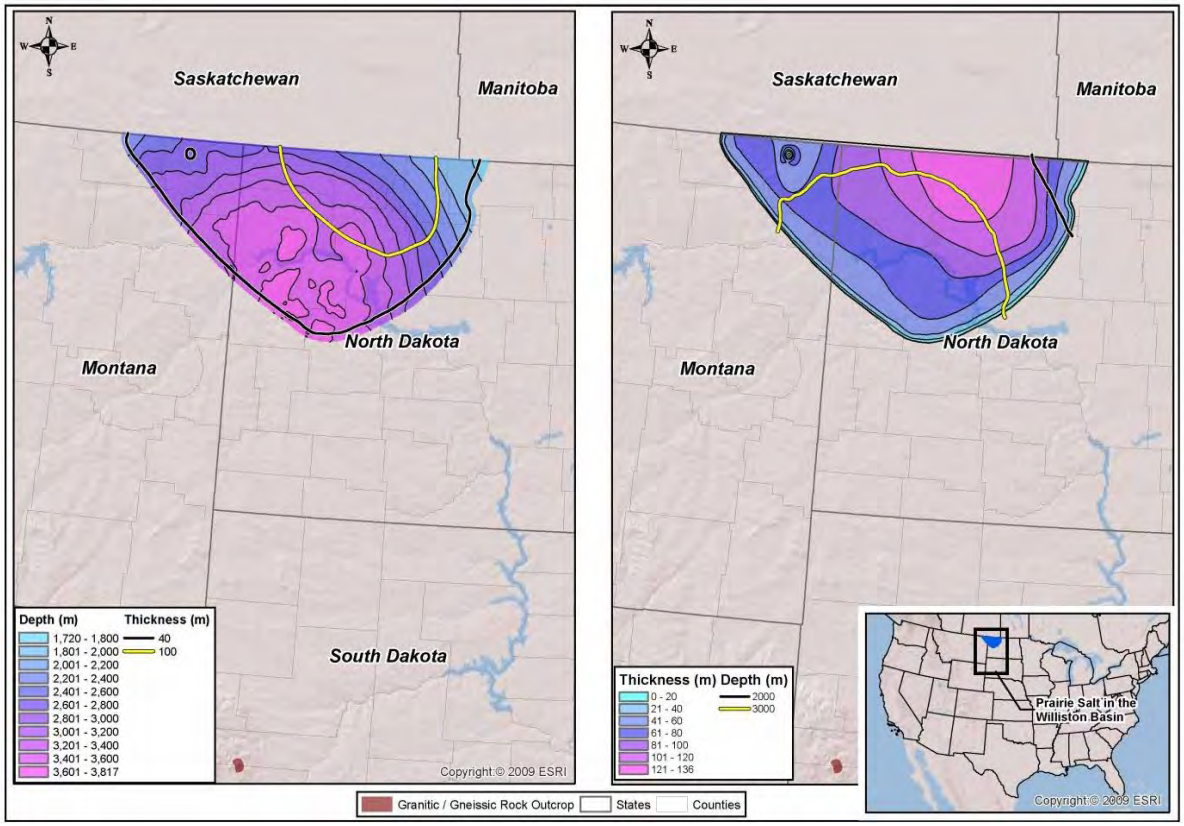

Figure 4-10. Depth to top and aggregate thickness of salt in the Devonian Prairie Formation in the Williston Basin.

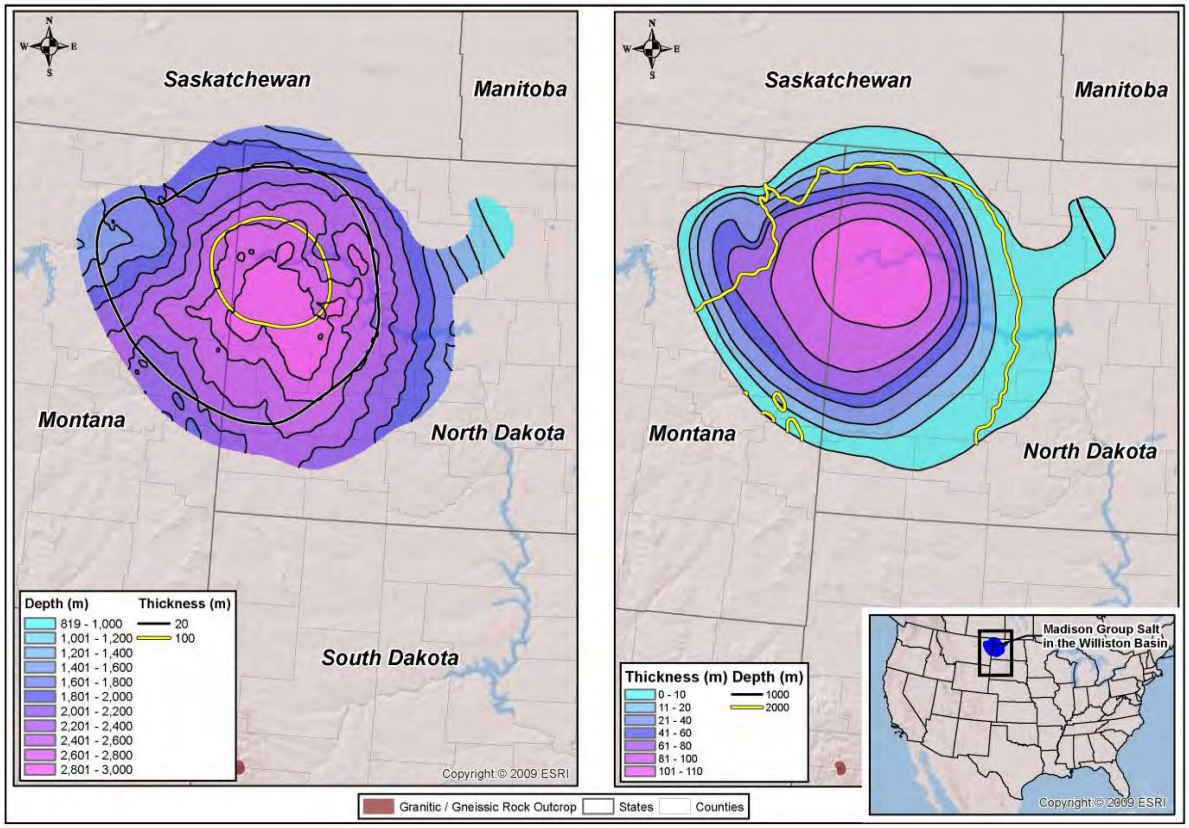

Figure 4-11. Depth to top and aggregate thickness of salt in the Mississippian Madison Group in the Williston Basin.

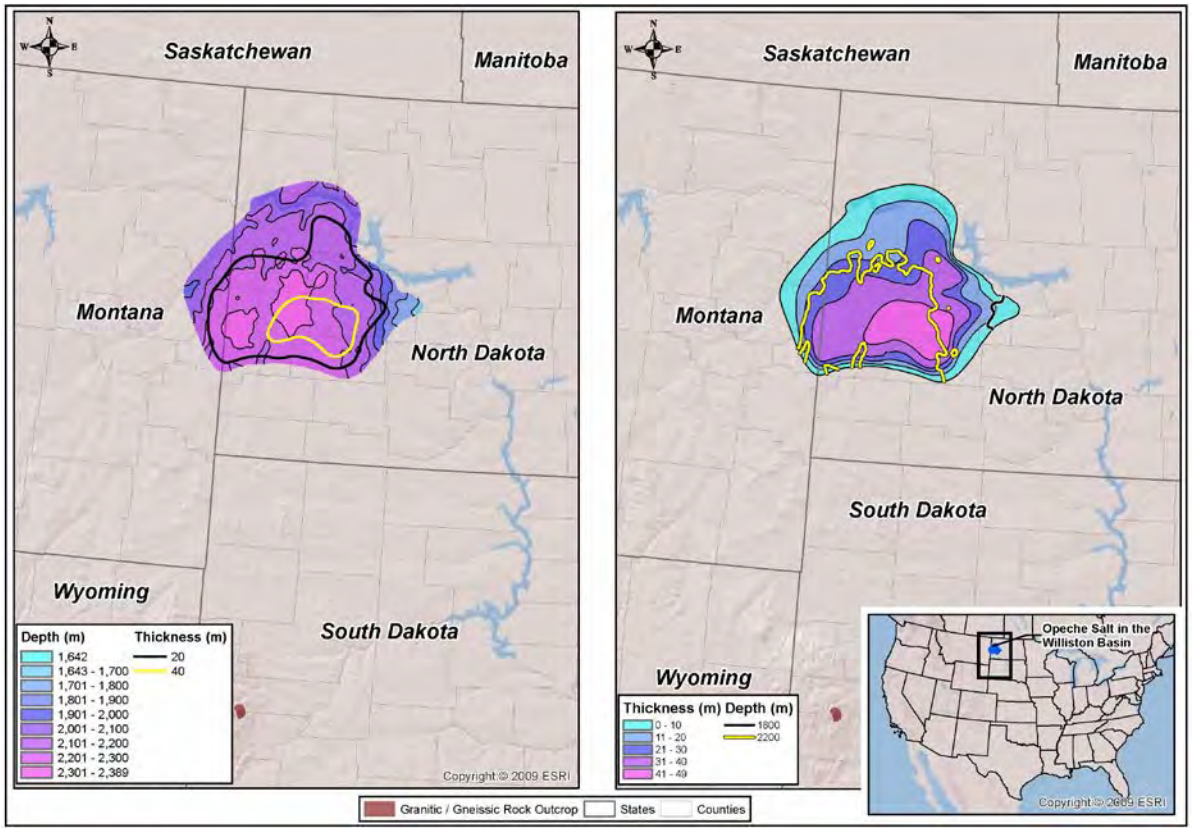

Figure 4-12. Depth to top and aggregate thickness of salt in the Permian Opeche Formation in the Williston Basin.

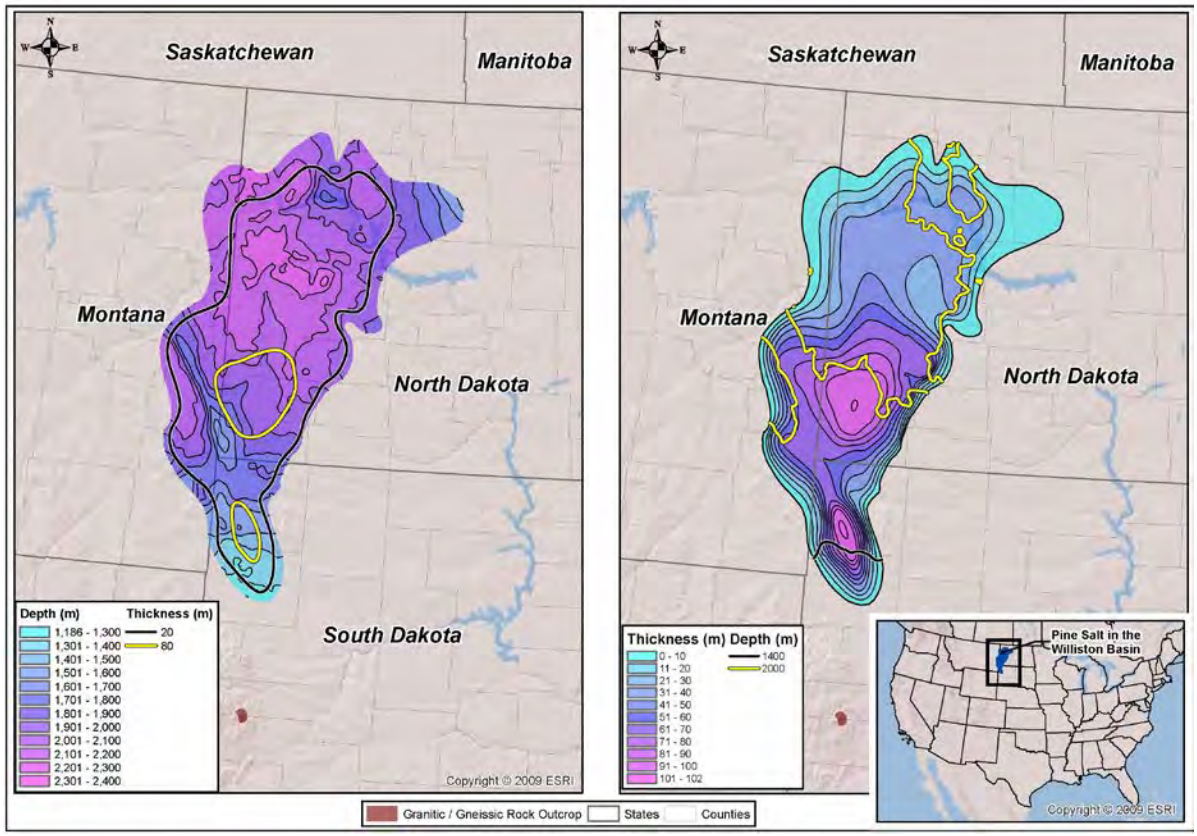

Figure 4-13. Depth to top and aggregate thickness of the Pine Salt of the Permo-Triassic Spearfish Formation in the Williston Basin.

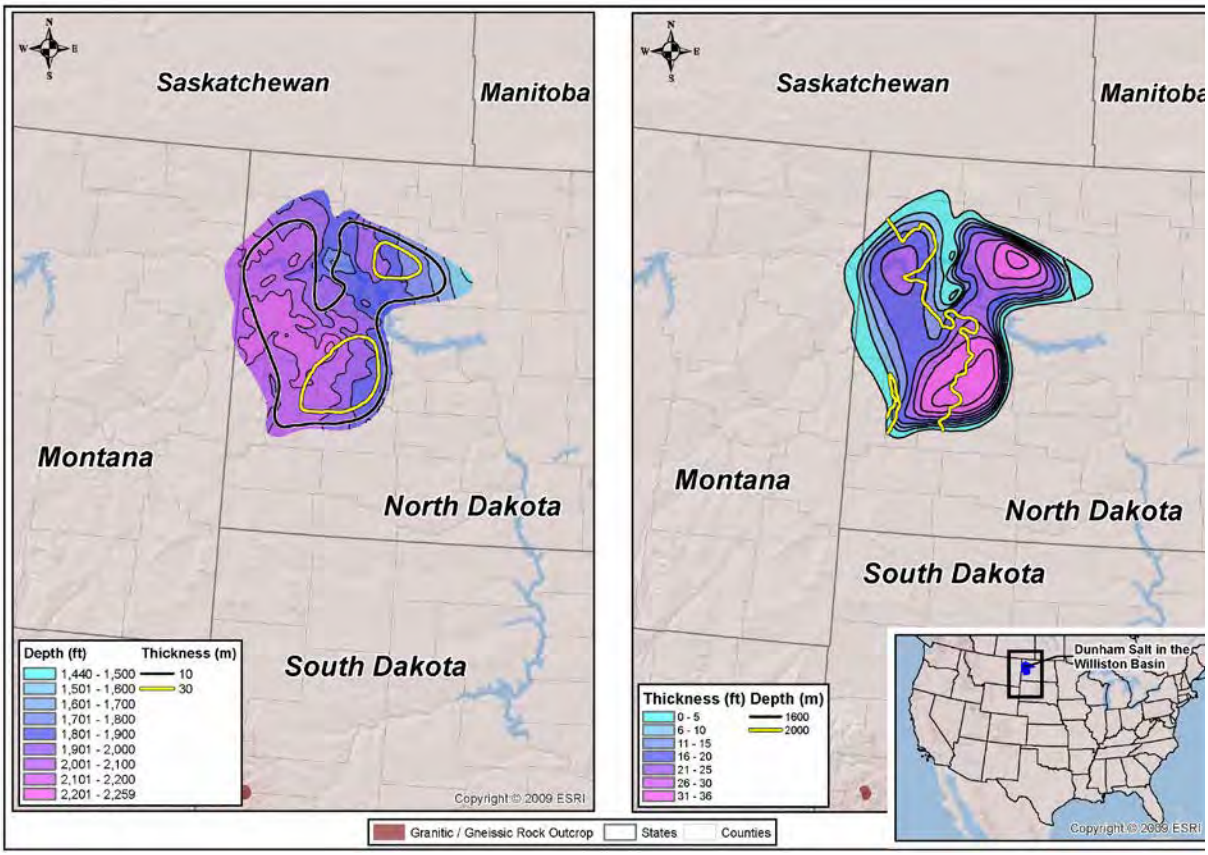

Figure 4-14. Depth to top and aggregate thickness of the Dunham salt in the Williston Basin.

4.2.6 Powder River Basin

The Powder River is a deep asymetric intermontane basin of Laramide-age with the strutural axis near the western margin. The sediments range in age from Cambrian to Tertiary and have a total thickness of greater than 5500 meters. The Paleozoic rocks are primarily marine in origin while the Mesozoic and younger rocks are increasingly of terrestrial origin (Dolton and Fox, 1996)

The Ervay Salt occurs within the Ervay Member of the Permian Goose Egg Formation and is roughly time equivalent to the Pine Salt of the Spearfish Formation in the Williston Basin, although their exact stratigraphic relationship is debated. It lies above the Permian Opeche Formation of both the Williston and Powder River Basins (Dolton and Fox, 1996). Salt ranges in depth from over 1700 meters in the southern and northeastern margins of the basin to 4000 meters along the basin axis on the western margin of the basin (Figure 4-15). The thickest salt, at only 30-40 meters, occurs in the northern half of the basin (Figure 4-15).

The data source used to create the GIS database for salt of the Powder River Basin is listed in Table 4-6

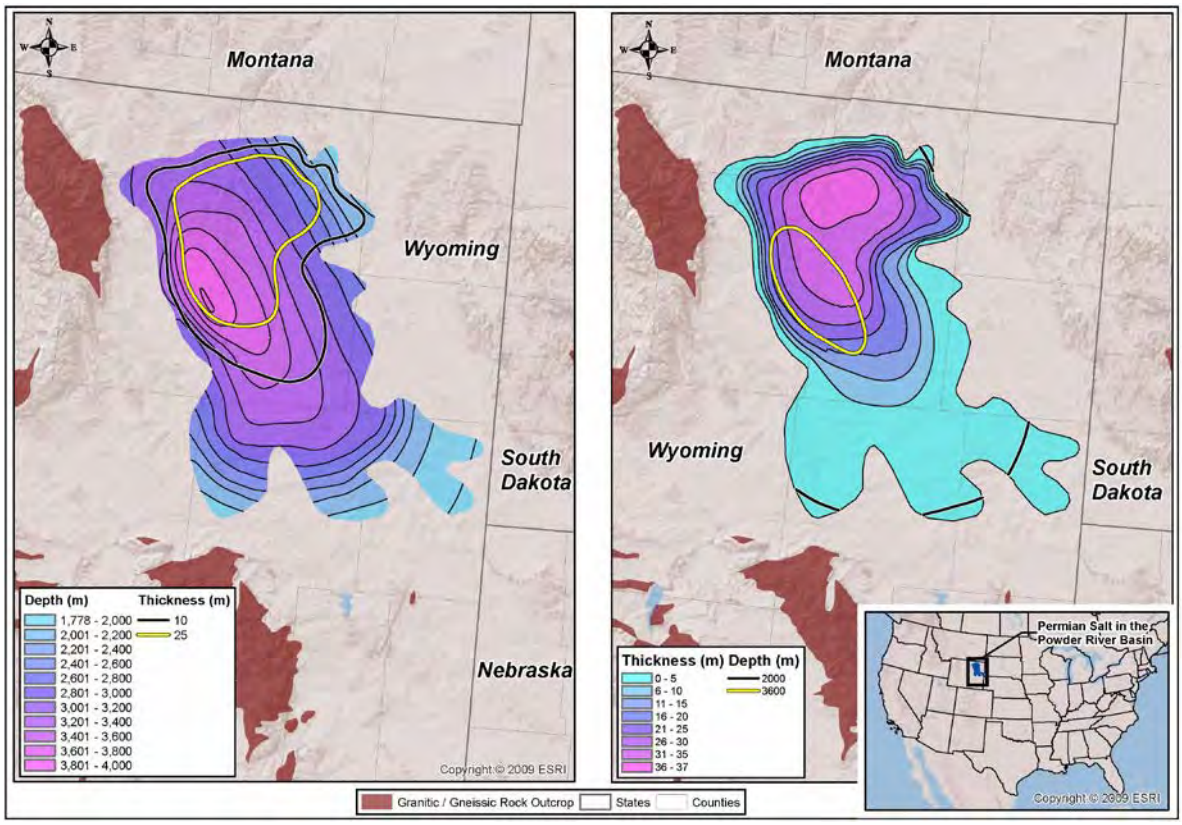

Figure 4-15. Depth to top and aggregate thickness of the Ervay Salt in Permian Goose Egg Formation in the Powder River Basin.

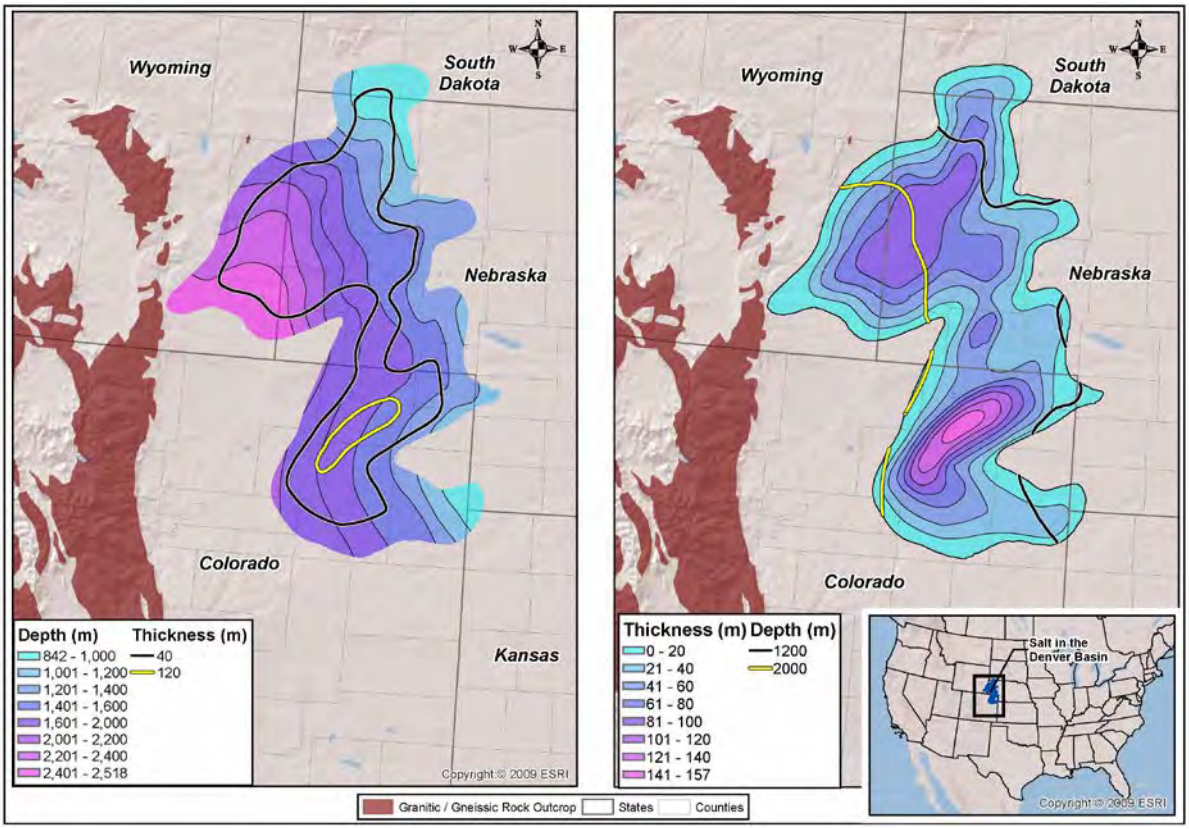

Figure 4-16. Depth to top and aggregate thickness of Permian salts of the northern Denver Basin.

4.2.7 Denver Basin

The Denver Basin is another asymmetric Laramide-age basin located southeast of the Powder River Basin that dips towards and is bounded on the west by the Front Range of the Colorado Rockies (Higley et al., 1996). Total depth of sediment approaches 4000 meters on the western margin. Paleozoic rocks include terrigenous sandstones and conglomerates shed off the ancestral Rocky Mountains, deltaic sediments and marine carbonates and shales.

Permian salts of the Denver Basin include thirteen separate units described by Oldham (1996). The thirteen salts vary in extent and thickness but have an aggregate thickness of up to 150 meters in the southern extent of the salts in northeastern Colorado (Figure 4-16). The oldest salt (13) is a thin salt that occurs at the top of the Chase Group (Lower Permian) and the youngest four salts (1-4) occur within the Goose Egg and Opeche Formations but below the level of the Ervay Salt in the Powder River Basin (Upper Permian). The middle salts (5, 6, and 7) occur within the Blaine Formation, which is the equivalent to the San Andres Formation in the Palo Duro Basin (Johnson and Gonzales, 1978). The Permian salts of the Denver Basin thus include salts that are time-equivalent or closely time equivalent to salt beds present in the Permian Basin to the southeast and the Powder River and Williston Basins to the north and northeast (Figure 4-2).

The depth to the top of salt in the Denver Basin ranges from roughly 800 to 1400 meters on the eastern side of the basin to as much as 2500 meters on the western side of the basin (Figure 4-16).

The data source used to create the GIS database for salt of the Denver Basin is listed in Table 4-6.

Table 4-6. GIS data sources for salts of the Powder River and Denver Basins

Salt	Reference	Source Features used in GIS Database
Permian salt of the Powder River and Denver Basins	Ege (1985)	Depth and isopach contours, extent of salt

4.2.8 Permian Basin (Delaware, Midland, Palo Duro and Anadarko Basins)

The Permian Basin, formally defined, includes the Delaware Basins and Midland Basins of west Texas and southeastern New Mexico. Early reports concerning the disposal of radioactive waste in salt began to informally broaden the definition of the Permian Basin to include the structural basins to the north (Palo Duro, Dalhart and Anadarko Basins) as well as areas of less structural relief that ramp towards these basins in eastern New Mexico, eastern Colorado and central Kansas. (Pierce and Rich, 1962; Bachman and Johnson, 1973). What this large region has in common is the presence of thick salt deposits (Figure 4-17). These deposits have historically been of interest in the US for HLW disposal with work focused on the Hutchinson salt of Kansas in the 1960s, the Salado salt of southeastern New Mexico in the early 1970s and the San Andres salt in west Texas beginning in the late 1970s (Lomenick, 1996).

The Permian Basin contains eight principal salt-bearing formations (Johnson and Gonzales, 1978) with older salts in the north and younger salts in the south (Figure 4-17). They are described in this section in order of decreasing age, and consist of the Hutchinson, Lower and Upper Clear Fork, San Andreas (Blaine), Artesia Group, Castile, Salado and Rustler (Figure 4-17 and Figure 4-18).

No attempt was made to include the salts of the Artesia Group or Rustler Formation in the GIS database because they generally contain thinner and more discontinuous pure salt, making them difficult to characterize or map over large areas (Pierce and Rich, 1962; Johnson and Gonzales, 1978; Hovorka, 1998). The extent of the Rustler Formation is limited to the Delaware and Midland Basin. The main salt-bearing unit in the Artesia Group is the Seven Rivers Formation. The Seven Rivers Formation lies below

the Salado Formation and above the San Andres Formation within the Midland Basin and southern portion of the Palo Duro Basin, its northernmost extent (Figure 4-18). These two salts are not discussed further in this report.

Data sources used to create the GIS database for salt of the Permian Basin are listed in Table 4-7.

Table 4-7. GIS data sources for salts of the Permian Basin

Salt	Reference	Source Features used in GIS Database
Salado	Johnson and Gonzales (1978)	Thickness contours
Salado	Hovorka (1998)	Elevation of marker bed on top of Salado
Salado	Powers and Richardson (2004a,b)	Depth of Salado Formation to the immediate north and south of WIPP site
Salado	New Mexico Tech Petroleum Recovery Research Center[1]; National Geothermal data System[2]	Data from 94 wells to determine top of Salado Formation in SE New Mexico
Castile	Johnson and Gonzales (1978)	Isopach contours, extent of salt
San Andres	Presley (1981)	Depth contours in Palo Duro Basin
San Andres	Johnson and Gonzales (1978)	Thickness contours and extent of salt, depth contours outside of Palo Duro Basin
San Andres	Zambito et al. (2012)	Discrimination of salt thickness in western Kansas
San Andres, Lower and Upper Clear Fork	Ege (1985)	Extent of salt in eastern New Mexico
Upper Clear Creek	Johnson and Gonzales (1978)	Depth and thickness contours, extent of salt
Lower Clear Creek	Johnson and Gonzales (1978)	Depth and thickness contours, extent of salt
Hutchinson	Johnson and Gonzales (1978)	Depth and isopach contours, extent of salt

[1] http://octane.nmt.edu/gotech/Petroleum_Data/allwells.aspx

[2] http://www.geothermaldata.org/

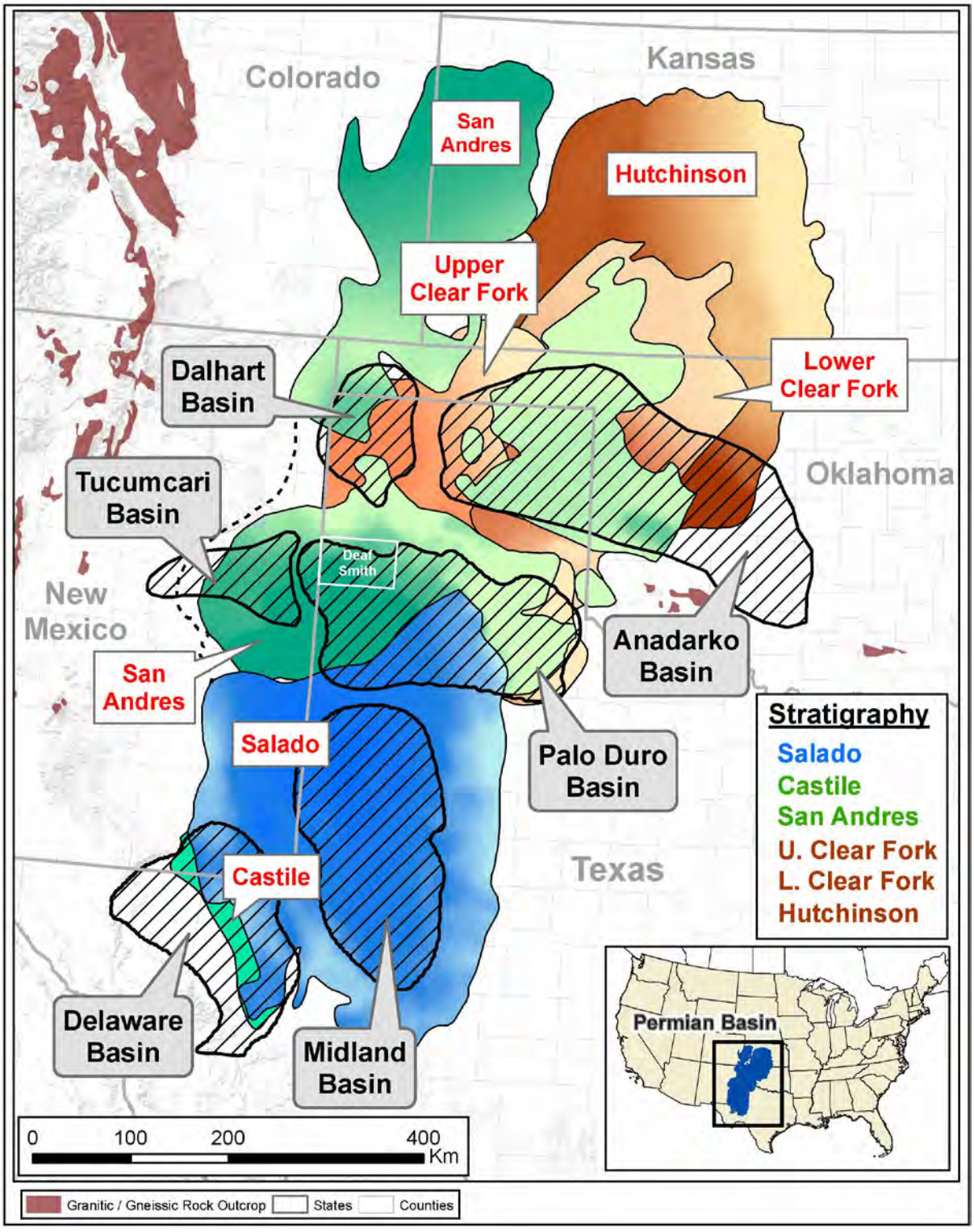

Figure 4-17. Overview of the distribution of major salt-bearing formations, their stratigraphic relationships and boundaries of sub-basins within the greater Permian Basin of Texas, New Mexico, Oklahoma, Kansas and Colorado. Brown to tan-shaded formations are Lower Permian, green to blue-shaded formations are Upper Permian. Color shading within formations indicates the relative depth to top of salt with darker shades indicating greater depth. Red labels identify the Hutchinson, Lower and Upper Clear Fork, San Andres, Castile and Salado formations. Sub-basin boundaries from Handford (1980) and Hovorka (1998). Deaf Smith County is shown for reference and discussed in text.

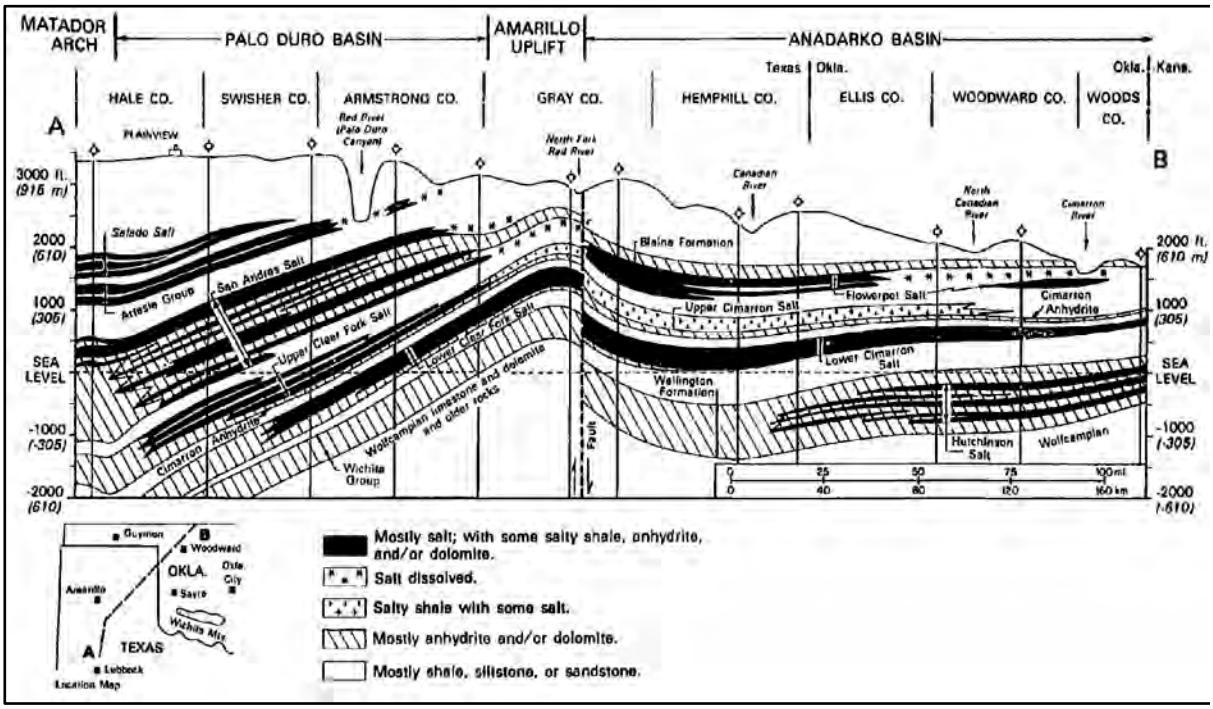

Figure 4-18. Regional cross-section of major salt formations in the Palo Duro and Anadarko Basins (from Johnson and Gonzales, 1978). This cross-section shows the stratigraphic relationship of all the major salt formations in the Permian Basin, from the lowermost Hutchinson Salt with a depositional center to the north, to the Salado Salt with a depositional center to the south. Cross-section is from southwest to northeast with "A" marking the Matador Arch (separating the southern margin of the Palo Duro Basin from the northern margin of the Midland Basin) and "B" marking the Oklahoma-Kansas state line within the Anadarko Basin (see figure inset).

4.2.8.1 Hutchinson Salt Member of the Wellington Formation

The Hutchinson Salt Member of the Permian Wellington Formation extends from central Kansas into western Oklahoma where it deepens within the Anadarko Basin (Figures 4-18 and 4-19). The Hutchinson Salt in Kansas was the subject of the earliest series of comphrensive studies and experiments aimed at selecting a suitable site for HLW disposal. The earliest experiments in 1961-1962 at the Carey Salt Mine near Hutchinson involved disposal of simulated liquid waste in a heated salt cavity beneath the floor of the mine (Lomenick, 1996). These experiments revealed that disposing of liquid HLW in salt was impractical and convinced the AEC that liquid waste would have to be solidified before being disposed of in a geologic repository.

In 1962 the AEC requested that ORNL carry out emplacement and thermal tests in salt using irradiated fuel assemblies (Limenick, 1963; 1996). The test, Project Salt Vault, was conducted at the Carey Salt Company mine northeast of Lyons (about 25 miles northwest of Hutchinson) between 1964 and 1967 (Lomenick, 1996). In 1970, the AEC announced selection of the same mine near Lyons as the site for a demonstration salt-mine repository. In early 1972 the AEC withdrew the plan for a demonstration repository at Lyons for several reasons, including recognition by the Kansas Geological Survey of unsealable oil and gas boreholes near the site and problems with salt solution mining activities at an adjacent mine (Lomenick, 1996).

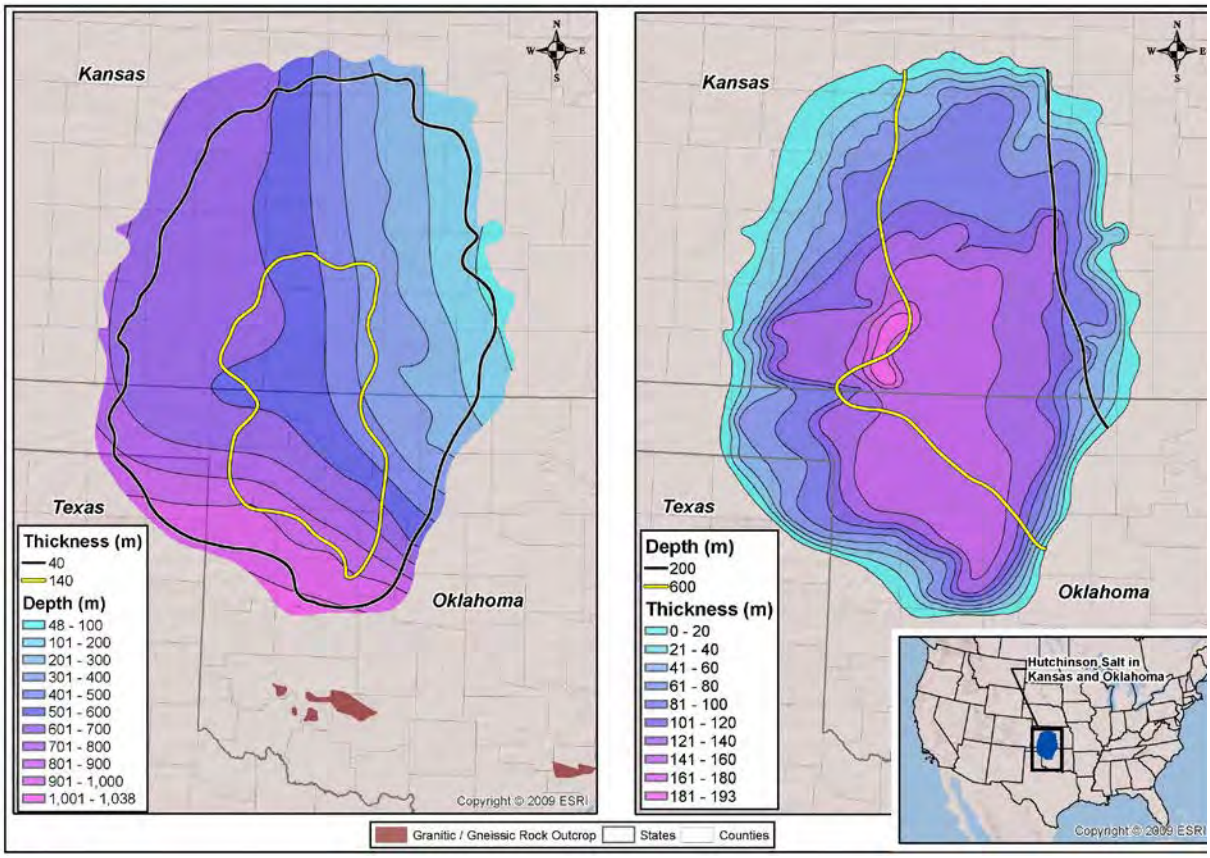

Figure 4-19. Depth to top and aggregate thickness of the Permian Hutchinson Salt.

The Hutchinson Salt Member in central Kansas consists of approximately 100 meters of flat-lying deposits of salt, shale and anhydrite, with salt compromising the bulk of the member. Bedded salt units are typical 5-6 meters thick and separated by thin beds of shale (Lomenick, 1963). Thickness of aggregate salt ranges from less than 100 meters on the margins of the salt deposit to more than 180 meters near its center (Figure 4-19). Depth to the top of salt ranges from about 100 meters at its eastern extent to more than 1000 meters in the Anadarko Basin of Oklahoma (Figure 4-19).

4.2.8.2 Salt of the Lower and Upper Clear Fork Formations (Lower and Upper Cimarron)

The Lower and Upper Clear Fork Formations of the Clear Fork Gourp are known as the Lower and Upper Cimmaron in the Anadarko Basin and north (Johnson and Gonzales, 1978). Salts of the Lower and Upper Clear Fork are the thickest in the Palo Duro, Anadarko and Dalhart Basins and thin farther north in southern and central Kansas (Figures 4-20 and 4-21). The Upper and Lower Clear Fork Formations are separated by primarily carbonates and shales of the Tubb Formation (Budnik and Smith, 1982). Both formations contain interbedded anhydrite and dolomite (Budnik and Smith, 1982). Individual massive salt beds are typically 2-8 meters thick (Johnson and Gonzales (1978). Depth and thickness ranges are similar for salt in the two formations, depending on location within basins, with the Upper Clear Fork having a somewhat greater thickness (Figures 4-20 and 4-21).

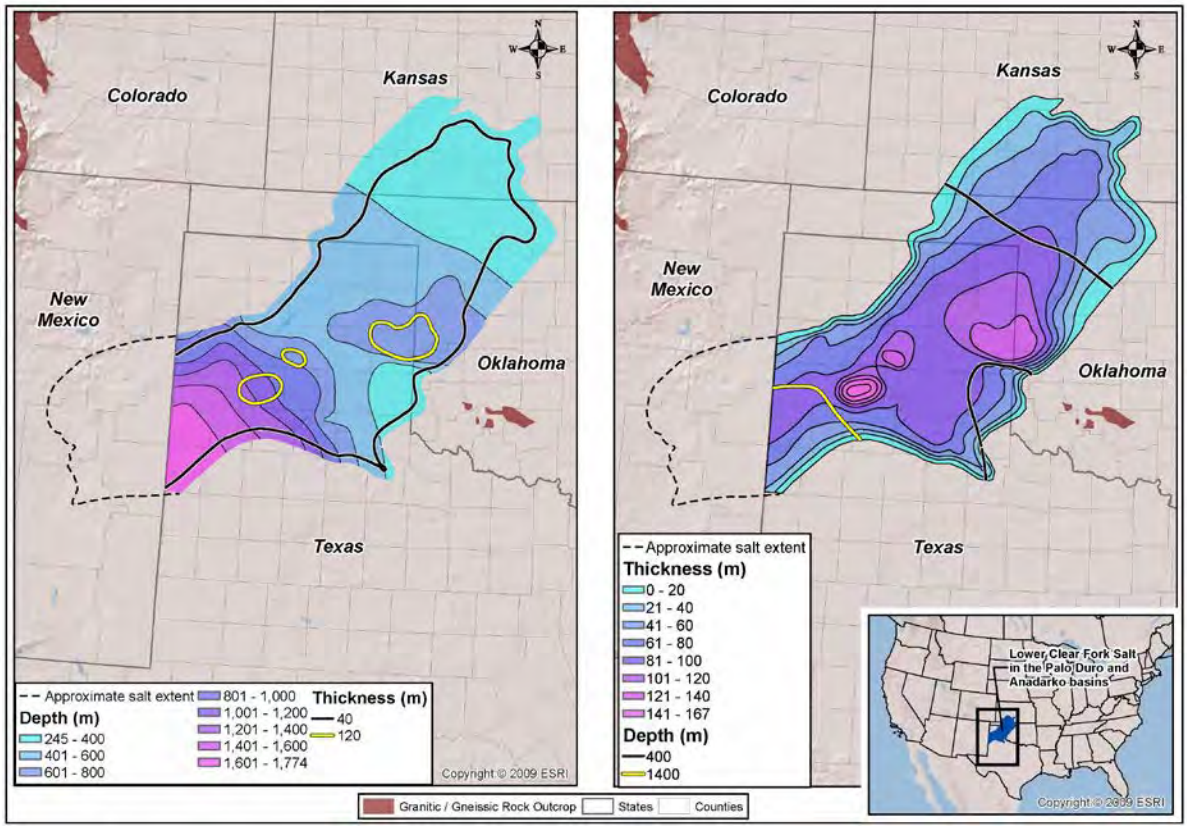

Figure 4-20. Depth to top and aggregate thickness of the Permian Lower Clear Fork Salt. Approximate western boundary of salt in New Mexico is interpreted from information in Ege (1985).

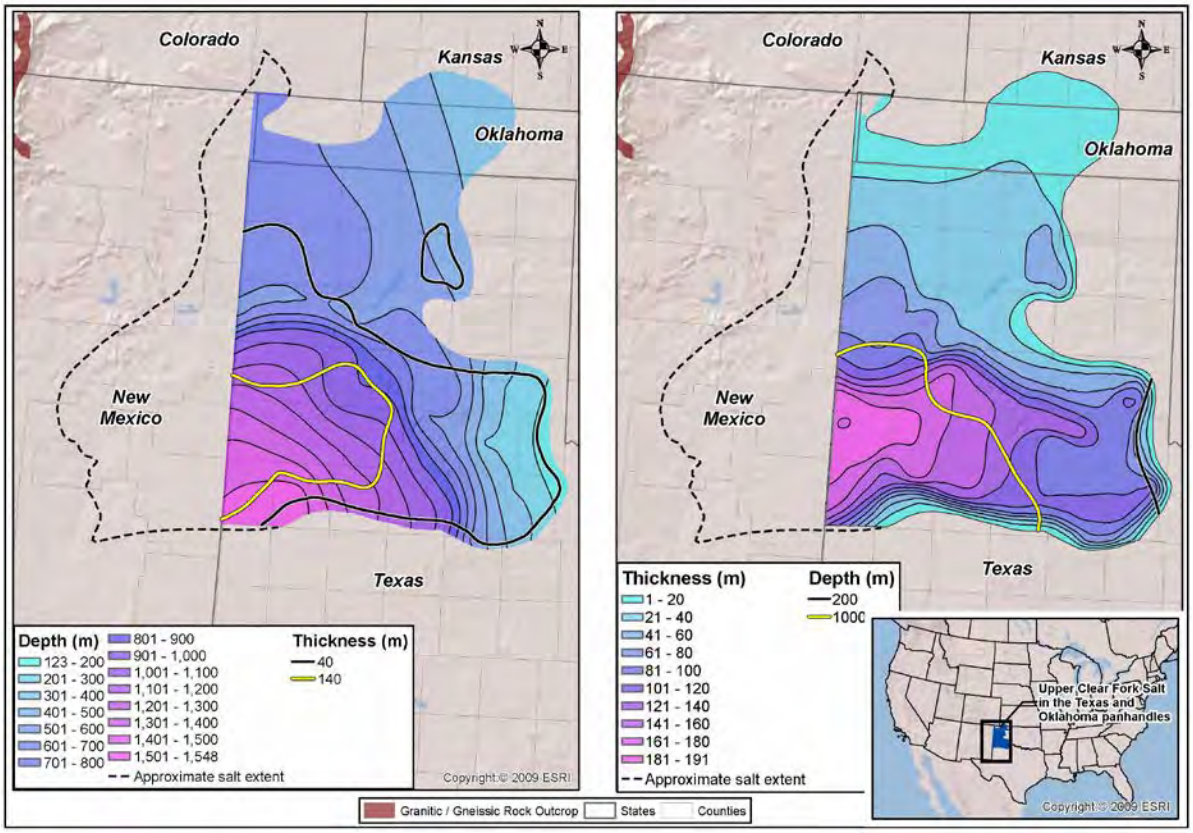

Figure 4-21. Depth to top and aggregate thickness of the Permian Upper Clear Fork Salt. Approximate western boundary of salt in New Mexico is interpreted from information in Ege (1985).

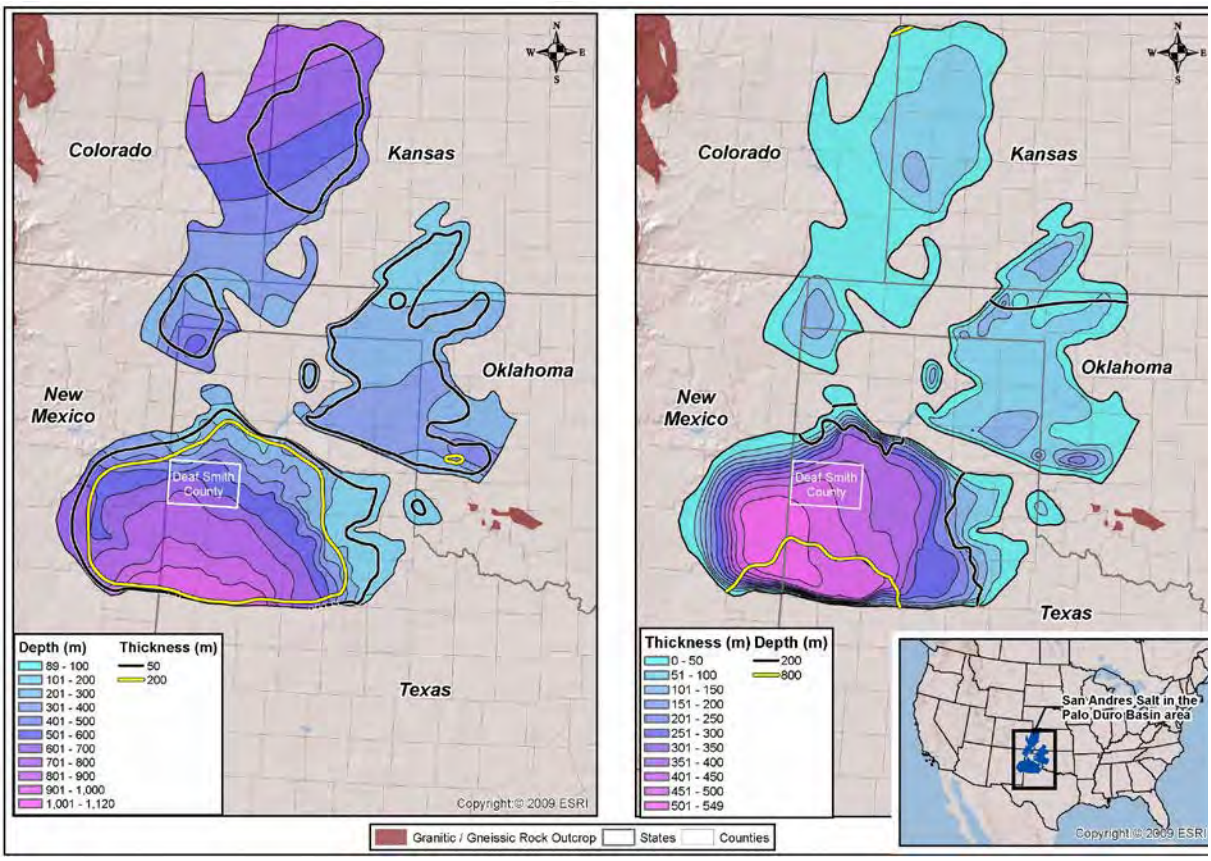

Figure 4-22. Depth to top and aggregate thickness of the salt in the Permian San Andres Formation. Deaf Smith County was one of three sites in the US selected for site characterization in 1986.

4.2.8.3 Salt of the San Andres Formation

Salt of the San Andres Formation is thickest in the Palo Duro Basin, reaching a maximum aggregate thickness of over 500 meters (Figure 4-22). Much of the basin has salt thicker than 200 meters. The salt thins to the north where is typically less than 150 meters thick. Deaf Smith County, in the northwestern part of the Palo Duro Basin (Figures 4-17 and 4-22), was recommended and approved in 1986 as one of three sites in the US to go forward for site characterization and the only site in salt (Lomenick, 1996). Individual massive salt horizons reach a thickness of 60 meters in the San Andres Formation and are interbedded with anhydrite and dolomite (Presley, 1981; see Figure 4-3). The depth to the top of the San Andres salt ranges from less than 200 meters in its eastern and northeastern extent to slightly more than 1000 meters at the southern margin of the Palo Duro Basin (Figure 4-22).

The San Andres Formation is known as the Blaine Formation farther to the north and east in the Dalhart and Anadarko Basins (and Denver Basin as previously discussed). The San Andres Formation in the Midland Basin is primarily dolomitic and does not contain salt (Johnson and Gonzales, 1978).

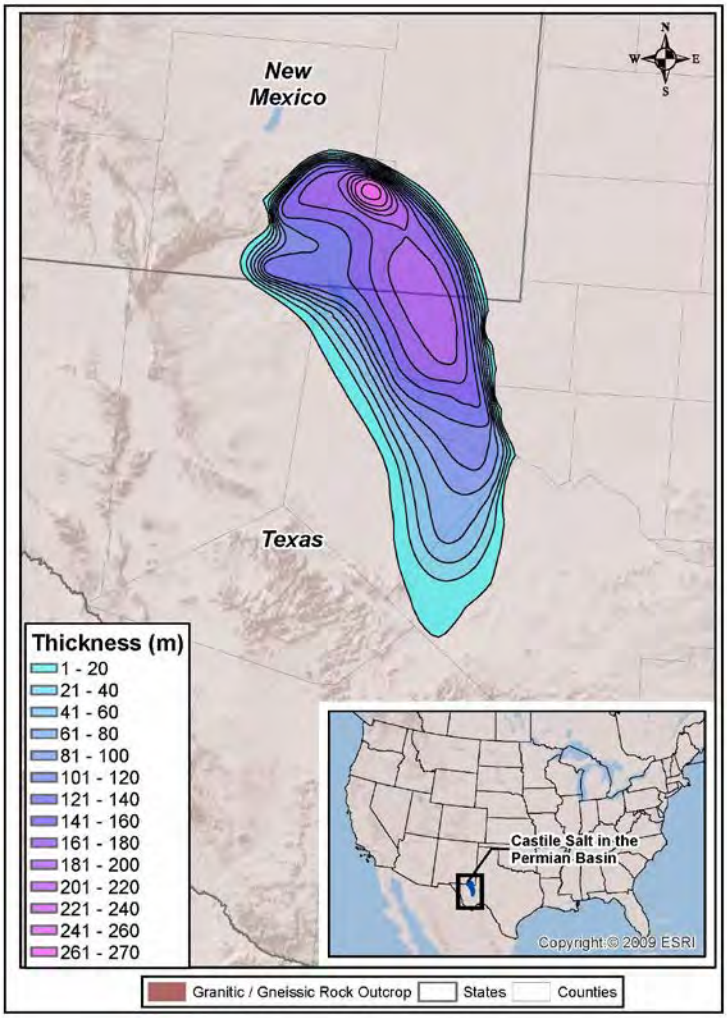

Figure 4-23. Aggregate thickness of salt in the Permian Castile Formation in the Delaware Basin.

4.2.8.4 Salt of the Castile Formation

The Castile Formation is confined to the Delaware Basin and is primarily anhydrite with lesser amounts of salt. The total formation thickness has a maximum thickness of more than 600 meters with aggregate salt thickness of as much as 270 meters (King, 1948; Johnson and Gonzales, 1978). Anhydrite occurs in three thick sequences overlain by salt. Four major anhydrite sequences dominate the Castile, separated by three intervals primarily composed of bedded salt (Hovorka, 1998). Individual bedded salt intervals reach typical thicknesses of approximately 100 meters. Variations in the aggregate thickness of salt are shown in Figure 4-23. No data has been identified that would allow construction of a reliable structural contour map for depth to the top of salt over the entire area of the Castile Formation.

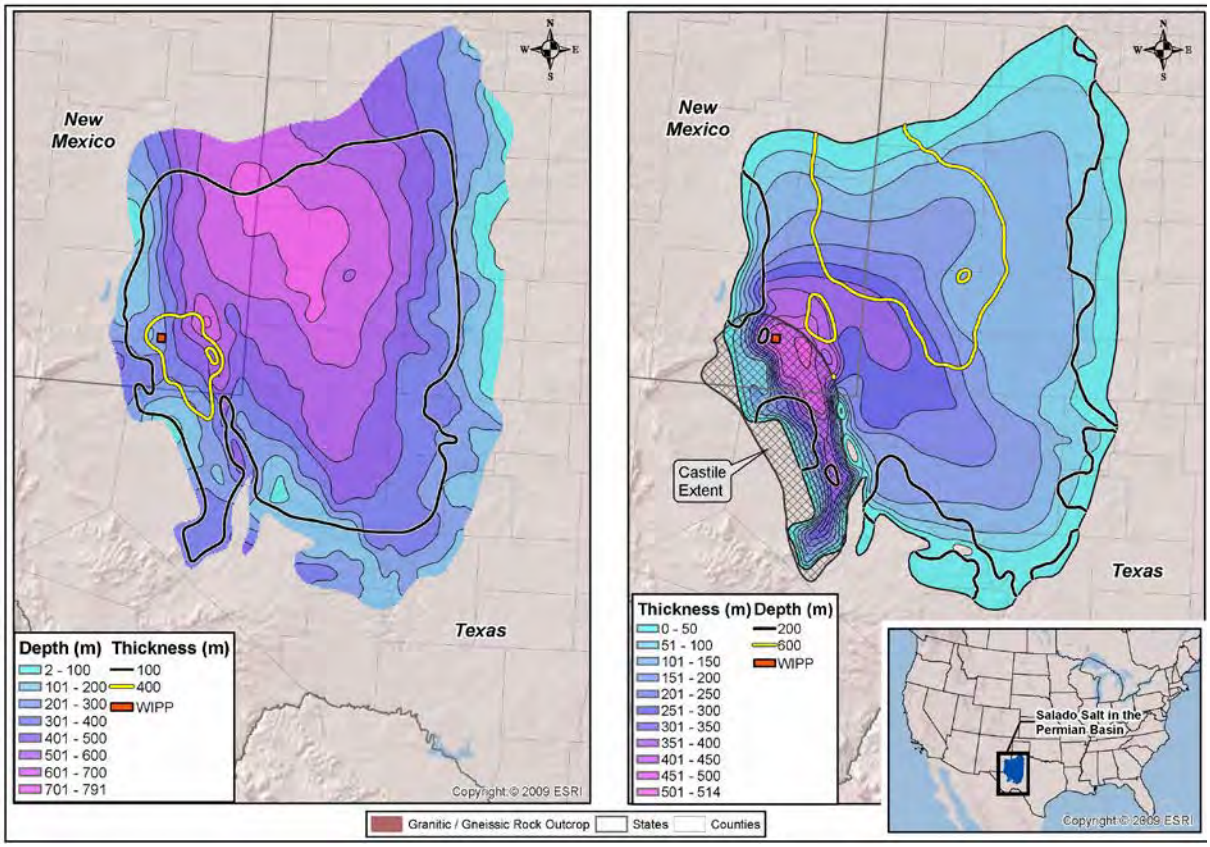

Figure 4-24. Depth to top and aggregate thickness of the salt in the Permian Salado Formation in the Delaware, Midland and Palo Duro Basins. Extent of the Castile Formation and the location of the WIPP site (red square) are shown for reference.

4.2.8.5 Salt of the Salado Formation

The Salado Formation fills the Midland Basin and parts of the Delaware and Palo Duro Basins. It is thickest in the Delaware Basin and thins as it extends to the east across the Midland Basin and north into the southern Palo Duro Basin (Figure 4-24).

Most of the Salado Formation is composed of greater than 70% salt with the remainder consisting of detrital materials and anhydrite. An area near the platform that divides the Midland from the Delaware Basin has consistently less than 70% salt (as little as ~50% salt due to the increased thickess of anhydrite layers towards the Delaware Basin (Hovorka, 1998; see Figure 4-25). Typical individual salt beds vary in thickness from 3-9 meters and are interbedded with shale and anhydrite with thicknesses of up to 3 and 10 meters, respectively (Hovorka, 1998). The salt bed in which the WIPP disposal area is constructed is 7 meters thick (Swift and Corbet, 2000).

The depth to the top of the Salado Formation ranges from less than 100 meters at its eastern and portions of its western margins, where it approaches the surface as an insoluble residue, to greater than 750 meters in the northern Midland Basin (Figure 4-24).

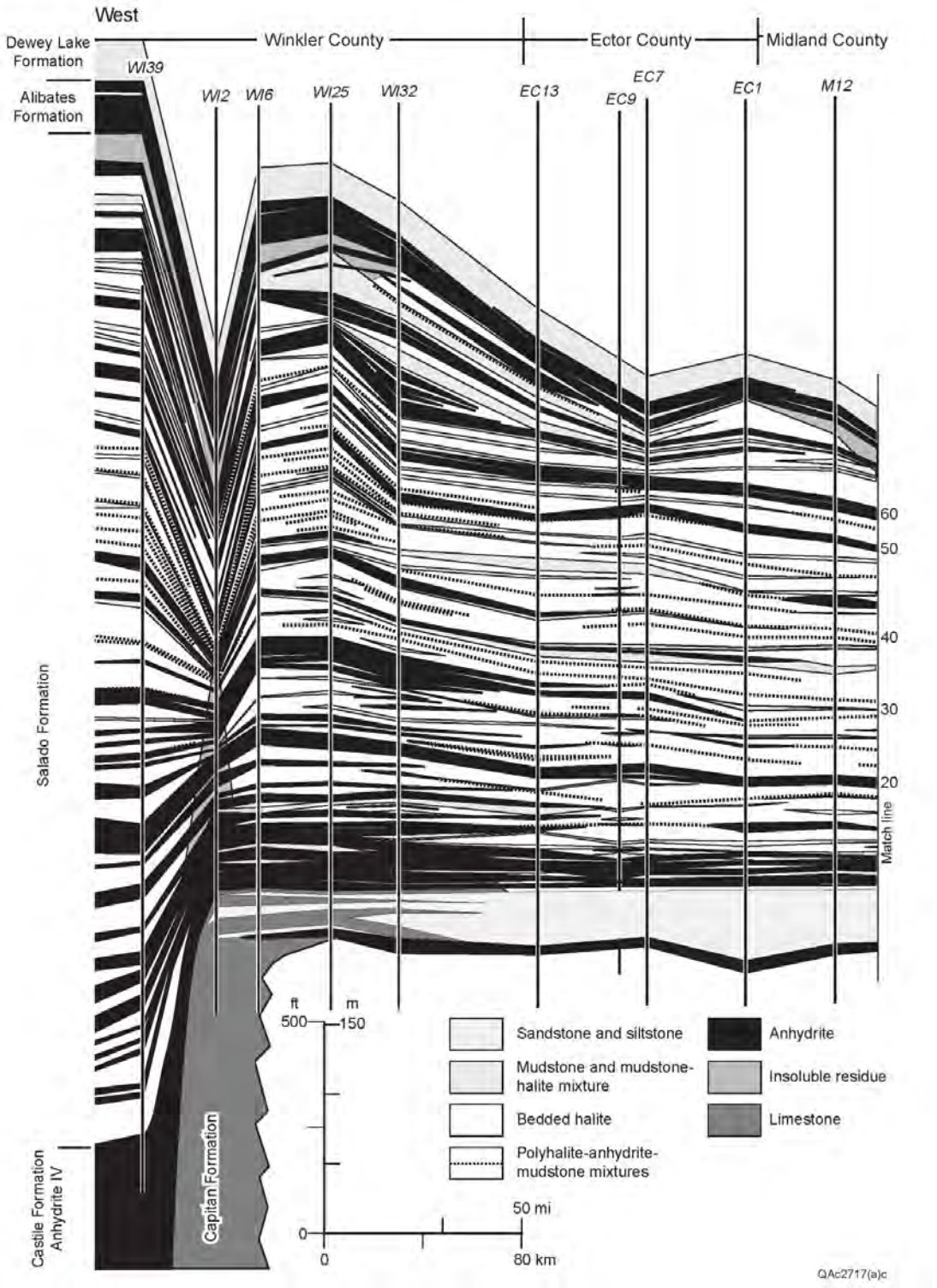

Figure 4-25. East-west cross-section of the western part of the Salado Formation and associated formations from Hovorka (1998). The cross-section is located in the southern half of the Midland Basin and extends from the eastern edge of the Delaware Basin (left) to the middle of the Midland Basin near Midland, Texas. The cross-section shows the internal stratigraphy of the Salado Formation, most notably the frequency and thickness of anhydrite and fine-grained detrital beds interlayered with the halite beds.

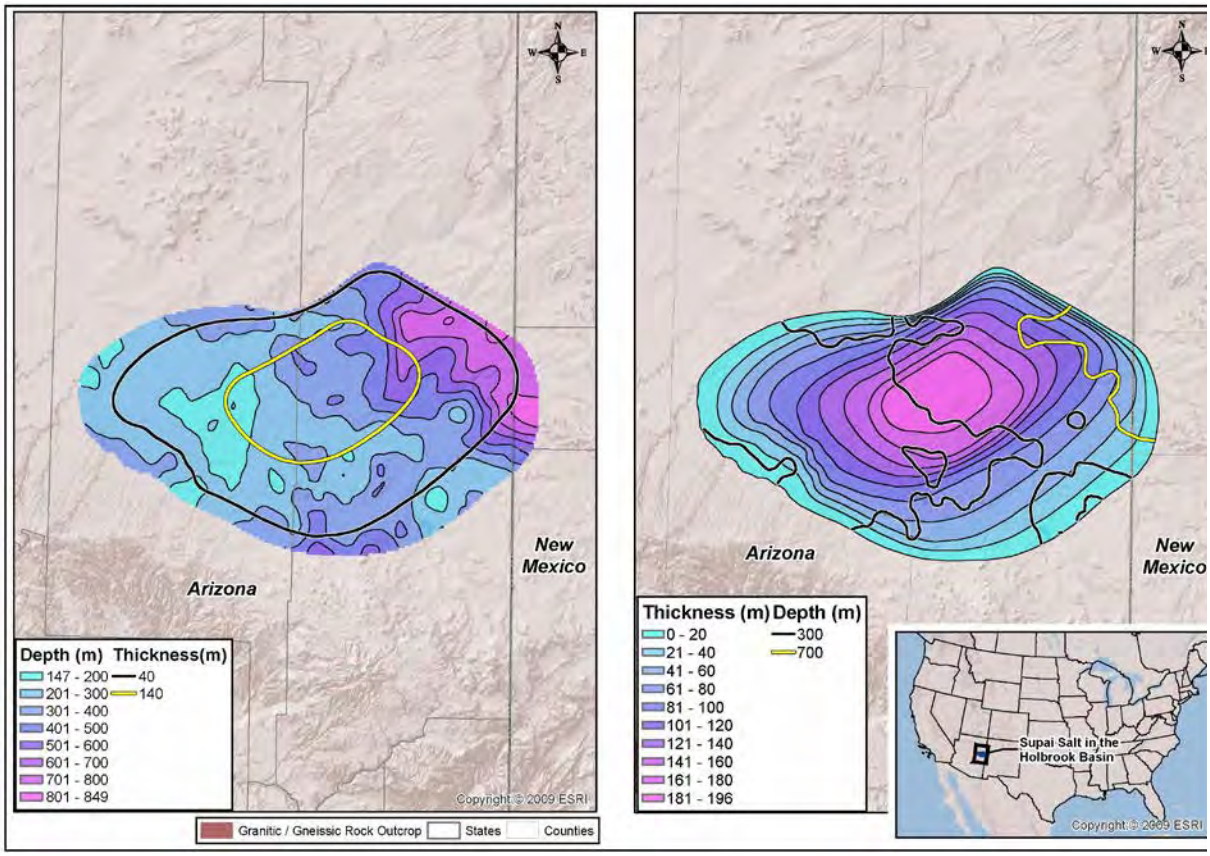

Figure 4-26. Depth to top and aggregate thickness of the salt of the Supai Formation in the Holbrook Basin of Arizona.

Holbrook Basin

The Holbrook Basin is a relatively shallow structural basin on the southern margin of the Colorado Plateau filled with roughly 800-1300 meters of Cambrian through Triassic sediments (Johnson and Gonzales, 1978). The thickest formation in the basin is the Permian Supai Formation which ranges in thickness from about 500-800 meters (Johnson and Gonzales, 1978). Salt deposited in a shallow marine environment occurs primarily in the upper part of the Supai Formation within the Corduroy Member (Rauzi, 2000). The salt is interbedded with shale, anhydrite and minor carbonate. Salt beds are typically 1-2 meters thick but range up to 9 meters in thickness (Rauzi, 2000).

Aggregate thickness of salt reaches more than 180 meters in the center of the basin (Figure 4-26). Depth to the top of the salt is from 150-500 meters throughout most of the basin, reaching 700-800 meters on the northeast basin margin (Figure 4-26).

4.2.9 Late Tertiary Salt in Basins of Arizona and Southern Nevada

In addition to the salt of the Holbrook Basin, several Miocene to early Pliocene salt bodies occur within the extensional basins of the Basin and Range Province of Arizona and an adjoining area of southern Nevada (Faulds et al., 1997). These salts are suggested to have formed in subsiding, internally drained basins via influx of saline groundwaters from upgradient saline sources (Faulds et al., 1997). The Great Salt Lake of Utah is suggested as a modern-day analog.

Rauzi (2002) has described both the known and potential occurrences of Tertiary salt deposits in Arizona in relationship to their use and potential as both salt resources and for solution-mined underground storage of natural gas or liquefied petroleum gas (LPG). From information in Rauzi (2002), we have created GIS data for the maximum extent of the known salt bodies, as well as depth and thickness information for each deposit (Figure 4-27). Depth to the top of the salt deposits ranges from 125 to 700 meters and maximum thickness ranges from 200 to greater than 1300 meters (Figure 4-27).

Salts of the Luke Basin and Red Lake Basin (also known as the Hualapai Basin) have garnered past interest as HLW disposal media primarily because of their extreme thickness (>1000 meters) at moderate depth and the relative massive nature of the halite without significant interbeds (Johnson and Gonzales, 1978). The Luke Basin salt underlies portions Luke Air Force Base and the City of Glendale. The salt is currently being solution mined by Morton Salt Company from two active wells and it hosts three LPG storage caverns (Rauzi, 2002).

Table 4-8. GIS data sources for salts of the Holbrook Basin and Tertiary basins of Arizona and Nevada

Salt	Reference	Source Features used in GIS Database
Supai salt of Holbrook Basin	Rauzi, 2000	Elevation and isopach contours, extent of salt
Tertiary salt deposits of Arizona and Nevada	Rauzi, 2002	Depth and thickness information, maximum extent of salt

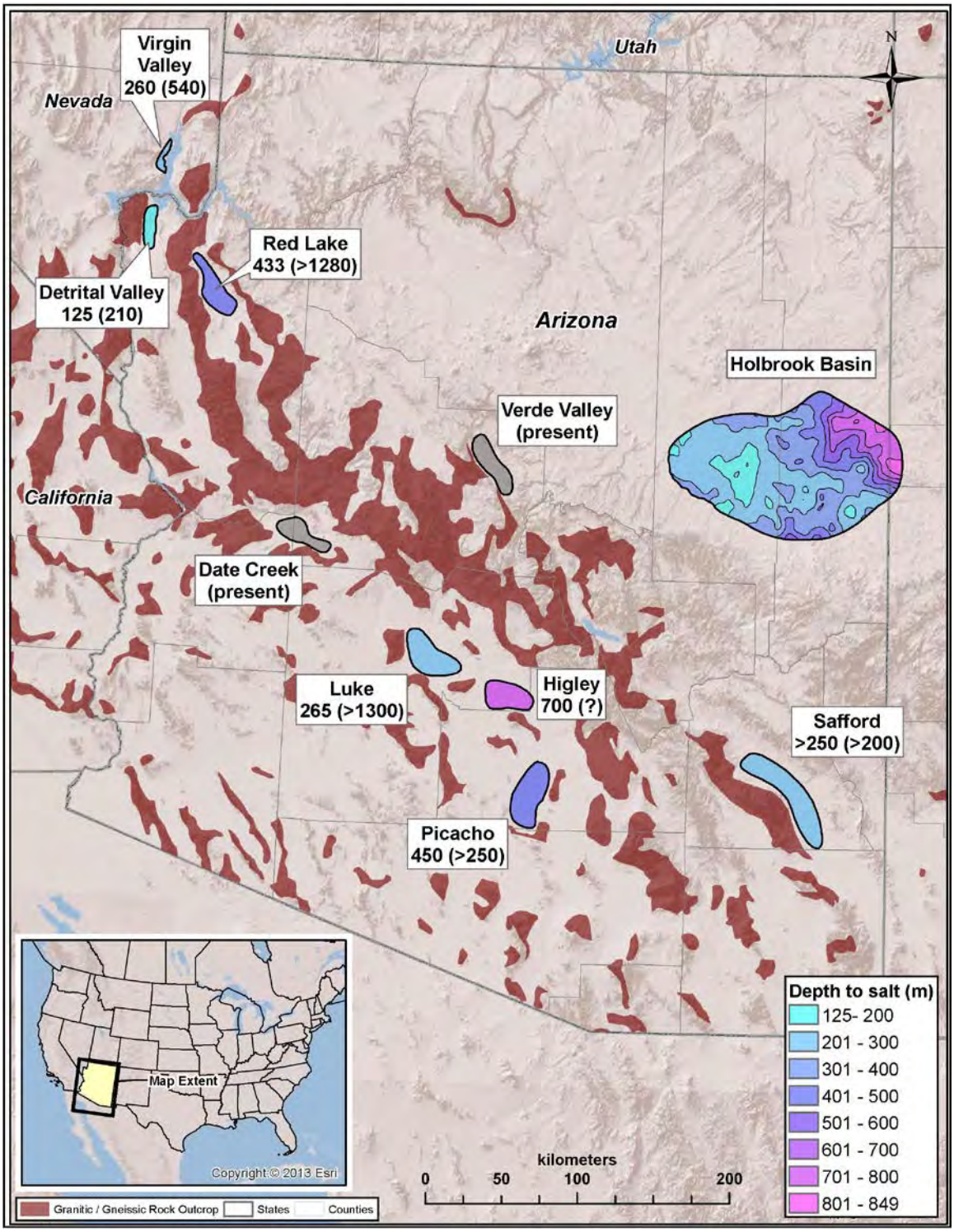

Figure 4-27. Location of salt basins in Arizona and adjoining area in southeastern Nevada. Depth to the top and maximum thickness (in parentheses) of each salt body are indicated in units of meters. Depth and thickness of salt in the Verde Valley and Date Creek Basin are not known well enough to provide depth and thickness values, but salt is known to be present. Data for approximate depths and thicknesses are from Johnson and Gonzales (1978) and Ege (1985), except for salt in the Holbrook Basin.

4.2.10 Gulf Coast Salt Domes

GIS data has been obtained for the location and shape of salt domes in the Gulf Coast region, as well as the approximate subsurface limit of the Jurassic Louann Salt, which is the deep source of the salt domes (Table 4-9). These features are displayed in Figure 4-2. Other information, such as the depth to the top of individual salt domes, is available in reports such as Beckman and Williamson (1990). The information related to Gulf Coast Salt Domes will be refined and additional information added to the GIS database in the future. The sections below provide an overview of the five salt basins in the Gulf Coast Region that contain salt domes, based on information provided in Johnson and Gonzales (1978).

Table 4-9. GIS source data for bedded salt and salt domes in the Gulf Coast Region

Salt	Reference	Source Features used in GIS Database
Louann	Available for download from USGS Digital Data Series 069–E http://pubs.usgs.gov/dds/dds-069/dds-069-e/	Approximate limit of middle Jurassic Salt in the Gulf Coast
Gulf Coast salt domes	Available for download from USGS Digital Data Series 069–E http://pubs.usgs.gov/dds/dds-069/dds-069-e/	Locations and shapes of salt diapirs in the Gulf Coast

4.2.10.1 North Louisiana Salt Dome Basin

At 13,000 square kilometers, the North Louisiana Salt Dome Basin is the smallest of five dome-bearing basins in the Gulf Coast Region. The basin is divided into small and large sub-basins that are separated by an E-W-oriented ridge. Nineteen salt domes, originating from the Jurassic Louann Salt were found within the basin. Vertical diapirism of the Louann Salt began in the early Cretaceous and ceased by middle Cretaceous. However, local arching and faulting continued into late Tertiary. Studies of Quaternary deposits showed no significant tectonic movements. Four of the domes occur about 1000 m below the ground surface, whereas others occur at shallower depth (<320 m). Some of the domes have been utilized for LPG storage, whereas six of the domes have saline water at the surface. The salt domes are associated with carbonates, marls, chalks, anhydrite, clay, sand, and shale.

Oil and gas are major resources in the basin. Salt, gravel and sand, gypsum, and anhydrite were also mined in the past. Most of the domes (15) are within 100 to 300 m of the ground surface. Some have been used for LPG storage, whereas others were mined for brine production.

4.2.10.2 Northeast Texas Salt Dome Basin

The Northeast Texas Salt Dome Basin is about 160 kilometers in diameter and major NE-oriented tectonic and depositional features bound the basin. Drilling in the basin identified 18 domes and the presence of an additional five domes is speculated. The domes are 1.5 to 8 km in diameter. Carbonates, evaporites, marls, chalks, anhydrite and sand and gravel occur as cap rocks or hosts to the salt intrusion. The parent Jurassic Louann bedded salt is at a depth of about 6100 to 6700 meters below the basin. Four of the deepest salt domes occur at about 1000 m below the surface, whereas seven are at <200 m depth.

A 0.006 mm/year uplift rate was estimated for the last 50 Ma and the domes have not been active since the late Tertiary based on detailed studies of Quaternary deposits.

Oil and gas resources accumulated along structural and stratigraphic traps associated with Jurassic, Cretaceous, and Tertiary formations. Most domes are barren of hydrocarbon deposits; three are utilized for oil and gas production. Salt production was mostly confined to subsurface mining and salt springs. Other resources include sand and gravel and lignite. LPG was deposited in three of the domes and another is utilized for multiple industry usage. The basin has 18 known salt domes; 14 of them occur 300 to 1000 m below the surface.

4.2.10.3 Mississippi Salt Dome Basin

The Mississippi Salt Dome Basin extends from SE Louisiana across Mississippi to SW Alabama for a distance of 400 km. Uplifted structural blocks and faults bound the NW-SE trending basin. Part of the basin occupies the Mississippi alluvial plain, whereas the rest is within the Gulf Coast plain. The basin contains 77 known and suspected salt domes at various depths and 58 of the domes have cap rocks. Limestone anhydrite, clay, shale, and unconsolidated Quaternary sandstone with minor shale and carbonates are associated with the Jurassic Louann salt intrusion. The parent salt is at 6400 m and at 3165 m along the northern flanks of the basin. About 12 domes occur below 3000 m, whereas the rest are at 300 to 600 m below the surface.

Oil and gas are major resources in the basin and 11 of 77 domes are significant producers. Two domes were used for salt production and two others for LPG storage. Other resources in the basin include sand and gravel, clay, brick clay, and limestone for Portland-cement production. About half of the 77 salt domes exceed a depth of 300 to 1000 m below the surface, seven are utilized for industrial usage, and others are more than 600 m below the surface.

4.2.10.4 Texas-Louisiana Coast Salt-Dome Basin

Salt diapirs and flowage have created complex geologic structures in the Texas-Louisiana coastal basin. The basin contains more salt domes than the combined number of domes discovered in the other four salt-dome basins. Stratigraphically, deltaic continental deposits interfingering with marine shales and clays are the dominant lithologic units associated with the salt domes. Most of the salt domes occur at about 1000 m below the surface except for four domes that occur at <360 m depth. One of the domes is shallower at 135 m and it is covered by thick cap rock that ranges in thickness from 80 to 160 meters.

The basin provides the most prolific petroleum source in the United States and it is found within Tertiary, Cretaceous and Jurassic rocks. Salt domes and salt tectonics provided the structural traps for the oil and gas resources. Of the known 143 domes, 77 are utilized for industrial usage, including oil and gas storage and salt production. Native sulfur, sand and gravel, limestone, clays, and gypsum are other resources. Even though many salt domes occur within the basin only four out of 139 were considered favorable for additional investigation for storage of waste by Johnson and Gonzales (1978).

4.2.10.5 South Texas Salt-Dome Basin

The South Texas Salt-Dome Basin is one of the smaller of the Gulf Coast basins and is confined to the southeastern part of Texas. The basin occurs within the Rio Grande Syncline bounded by high-angle normal faults with up to 150 m of displacements related to salt flowage. Marine and continental deposits of Tertiary sands, clays, and sandstone associated with salt diapirs constitute the geology of the basin. Six salt domes, one of which is the deepest (4300 m) and the largest in the US, have been identified in the basin. Two other domes are at 1900 m below the ground surface and the shallowest is at 250 to 300 below the surface.

Major oil and gas production is from Tertiary limestone and sandstone reservoirs and the salt domes. Potash, gypsum, and low-grade uranium are known to occur within the basin.

4.2.11 Description of Other Salts

The following salt bodies are briefly described based on information in Johnson and Gonzales (1978) and Ege (1985). Information for the first five salt occurrences listed, in the western US, is illustrated in Figure 4-28. The location of the Saltville and southern Florida salt occurrences are illustrated in Figure 4-2.

1. **Sevier Valley** (Utah): The salt deposit occurs in central Utah. Up to 60 m of salt was exposed at a quarry and estimated to be about 300 m in thickness. Even though the salt is brick red in color due to red clay, it is 95 to 97 percent halite. Exploratory wells intersected the salt deposit at variable depths that ranged from 1800 to 3600 meters. The salt layers are generally thin (<20 m) except for the north-central area where more than 600 m of salt was encountered. The salt is generally deformed.
2. **Eagle Valley** (Colorado): The deposit consists of Pennsylvanian clastic and evaporite rocks on the western side of the Rocky Mountains in northwestern Colorado. Halite occurs 450 m below the surface in association with anhydrite, shale, and siltstone to a maximum depth of 1600 meters. The evaporite deposit is deformed.
3. **Piceance Basin** (Colorado): Two halite-bearing zones associated with nahcolite are known within the Parachute Creek Member of the Early Tertiary (Eocene) Green River Formation. Salt deposits of the Piceance basin are at moderate depth and individual layers are thin. Dissolution of the upper salt is probably an ongoing process.
4. **Green River Basin** (Wyoming): Salt layers of the Green River basin are usually mixed with trona and are thin (<1 m) units of almost pure halite that occur locally as part of a thicker evaporite bed.
5. **Idaho-Utah-Wyoming Borde**r: The halite deposit is interbedded with red shale, anhydrite, and limestone. It is impure and discontinuous and occurs in a structurally complex setting.
6. **Saltville Area (Virginia)**: Salt occurs as a tectonic breccia up to 200-300 meters thick primarily in the upper member of the Mississippian Maccrady Formation (Cooper, 1966). The tectonic breccia occurs within a large synclinal fold and is mixed with brecciated fragments of shale, anhydrite, limestone and dolomite. Salt comprises the largest percentage of the breccia.
7. **Southern Florida**: The thin salt beds (<3 m) are associated with anhydrite, limestone, dolomite, and minor amounts of dark shale. The salt beds were intersected in deep wells more than 3300 m below the ground surface (Figure 4-2).

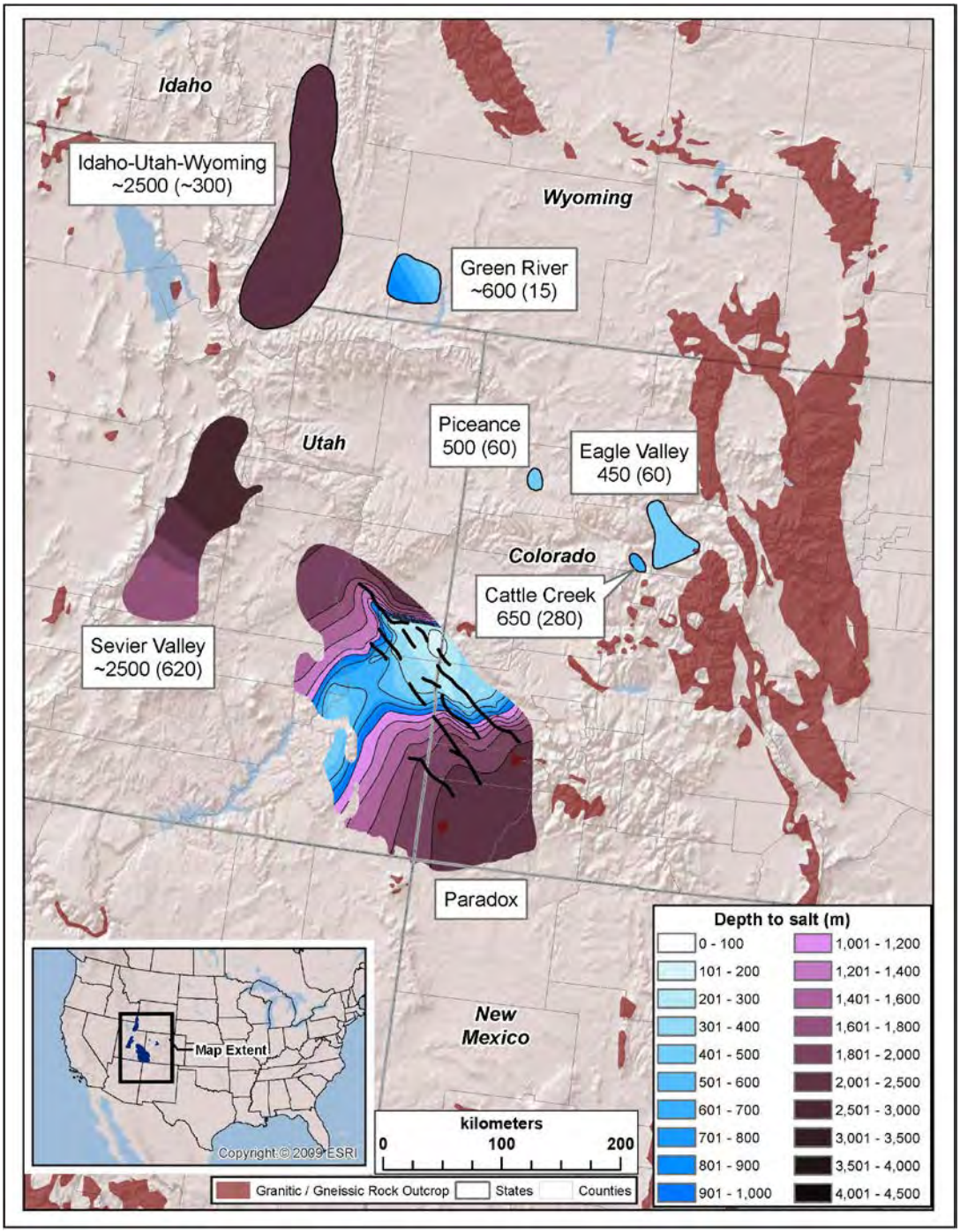

Figure 4-28. Location of salt bodies in Colorado, Utah and Wyoming. Depth to top and maximum thickness (in parentheses) of each salt body is listed in units of meters. More detailed information for the Paradox salt is illustrated in Figure 4-8. Data for approximate depths and thicknesses are from Johnson and Gonzales (1978) and Ege (1985), except for salt in the Paradox Basin.

4.3 Shale and Other Clay-Bearing Rocks

(An updated discussion of shale is presented in Section 5 of the main report).

4.4 Granitic (Crystalline) Rock

Data for granitic rock in the contiguous United States were obtained from Garrity and Soller (2009), a digital database of the geology of North America. Granitic, or crystalline, rocks in the GIS database are broadly divided into granitic (igneous) or gneissic (metamorphic) rock (Figure 4-29). Using designations from Garrity and Soller (2009), granitic rock types in the database include granite, felsite, intermediate plutonic rocks, and tonalite. Gneissic rock types include orthogneiss, paragneiss, tonalite gneiss, sedimentary and volcanic gneiss, and undivided gneissic rocks.

Granitic rocks are found in several distinct geologic and tectonic settings within the contiguous US:

1. Northern Appalachians: Large areas of crystalline rocks exposed across much of upstate New York, New Hampshire, and Vermont that are part of the Phanerozoic crystalline rock terrains. The Adirondacks crystalline rocks are part of a shield area.

2. Central and Southern Appalachians: Tectonically exposed Precambrian rocks forming considerable topography in the southeastern states of Virginia through Georgia. They are generally deformed and metamorphosed.

3. Central Midwest: Tectonically exposed crystalline basement rocks that form the Ouachita Mountains magmatic province of southern Oklahoma and the Llano uplift of central Texas.

4. Northern Midwest: Large areas of Wisconsin and Minnesota that contain Precambrian crystalline rocks that are part of the southern Canadian Shield.

5. Rocky Mountains: Mountain ranges running from the Canadian border to central New Mexico containing extensive Proterozoic crystalline-rock terrains.

6. Basin and Range: Region containing Proterozoic and Phanerozoic crystalline-rock terrains that are highly faulted and covered by Tertiary volcanic rocks.

7. Pacific Coast and the Sierra Nevada: A large region of the western US with outcrops of crystalline rock from the Mexican border through California and the length of the Sierra Nevada. Blocks also occur along the coast south of San Francisco and across the California-Oregon border. The Cordilleran batholiths are marginal to Precambrian basement.

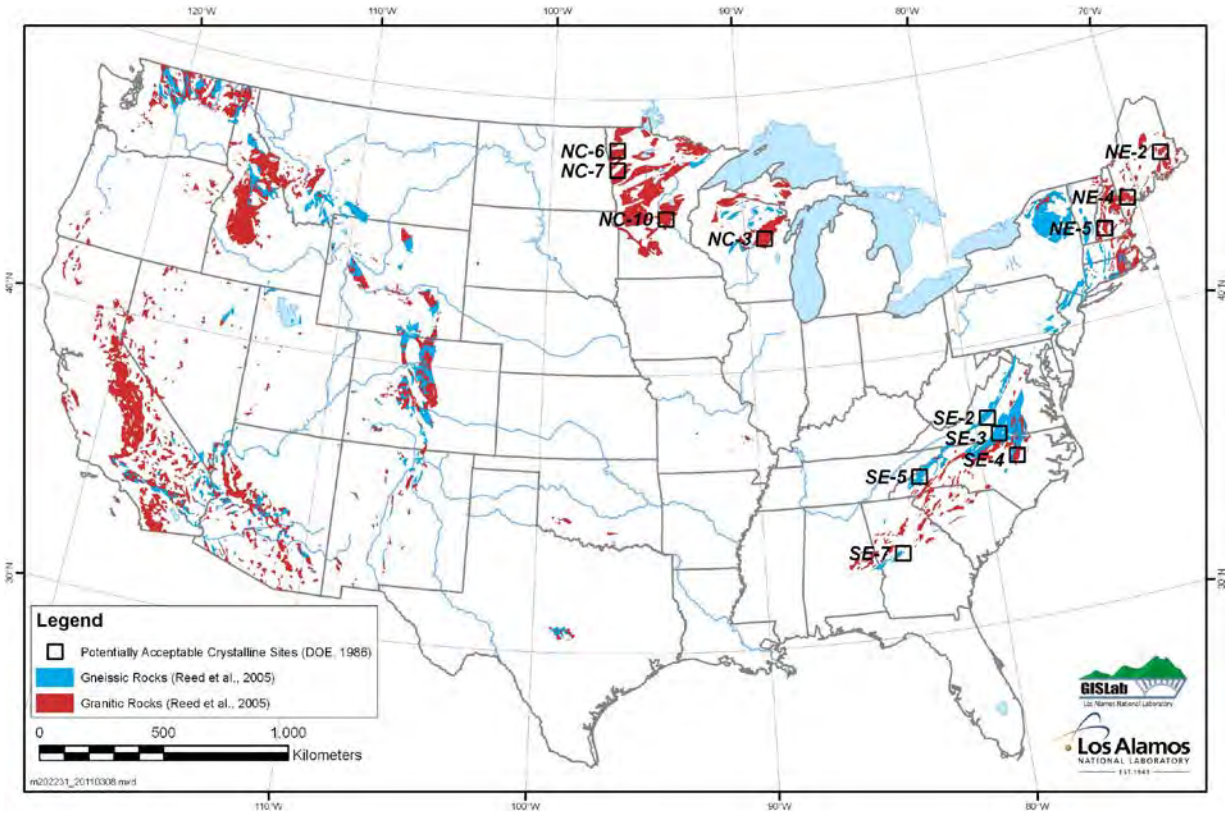

Figure 4-29. Surface exposures of granitic and gneissic crystalline rock in the contiguous United States. Shown for reference are the locations of the twelve Potentially Acceptable Crystalline Sites identified as part of the DOE Crystalline Repository Project of the early and mid-1980s (DOE, 1986b).

4.5 Crystalline Basement Rock

(An updated discussion of crystalline basement rock is presented in Section 4 of the main report).

5. Rock Properties and In-Situ Conditions for Shale Estimated from Sonic Velocity Measurements

Summary - this section presents the development of methods to assess hydrological and geomechanical properties and conditions for shale formations based on sonic velocity measurements. Publically available data sets have been identified for shales under investigation for nuclear waste disposal in Europe and from shales of interest for oil exploration and production in the North Sea. These data have been used in the development of several correlations which link properties to sonic compressional velocity. The advantage of using correlations based on sonic velocity is that properties can be estimated from geophysical logs. This information is often more readily available than direct property measurements on core that would otherwise be required. Furthermore, geophysical logs typically provide a continuous readout along wells that can be more readily used to characterize spatial variability in properties. The correlations developed are then used to assess properties and conditions in several shale formations of interest within the United States which have publically available data on sonic velocity. Some of the proposed correlations have been previously investigated by others and comparisons between correlations are reasonably consistent. The approach has been extended here to other properties as well as in-situ conditions, in particular, a method to estimate pore-fluid pressure. A method is also developed and used to account for anisotropy for properties where sufficient information is available to assess directional dependence. Some of the correlations, in particular estimation of sonic velocity parallel to bedding from normal to bedding sonic velocity measurements, and estimation of clay content from sonic velocity were found to be weak, indicating that additional independent measurements are desirable to supplement such estimates. Several of the correlations were also constructed from small data sets and require additional data for greater confidence. Similarly, several factors that can influence properties have not been investigated here, including confining stress, fluid saturation conditions, and the organic content of shale. Further verification is also needed for many of the parameter estimates for the US shale formations analyzed; therefore, they should be viewed as initial estimates.

Data for assessing the properties of shale formations for nuclear waste disposal are often limited by a lack of direct measurements, either performed in-situ or on laboratory samples taken from the formation. Here we use the term “shale” as a general term describing any fine-grained argillaceous, or clay-rich, clastic rock, including mudstones, claystones, and argillites. The USGS definitions indicate that mudstone is a term that encompasses claystones, shales, argillites, and siltstones (USGS 2013), and might be a more suitable generic term for rock type studied here. In this section, correlations for estimating hydrological and geomechanical formation properties and in-situ conditions from sonic velocities are developed from data on shale formations that lie outside of the United States. The advantage of using correlations based on sonic velocity is that properties can be estimated from geophysical logs. This information is often more readily available than direct property measurements on core that would otherwise be required. Furthermore, geophysical logs typically provide a continuous readout along wells that can be more readily used to characterize spatial variability in properties. The correlations developed are then used to assess properties and conditions in several shale formations of interest within the United States.

5.1 DATA USED TO DEVELOP THE CORRELATIONS

Data used for developing the correlations are given in Tables 5-1 through 5-3. Table 5-1 is based on formations reported on by Boisson (2005), who documented characteristics of shale formations being investigated for high-level nuclear waste disposal. The data are generally presented in terms of a maximum, minimum, and "best" value for each parameter. Table 5-1 presents the "best" values, or in cases where only a maximum and minimum were presented, the average is used as "best". Furthermore, the porosity data are averaged over different types of porosity measurements that were reported (e.g., as determined by water content and grain density, or by mercury injection). Clay content is the mass of all clay mineral types divided by the total rock mass. Permeabilities are converted from reported hydraulic conductivities measured either in-situ or on core samples in the laboratory. The uniaxial compressive strength and permeabilities were reported in terms of directional values for some of the formations, but in many cases orientation is not known. In addition, more recent and/or more complete information for some parameters and formations was found from other sources, as indicated in Table 5-1.

Additional types of properties data for some of the same formations reported on by Boisson (2005) but taken from a variety of other sources are given in Table 5-2. This table provides bulk density, Young's modulus, shear strength, cohesive strength, friction angle, and tensile strength. For the Opalinus Clay-Mont Terri, Opalinus Clay-Benken, Callovo-Oxfordian, and Tournemire argillite, directional values of Young's modulus are available. Similarly, for the Opalinus Clay-Mont Terri, Opalinus Clay-Benken, and Callovo-Oxfordian Clay, cohesive strength, and tensile strength have directional information related to the parameters.

Table 5-1. Data from Boisson (2005) (except as noted)

formation	sonic velocity (m/s)	porosity	clay content	uniaxial compressive strength (MPa)	depth (m)	maximum burial depth (m)	permeability (in-situ, m^2)	permeability (lab, m^2)
Boom Clay	1710[(1)] (1970)[(1)]	0.38[(6)]	0.600	2.21*	176	176	2.31E-19 (4.78E-19)	3.34E-19 (7.27e-19)
Oxford Clay	1776[(2)] (1798)[(2)]	0.42[(7)]	0.560	2.21*	265	-	-	-
Ypresian Clay	1805*	0.422[(8)]	0.605	1.47*	324	471	3.78E-17*	6.74E-19[(8)] (8.03e-19)[(8)]
Opalinus Clay – Mont Terri	2620[(3)] (3350)[(3)]	0.137[(3)]	0.597	15[(3)] (11)[(3)]	235	1353	4.19E-21 (1.94E-20)	7.14E-21[(3)] (2.04E-20)[(3)]
Spanish Reference Clay	2642*	0.290	0.775	2.94*	147	265	1.29E-19*	1.92E-18*
Callovo-Oxfordian Clay	2900[(4)] (3400)[(4)]	0.16[(4)]	0.450	21[(4)]	412	-	3.39E-22*	7.90E-21[(4)] (1.02e-20)[(4)]
Konrad mine – lower Cretaceous Claystone	2925*	-	0.583	-	250	-	-	-
Konrad mine – lower Cretaceous Claystone – Albian	2972*	-	0.496	-	250	-	1.02E-17	-
Opalinus Clay – Zurich Weinland	3030[(4)] (4030) [(4)]	0.124[(4)]	0.533	29.4 (27.9)	544	1588	2.91E-21* (1.08E-20)	1.92E-21 (9.90E-21)
Tournemire argillite	4434[(5)] (3799)[(5)]	0.090[(9)]	0.550	32.4	250	1000	2.00E-21[(10)] 6.00E-21[(10)]	1.05E-21*
Konrad mine – lower Cretaceous Claystone – Callovo	3774*	0.099	0.517	73.5	912	912	1.15E-18	-
Palfris formation – Wellenberg	4586*	0.013	0.430	47.1 (52.9)	397	> 3000	3.32E-19*	6.50E-21[(11)]*
Boda claystone	5094*	0.012	0.400	115	294	>3000	9.62E-20*	-

Note: for directionally-sensitive parameters (sonic velocity, uniaxial compressive strength, permeability) values for both normal and parallel to bedding are shown where available; first values are for orientation normal to bedding followed by numbers in parentheses for values parallel to bedding. Single values are for normal to bedding unless marked with * indicating orientation is unknown.

Sources other than Boisson (2005): [1] Dehandshutter et al. (2005a); [2] Kerner et al. (1989); [3] Bock (2009); [4] Wenk et al. (2008); (5) Zinszer et al. (2002); [6] Shaw (2010); [7] Midttøme et al. (1998); [8] Piña-Diaz (2011); [9] Matray et al. (2007); [10] Millard and Rejeb (2008); [11] Fedor et al. (2008)

Table 5-2 . Additional Properties of Some Formations from Table 5-1.

formation	saturated bulk density (kg/m^3)	Young's modulus (GPa)	shear modulus (GPa)	Poisson's Ratio	cohesive strength (MPa)	friction angle (degrees)	tensile strength (MPa)
Boom Clay	2050[1]	0.35*[9]	0.04*[15]	0.4*[19]	0.24*[15]	18*[15]	0.1*[17]
Oxford Clay	1940[2]	0.1*+[10]	0.034*$[10][20]	0.47*[20]	0.17*+[10]	20.3*[17]	-
Ypresian Clay	2000[1]	0.042*[11]	0.017*$[11]	0.25*[11]	0.36*[11]	10.6*[11]	-
Opalinus Clay – Mont Terri	2430[3]	4[3] (10)[3]	2.4$@ [3]	0.29@[3]	3[3] (4)[3]	22[3]	0.6[3] (1.2)[3]
Callovo-Oxfordian Clay	2480[4]	4.0[12] (5.6)[12]	2.4*[16]	0.3*[12]	3.0[12] (7.0)[12]	22.5*[12]	2.6*[18]
Opalinus Clay – Zurich Weinland	2520[4]	5.0[13] (10.5)[13]	2.0$[13]	0.25[13]	1.6[13] (7.6)[13]	22*[13]	1.2[13] (2.7)[13]
Tournemire argillite	2551#[5]	7.0[14] (22.0)[14]	2.0[14]	0.16[21]	-	-	-
Konrad mine – lower Cretaceous Claystone – Callovo	2585#[6]	-	-	-	-	-	-
Palfris formation - Wellenberg	2629#[7]	-	-	-	-	-	-
Boda claystone	2803##[8]	-	-	-	-	-	-

Note: for directionally-sensitive parameters (all of the above with the exception of bulk density) values for both normal and parallel to bedding are shown where available; first values are for orientation normal to bedding followed by numbers in parentheses for values parallel to bedding. Single values are for normal to bedding unless marked with * indicating orientation is unknown.

saturated bulk density based on porosity and grain density

saturated bulk density based on porosity and dry bulk density

+ extrapolated to zero confining stress

$ computed using Poisson ratio and Young's modulus

[@] computed from approximation reported by Bock (2009) $\frac{1}{G_n} = \frac{1}{E_n} + \frac{1}{E_p} + \frac{2\upsilon_p}{E_p}$, where G_n is the shear modulus normal to bedding, E_n is Young's modulus normal to bedding, E_p is Young's modulus parallel to bedding, and υ_p is Poisson's ratio parallel to bedding. Bock (2009) gives a value of 0.35 for υ_p.

Sources: [(1)] Lima et al. (2012); [(2)] Midttøme et al. (1998); [(3)] Bock (2009); [(4)] Wenk et al. (2008); [(9)] Matray et al. (2007); [(6)] EAEC (1984); [(7)] Baeyens and Bradbury (1994); [(8)] Fedor et al. (2008); [(9)] Shaw (2010); [(10)] Kutschke and Vallejo (2012); [(11)] Piña-Diaz (2011); [(12)] Charlier et al. (2013); [(13)] Volckaert (2004); [(14)] Giraud et al. (2007); [(15)] Dehandshutter et al. (2005b); [(16)] Jougnot et al. (2010); [(17)] Burland et al. (1977); [(18)] Ghorbani et al. (2009); [(19)] Bastiens et al. (2007); [(20)] Kerner et al. (1989); [(21)] Niandou et al. (1997)

Similar data are available from Horsrud (2001), who also developed several correlations between sonic velocity and petrophysical parameters. These data are mainly from formations in the North Sea that are of interest for petroleum resource development. The data presented by Horsrud (2001) are given in Table 5-3.

Table 5-3. Rock Properties Data from Horsrud (2001)

formation	sonic velocity (m/s)*	porosity	clay content	uniaxial compressive strength (MPa)*	Young's modulus (GPa)*	shear modulus (GPa)*	depth (m)
Mo Clay	1706	0.72	0.25	1.67	0.30	0.19	0
Smectite	1757	0.57	0.99	2.08	0.22	0.10	0
London Clay	1796	0.45	0.65	1.67	0.07	0.10	0
Tertiary Miocene	1886	0.55	0.53	6.25	0.81	0.29	1370
Tertiary Paleocene-3	2143	0.31	0.52	7.92	1.04	0.42	1940
Tertiary Paleocene-2	2413	0.34	0.56	12.92	1.93	0.71	1870
Tertiary Paleocene-1	2439	0.31	0.34	12.50	1.63	0.71	1720
Upper Jurassic-1	2529	0.3	0.32	7.92	1.11	0.42	3160
Upper Jurassic-3	2966	0.17	0.47	18.33	2.59	1.01	2550
Triassic	3018	0.15	0.65	13.33	2.00	0.91	2440
Upper Jurassic-2	3185	0.1	0.58	27.08	3.85	1.36	2630
Middle Jurassic	4818	0.03	0.49	77.50	12.22	5.39	4870

* normal to bedding

As can be seen from Tables 5-1 and 5-3, the formations reported on by Boisson (2005) are at depths less than 1000 m whereas the formations selected by Horsrud (2001) are mainly at depths greater than 1000 m. However, the maximum burial depths of several of the Boisson (2005) formations were at some time in the past greater than 1000 m. Although the Horsrud (2001) measurements were made normal to bedding, Horsrud (2001) reports that velocities parallel to bedding ranged from 0 to 25% larger than the normal-to-bedding velocities. The Mo Clay data in Table 5-3 show a high porosity of 0.72 and a low clay content of 0.25. Based on information from the "Geosites in Denmark" website (see references), the Mo Clay is a diatomite. The data for this formation were not used in the correlations given below because of the low clay content and the substantially different hydro-mechanical character of diatomite as compared with most shales.

5.2 THE DEVELOPMENT OF CORRELATIONS TO ASSESS FORMATION PROPERTIES AND CONDITIONS

5.2.1 Treatment of Anisotropic Sonic Velocities

The sonic velocity data show in several cases that the compressional sonic velocity, V_p, is different normal and parallel to bedding. The effects of anisotropy have to be considered in order to use sonic velocity as an independent variable to correlate with rock properties. Certain properties, such as porosity and bulk density, are not directional. If one formation has isotropic behavior and a single value of V_p and another formation having the same porosity is anisotropic with two different values of V_p depending on direction, which velocity from the anisotropic formation should be used in the correlation? The selection of a single velocity from an anisotropic system appears to be ambiguous. A pragmatic selection that has been found to be suitable is the geometric mean of the parallel, V_{pp}, and normal, V_{pn}, sonic velocities, $V_{pm} = \sqrt{V_{pn}V_{pp}}$. For anisotropic properties, it could be argued that the velocity and property directions should be used consistently, i.e., the correlation for a property normal to bedding should use the velocity normal to bedding. However, there does not seem to be much advantage to this method over using the geometric mean velocity. Instead, estimates for property values for an orientation parallel to bedding use a scaling factor called the anisotropy factor. The anisotropy factor is computed as the ratio of the velocity parallel and normal to bedding ($V_{pr} = V_{pp}/V_{pn}$) raised to a power that is determined empirically. A property value for a parallel-to-bedding orientation is then computed by multiplying the normal-to-bedding property value by the anisotropy factor.

To implement the approach outlined above requires a means of estimating the bedding-parallel velocities for cases in Tables 5-1 where these data do not exist and for all cases in Table 5-3. Only six of the formations have measurements of sonic velocity normal and parallel to bedding in Table 5-1. A plot of the velocity ratio against the normal velocity is shown in Figure 5-1.

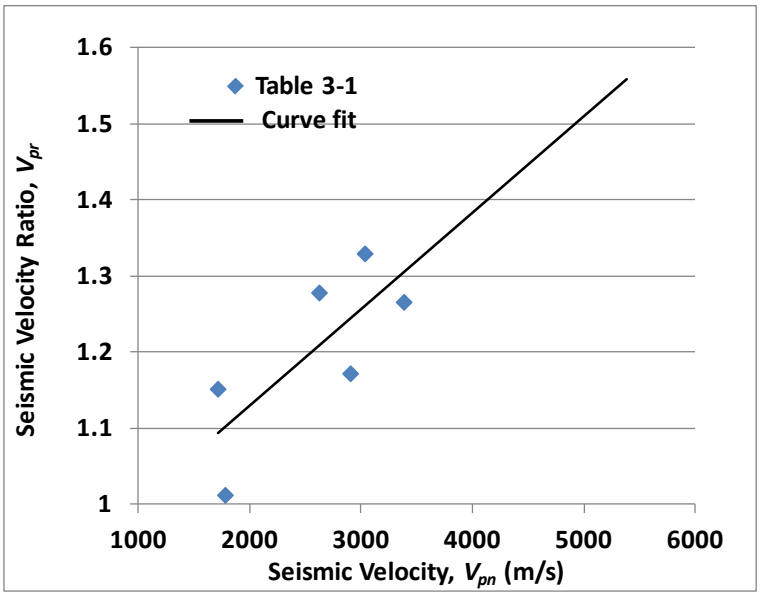

Figure 5-1. Velocity ratio plotted against the sonic velocity normal to bedding.

The values in Table 5-3 are all normal to bedding, but Horsrud (2001) stated that velocities parallel to bedding ranged from 1 to 1.25 times the normal velocity. The normal velocities measured by Horsrud

include one sample with a normal velocity of 4818 m/s. Given that this sample has a velocity ratio of 1.25 (or smaller), it seems that the steadily increasing velocity ratio out to 5000 m/s in the normal velocity is not reasonable. To represent this (somewhat fuzzy) information in the correlation, a point is added at 5000 m/s with a velocity ratio of 1.3. Furthermore, the correlation is performed using transformed variables to help account for limiting behavior, similar to that used by Ingram and Urai (1999). The velocity limits are set to a minimum of 1500 m/s, which corresponds to the sonic velocity in water and a maximum of 7000 m/s, which was found to be a suitable upper limit by inspection. The log-transformed variable used as the independent variable for the velocity ratio is $V_{pnt} = -\log\left(\frac{V_{pn}-1500}{7000-V_{pn}}\right)$, which approaches infinity as the velocity goes to 1500 m/s and negative infinity as velocity goes to 7000 m/s. For the velocity ratio itself, the transformed variable is $V_{prt} = -\log\left(\frac{V_{pr}-1}{1.4-V_{pr}}\right)$, which goes to infinity as V_{pr} tends to 1 and to negative infinity as V_{pr} tends to 1.4, which acts as an upper limit for the velocity ratio. The correlation of the velocity ratio with the normal velocity is shown in Figure 5-2. The correlation equation is given in Equation (5-1), which has a root-mean-square error of 0.068 in the velocity ratio. A plot of the correlation in terms of physical variables is shown in Figure 5-3.

$$V_{prt} = 0.4482\, V_{pnt}^2 + 0.3298\, V_{pnt} - 0.4825 \tag{5-1}$$

The correlation was then applied to the values in Tables 5-1 and 5-3 to provide parallel velocities for cases in which a parallel velocity was not available. A normal orientation is assumed for those cases in Table 5-1 in which the orientation of the sonic velocity measurement was not identified. Given the small data set available to develop the correlation and the weak correlation that has been demonstrated, it is clearly preferable to have measurements for velocities both normal and parallel to bedding rather than relying on the correlation.

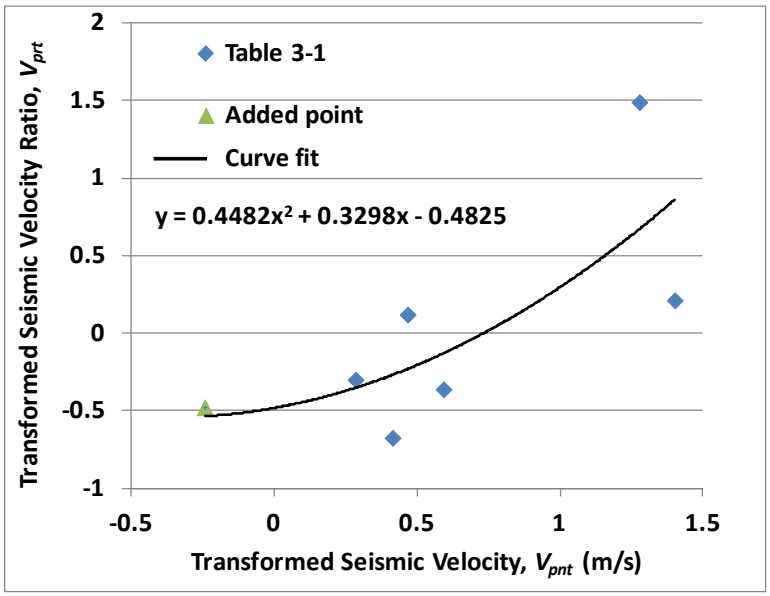

Figure 5-2. Seismic velocity ratio correlation with normal sonic velocity using transformed variables.

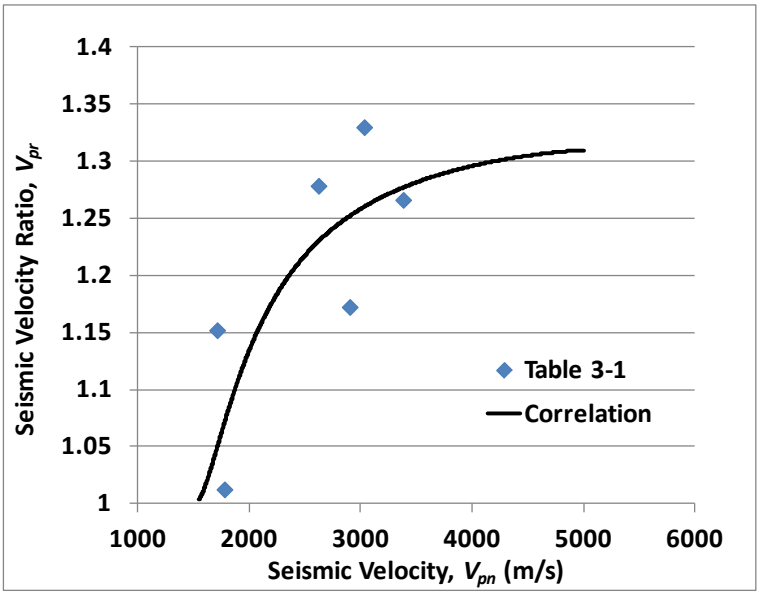

Figure 5-3. Seismic velocity ratio correlation with normal sonic velocity using physical variables.

5.2.2 The Porosity – Seismic Velocity Correlation

The relationship between porosity (ϕ) and V_p was originally investigated by Wyllie et al. (1956; 1958). The correlation was further investigated by Han et al. (1986) for sandstones accounting for the influence of clay content. Horsrud (2001) presented a correlation between ϕ and V_p for shales. A similar transformed sonic velocity is used for the porosity correlation as used in Section 5.2.1; however, here the geometric mean of the normal and parallel sonic velocities, V_{pm}, is used. The transformed sonic velocity is given by $V_{pmt} = \log\left(\frac{V_{pm}-1500}{7000-V_{pm}}\right)$. The transformed variable used for ϕ is $\phi_t = \log\left(\frac{1-\phi}{\phi}\right)$, which goes to negative infinity as porosity goes to 1 and to infinity as porosity goes to 0. The correlation for the transformed porosities and sonic velocities using data from Tables 5-1 and 5-3 is shown in Figure 5-4.

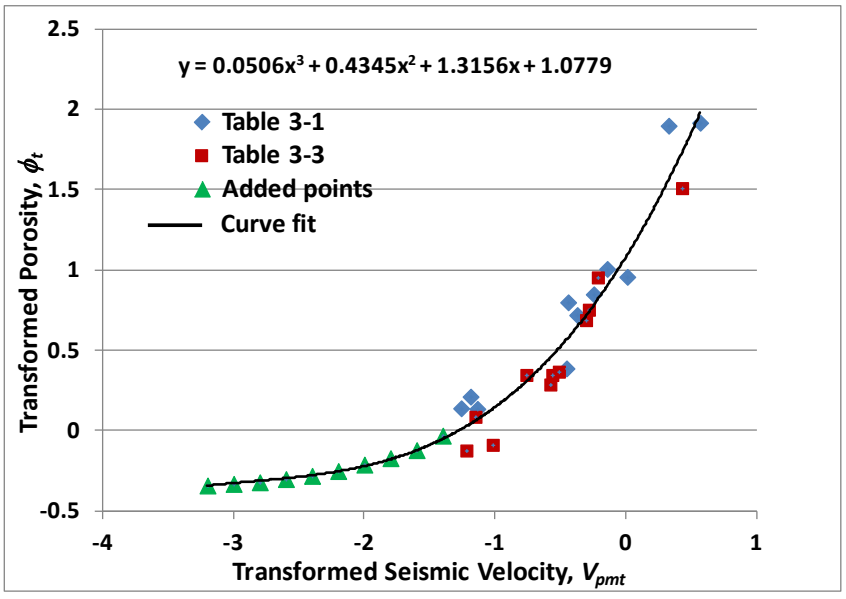

Figure 5-4. Porosity and sonic velocity correlation using transformed variables.

The polynomial correlation tends to result in unreasonable results beyond the limit of the data, and in particular will generate reversals in the velocity-porosity curve at low values of the velocity. The green points in Figure 5-4 are used such that the polynomial correlation remains reasonable for extrapolations at low values of V_{pmt} (which is also for low values of V_{pm}) beyond the range of the existing data.

The correlation is given in Equation (5-2), which has a root-mean-square error (RMSE) of 0.056.

$$\phi_t = 0.0506\, V_{pmt}^3 + 0.4345\, V_{pmt}^2 + 1.3156\, V_{pmt} + 1.0779 \quad (5\text{-}2)$$

The comparison of the correlation with the data using the physical variable is shown in Figure 5-5. The data point from Table 5-3, not used for the correlation shown in Figure 5-5, is for the Mo Clay, as discussed in Section 5.1. The Horsrud (2001) correlation, which is based on the Table 5-3 data, predicts higher values of porosity, particularly at the extremes of the velocity spectrum.

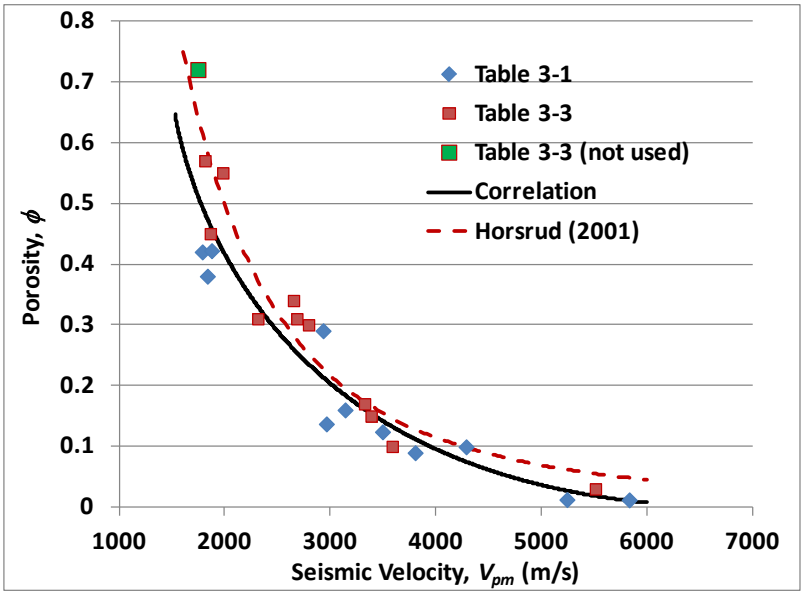

Figure 5-5. Porosity and sonic velocity correlation using physical variables.

5.2.3 The Bulk Density – Seismic Velocity Correlation

After finding the relatively strong correlation between ϕ and V_{pm}, it is reasonable to expect a correlation between the saturated bulk density, ρ_b, and V_{pm}. The correlation uses the transformed velocity, V_{pmt}, described in Section 5.2.2 and a transformed bulk density, $\rho_{bt} = \log\left(\frac{\rho_b - 1000}{2900 - \rho_b}\right)$, where 1000 kg/m^3 represents the minimum bulk density (equal to that of water for a porosity of 1) and 2900 kg/m^3 represents a maximum bulk density. The data and correlation are shown in Figure 5-6 and the correlation equation is given in Equation (5-3), which has an RMSE of 33 kg/m^3 for ρ_b. Given the bulk density and the porosity, the grain density, ρ_g, may be computed by $\rho_g = \frac{\rho_b - \phi\rho_w}{1-\phi}$, where ρ_w is the density of the resident fluid that saturates the pore space.

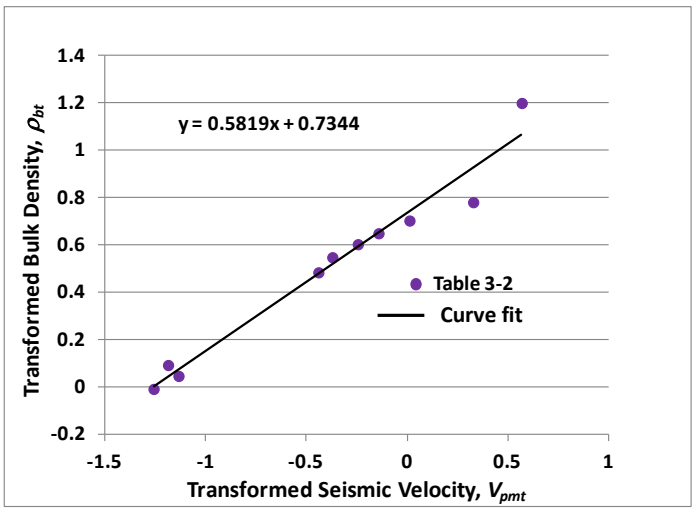

Figure 5-6. Bulk density and sonic velocity correlation using transformed variables.

$$\rho_{bt} = 0.5819\, V_{pmt} + 0.7344 \quad (5\text{-}3)$$

The correlation comparison with the data in physical variables is shown in Figure 5-7.

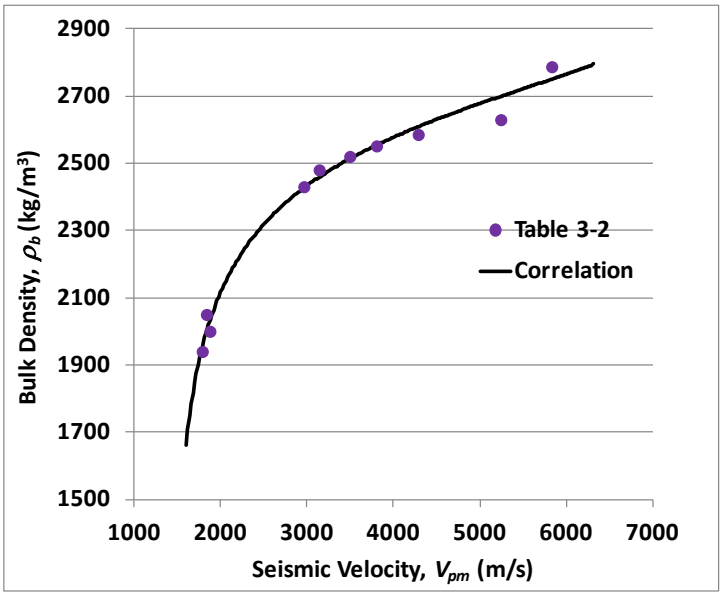

Figure 5-7. Bulk density and sonic velocity correlation using physical variables.

5.2.4 The Clay Content – Seismic Velocity Correlation

The behavior of shale formations with respect to compaction and permeability is affected by the clay content of the rock (Yang and Aplin, 2004; 2010). Thus, it is important to establish clay content to carry out additional parameter estimation. This correlation uses the transformed sonic velocity, V_{pmt}, described in Section 5.2.2 and the clay content mass fraction, X, as shown in Figure 5-8. The correlation function in Equation (5-4) has an RMSE of 0.098. A correlation plot in terms of the physical variables is shown in Figure 5-9. The data point from Table 5-3 that is not used for the correlation shown in Figure 5-9, is for the Mo Clay, as discussed in Section 5.1.

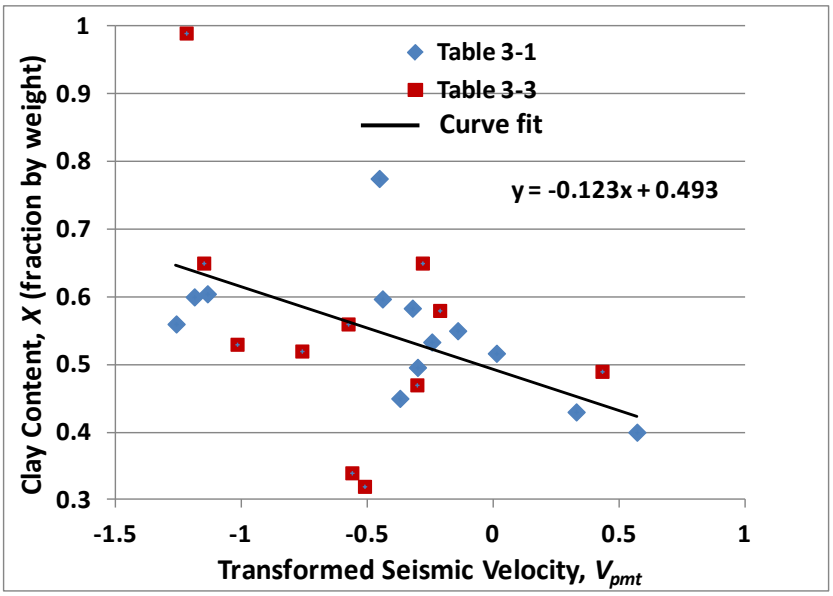

Figure 5-8. Clay content and sonic velocity correlation using transformed sonic velocity.

$$X = -0.123\, V_{pmt} + 0.493 \qquad (5\text{-}4)$$

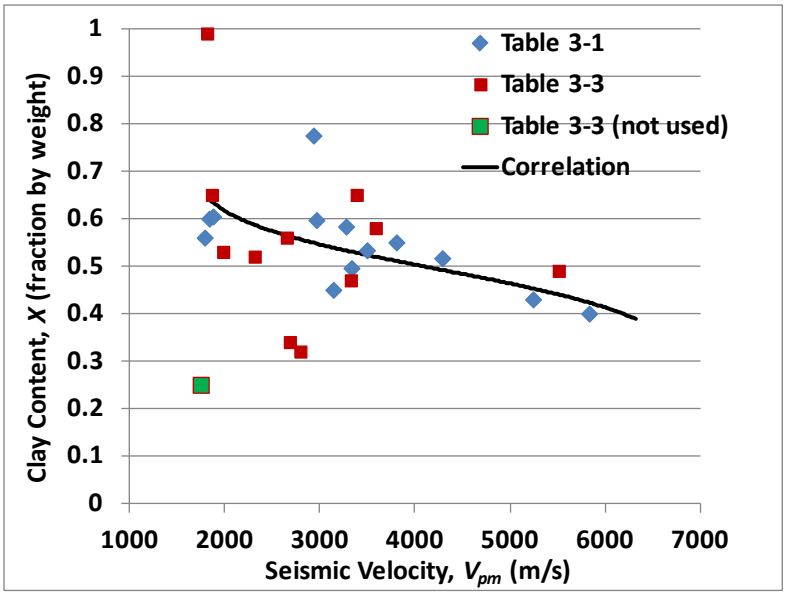

Figure 5-9. Clay content plotted against the physical sonic velocity.

As shown in Figure 5-9, the clay content correlation with sonic velocity is weak. This is expected based on the weak correlation found by Yang and Aplin (2010) between porosity and clay content. On the other hand, more than 85% of the values for clay content fall within the range of 0.4 to 0.65. Another question concerning the correlation is that the clay content values given in Tables 5-1 and 5-3 are the mass fractions of clay minerals, whereas Yang and Aplin (2010) defined the clay content as the mass fraction for grain sizes less than 2μm. Yang and Aplin (2010) demonstrated that the clay mass fraction correlates

much more strongly with the Atterberg liquid limit. However, there is some question as to whether this attribute is applicable to stiff clays and shales (Bock 2001).

5.2.5 The Permeability – Porosity - Clay Content Correlation

Yang and Aplin (2010) have published a correlation relating bedding-normal permeability (k) with ϕ and X_c for marine mudstones, where X_c is the mass fraction of grains less than 2 microns in size. The correlation is supported by a large data set of 376 data points covering a wide range of porosity and clay content. The correlation is given by Equation (5-5),

$$\ln(k) = -69.59 - 26.7\,X_c + 44.07\,X_C^{0.5} + \left(-53.61 - 80.03\,X_c + 132.78\,X_C^{0.5}\right)e + \left(86.61 + 81.91\,X_c - 163.61\,X_C^{0.5}\right)e^{0.5} \quad (5\text{-}5)$$

where k is the permeability in m^2 and e is the void ratio given by $e = \phi/(1-\phi)$. Given limited information concerning X_c, the clay mineral mass fraction, X, from Section 2.3 is used as a proxy for the clay-size mass fraction, X_c.

Permeability estimates from a known value of V_{pm} can be computed using Equation (5-5) by using Equations (5-2) and (5-4) for porosity and clay content, respectively. The results compared with the Table 5-1 bedding-normal permeability data is shown in Figure 5-10.

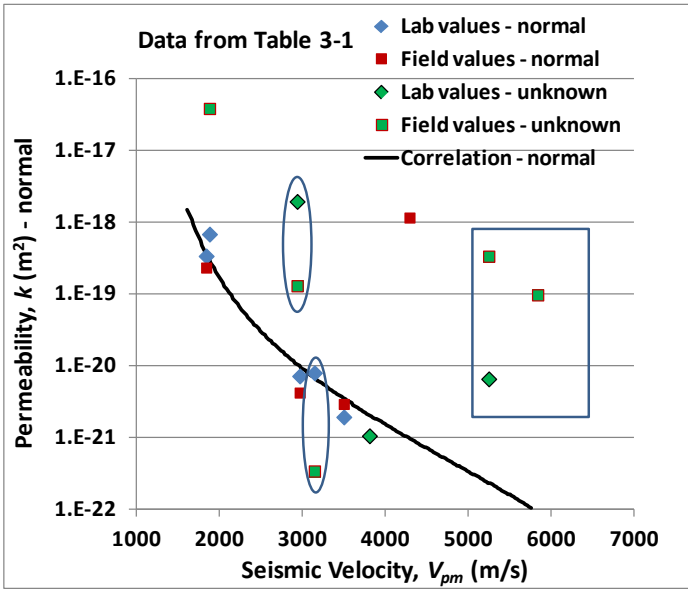

Figure 5-10. Permeability correlation normal to bedding (using Equations 5-2, 5-4, and 5-5) compared with measurements. Note: see text near end of this section concerning ovals and rectangle.

The labeling "normal" and "unknown" in the legend of Figure 5-10 refers to the orientation of the permeability measurement relative to bedding. For quantities like permeability that range over a factor of 10 or more in magnitude, it is better to describe the correlation error in terms of the logarithm of the variable because the magnitude of the error typically scales with the value of the permeability. The RMSE range of the correlation for log permeability relative to the laboratory data normal to bedding is ± 0.21. The RMSE range for $\log(k)$, $\log(k) \pm 0.21$, is equivalent to a range in permeability in which permeability is multiplied by a factor of 1.6 and divided by a factor of 1.6.

The correlation is extended to provide permeability parallel to bedding by scaling the normal to bedding permeability by an anisotropy factor, A_f, given by Equation (5-6),

$$A_f = V_{pr}^{\omega} \tag{5-6}$$

where ω is the empirical anisotropy coefficient and V_{pr} is the parallel to normal sonic velocity ratio. The calibrated value of ω is 4.6. The RMSE of the correlation for log permeability relative to the laboratory data parallel to bedding is 0.15, or a factor of 1.4 for the permeability. The results are shown in Figure 5-11.

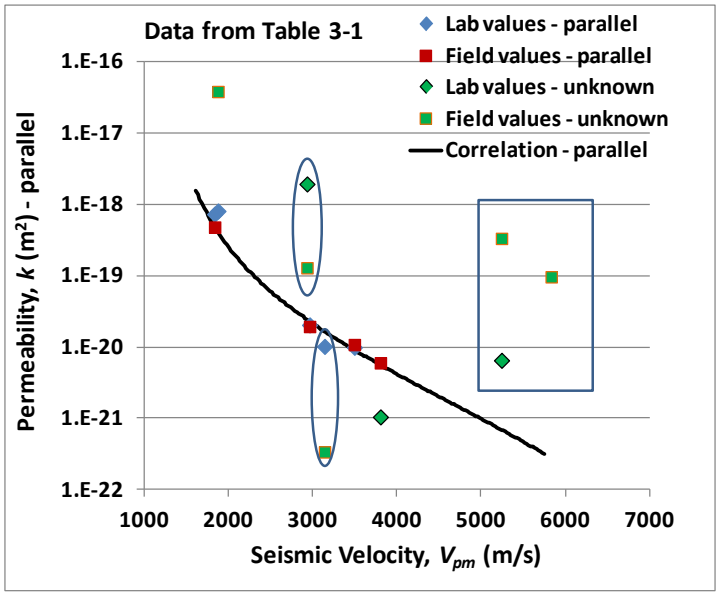

Figure 5-11. Permeability correlation parallel to bedding (using Equations 5-2, 5-3, and 5-4 and 5-6) compared with measurements. Note: see text near end of this section concerning ovals and rectangle.

In Figures 5-10 and 5-11, the estimated permeabilities are close to the lab measurements, with two exceptions: the Spanish Reference Clay and the Palfris Formation at Wellenberg. The points outlined by the blue rectangle are for the Palfris Formation at Wellenberg and the Boda Claystone. These have porosities of approximately 0.01, which lies outside the range of values (0.04 to 0.78) investigated by Yang and Aplin (2010). Four other in-situ measurements also fall far off the correlation line. In-situ measurements can be affected by larger-scale features of the formation and would generally lead to higher permeabilities (Neuzil, 1994). However, two cases circled on Figure 5-10, the Callovo-Oxfordian Clay (the lower oval) and the Spanish Reference Clay (the upper oval), are found to have in-situ permeabilities that are significantly less than the laboratory values. The reason for this behavior is not known. The same two ovals are shown in Figure 5-11. The laboratory value in Figure 5-11 with unknown orientation at a velocity of 3800 m/s is for the Tournemire argillite. This value falls off the correlation line by about a factor of 4; however, it is also shown in Figure 5-10 and appears to be roughly consistent with a normal-to-bedding orientation.

5.2.6 The Porosity–Maximum Effective Stress–Clay Content Correlation

With estimates for ϕ and C, the maximum effective stress (σ_v') experienced by the formation can be estimated using the results of Yang and Aplin (2004). Their correlation representing the physical burial compaction of mudstones relates ϕ, X_c, and σ_v' is given in Equation (5-7),

$$e = 0.3024 + 1.6867\,X_c + 1.9505\,X_C^2 - (0.0407 + 0.2479\,X_c + 0.3684\,X_C^2)\ln\left(\frac{\sigma_v'}{100}\right) \quad (5\text{-}7)$$

where $\sigma_v' = \sigma_v - p$ is the maximum effective stress in kPa experienced by the formation, σ_v is the total stress, p is the pore-fluid pressure, and $e = \phi/(1-\phi)$ is the void ratio. As for their permeability correlation discussed in Section 5.2.5, the correlation covers a wide range of ϕ and X_c and is based on a large laboratory data set of 200 values and a much larger data set based on wireline log interpretations consisting of about 3600 data points. The effective stress is evaluated for values up to 40 MPa. As for permeability in Section 5.2.5, the clay mineral fraction, X, is used as a proxy for X_c.

Equation (5-7) cannot be compared directly with the data presented in Section 5.1. However, by using Equation (5-7), it is possible to estimate the present-day pore fluid pressure. Pore fluid pressure is a difficult condition to measure in very low permeability formations characteristic of shale rock (Neuzil, 1993). Pore fluid pressures are important for shale rock, however, because they are frequently "abnormal", i.e., not hydrostatic. Abnormal overpressures can mean that the formation is more vulnerable to mechanical damage by fracture. In order to estimate pore fluid pressure, a correlation for the uniaxial compressive strength and its relationship with the overconsolidation ratio are also needed. These correlations and how they can be combined with Equation (5-7) to estimate pore fluid pressure are described in the next two sections.

5.2.6.1 The Uniaxial Compressive Strength – Seismic Velocity Correlation

The uniaxial compressive strength (UCS) is the compressive load placed on an unconfined rock sample required to cause fracture. A strong correlation has been noted between the UCS and V_p by both Ingram and Urai (1999) and Horsrud (2001) for mudrocks and shales. The correlation is computed using the transformed sonic velocity, V_{pmt}, described in Section 5.2.2 and a log-transformed uniaxial compressive strength, $\log(UCS)$. The correlation plot using transformed variables is shown in Figure 5-12. The correlation equation is given by Equation (5-8) and has an RMSE of 0.13 for $\log(UCS)$, or a factor of 1.3 for UCS.

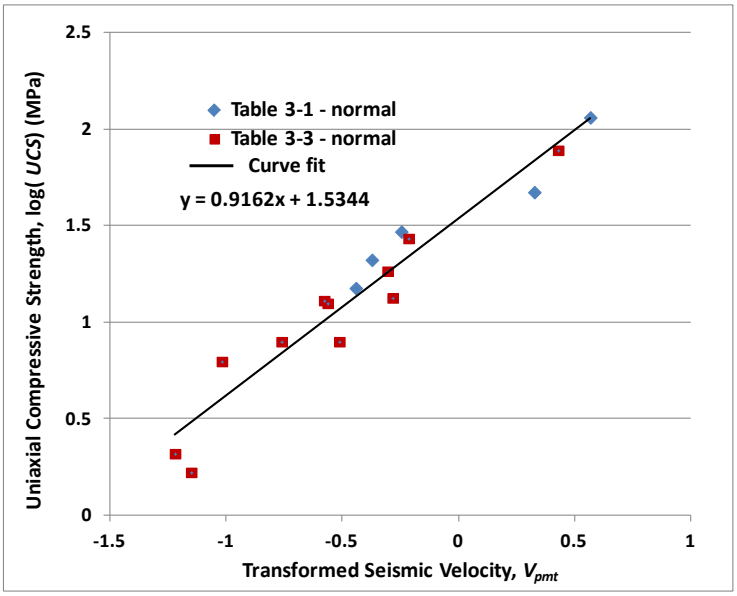

Figure 5-12. Uniaxial compressive strength normal to bedding and sonic velocity correlation using transformed variables.

$$\log(\text{UCS}) = 0.9162\,V_{pmt} + 1.5344 \quad (5\text{-}8)$$

The correlation comparison with the data in physical variables is shown in Figure 5-13. In addition to the measured uniaxial compressive strength normal to bedding, data in which the orientation of the measurement is unknown or parallel to bedding are also shown, although these were not used to develop the correlation. The results suggest that anisotropy in uniaxial compressive strength is not strong. The normal value not used from Table 5-3 is for the Mo Clay as discussed in Section 5.1. Correlation plots based on correlations developed by Horsrud (2001) and Ingram and Urai (1999) are also presented in Figure 5-13. The correlation developed here is closer to the Horsrud (2001) correlation, but has some of the character of the Ingram and Urai (1999) correlation at the extremes of the velocity spectrum.

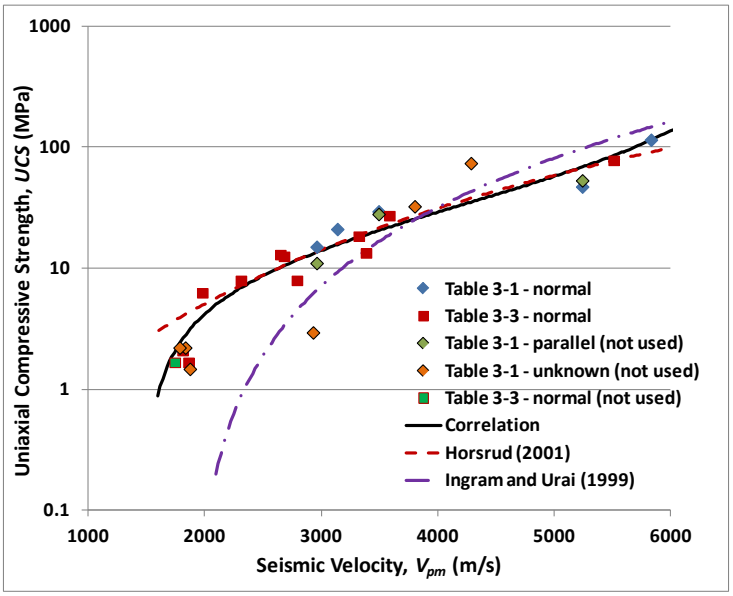

Figure 5-13. Uniaxial compressive strength and sonic velocity correlation using physical variables.

5.2.6.2 Linking the Overconsolidation Ratio to Seismic Velocity

The overconsolidation ratio (OCR) is the maximum effective stress experienced by a formation divided by the present-day effective stress. Ingram and Urai (1999) proposed the following brittleness index (BRI) for mudrocks,

$$\text{BRI} = \frac{\text{UCS}}{\text{UCS}_{\text{NC}}} \tag{5-9}$$

where UCS_{NC} is the uniaxial compressive strength for a normally-consolidated rock. Normal consolidation means that the present-day effective stress is the maximum effective stress. Ingram and Urai (1999), based on results from Horseman et al. (1986), suggest that UCS_{NC} can be estimated from the following,

$$\text{UCS}_{\text{NC}} = 0.5\sigma_{NC} \tag{5-10}$$

where σ_{NC} is the effective stress for normal consolidation at the present-day depth. Using the definitions of bulk density and effective stress, the value of σ_{NC} may be computed from the following,

$$\sigma_{NC} = \rho_b g D - p_{hs} \tag{5-11}$$

where p_{hs} is the hydrostatic pressure equal to $\rho_w g D$, $\rho_w$is the density of the pore fluid, D is the present-day burial depth, and g is the acceleration of gravity. This is based on the approximation that the entire

stratigraphic column can be represented by the formation bulk density, ρ_b, and that the pore fluid density is known or can be reasonably approximated. Therefore, using Equations (5-8), (5-10) and (5-11), the brittleness index in Equation (5-9) may be computed. Nygård et al. (2006) proposed that the brittleness index could be related to the overconsolidation ratio by the following:

$$\mathrm{OCR} = \mathrm{BRI}^{\kappa} \tag{5-12}$$

Nygård et al. (2006) found a value of ω of about 1.1, however, evaluations conducted here have found a value of 0.7 is better suited for the determination of pore pressure. Using Equation (5-12) to compute the OCR and Equation (5-7) to compute the maximum effective stress, σ_v', the present-day effective stress, σ_{pd}, is,

$$\sigma_{pd} = \frac{\sigma_v'}{\mathrm{OCR}} \tag{5-13}$$

The present-day effective stress is also given by,

$$\sigma_{pd} = \rho_b g D - p \tag{5-14}$$

Equation (5-14) may be used to determine the present-day pore fluid pressure, p. The pore fluid overpressure, $p_{op} = p - p_{hs}$, is the difference between the pore fluid pressure and the hydrostatic pressure.

BRI is also important for evaluating whether the rock is subject to brittle or ductile failure. Ingram and Urai (1999) determined that the failure mode is expected to be brittle for a BRI greater than 2 and is expected to behave as a ductile material at lower values of the BRI.

5.2.7 Young's Modulus - Seismic Velocity Correlations

Data for Young's modulus normal to bedding (E_n) and parallel to bedding (E_p) are given in Tables 5-2 and 5-3. The plot of the log-transformed E_n against the transformed sonic velocity, V_{pmt}, described in Section 5.2.2 is shown in Figure 5-14. The polynomial correlation tends to estimate unreasonable results beyond the limit of the data, and in particular will generate reversals in the velocity-Young's modulus curve at high values of the velocity. The green points in Figure 5-15 are used such that the polynomial correlation remains reasonable for extrapolations at high values of V_{pmt} (which is also for high values of V_{pm}) beyond the range of the existing data. The correlation is given in Equation (5-15) and has an RMSE of 0.25 for $\log(E_n)$ or a factor of 1.8 for E_n.

$$\log(E_n) = 0.111\, V_{pmt}^3 - 0.3395\, V_{pmt}^2 + 0.8125\, V_{pmt} + 0.8228 \tag{5-15}$$

The correlation is shown in physical variables along with the data in Figure 5-15. The "not used" data point from Table 5-3 is the Mo Clay as discussed in Section 5.1. Figure 5-15 also presents the correlation developed by Horsrud (2001). The correlation given by Equation (5-15) lies close to the Horsrud (2001) correlation, except at the low end of the velocity spectrum.

The correlation for Young's modulus parallel to bedding is developed using the anisotropy coefficient as described in Section 5.2.5 for permeability. The calibrated anisotropy coefficient, ω, is 4.8. The resulting comparison with data is shown in Figure 5-16. The RMSE for the parallel Young's modulus correlation is 0.49 for $\log(E_n)$ or a factor of 3.1 for E_p. The large error in this case is driven mainly by the large relative errors incurred at low values of Young's modulus where the correlation curve becomes steep.

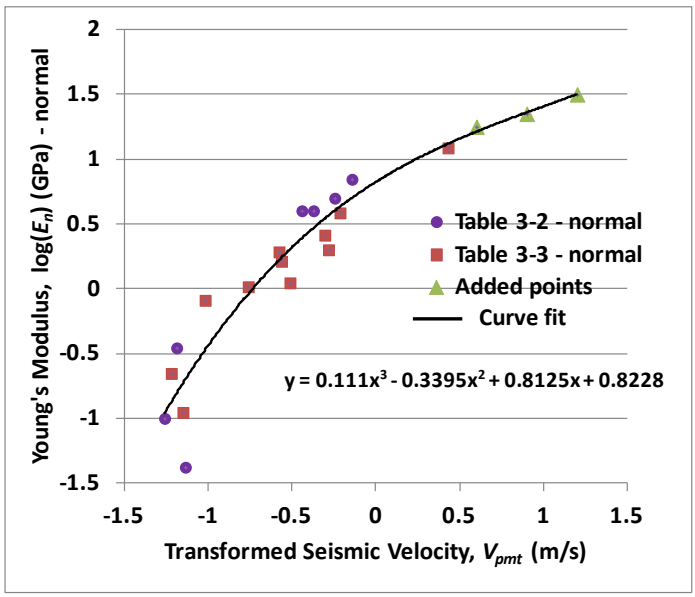

Figure 5-14. Correlation for Young's modulus normal to bedding with sonic velocity using transformed variables.

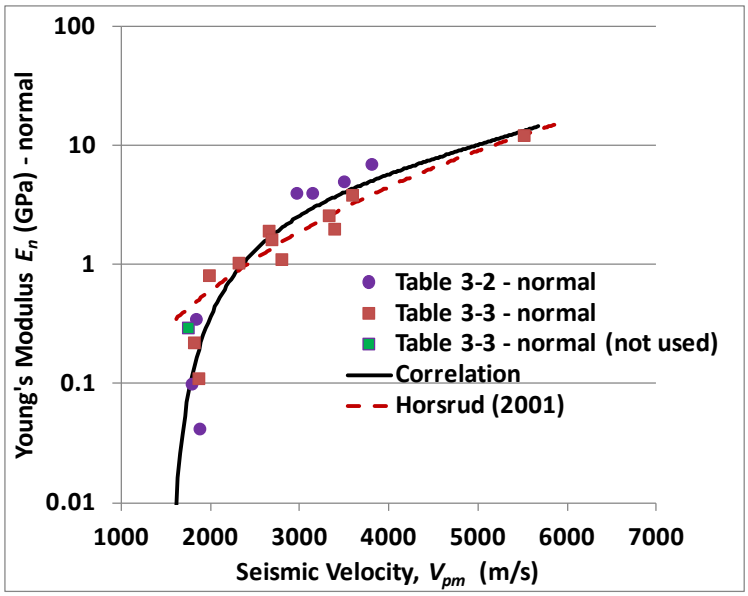

Figure 5-15. Correlation for Young's modulus normal to bedding with sonic velocity using physical variables.

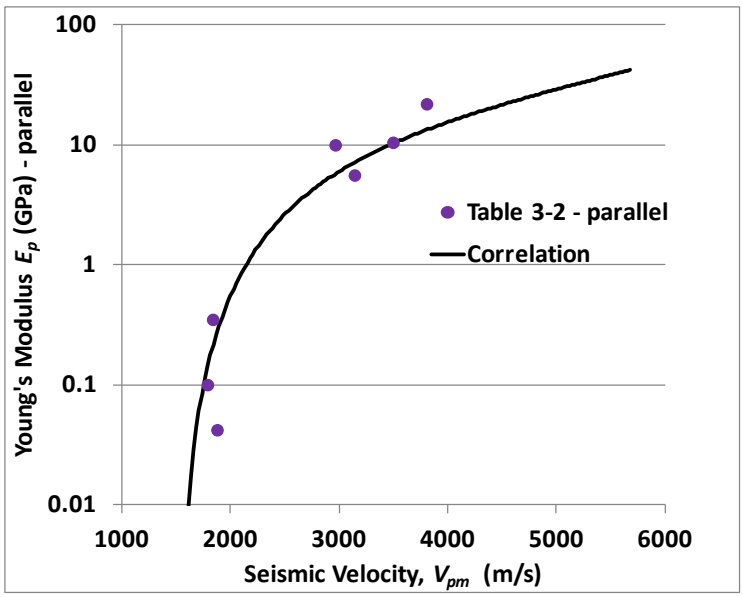

Figure 5-16. Correlation for Young's modulus parallel to bedding with sonic velocity.

5.2.8 Shear Modulus – Seismic Velocity Correlation

Data for shear modulus (G) are given in Tables 5-2 and 5-3. Insufficient data were available to assess anisotropic effects, with data limited to either normal-to-bedding or unknown orientation. The plot of the log-transformed G against the transformed sonic velocity, V_{pmt}, described in Section 5.2.2, is shown in Figure 5-17. The polynomial correlation tends to result in unreasonable results beyond the limit of the data, and in particular will generate reversals in the velocity-shear modulus curve at high values of the velocity. The green points in Figure 5-17 are used such that the polynomial correlation remains reasonable for extrapolations to high values of V_{pmt} (which is also for high values of V_{pm}) beyond the range of the existing data. The correlation is given in Equation (5-16) and has an RMSE of 0.25 for $\log(G)$ or a factor of 1.8 for G.

$$\log(G) = 0.1556\, V_{pmt}^3 - 0.4077\, V_{pmt}^2 + 0.7162\, V_{pmt} + 0.4279 \qquad (5\text{-}16)$$

The correlation is shown in physical variables along with the data in Figure 5-18. The "not used" data point from Table 5-3 is the Mo Clay as discussed in Section 5.1. As for Young's modulus, the correlation developed here lies close to the Horsrud (2001) correlation, except at the low end of the velocity spectrum.

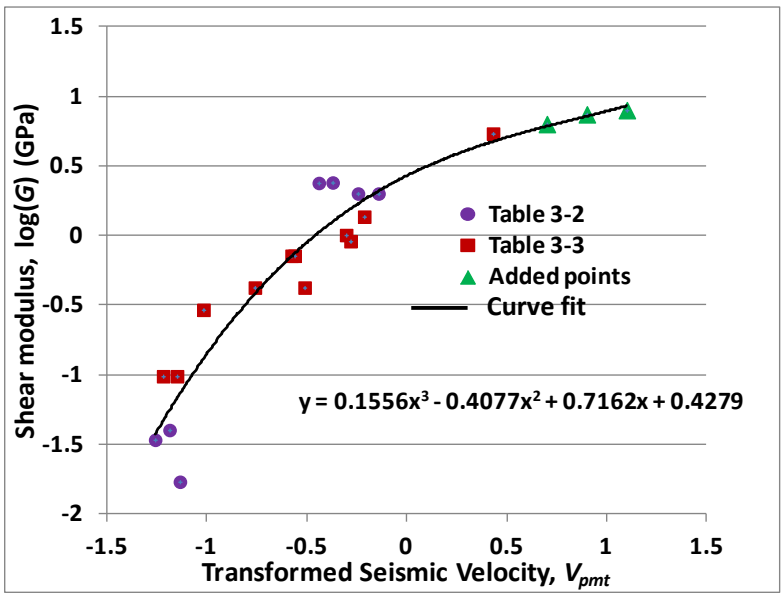

Figure 5-17. Correlation for shear modulus with sonic velocity using transformed variables.

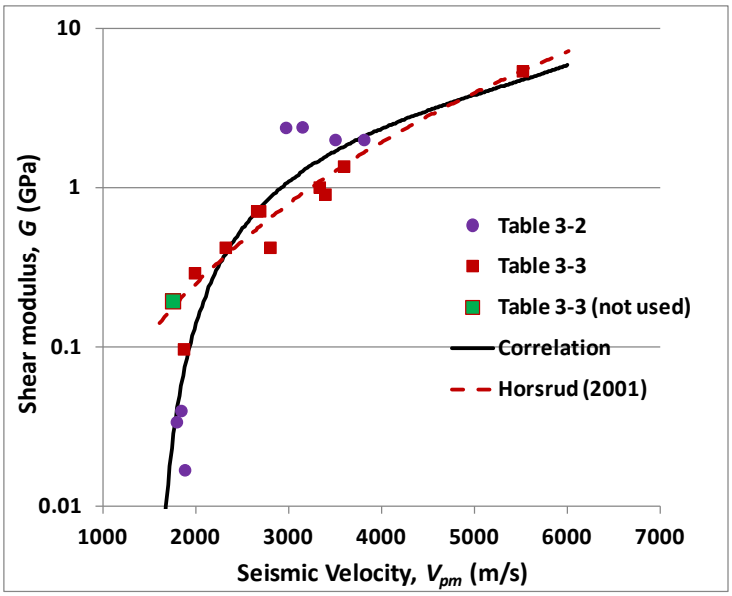

Figure 5-18. Correlation for shear modulus with sonic velocity using physical variables.

5.2.9 Poisson's Ratio - Seismic Velocity Correlation

Data for Poisson's ratio are given in Table 5-2. Insufficient data were available to assess anisotropic effects. Furthermore, orientation information was generally unavailable; therefore, the data and results are treated as effectively isotropic. The plot of the transformed Poisson's ratio, $\upsilon_t = \log\left(\frac{0.5-\upsilon}{\upsilon}\right)$, against the transformed sonic velocity, V_{pmt}, as described in Section 5.2.2, is shown in Figure 5-19. The correlation equation is given in Equation (5-19) and has an RMSE of 0.077 for υ. The correlation did not include the value for the Ypresian Clay from Table 5-2. The plot of the correlation with the data using physical variables in Figure 5-20 shows that the Ypresian Clay (indicated by the light green-filled symbol) deviated significantly from the trend of the other formations. It is possible that the discrepancy is caused

by the measurement method. The Ypresian Clay Poisson's ratio was determined from a uniaxial compression test (Piña-Diaz 2011) that would not maintain undrained conditions. This contrasts with the measurement reported for the Boom Clay (υ = 0.425), also at a low sonic velocity similar to the Ypresian Clay, which was for undrained conditions.

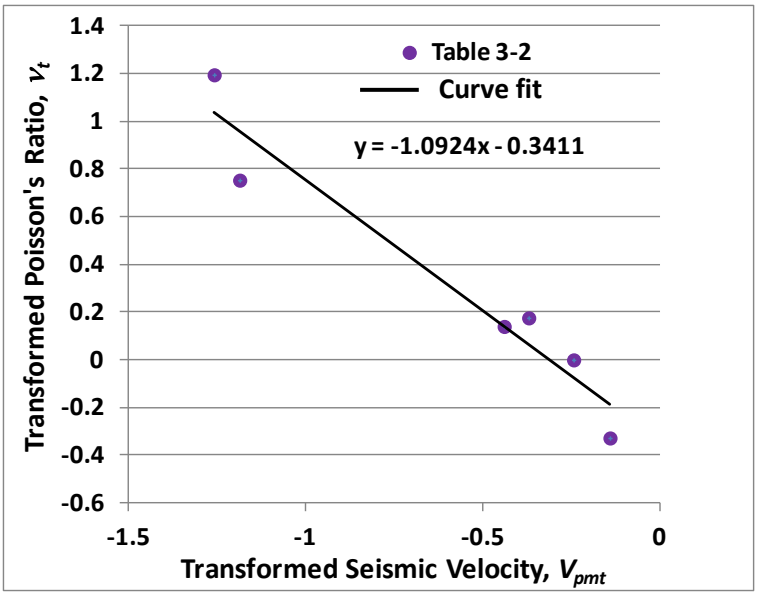

Figure 5-19. Correlation for Poisson's ratio with sonic velocity using transformed variables.

$$\upsilon_t = -1.0924\, V_{pmt} - 0.3411 \tag{5-17}$$

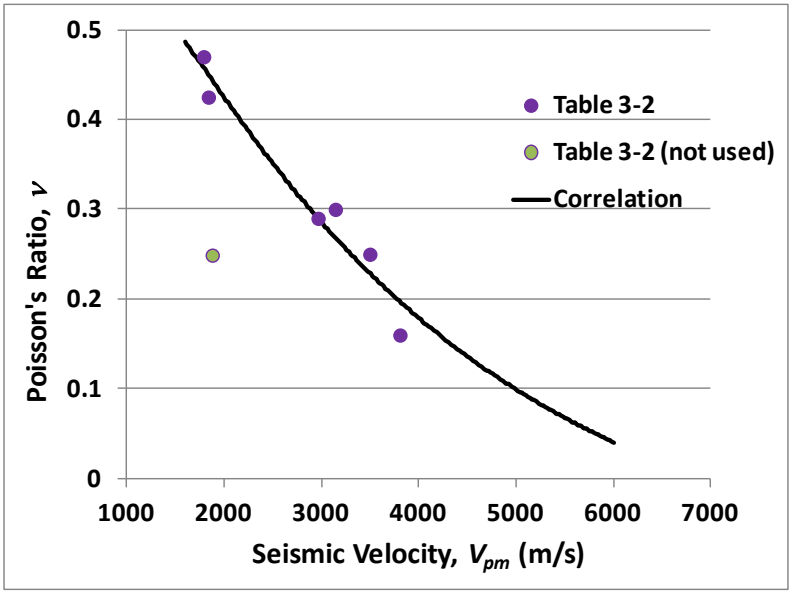

Figure 5-20. Correlation for Poisson's ratio with sonic velocity using physical variables.

5.2.10 Cohesive Strength - Seismic Velocity Correlations

Cohesive strength is a parameter in the Mohr-Coulomb model for rock failure under shear stress. Data for cohesive strength (c) are given in Table 5-2. The plot of the log-transformed cohesive strength normal to

bedding, $\log(c_n)$ against the transformed sonic velocity V_{pmt}, as described in Section 5.2.2, is shown in Figure 5-21. The correlation given in Equation (5-18) has an RMSE for $\log(c_n)$ of 0.16, or a factor of 1.5 for c_n.

$$\log(c_n) = 1.1461\, V_{pmt} + 0.7737 \quad (5\text{-}18)$$

The correlation for cohesive strength normal to bedding against sonic velocity using physical variables is shown in Figure 5-22. The cohesive strength parallel to bedding was developed by using the anisotropy factor discussed in Section 5.2.5. The calibrated anisotropy parameter,, is 3.5. The correlation for cohesive strength parallel to bedding is shown in Figure 5-23 and has an RMSE of for $\log(c_p)$ of 0.14, or a factor of 1.4 for c_p. Although the data are limited for these correlations, Wong and Kenter (1993) have also suggested that cohesive strength and the sonic velocity may be correlated. However, further work is needed to better establish these correlations.

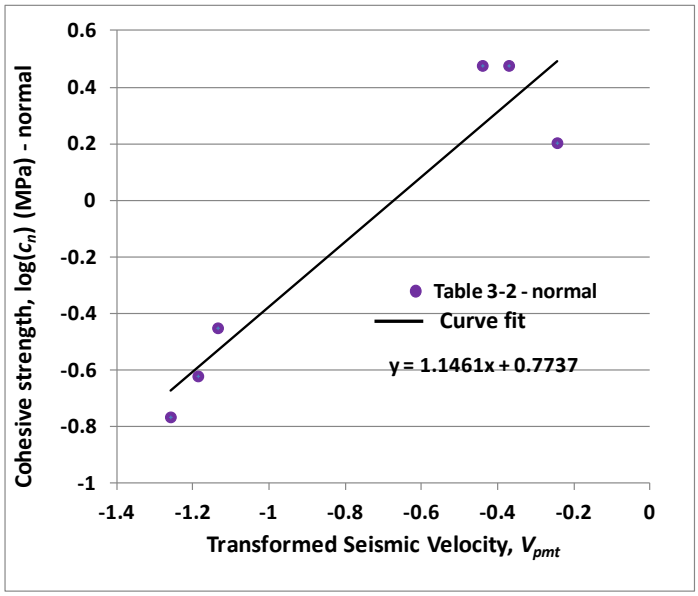

Figure 5-21. Correlation for cohesive strength normal to bedding with sonic velocity using transformed variables.

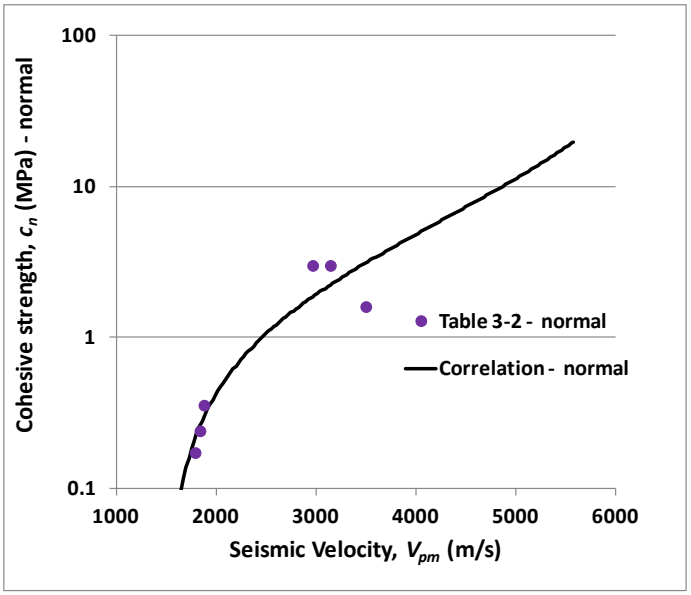

Figure 5-22. Correlation for cohesive strength normal to bedding with sonic velocity using physical variables.

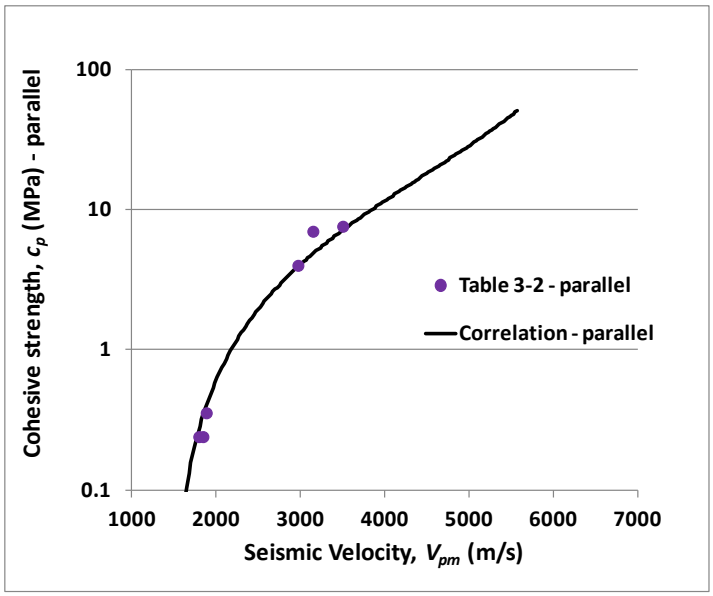

Figure 5-23. Correlation for cohesive strength parallel to bedding with sonic velocity.

5.2.11 Friction Angle - Seismic Velocity Correlation

Friction angle is a parameter in the Mohr-Coulomb model for rock failure under shear stress. Data for friction angle (φ) are given in Table 5-2. Insufficient data were available to assess anisotropic effects. Furthermore, orientation information was generally unavailable; therefore, the results are treated as effectively isotropic. The plot of φ against the transformed sonic velocity V_{pmt}, as described in Section 5.2.2, is shown in Figure 5-24. The correlation given in Equation (5-19) has an RMSE of 0.85 degrees for φ.

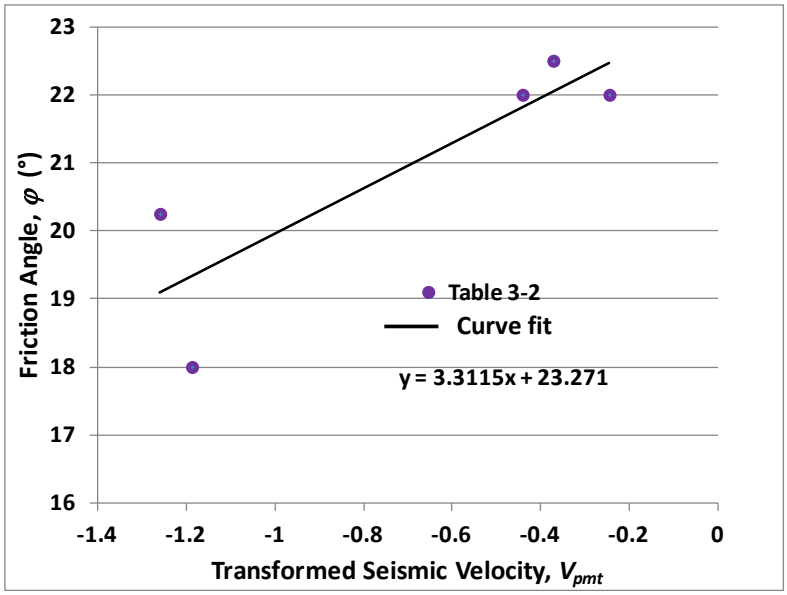

Figure 5-24. Correlation for friction angle with sonic velocity using transformed variables.

$$\varphi = 3.3115\, V_{pmt} + 23.271 \qquad (5\text{-}19)$$

The correlation for cohesive strength normal to bedding against sonic velocity using physical variables is shown in Figure 5-25. As in Section 5.2.9 for Poisson's ratio, the Ypresian Clay is an outlier that was not used in the friction angle correlation. It is shown as the point not used in Figure 5-25. This appears to be in a range of sonic velocities where friction angle changes rapidly, making an assessment of the friction angle problematic at velocities below 2000 m/s. Horsrud (2001) developed a correlation with friction angle but did not present any of the data behind the correlation. Horsrud's (2001) observation that the friction angle of shale tends to lie between 45° and 60° is not consistent with the available data found to develop the correlation in this report. Further work is needed to establish the friction angle correlation with sonic velocity, however, Wong and Kenter (1993) also suggested that friction angle and the sonic velocity may be correlated.

It is interesting to note that Ingram and Urai (1999) found a correlation between the specific surface area of shale and the friction angle. The specific surface area is a measure of the total hydratable surface in a rock. If the friction angle correlation with velocity is found to hold more generally, then it may be possible to obtain surface area from the sonic velocity. This is useful for geochemical models involving reactions with the rock surface.

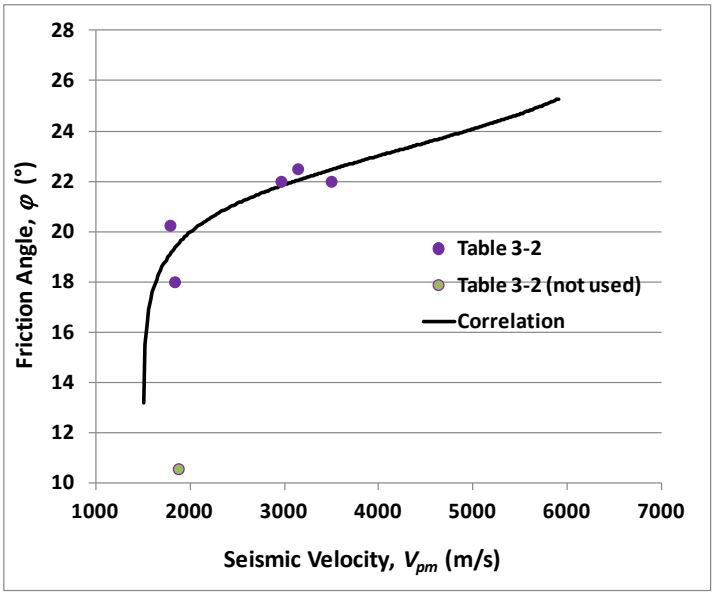

Figure 5-25. Correlation for friction angle with sonic velocity using physical variables.

5.2.12 Tensile Strength – Seismic Velocity Correlations

Data for tensile strength (τ) are given in Table 5-2. The plot of the log-transformed tensile strength normal to bedding, $\log(\tau_n)$ against the transformed sonic velocity, V_{pmt}, as described in Section 5.2.2, is shown in Figure 5-26. The correlation given in Equation (5-20) has an RMSE for $\log(\tau_n)$ of 0.034, or a factor of 1.1 for τ_n.

$$\log(\tau_n) = 1.1166\, V_{pmt} + 0.3164 \qquad (5\text{-}20)$$

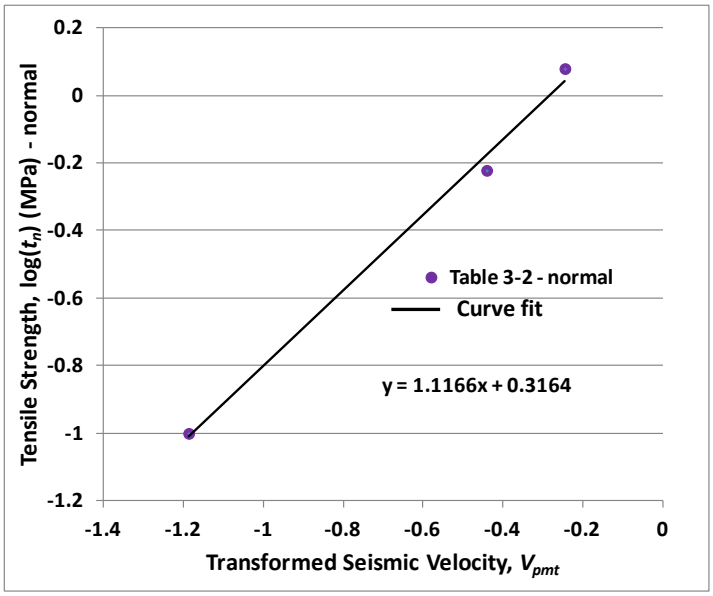

Figure 5-26. Correlation for tensile strength normal to bedding with sonic velocity using transformed variables.

The correlation for tensile strength normal to bedding against sonic velocity using physical variables is shown in Figure 5-27. The tensile strength parallel to bedding was developed by using the anisotropy factor discussed in Section 5.2.5. The calibrated anisotropy parameter,, is 3.3. The correlation for

cohesive strength parallel to bedding is shown in Figure 5-28 and has an RMSE for $\log(\tau_p)$ of 0.19, or a factor of 1.5 for τ_p.

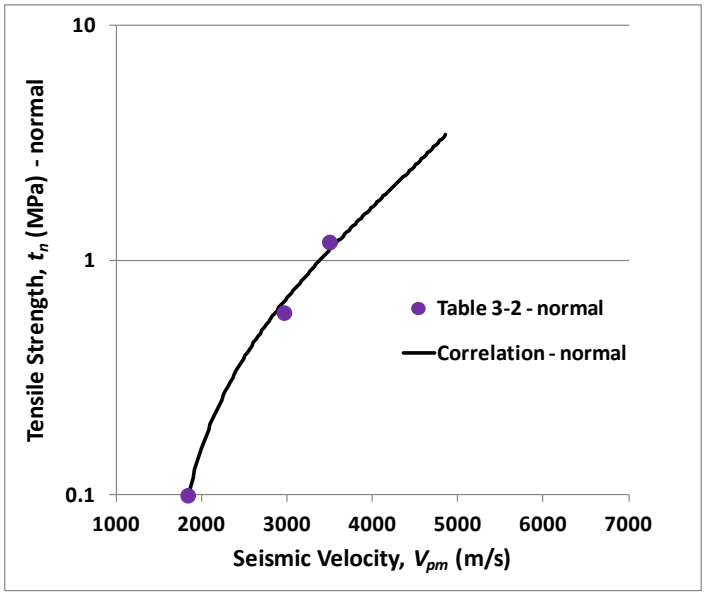

Figure 5-27. Correlation for tensile strength normal to bedding with sonic velocity using physical variables.

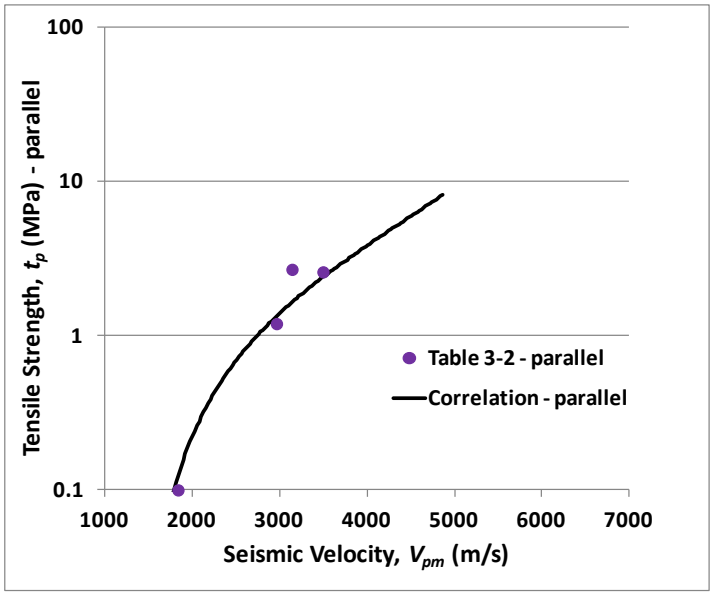

Figure 5-28. Correlation for tensile strength parallel to bedding with sonic velocity.

5.3 APPLICATION TO US SHALE FORMATIONS

The correlations developed in Section 5.2 are now applied to evaluate properties of specific sites in the United States. The formations analyzed are the Barnett shale, Haynesville shale, Pierre shale, New Albany, Antrim, Eagle Ford, Marcellus, Woodford, and Monterey. The locations of the various shale formations are shown in Figure 5-29.

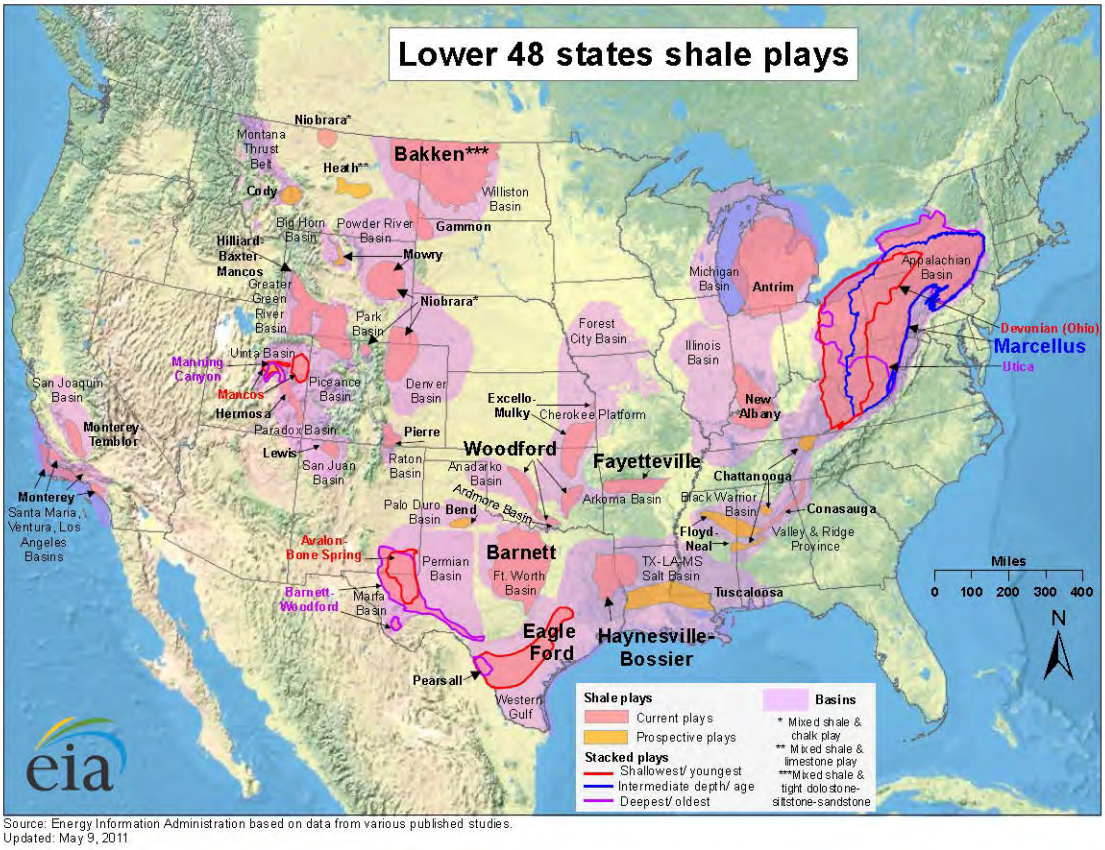

Source: Energy Information Administration based on data from various published studies.
Updated: May 9, 2011

Figure 5-29. Map of U.S. shale gas and shale oil plays (EIA 2011).

5.3.1 Inputs

The correlation inputs are the normal and parallel sonic velocities and an average formation depth. As for the development of correlations described in Section 5.2, if the velocity parallel to bedding is not available, it is estimated using the velocity ratio correlation given by Equation (5-1). Table 5-4 gives the requisite inputs for the formations. The formation water density is also an input, however, for the current analysis, a fresh water density of 1000 kg/m^3 was assumed.

Table 5-4. Inputs for Properties Estimation.

Formation	V_{pn} (m/s)	V_{pp} (m/s)	D (m)
Barnett Shale	4031[(1)]	NA	1000[(2)]
Haynesville Shale	3628[(1)]	NA	3000[(3)]
Pierre Shale (1)	2164[(4)]	2243[(4)]	152[(4)]
Pierre Shale (2)	3140[(5)]	3768[(5)]	1520[(5)]
New Albany Shale	3600[(6)]	4500[(6)]	520[(7)]
Antrim Shale	3174[(8)]	4057[(8)]	328[(8)]
Eagle Ford Shale	4016[(9)]	4083[(9)]	3234[(9)]
Marcellus Shale	3500[(10)]	NA	1920[(10)]
Woodford Shale	4008[(11)]	NA	1220[(11)]
Monterey Shale	4844[(12)]	5310[(12)]	2.7[(12)]

Sources: [(1)] Montaut (2012); [(2)] Bruner and Smosna (2011); [(3)] Nunn (2012); [(4)] McDonal et al. (1958); [(5)] Tosaya (1982); [(6)] Johnston and Christensen (1995); [(7)] CNX/GTI (2008); [(8)] Liu (1997); [(9)] Sondhi (2011); [(10)] Hardage (2013); [(11)] Verma et al. (2013); [(12)] Liu (1994)

5.3.2 Correlations Results

With the sonic velocities from Section 5.3.1, the correlations from Section 5.2 may be used to compute hydrological and geomechanical parameters. These results are shown in Table 5-5. Outputs shaded in blue are rock parameters, while outputs shaded in rose are formation conditions (e.g., effective stress, brittleness index, and overconsolidation ratio) that lead to the estimation of pore pressure.

Table 5-5. Estimated Parameters Using Seismic Velocity Correlations from Section 5.2.

Parameters	Barnett Shale	Haynesville Shale	Pierre Shale (1)	Pierre Shale (2)	New Albany Shale
Inputs (from Table 4)					
V_{pn} (m/s)	4031	3628	2164	3140	3600
V_{pp} (m/s)	NA	NA	2243	NA	4500
D(m)	1000	3000	152	1524	518
Outputs					
V_{pp} (m/s)	5226	4665	2530	3975	4626
ϕ	0.055	0.084	0.36	0.13	0.094
e	0.059	0.092	0.56	0.15	0.103
ρ_b (kg/m^3)	2640	2590	2220	2530	2580
ρ_{bd} (kg/m^3)	2580	2510	1860	2400	2490
ρ_g (kg/m^3)	2640	2600	2410	2550	2590
X (fraction)	0.48	0.50	0.60	0.52	0.50
k_n(m^2)	6.0E-22	1.2E-21	7.4E-20	2.9E-21	1.4E-21
k_p(m^2)	1.8E-21	3.6E-21	8.6E-20	8.8E-21	3.6E-21
UCS (MPa)	43	32	5.9	22	29
E_n (GPa)	8.1	6.3	0.70	4.3	5.8
E_p (GPa)	24	18	0.81	12.8	14
G (GPa)	3.2	2.5	0.29	1.7	2.4
υ	0.13	0.17	0.39	0.22	0.18
c_n (MPa)	8.0	5.5	0.66	3.4	4.9
c_p (MPa)	20	14.0	0.7	8.8	11
φ (degrees)	24	23	21	23	23
τ_n (MPa)	2.8	1.9	0.24	1.2	1.7
τ_p (MPa)	6.6	4.6	0.27	2.9	3.6
σ'_v (MPa)	48	41	9.3	33	40
σ_{NC} (MPa)	16	47	1.8	23	8.0
UCS_{NC} (MPa)	8.0	23	0.9	11	4.0
BRI	5.4	1.4	6.5	1.9	7.3
OCR	3.3	1.2	3.7	1.6	4.0
σ_{pd} (MPa)	15	33	2.5	21	10
p (MPa)	11	43	0.79	17	3
p_{hs} (MPa)	9.8	29	1.5	15	5.1
p_{op} (MPa)	1.45	14	-0.70	2.0	-1.8

Table 5-5 (continued). Estimated Parameters Using Seismic Velocity Correlations from Section 5.2.

Parameters	Antrim Shale	Eagle Ford Shale	Marcellus Shale	Woodford Shale	Monterey Shale
Inputs (from Table 4)					
V_{pn} (m/s)	3174	4016	3500	4008	4844
V_{pp} (m/s)	4057	4843	NA	NA	5310
D(m)	328	3234	1920	1219	2.7
Outputs					
V_{pp} (m/s)	4024	5206	4485	5195	6339
ϕ	0.13	0.067	0.10	0.057	0.033
e	0.15	0.071	0.11	0.060	0.035
ρ_b (kg/m^3)	2530	2620	2580	2640	2680
ρ_{bd} (kg/m^3)	2390	2550	2480	2580	2650
ρ_g (kg/m^3)	2550	2630	2590	2640	2680
X (fraction)	0.52	0.49	0.50	0.48	0.46
k_n(m^2)	2.9E-21	8.0E-22	1.5E-21	6.2E-22	3.0E-22
k_p(m^2)	8.1E-21	1.7E-21	4.5E-21	1.8E-21	4.4E-22
UCS (MPa)	22	38	29	43	60
E_n (GPa)	4.3	7.3	5.7	8.0	10.4
E_p (GPa)	11	15	17	23	15
G (GPa)	1.8	2.9	2.3	3.1	3.9
υ	0.22	0.14	0.18	0.13	0.094
c_n (MPa)	3.4	6.8	4.8	7.8	12
c_p (MPa)	8.0	13	12.5	20	17
φ (degrees)	23	23	23	24	24
τ_n (MPa)	1.2	2.4	1.7	2.7	4.1
τ_p (MPa)	2.7	4.4	4.1	6.5	5.6
σ'_v (MPa)	33	45	39	47	53
σ_{NC} (MPa)	4.9	51	30	20	0.045
UCS_{NC} (MPa)	2.5	26	15	9.8	0.023
BRI	8.9	1.5	2.0	4.4	2700
OCR	4.6	1.3	1.6	2.8	250.0
σ_{pd} (MPa)	7	34	25	17	0.21
p (MPa)	1.01	49	24	15	-0.14
p_{hs} (MPa)	3.2	32	19	12	0.027
p_{op} (MPa)	-2.2	17	5.2	2.7	-0.17

V_{pn} : compressional sonic velocity normal to bedding; V_{pp} : compressional sonic velocity parallel to bedding; D: present-day formation depth; ϕ: porosity; e: void ratio; ρ_b: brine-saturated bulk density; ρ_{bd}: dry bulk density; ρ_g: grain density; X: mass fraction of clay minerals; k_n: brine permeability normal to bedding; k_p: brine permeability parallel to bedding; UCS: uniaxial compressive strength normal to bedding; E_n: Young's modulus normal to bedding; E_p: Young's modulus parallel to bedding; G: shear modulus normal to bedding; υ: Poisson's ratio (isotropic); c_n: cohesive strength normal to bedding; c_p: cohesive strength parallel to bedding; φ: friction angle (isotropic); τ_n: tensile strength normal to bedding; τ_p: tensile strength parallel to bedding; σ'_v: maximum effective stress experienced by the formation; σ_{NC}: effective stress at the present-day

depth for normal consolidation at hydrostatic pore pressure; UCS_{NC}: uniaxial compressive strength for normal consolidation at present-day depth; BRI: brittleness index; OCR: overconsolidation ratio; σ_{pd}: present-day effective stress; p: present-day pore-fluid pressure; p_{hs}: hydrostatic pressure at present-day depth; p_{op}: pore-fluid overpressure (or underpressure if negative) $(p - p_{hs})$.

At this point, the bulk of the output values in Table 5-5 have not been independently verified and should be treated as initial estimates. In particular, the correlations for Poisson's ratio, cohesive strength, friction angle, and tensile strength were built from a small number of measured values. The following four subsections provide some independent comparisons for some of the parameter estimates for the Barnett, Haynesville, Pierre, and Monterey Shales.

5.3.3 Barnett Shale

Bruner and Smosna (2011) give an average porosity of 0.06 for Barnett shale, which is reasonably close to the correlation value of 0.055 in Table 5-5. Parshall (2008) cites a range of 10^{-19} m^2 to 10^{-21} m^2 for Barnett Shale permeability. The correlation is on the low end of this range with 6.0 x 10^{-22} m^2 for normal to bedding and 1.8 x 10^{-21} m^2 parallel to bedding. It is anticipated that permeability computed from the correlation will generally tend to the low end of the range because the correlation represents undisturbed matrix permeability and damage (e.g., fracturing) would lead to higher values. The pore pressure is found to be slightly overpressured, consistent with observations reported by Bruner and Smosna (2011).

5.3.4 Haynesville Shale

Pope et al. (2010) give a porosity range of 0.06 to 0.12 for the Haynesville Shale, which is consistent with the correlation value of 0.084. The permeability computed from the correlation is 1.2 x 10^{-21} m^2 normal to bedding and 3.6 x 10^{-21} m^2 parallel to bedding. Wang and Hammes (2010) give a range of roughly 10^{-19} m^2 to 10^{-21} m^2 for Haynesville Shale permeability. Pressure gradients in the Haynesville Shale range from about 0.67 to 0.9 psi/ft (0.0152 to 0.0204 MPa/m) Wang and Hammes (2010). At a depth of 3000 m, this corresponds to pressures of 45 to 61 MPa, while the estimated pore pressure in Table 5-5 is 43 MPa. For a static water pressure of 29 MPa, this gives an overpressure of 16 to 32 MPa, with the Table 5-5 estimate at 14 MPa.

5.3.5 Pierre Shale

The Pierre shale is evaluated at two depths, 152 m and 1524 m. The estimated porosities from Table 5-5 are 0.36 and 0.13, respectively. Porosities reported by Nichols (1992) at depths ranging from 123 to 181 m was 0.36 and for 1500 m depth, Tosaya (1982) reports a porosity of 0.145. For porosity in the range of 0.3 to 0.4, Neuzil reports permeabilities for the Pierre Shale range from 2 x 10^{-21} to 5 x 10^{-19} m^2, a range covering both normal and parallel to bedding. The values in Table 5-5 are 7.4 x 10^{-20} m^2 normal to bedding and 8.6 x 10^{-20} m^2 parallel to bedding. These lie within the observed range although they do not tend to fall at the lower end of the observations as expected. Neuzil (1993) reports on underpressures on the order of -100 m head, or about -1 MPa at depths of 150 m, which is close to the estimated value in Table 5-5 of -0.70 MPa.

5.3.6 Monterey Shale

The velocity measurements reported in Tables 5-4 and 5-5 for the Monterey Shale are on a low-organic-content sample from an outcrop. In addition to sonic velocities, measurements of porosity and dry bulk density were performed and reported in Liu (1994). The value of porosity is 0.05 and 2730 kg/m^3 for dry bulk density. The estimated values of these parameters from Table 5-5 are 0.033 for porosity and 2650 kg/m^3 for dry bulk density.

5.4 Conclusions of Section 5

Correlations for estimating hydrological and geomechanical formation properties and in-situ conditions from sonic velocities have been developed from data on shale formations that lie outside the United States. These correlations have been applied to estimate properties for several large shale formations in the United States. The advantage of using correlations based on sonic velocity is that properties can be estimated from geophysical logs. This information is often more readily available and in greater quantity than direct property measurements on core that would otherwise be required. Furthermore, geophysical logs provide a continuous readout along wells that can be more readily used to characterize spatial variability in properties.

Correlations developed for porosity, uniaxial compressive strength, Young's modulus, and shear modulus with the compressional sonic velocity are reasonably consistent with other correlations that have been documented in the scientific literature. The approach has been extended here to include several other properties: bulk density, clay content, permeability, Poisson's ratio, cohesive strength, friction angle, and tensile strength. The correlation for permeability is based on an existing correlation that requires porosity and clay content as inputs. However, this correlation is limited to the permeability of the undisturbed rock matrix. Therefore, ways to estimate bulk-rock permeability are still needed.

Anisotropy is often found in many shale properties as a result of their bedding structure. A method to account for anisotropy in the property correlations has been developed and applied to correlations for permeability, Young's modulus, cohesive strength, and tensile strength.

A method for the estimation of in-situ effective stress and pore-fluid pressure has also been developed. This is based on combining previously developed correlations for the maximum effective stress experienced by the formation, which requires porosity and clay content as inputs, as well as correlations linking the uniaxial compressive strength with the over-consolidation ratio.

Correlations for the bedding-parallel sonic velocity with the normal to bedding sonic velocity and for clay content with the mean sonic velocity were found to be relatively weak and should be supplemented with additional independent measurements if possible. All of the correlations require additional development and verification. In particular, correlations for Poisson's ratio, cohesive strength, friction angle, and tensile strength need to be checked with additional data because of a very limited number of documented values that could be identified to create the correlations. Several factors that can influence properties have not been investigated here, including confining stress, fluid saturation conditions, and the organic content of shale. Further verification is also needed for many of the parameter estimates in Table 5-5; therefore, they should be viewed as initial estimates.

6. Repository Siting Guidelines for Alternative Host Rocks

6.1 Introduction

The Regional Geology work package focuses on the distribution of specific geologies in the US, review of past and current siting guidelines in both the US and other countries, and assessments of how siting within alternative geologies could be impacted by a future US siting framework that included preliminary screening guidelines. It is not within our scope to develop siting guidelines for early site screening, but we are reviewing past US and international siting guidelines and examining how the most basic geologic and siting guidelines could impact future siting in salt, shale and crystalline rock at the regional and national scale. Examples of these approaches are given in Sections 6.4 and 6.5 of this report.

The nuclear waste programs of Canada and the UK have modified their approach to repository siting since the late 1990s, with a much greater emphasis on transparency and public participation from the earliest phases of repository development (Rechard et al., 2011b). An important aspect of their approach is the early establishment of a transparent siting process and site screening guidelines to build trust that the siting process is fair and to determine relatively quickly whether a proposed site meets basic suitability requirements or is clearly unsuitable before proceeding to more detailed and time-intensive process of site evaluation and selection. Applications of initial siting guidelines for specific sites in the UK and Canada are discussed extensively in Section 5 of Rechard et al. (2011b).

Canada recently entered into a consent-based waste management framework with communities expressing interest in undergoing an initial site screening based on the following initial screening criteria (NWMO, 2010):

- The site must have available land of sufficient size to accommodate the surface and underground facilities.
- This available land must be outside of protected areas, heritage sites, provincial parks and national parks.
- This available land must not contain known groundwater resources at the repository depth that could be used for drinking, agriculture or industrial uses, so that the repository site is unlikely to be disturbed by future generations.
- This available land must not contain economically exploitable natural resources as known today, so that the repository site is unlikely to be disturbed by future generations.
- This available land must not be located in areas with known geological and hydrogeological characteristics that would prevent the site from being safe

The initial siting guidelines are intended to identify conditions at a potential site that would exclude it from for further consideration in the site selection process.

Siting criteria recently adapted in the UK and intended to be as broad and high-level as possible called for excluding any area that contained exploitable natural resources (coal, oil and gas, oil shale, industrial minerals and metal ores) or freshwater aquifers or shallow porous formations present at potential repository depths (Defra, 2008).

The approach planned in this work package is to consider siting guidelines that based on past experiences of the US and other national programs could reasonably be evaluated across broad regional areas using

existing information and data. These guidelines will provide insight into the siting guidelines that would need to be considered at the site screening and site evaluation stages of repository development. As work continues, siting guidelines will be evaluated both singly and in combination with other siting guidelines to determine their potential impact on the availability of alternative host rock formations at suitable depth and of sufficient thickness to host a mined repository (see Sections 6.4 and 6.5 of this report).

6.2 Siting Guidelines considered in the US for Alternative Media

The earliest siting guidelines to be formally implemented in the US were developed for the Demonstration Repository in Salt at Lyons, Kansas (Culler, 1971, as reported in Lomenick, 1996):

1. The salt formation should be bedded approximately horizontal and relatively undisturbed structurally so that the previous R&D work on this disposal concept would be applicable.
2. The formation should extend a considerable horizontal distance, measuring at least several tens of kilometers.
3. The formation should not be less than 150 m (500 ft) deep or 60 m (200 ft) thick.
4. At the disposal site, the depth to the top of the salt formation should not be greater than 600 m (2000 ft) because of both the increased cost and the increased difficulty of operating at greater depths.
5. The formation should not have associated with it, or be in the immediate vicinity of, potentially valuable reserves of petroleum or other mineral resources.
6. The area should be tectonically stable.
7. The area should contain a deeply buried, permeable formation into which substantial volumes of artificial brine resulting from the dissolving of the excess salt produced during the mine-excavation phase could be injected.
8. It must be possible at least to infer a reasonable measure of geologic information about a specific site in order to evaluate even its preliminary acceptability, pending further detailed investigation. Because of the geologic nature of salt deposits, these inferences could be based on information obtained from either accessible mines in the area or from a rather large number of existing boreholes that penetrate the formation.

Siting guidelines for shale were defined as part of the extensive study of the Pierre Shale by Shurr (1977):

1. Depth. Potential specific isolation horizon (the zone in which an isolation facility would be constructed) should be from 1, 000 to 3,000 feet (305-914 m) below land surface; shallower depths may be considered, but are less desirable.
2. Shale thickness. Maximum thickness of the isolation medium is to be preferred. The minimum shale thickness acceptable is 500 feet (152m).
3. Overburden thickness. Minimal thickness of sand, gravel, or other overlying material above the Pierre Shale is preferred. Maximum permitted is 2,500 feet (762 m) (in order to have at least 500 feet (152 m) of shale and be no more than 3,000 feet (914 m) deep).
4. Lithology and mineralogy. The entire Pierre section must be reasonably uniform shale with few if any beds of sandstone or other permeable rocks. One or more potential isolation horizons, at least 50 feet (15 m) thick, must exist. Expandable clays in the shale are undesirable within the isolation zone.
5. Penetrations (boreholes). Boreholes of any kind are undesirable, particularly if they penetrate to rocks beneath the Pierre Shale. It is recognized that some holes, either preexisting or bored during detailed search for isolation sites, are necessary to provide geologic information at depth.
6. Structure. Beds should be nearly horizontal, having maximum dips of 5° and no known faults or folds within several miles of the isolation site.
7. Seismicity. Future seismic activity is highly undesirable; regions of recorded epicenters should be avoided.

8. Topography. Minimal topographic relief is desirable.
9. Mineral and water resources. It is undesirable to consider a potential site near exploitable mineral or water resources, either at or below the surface.

These guidelines were defined specifically for the Pierre Shale, but could apply to any shale formation.

The Crystalline Repository Project (DOE, 1986b) was the first and only U.S. repository project to formally apply systematic screening criteria at the national to regional to area to site screening stages (DOE, 1986b). The Crystalline Repository Project used the following criteria for the first stage of screening as part of the national survey of granitic rocks:

1. Exposed or near-surface crystalline rocks
2. Rock mass size
3. Vertical movements
4. Faulting
5. Earthquakes
6. Seismically induced ground motion
7. Quaternary volcanic rocks
8. Mineral deposits
9. High-temperature convective ground-water systems
10. Hydraulic gradients incorporating regional topographic variations
11. Erosion

In the next stage of screening, the regional survey that would support region-to-area screening, the Crystalline Repository Project used a slightly different and more detailed set of considerations:

1. Structure, stratigraphy, depth, thickness and continuity of rock formations
2. Regional flow characteristics of groundwater systems
3. Physical characteristics of major formations (lithology and mineralogy)
4. Occurrence of natural resources and their current and future production potential
5. Existence of folds and faults
6. General surface characteristics
7. Seismic history of the region
8. Dedicated land use areas
9. Threatened and endangered species
10. Population centers
11. Transportation systems

6.3 Data for Representative Siting Guidelines

The siting guidelines proposed for alternative repository host rocks have several items in common. The first has to do with the geometry and characteristics of the host rock including size (extent), depth and thickness. Others have to do with the proximity of natural resources (oil and gas, minerals, groundwater), seismicity, topography, and population distribution. Based on review of siting guidelines considered in the US and other national programs, we have to date included data for a number of potential siting

guidelines in the GIS database (Table 6-1). These guidelines include data related to formation geometry, natural hazards, cultural features and natural resources. Other data for siting guidelines planned in the future but not yet fully implemented as part of the GIS database include data for freshwater and saline reservoirs and data related to crustal temperature and geothermal resources such as geothermal gradient and heat flow. We also include data for transportation infrastructure such as railways and roads as well as other data potentially relevant to siting.

Table 6-1. Data Relevant to Potential Siting Guidelines for Geologic Media (Deep boreholes in Crystalline Basement, Mined Repositories in Granite, Salt or Shale)

Potential Siting Guideline	**Applicable Geologic Media**	**Source**
Population Distribution and Density	All media	LandScan (2010), McKee et al. (2014) and courtesy of Femi Omitaomu and Randy Belles (ORNL)
Natural Resources (Oil and Natural Gas)	All media	Biewick (2008)
Federal Lands	All media	National Atlas of the United States (2005)
Quaternary Faults and Plio-Quaternary Volcanism	All media	USGS (2006); Garrity and Soller (2009)
Seismic Ground Motion Hazard	All media	Petersen et al. (2011)
Topography and Smoothed Slope	All media	NOAA (2006); Slope calculated at LANL
Depth to Crystalline Basement	Deep Borehole	Southern Methodist University Geothermal Laboratory, courtesy of Maria Richards
Structure within Crystalline Basement	Deep Borehole	Sims et al. (2008)
Horizontal Stress	All media (primarily Deep Borehole)	Heidbach et al. (2008)
Temperature at Depth	Deep Borehole	Geology, Minerals, Energy, and Geophysics Science Center (USGS) courtesy of Colin Williams
Geometry and Depth of Geologic Formations	All media	Multiple sources described in Section 4 of this report

6.3.1 Population Distribution and Density

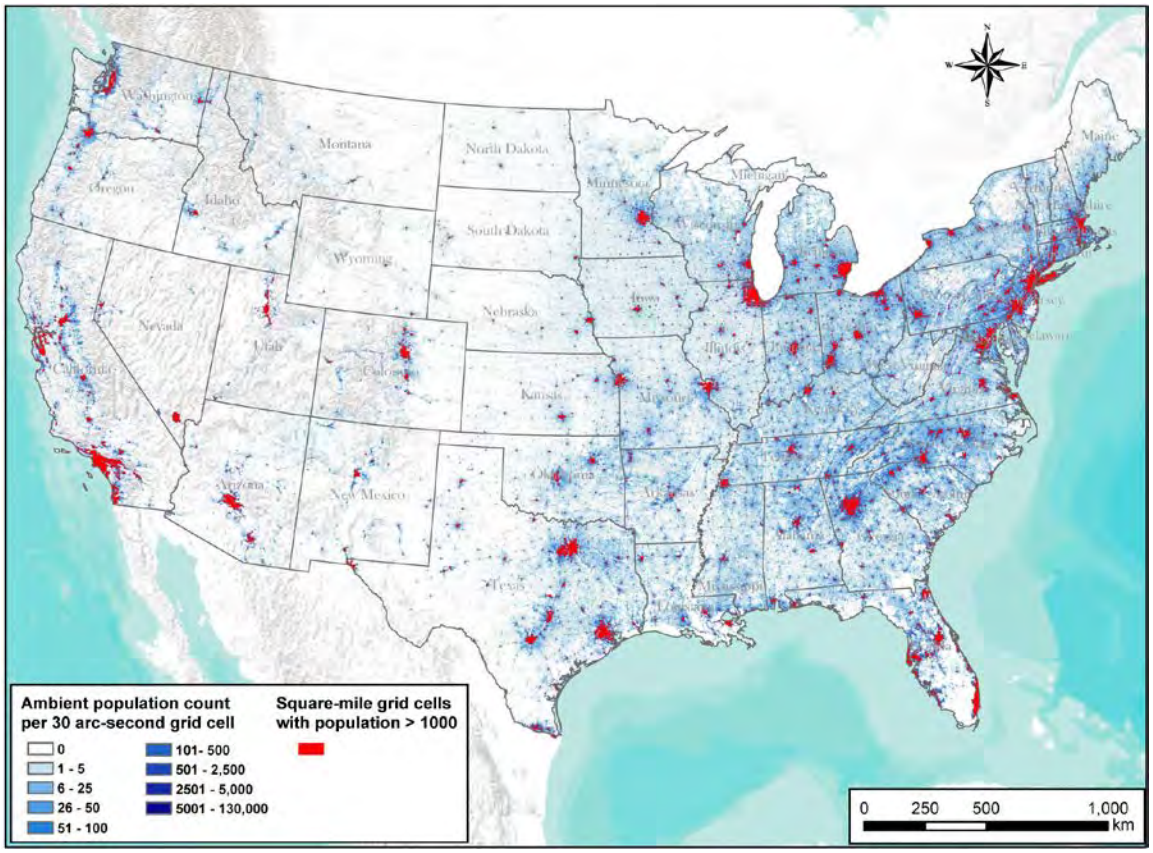

Figure 6-1. Population distribution and density in the contiguous US based on 2010 LandScan data.

Proximity to population is a primary siting consideration based on minimizing radiation hazard to humans. Population data for the US was obtained from the LandScan High Resolution Global Population Data Set (LandScan, 2010). The LandScan data is the highest resolution population data available and is represented as "ambient" population, which is the population averaged over a 24 hour period (LandScan, 2010). The data can be processed and visualized in different ways depending on need (Figure 6-1). The first method displayed here (in blue) is an approximation of population density, based on counts within 30 arc-second cells, which are ~ 1 square kilometer at the equator but diminish in size as latitude increases. Although not represent a true population density because the size of the area changes, it is a close approximation that is useful for visualization of population distribution at the national scale. The second method (in red) shows square-mile cells within the US containing more than 1000 persons, consistent with siting criteria discussed in the NWPA and implemented as part of site screening for the DOE Crystalline Repository Project (DOE, 1986b). The two representations of population distribution are consistent, showing the highest population density in the eastern US with population densities in excess of 1000 persons per square mile restricted to the urban areas of the US. ORNL has provided us with population distribution projections for 2030 and 2050 that are available for the Regional Geology database but not shown in this report (McKee et al., 2014). At the national scale, the projections for 2030 and 2050 are not visibly different than the population distribution for 2010.

6.3.2 Natural Resources (Oil and Natural Gas)

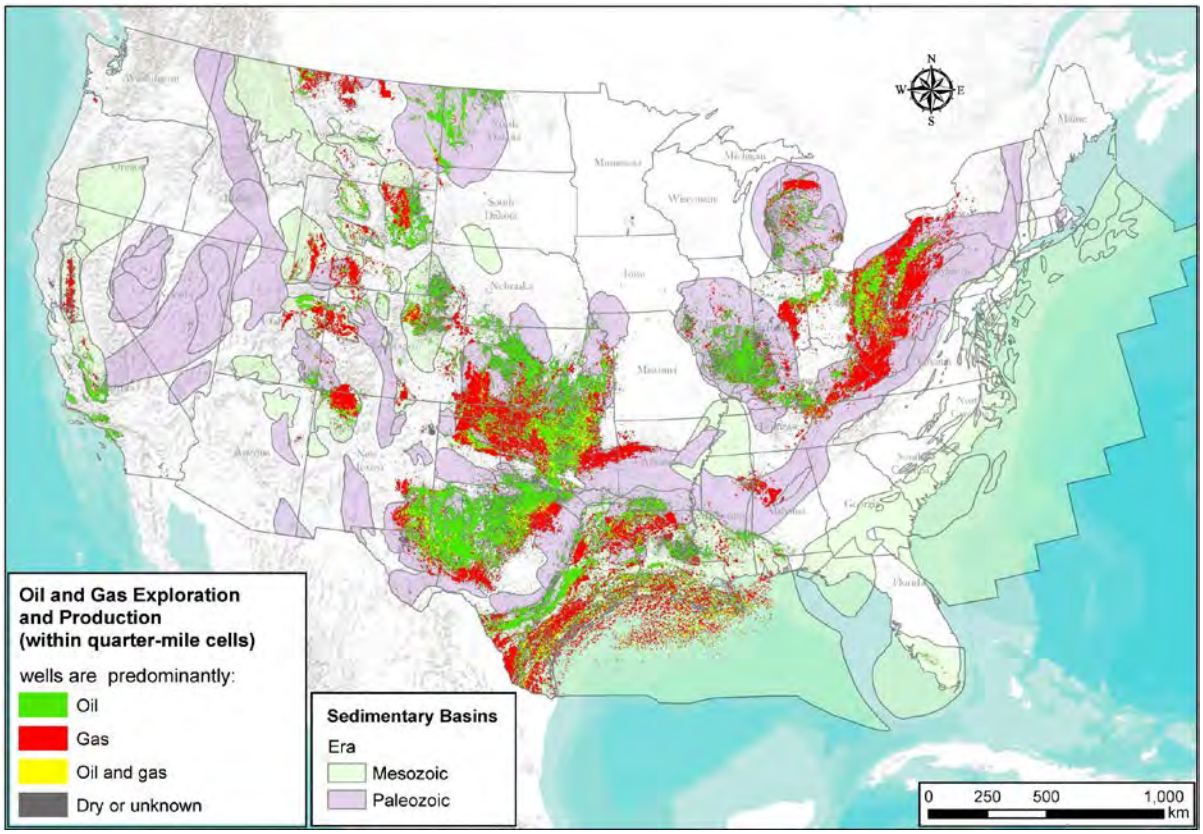

Figure 6-2. Distribution of oil and natural gas production in the contiguous US. Paleozoic and Mesozoic structural basins of the US are shown for reference (Coleman and Cahan, 2013). Cell sizes of oil and gas areas are exaggerated in figure to increase visibility.

Areas of oil and gas exploration production indicate where relative dense and deep drilling in the US has occurred and likely will occur in the future (Figure 6-2). Drilling depths are generally greater than a few hundred meters and well below the depth of the majority of drinking water wells. Deep drilling is considered the most common mechanism of human intrusion of a mined geologic repository. Compared to other natural resources that might be mined or drilled, oil and gas represent the most widely distributed natural resource within the US and therefore impact the largest areas of the US. The map for the distribution of oil and gas exploration and production in the US represents over three million wells and is the most complete database of wells available for the US (Biewick, 2008).

Well location is represented by quarter-mile cells, where each cell has some number of wells that predominately produce oil, gas, oil and gas, or are dry or unknown (see legend, Figure 6-2). Displaying the data in this way avoids the issue of using proprietary data from the oil and gas industry. Although substantial new drilling has occurred in the US since this data was finalized in 2005-2006, most new drilling represents “infilling” of areas of previous exploration and production versus drilling in new areas (for example, the Williston Basin of North Dakota). For this reason, the distribution of past drilling can be considered to approximate the distribution of future drilling.

6.3.3 Federal Lands

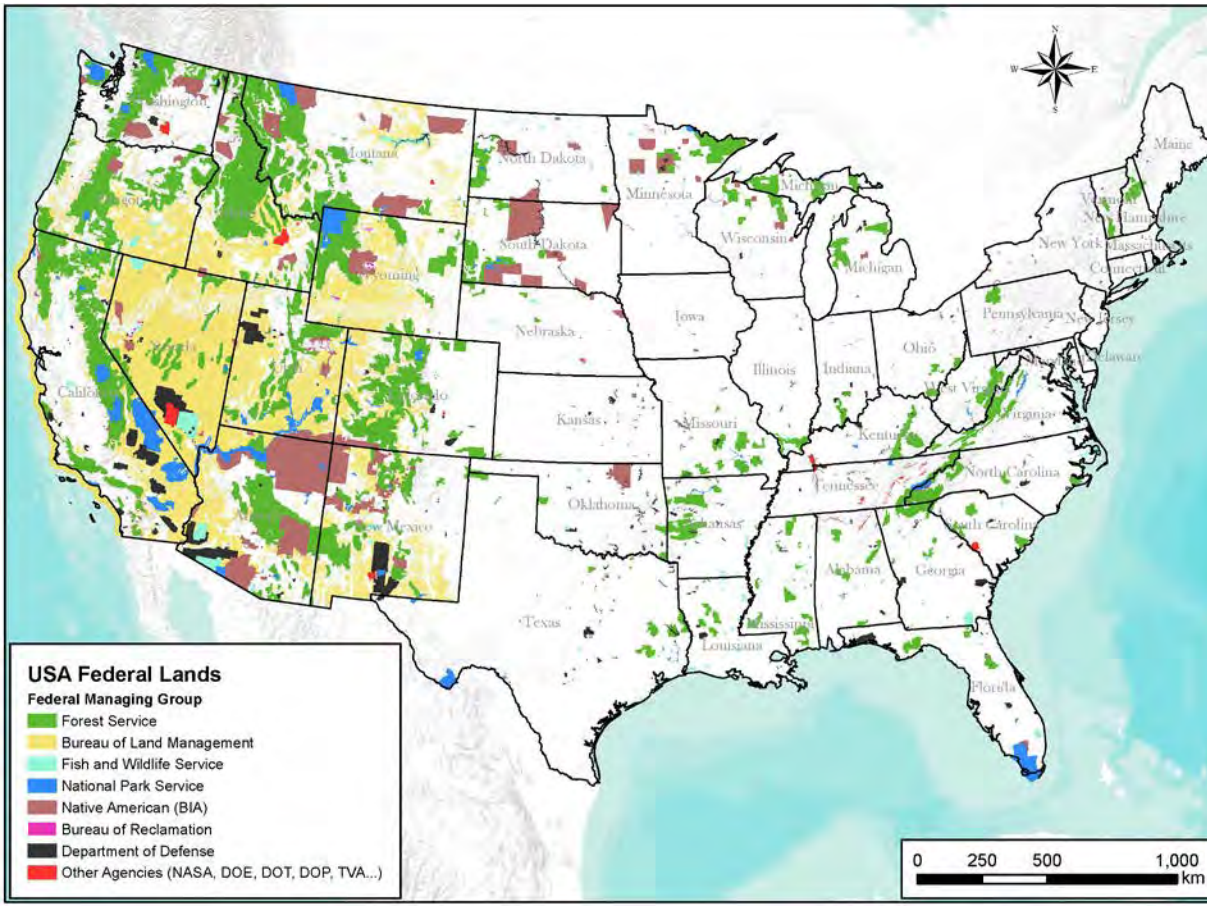

Figure 6-3. Federal lands in the contiguous US.

The location of Federal lands is potentially important for repository siting because certain types of lands (e.g., National Parks and National Wildlife Refuges) are considered protected national and cultural assets. The greatest areas of Federal lands are located in the western US and administered by the National Forest Service or the Bureau of Land Management (Figure 6-3). From another perspective, the GAO (1979) recommended that Federal lands (specifically DOE reservations) be given first consideration for nuclear waste disposal sites. The GAO noted that DOE sites are already federally owned and several are in remote locations. Certain Federal lands could also potentially be considered for siting of disposal or storage demonstration facilities.

6.3.4 Quaternary Faults and Plio-Quaternary Volcanism

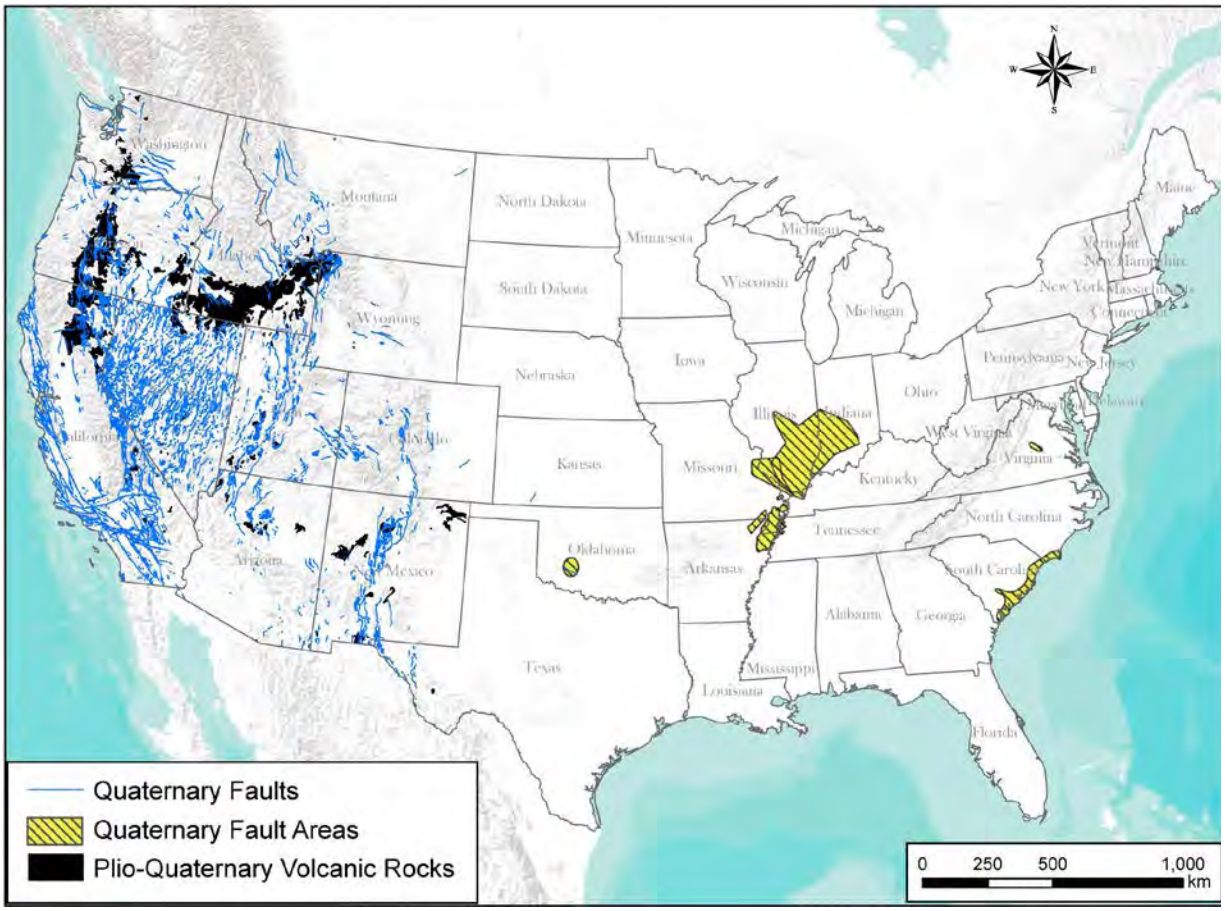

Figure 6-4. Distribution of Quaternary faults, fault areas and Plio-Quaternary volcanic rocks in the contiguous US.

Active faulting and volcanism represent features and events that could potentially compromise the ability of a geologic repository to isolate waste. The major region of active faulting in the US occupies many of the western states while the most active areas of volcanism are the Cascade volcanoes of Washington and Oregon and the Snake River/Yellowstone system of Idaho and Wyoming. Scattered basaltic volcanoes of small volume have erupted during the last 10,000 years in Arizona, New Mexico, Utah, California, and Oregon. Data for their distribution of faults and volcanoes in the US are important for identifying regions of active tectonics. The fault locations and areas depicted in Figure 6-4 represent faults believed to have produced earthquakes of greater than magnitude 6 during the Quaternary Period (USGS, 2006). Combined with data for the distribution of Pliocene and Quaternary volcanism (Garrity and Soller, 2009), which indicate areas that have been volcanically active in the past 5.3 million years, these data indicate regions that are likely to be tectonically active in the next few million years. Taken together, these regions include much of the western US, as well as the New Madrid and Charleston regions of the eastern US.

6.3.5 Seismic Ground Motion Hazard

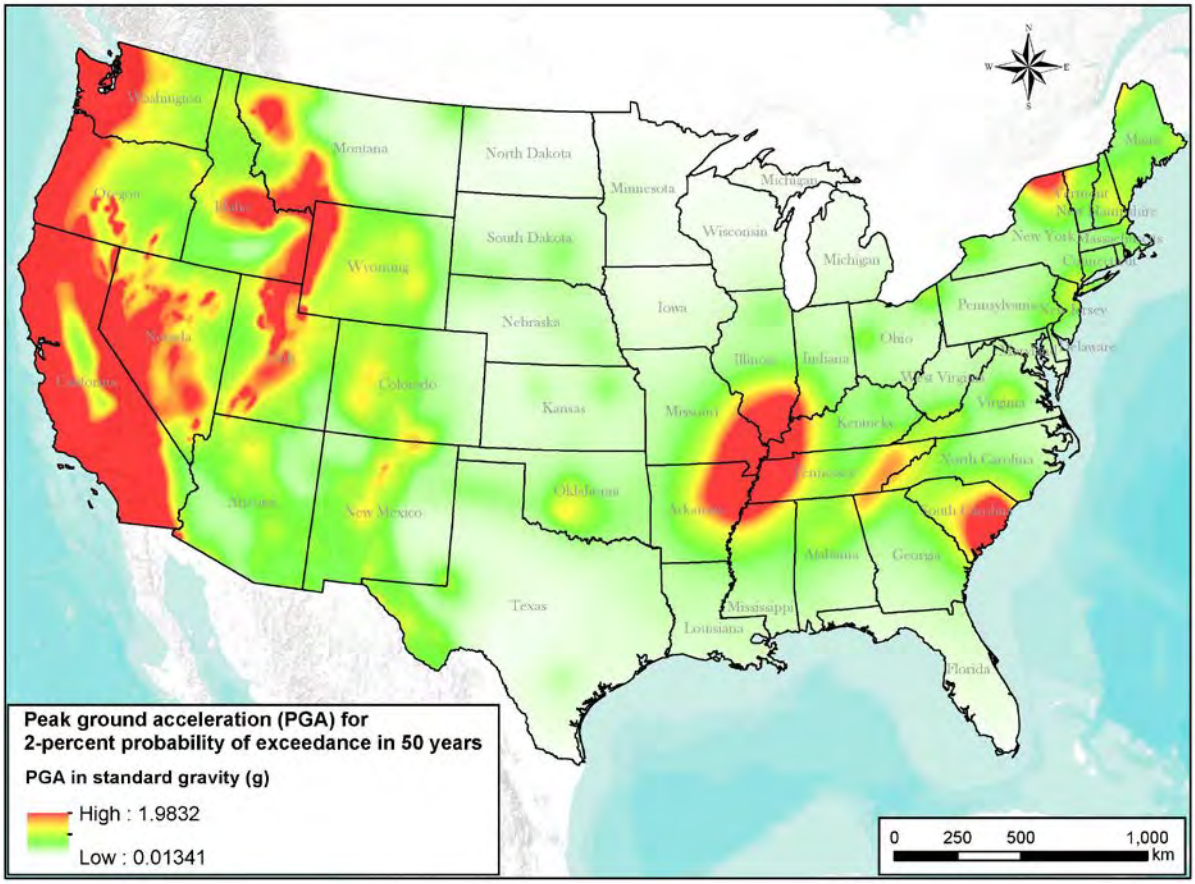

Figure 6-5. Seismic ground motion hazard map of the contiguous US. Color values represent peak ground acceleration with a probability of exceedance of 2% in 50 years.

Strong seismic ground motion produced by fault displacement can adversly impact repository facilities and infrastructure and is indicative of regions of tectonic activity (Figure 6-5). The seismic ground motion hazard is represented as the probability of exceeding a certain peak ground acceleration within a defined period of time, for example, a probability of 2% in 50 years (Figure 6-5; data from Petersen et al. 2011). Since ground motion is caused by fault displacement, the distribution of the ground motion hazard mirrors the distribution of Quaternary faults and fault areas in the US (Figure 6-4).

6.3.6 Topography and Smoothed Slope

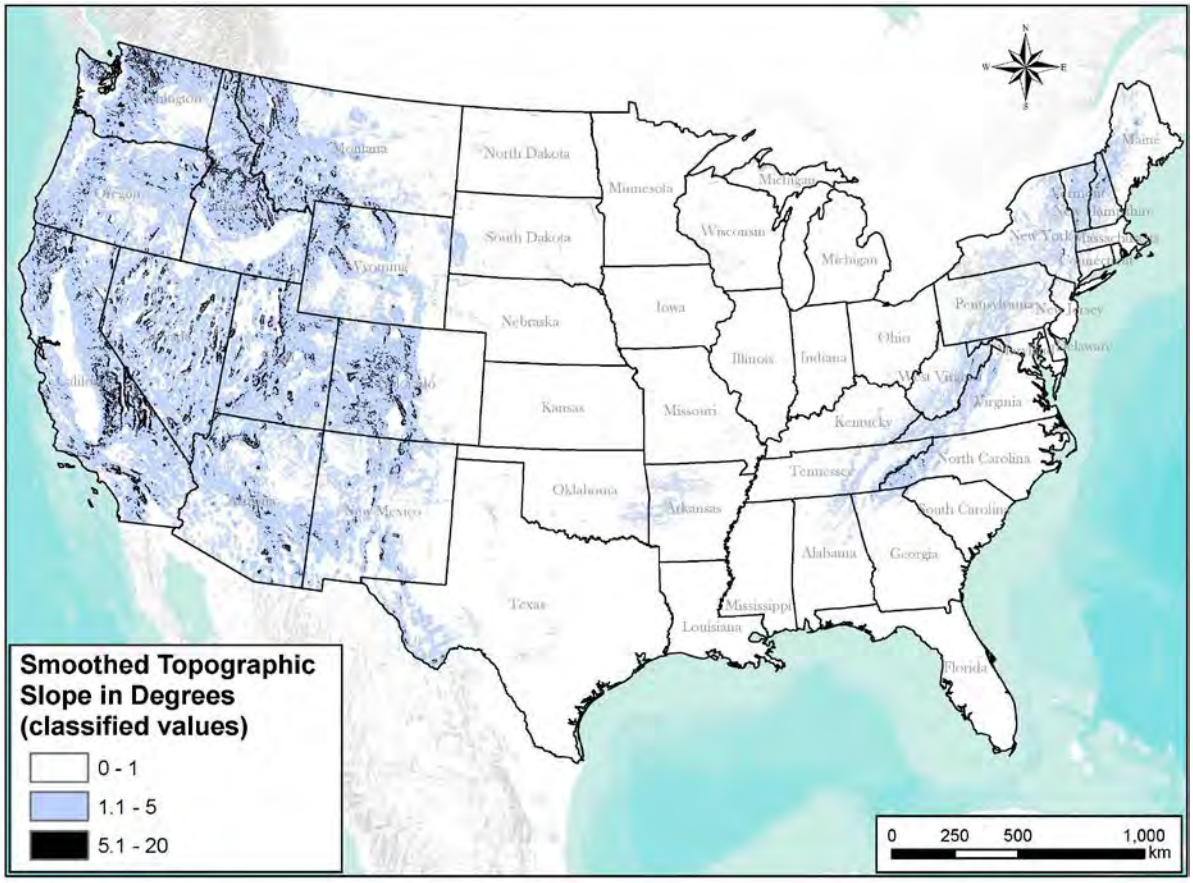

Figure 6-6. Topographic slope in the contiguous US classified by slope angle over a smoothing distance of 3 km.

Topography and topographic relief (represented here as smoothed slope) is a siting consideration for several reasons. Steep topography is a primary indicator of recent uplift and tectonism, high erosion rates, and increased landslide hazard from steep slopes (e.g., Montgomery and Brandon, 2002), Topography also exerts a primary control on hydraulic flow and groundwater recharge and discharge. These processes affect the isolation capability of a repository. Topographic data in the form of a global DEM was acquired from the ETOPO2 data set (NOAA, 2006). The average slope within 3-km grid cells was calculated using tools in the ArcGIS software that compares elevation values in adjacent DEM cells. The resulting grid of slope values quantifies the degree of topographic slope and relief for different regions of the US (Figure 6-6). Areas of more complex topographic relief are expected to have more complex groundwater systems driven by hydraulic gradients that are more variable over shorter distances.

The results can be represented and displayed as either classified or continuous values (Figures 6-6 and 6-7). The classified data is useful for quantifying areas of the US that are almost completely flat (<1 degree of slope), as well as their distance from areas of higher relief. Essentially flat areas far (>100 km) from areas of significant topographic relief would be expected to have groundwater systems with extremely low groundwater flow rates because of a regionally low hydraulic gradient. These regions include much of the interior US (Figure 6-6).

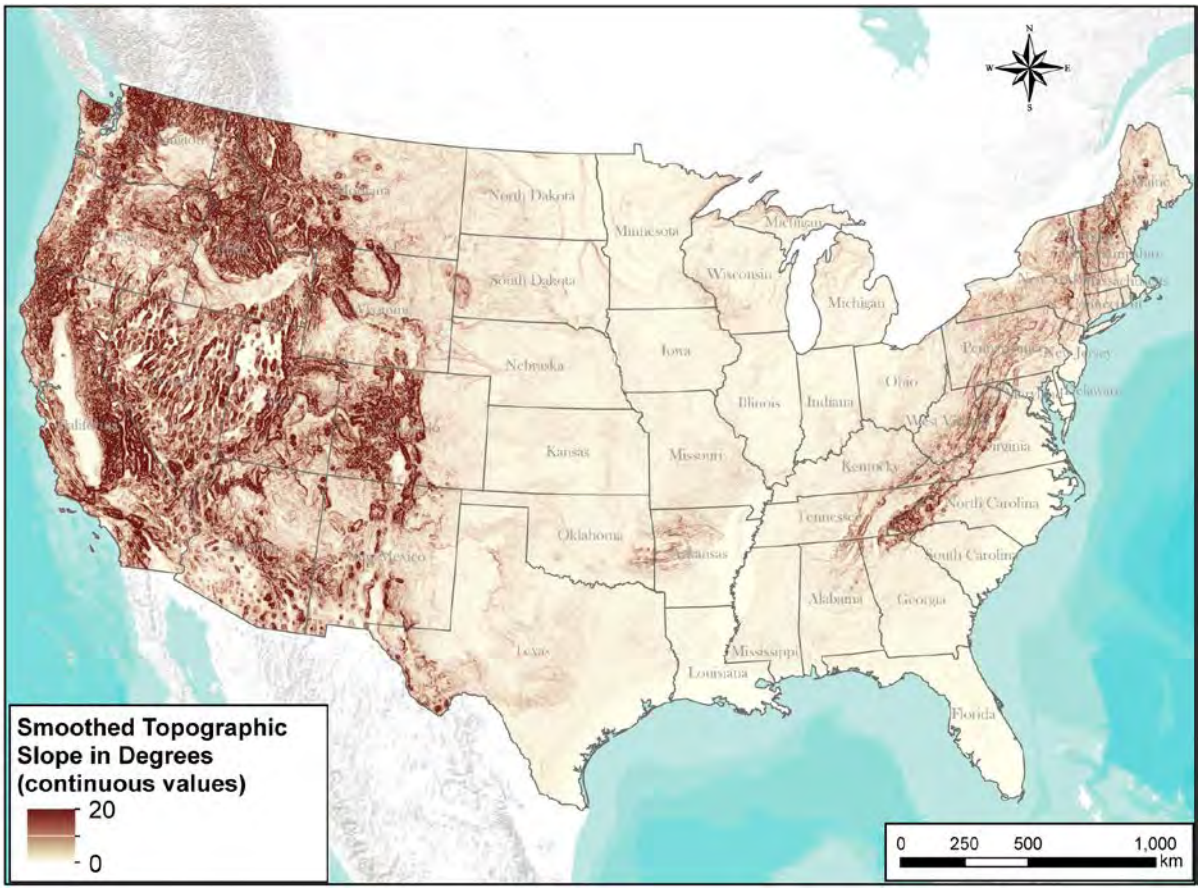

Figure 6-7. Topographic slope in the contiguous US displayed as continuous values over a smoothing distance of 3 km.

The continuous data representation provides a view that more closely resembles topographic variations and provides a higher fidelity view of areas of very low or very high topographic slope (Figure 6-7).

Several features related to tectonic uplift are worth noting that are apparent by inspection of Figures 6-6 and 6-7. The Sierra Nevada Range has one of the highest contemporary uplift rates in the US (Hammond et al., 2012), consistent with high slope angles in the upper end of the range for the contiguous US. Likewise, a region of the southern Appalachian range in western North Carolina has anomalously high slope angles compared to much of the rest of the range (Figure 6-7). Based on geomorphic evidence, it has been proposed that this region has experienced tectonic rejuvenation possibly due to mantle processes beginning in the Miocene (Gallen et al., 2013).

6.3.7 Crustal Stability versus Active Tectonics

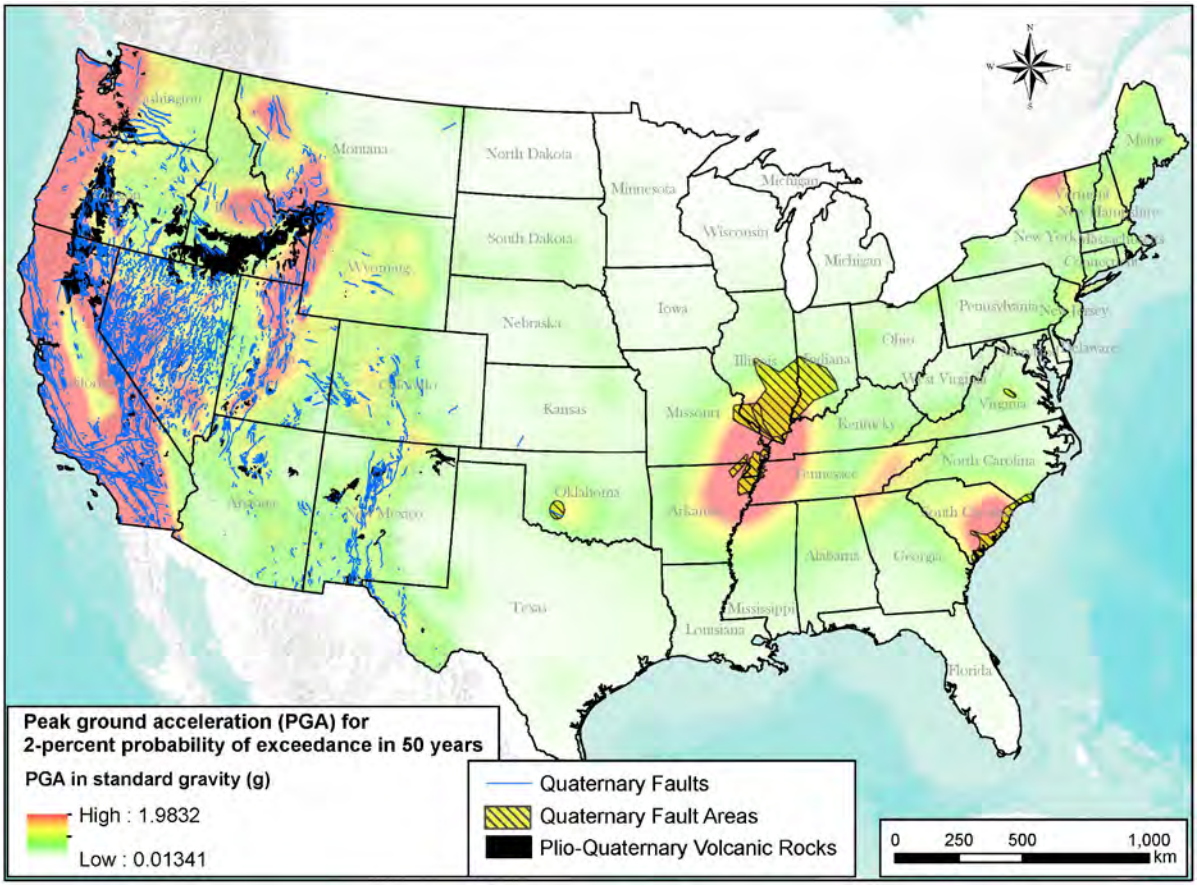

Figure 6-8. Seismic hazard and distribution of Quaternary faulting and Plio-Quaternary volcanic rocks in the contiguous US. In combination, these features indicate areas that are considered tectonically active in the US.

Data layers for potential siting guidelines can be combined on a single map to provide better insight on potential siting opportunities and challenges. For example, the distribution of Quaternary faults, volcanism and strong seismic ground motion hazard delineate the" tectonically active" regions of the US (Figure 6-8). Tectonic activity on the continental scale is dominated by the tectonic activity in the western US. The western US also incorporates the highest elevations and topographic relief in the US (compare Figure 6-7) due to tectonic uplift over the last 100 million years. The major tectonically active areas in the eastern US are the New Madrid and Charleston regions. Large regions of the US mid-continent are tectonically stable with no evidence of significant tectonism in the past several hundred million years.

6.3.8 Depth to Crystalline Basement

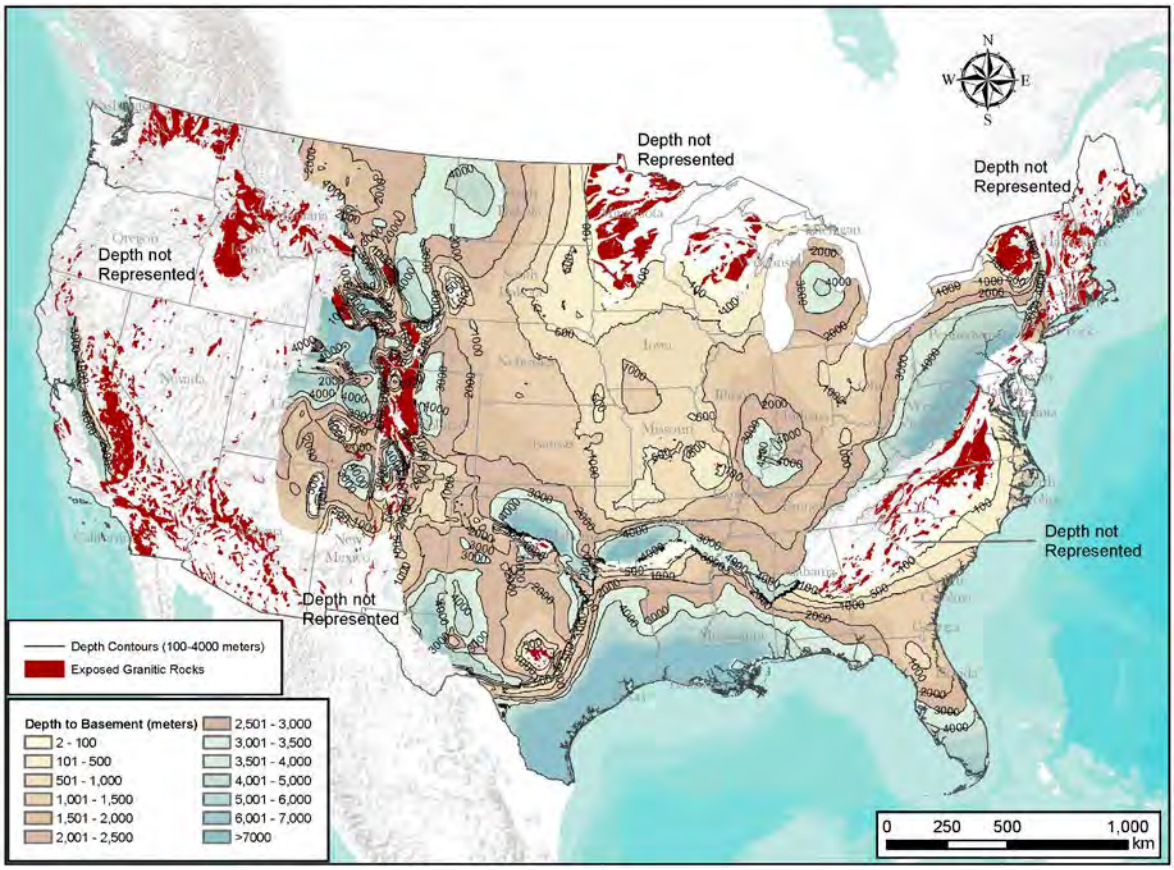

Figure 6-9. Depth to crystalline basement and distribution of granitic outcrop (red). Color-shading represents the depth to basement with yellow-brown representing depths of up to 3 kilometers and greens representing major basin areas with basement depth of greater than 3 kilometers.

Digital data for sediment thickness was obtained from the Southern Methodist University (SMU) Geothermal Laboratory (http://smu.edu/geothermal/). Data for sediment thickness can be converted to depth to crystalline basement by subtracting the sediment thickness from digital topography. The SMU dataset contains approximately 216,000 data points spanning much of the US. Data is not included for the tectonically active regions of the western US because sediment thickness and depth to basement is complex and highly variable over short distances due to intensive faulting. Each data point in the SMU dataset has a z-value that is equivalent to sediment thickness at that location. For inclusion in the GIS database, we subtracted sediment thickness values from the corresponding ground elevation values (to convert the values to basement depth) and then contoured the resulting data points. We used the contour data to interpolate a continuous 3D surface representing the depth to basement (Figure 6-9). The GIS data shown in Figure 6-9 can be queried to show only areas of the US that have crystalline basement at a depth of 2 kilometers or less (Figure 6-10).

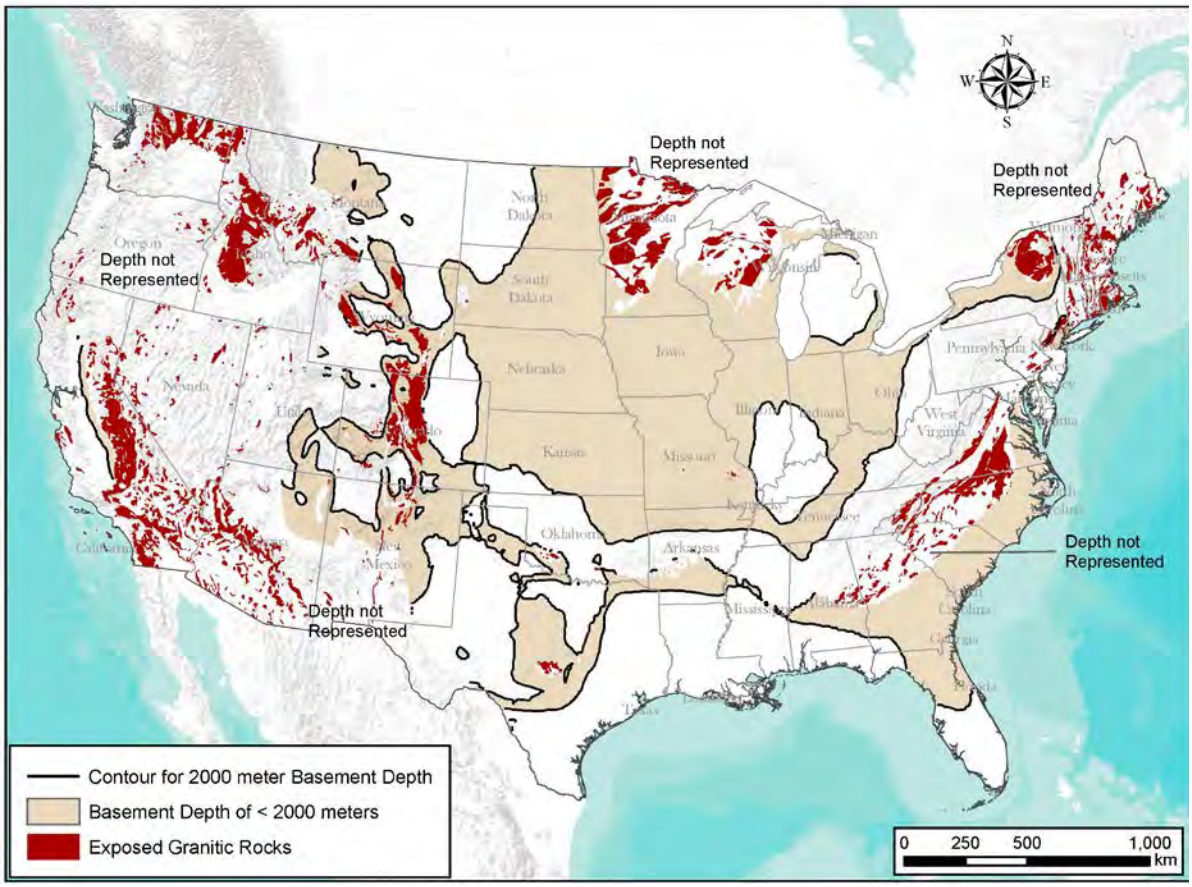

Figure 6-10. Distribution of crystalline basement at a depth of less than 2 kilometers and granitic outcrop (red) in the contiguous US.

Brady et al. (2009) and Arnold et al. (2011) present a reference design for deep borehole disposal that accomodates waste and seal material in the lower 2000-3000 meters of a borehole penetrating crystalline basement rock. For a maximum borehole depth of 5000 meters, crystalline basement at a maximum depth of 2000 meters is prefered.

Figure 6-10 shows the distribution of large and continous areas of the US where crystalline basement is at a depth of 2000 meters or less, including surface exposures of crysalline rock. These regions meet the technical site selection guidelines for a deep borehole demonstration site (Arnold et al., 2013). Other site selection guidelines would also have to be considered and are discussed briefly in section 6.4 of this report.

6.3.9 Structures within Crystalline Basement

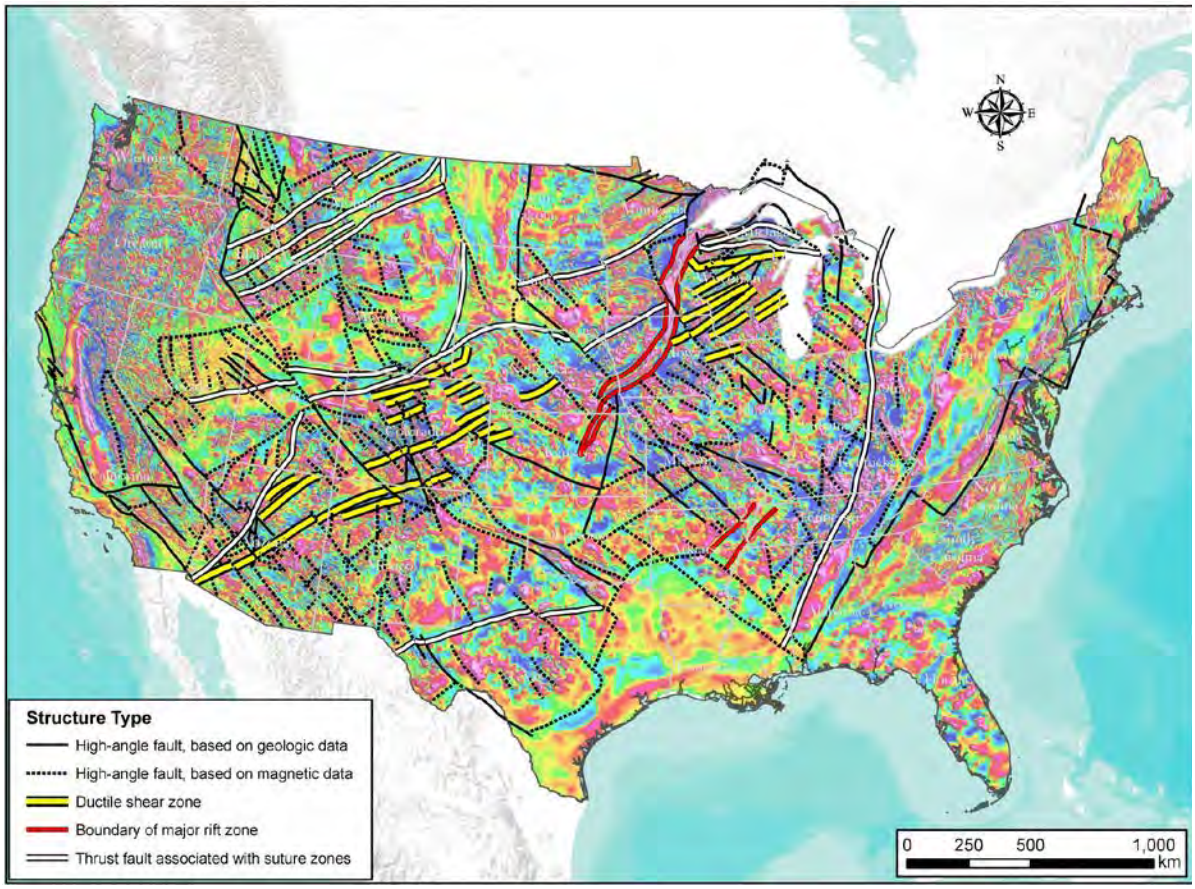

Figure 6-11. Aeromagnetic map and basement structure of the contiguous US from data presented in Sims et al. (2008).

Structures within crystalline basement rocks are interpreted primarily from geophysical data combined with generally less abundant geologic data that includes borehole data and interpretations of geologic data (Figure 6-11). Linear features and discontinuities in aeromagnetic data are generally interpreted to represent structures (faults, shear zones) that have offset and juxtaposed rocks with contrasting magnetic properties (Sims et al., 2008). These features largely formed during major tectonic episodes that took place during the Archean and Proterozoic Eons with episodic reactivation into the late Proterozoic (Sims et al., 2008).

The major impact to siting is that basement structures represent zones of geologic complexity or higher groundwater permeability. Basement structures present potential drilling problems as well as hydrologic conditions that could adversely affect waste isolation (Arnold et al., 2013).

6.3.10 Horizontal Stress

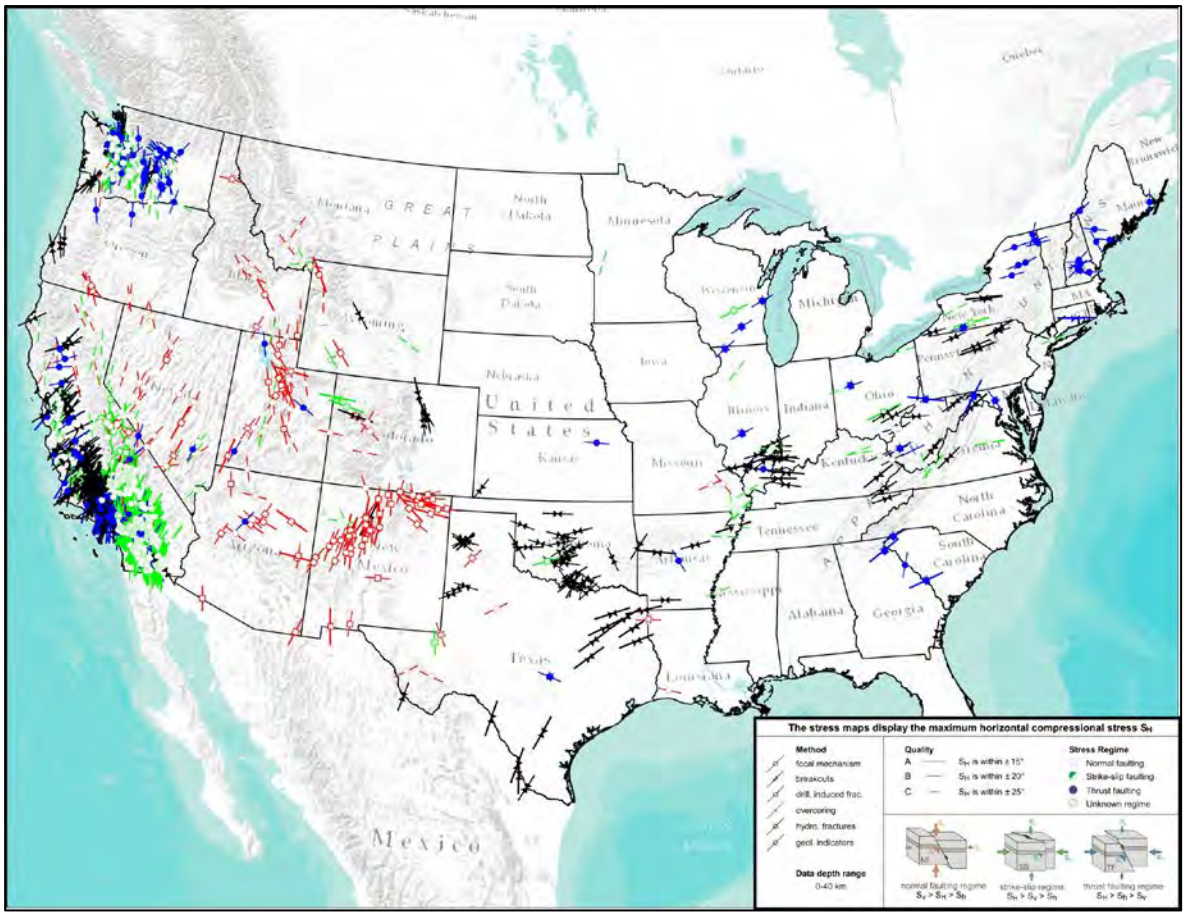

Figure 6-12. Map of maximum horizontal compressional stress in the contiguous US. Map legend is directly from Heidbach et al. (2009).

Data for horizontal stress in the US was acquired from the World Stress Map Project (Heidbach et al., 2008). Technical siting guidelines related to horizontal stresses in the crust relative to deep borehole disposal are discussed in detail by Arnold et al. (2013). Large differential horizontal stresses can compromise borehole integrity through breakouts oriented in the direction of the minimum horizontal stress. Relatively homogeneous regions of the US with low differential stress, such as the mid-continent region, are therefore more favorable for a deep borehole disposal demonstration site (Arnold et al., 2013).

6.3.11 Temperature at Depth

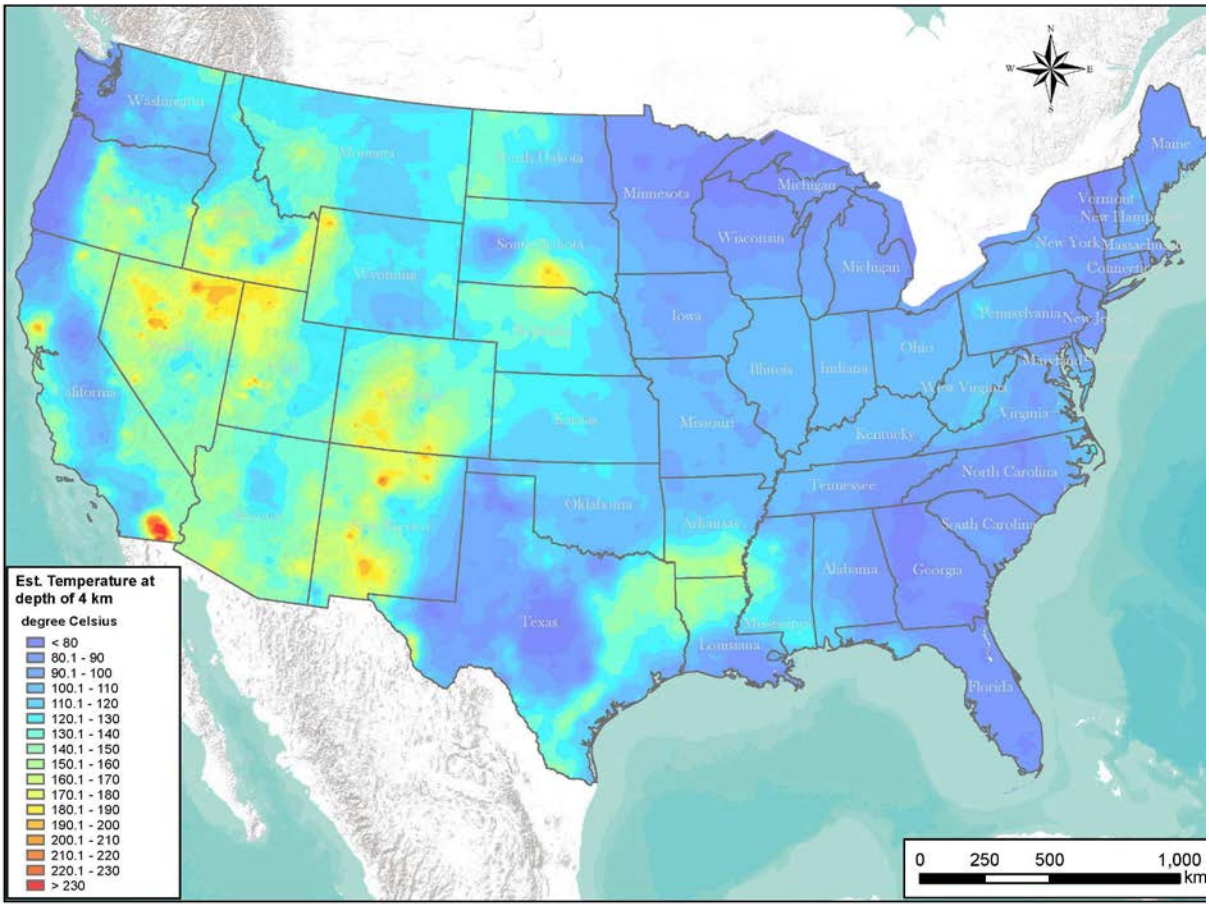

Figure 6-13. Estimated Temperature at a depth of 4 kilometers for the contiguous US.

Temperature at depth, along with geothermal gradient and heat flux, indicates areas that could potentially be explored for geothermal resources. Temperatures at depth estimates also provide the expected temperatures within the waste disposal zone of a deep borehole disposal system (Brady et al., 2009; Arnold et al., 2011). Data for temperature at depths of 2, 3 and 4 kilometers was obtained through the courtesy of Dr. Colin F. Williams, Director of the USGS Geology, Minerals, Energy, and Geophysics Science Center (Figure 6-13). Temperature at depth estimates are derived from surface heat flow data, sediment thickness data, and thermal conductivity and radioactive heat content estimates using methods presented in Blackwell et al. (2007). Higher crustal temperatures at depth and associated geothermal resources are more prevalent in the western US while large areas of the middle and eastern US are relatively cool at depth.

6.3.12 Geometry and Depth of Geologic Formations

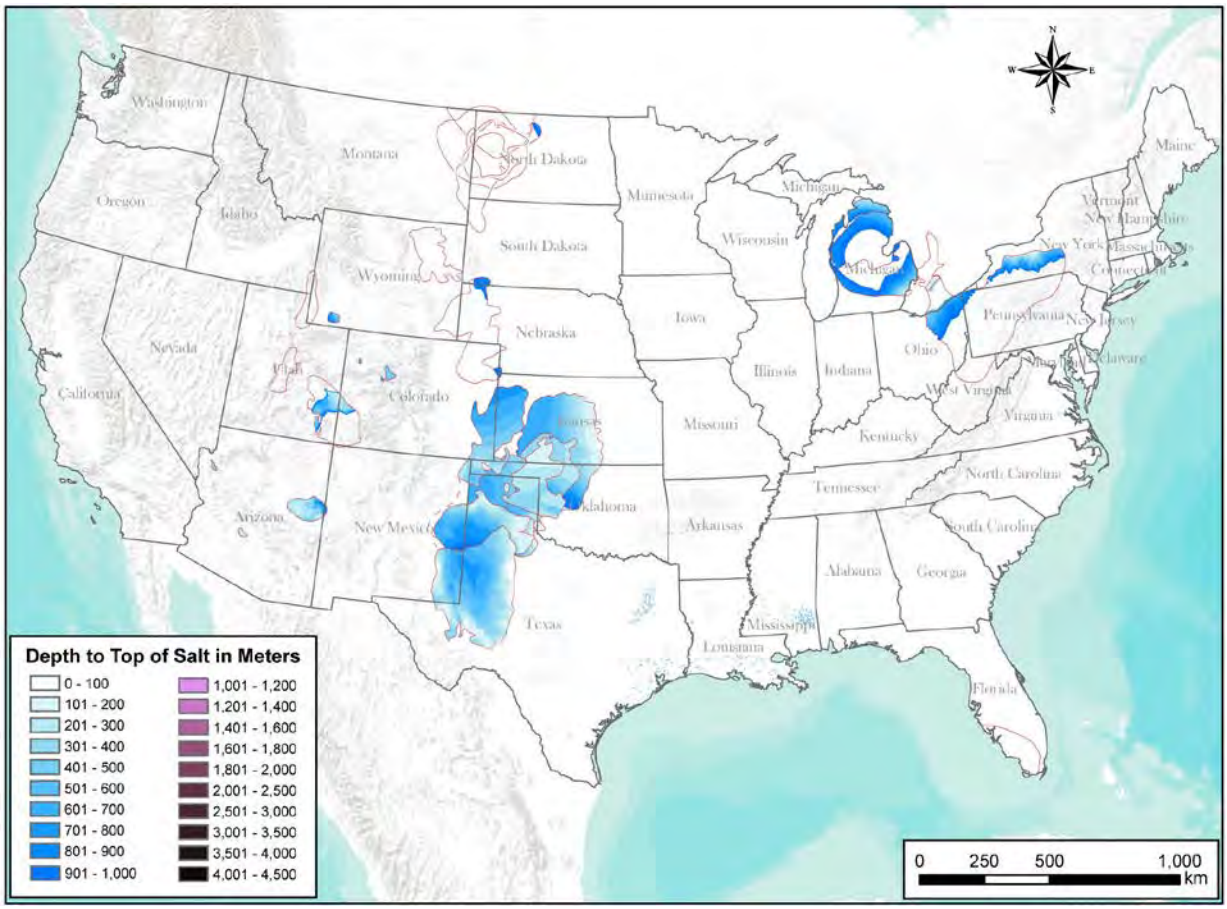

Figure 6-14. Distribution of salt formations in the US where the top of the formation is at a depth of less than 1000 meters.

In Section 4 of this report, we presented depth and thickness data for a large number of salt and shale formations. Figure 6-14 depicts the distribution of all salt deposits in the US with tops at a depth of 1000 meters or less. Depth to a the top of a potential repository host formation is a potential siting guideline that would determine whether a specific formation could potentially host a repository. A formation that is thin and occupies only the upper 100 meters of the near-surface enviornment, for example, would not provide enough overburden to ensure adequate waste isolation. At the opposite extreme, formations within the central portions of deep sedimentary basins may lie at a depth of several kilometers or more and are too deep for practical site characterization and construction of a mined repository. Other portions of these formations may be situated at shallower depths near basin margins or outside of basins and would provide more suitable sites for hosting a repository. Repository design concepts and experience in the US and other countries suggest that the maximum depth for a mined repository is approximately 1000 meters, with most designs lying within a depth range of 200-800 meters (EPRI, 2010). At depths greater than 1000 meters excavation becomes more difficult and expensive. For the purposes of ensuring geologic isolation of HLW, no need has been identified to position a repository at a depth greater than 1000 meters.

Major bedded salt deposits at shallow depth occur in only two regions of the US, the Permian Basin region and and the region encompassing the Appalachian and Michigan Basins (Figure 6-15). Lessor

volumes of salt occur at shallow depths in the Holbrook Basin of Arizona, the Paradox Basin of Utah,the margins of the Denver and Williston Basins, and the smaller basins of Arizona, Colorado and Wyoming.

6.4 Relationship between Geology and Siting Guidelines at the National Scale

One of the chief values of a GIS database is that it allows analysis and display of the attributes of individual data sets as well as multiple data sets in relationship to one another. In the previous section of this report, for example, we used the visualization capabilities of the GIS database and the depth data for all salts to show only the salts bodies that lie at a depth of less than 1000 meters. We also combined data to show the relationship between faulting, volcanism and seismic hazard.

With these capabilities, the GIS database can be used to address several fundamental questions related to potential host rocks and potential siting guidelines for HLW disposal

- Where are potential suitable host rocks located within the US?
- What are the spatial relationships between potential host rocks and other natural or cultural features that may be favorable or unfavorable to repository siting?
- Does a particular region or host-rock occurrence satisfy conditions that may be important for hosting a repository?

An example of the relationship between geology and potential siting is shown in Figure 6-15. In this example, the distribution of salt conditional on depth (<1000 meters) is displayed in relationship to topographic slope, population density (square mile areas with greater than 1000 persons) and a reference contour for a 2% probability of PGA exceeding 0.1g in 50 years.

The topographic features and seismic ground motion hazard define the major tectonically active regions of the US. The major salt deposits lie within areas of stable crust and have not been disrupted and dissolved over long periods of geologic time. Thus, active tectonics is probably not a significant siting factor for these salt deposits. The other key siting guideline included in Figure 6-15 is population distribution and density. As noted earlier in this report, high population density was a factor in deferring further site screening activities within the Michigan and Appalachian Basins region in the 1980s (DOE, 1986a). Population density is less of a potential issue in the Permian Basin region (Figure 6-15). Not shown in this example is the distribution of oil and gas resources (Figure 6-2), which historically has been a potential siting issue in the Permian Basin region (Lomenick, 1996).

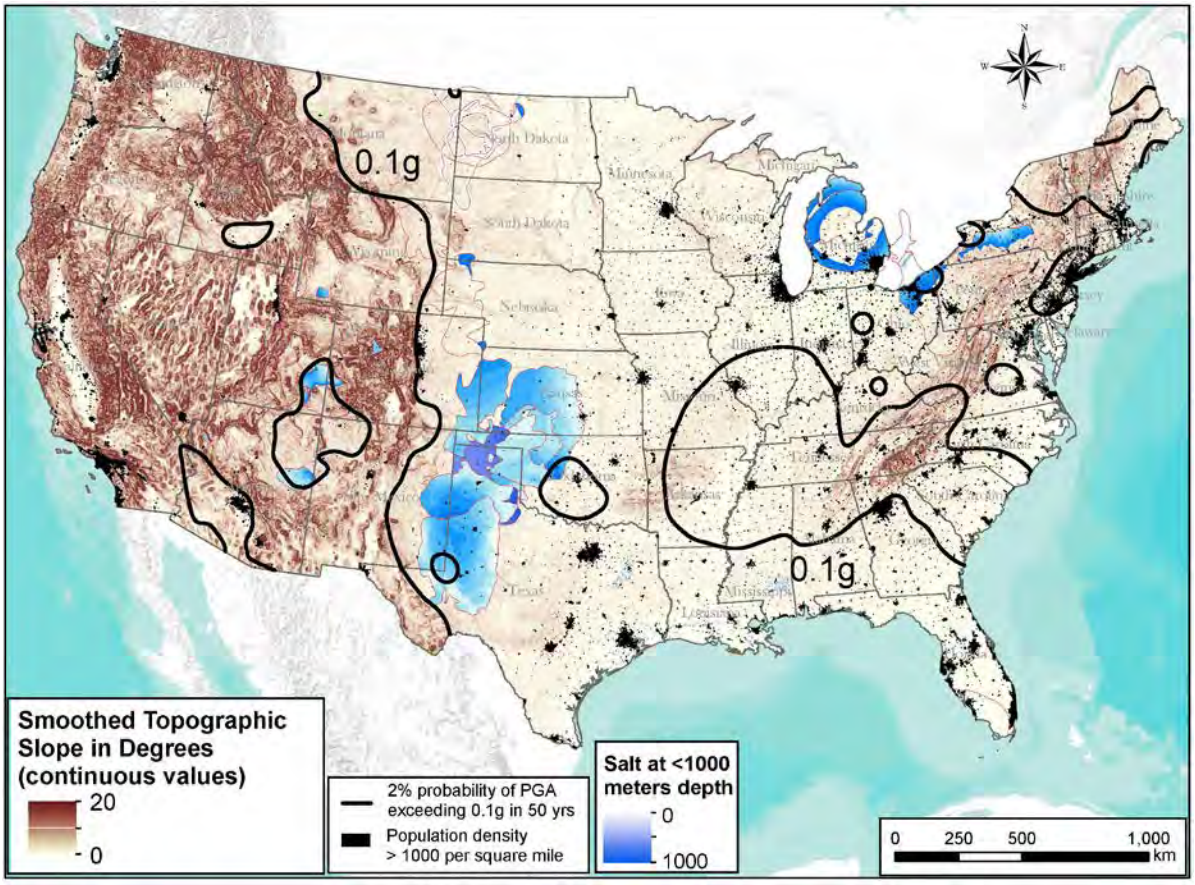

Figure 6-15. The distribution of salt formations with tops at a depth of <1 km combined with data for topographic slope, seismic peak ground acceleration and population distribution.

Similar to depth of salt or shale, depth to crystalline basement is a primary siting guideline for a borehole disposal system (Arnold et al., 2013). The favored depth is less than 2 kilometers, allowing a waste emplacement zone at a maximum depth of between 3-5 kilometers (Arnold et al., 2013). Other factors important for siting of a deep borehole disposal system include avoidance of recent faulting, volcanism and potentially high seismic ground motion, all of which indicate areas of current crustal instability (Figure 6-16). The most extensive region of the US meeting these guidelines is the upper mid-continent region of the US, an area underlain primarily by the southern extent of Archean basement terranes surrounded by accreted Proterozoic-age basement terranes. This region has not experienced major tectonism for at least the last several hundred million years.

Deep crystalline basement has tectonic structures whose nature and location can be interpreted through a combination of geophysical and geologic data (Figures 6-11 and 6-17, based on the work of Sims et al., 2008). Shallow basement beneath the stable mid-continent region has a number of major structures including the Midcontinent Rift, ductile shear zones and suture zones (Figure 6-17). These structures represent features that could present drilling difficulties or impact post-closure safety due to relatively permeable flow paths (Arnold et al., 2013). The impact of these structures to a deep borehole disposal system could be mitigated by a strategy of avoidance and siting away from major structures.

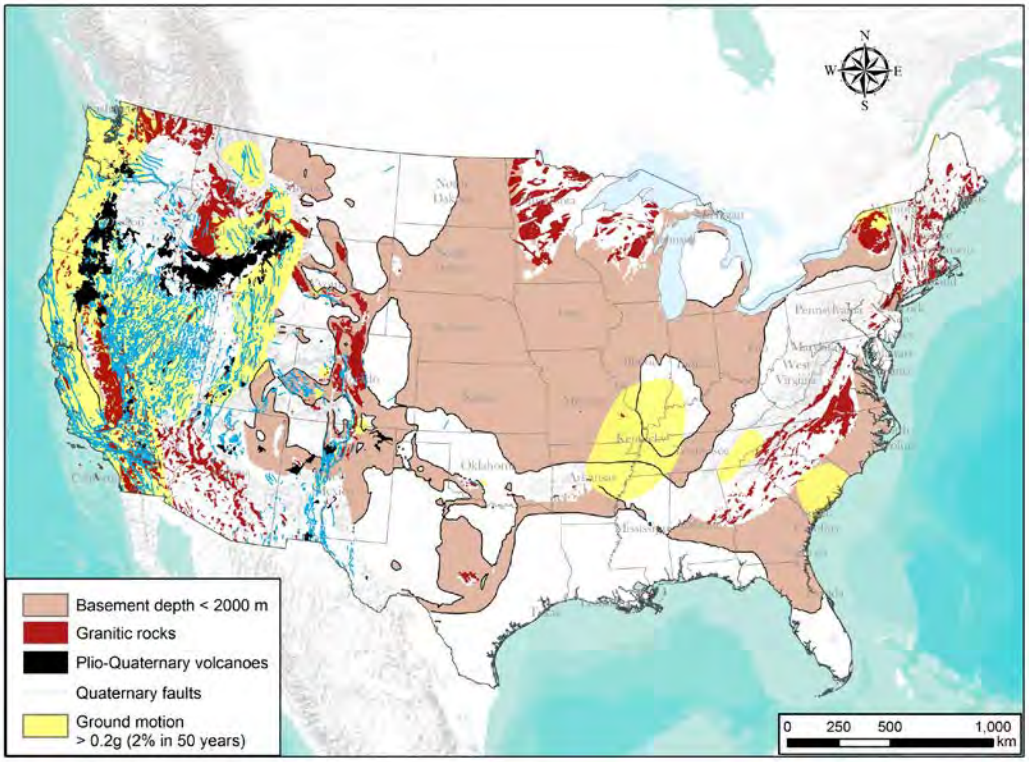

Figure 6-16. Location of crystalline basement in the contiguous US at a depth of less than 2000 meters. Included within this classification are exposed crystalline ("granitic") rocks at the surface. Also shown are the distribution of Quaternary faulting, volcanism, and seismic hazard (yellow shading = 2% probability of exceeding 0.2 g in 50 years), which indicate areas of recent tectonic activity in the US.

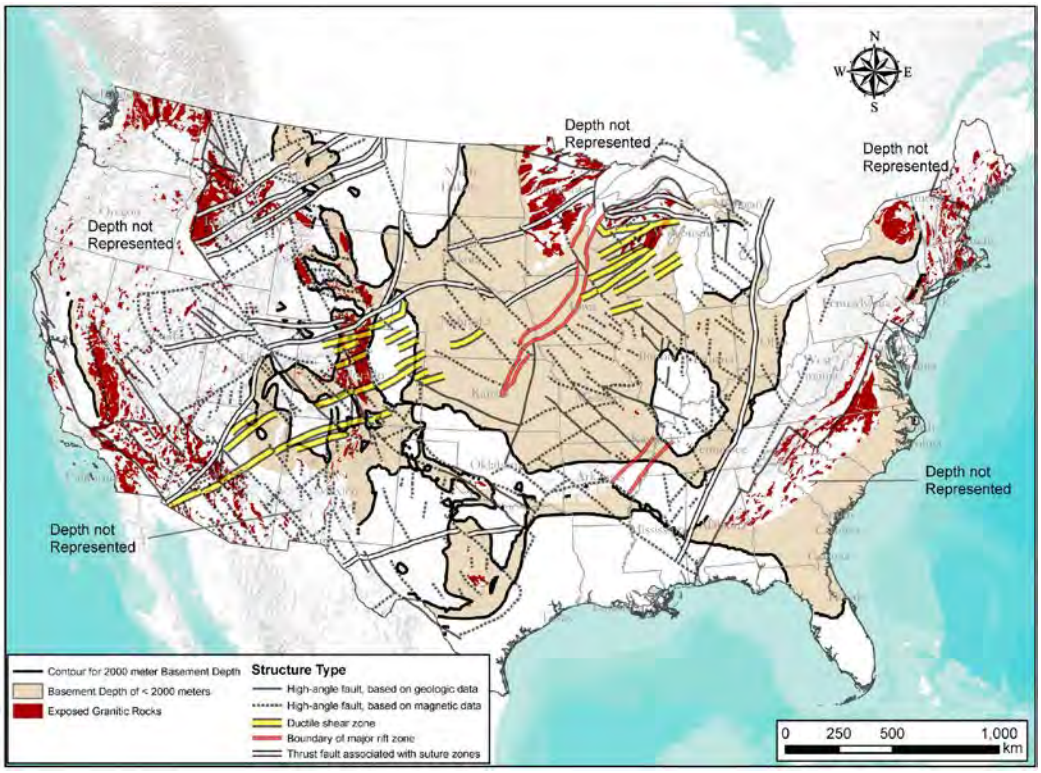

Figure 6-17. Crystalline basement at a depth of less than 2000 meters in the contiguous US displayed with the type and location of structural features within crystalline basement (structures from Sims et al., 2008).

The last example at the national scale shows the relationship between outcrops of granitic crystalline rock, topographic slope, seismic hazard, and population distribution and density (Figure 6-18). Granitic rocks were classified into two groups, conditional on whether they occupied flat terrain (<1 degree of smoothed slope) or steeper terrain (>1 degree of smoothed slope). Minimal topographic relief was considered a favorable characteristic during the region-to-area screening for the Crystalline Repository Project in the 1980s (DOE, 1986b). Topography was evaluated along with seismic hazard, population distribution and density (> 1000 persons per square mile) and several other factors discussed at the beginning of Section 6.2 (DOE, 1986b). Crystalline rocks were screened in three regions referred to as the North Central, Northeastern and Southeastern Regions. The great majority of crystalline rocks in these regions are on subdued terrain with low seismic hazard and numerous areas available that are separated from areas of high population density (Figure 6-18). Thus, at the national and regional scale, the qualitative results using data in the GIS database are consistent with the results of the Crystalline Repository Project's region-to-area screening results obtained in the 1980s.

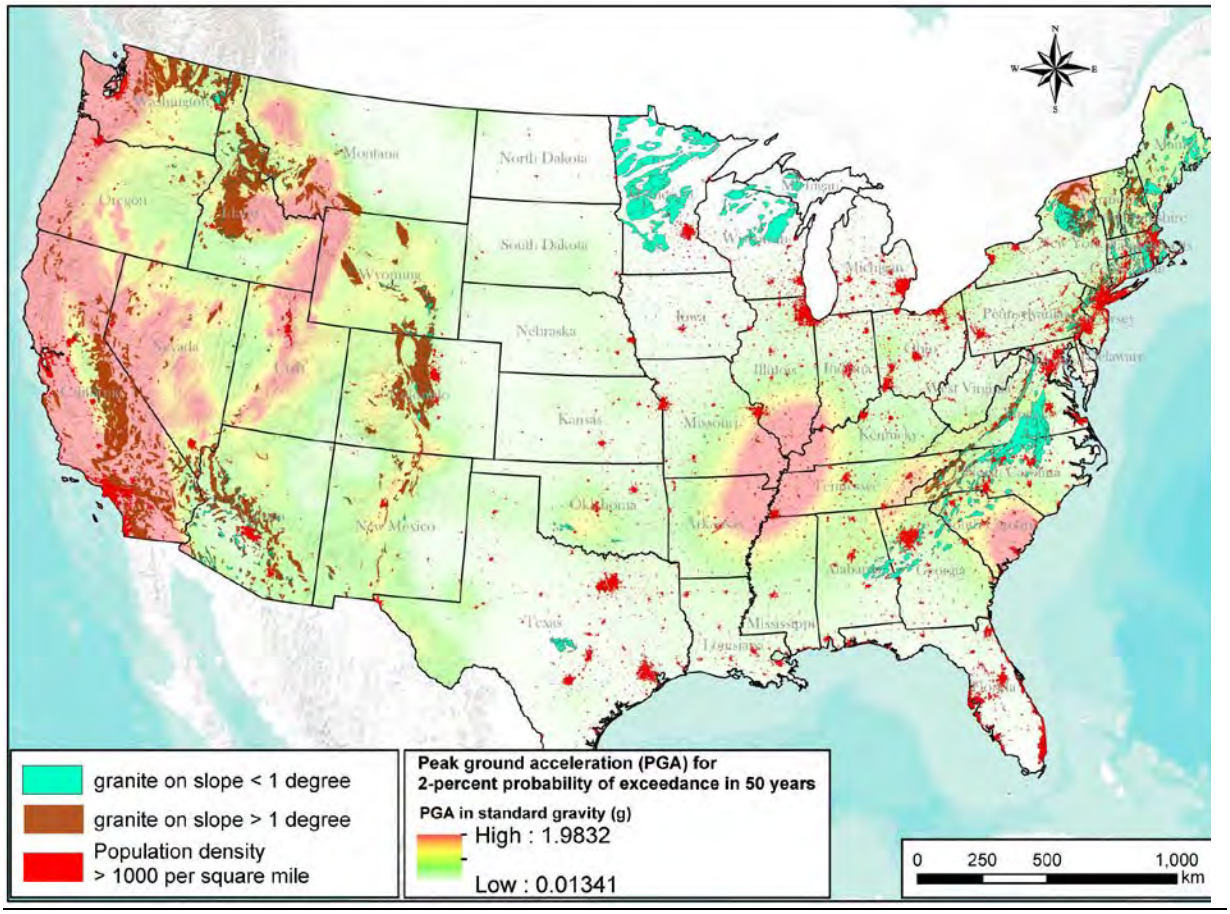

Figure 6-18. Distribution of granitic rocks in the contiguous US (classified by location relative to topographic slope), seismic hazard and population distribution and density.

6.5 Relationship between Geology and Siting Guidelines at the Regional Scale

Similar analyses can be performed at the regional scale to focus on specific geologic formations. The first example starts with the basic geological constraint of the formation depth and thickness, in this case the salt of the Salina Group in the Michigan Basin. The Salina salt was filtered for the portions of the salt group lie at a depth between 300 and 1000 meters, and, secondarily, a thickness of greater than 60 meters (Figure 6-19). The thickness constraint is somewhat artificial because the Salina Group is comprised of several major salt intervals having different thicknesses. The depth parameter is appropriate however as it represents the depth to the top of the shallowest salt deposit. Most importantly, the goal was to develop a method that can be applied to any host rock body, not to find a particular solution for the Salina Group. This example shows that certain parts of the formation would be appropriate where others would not, assuming that siting guidelines specify a depth interval for the repository.

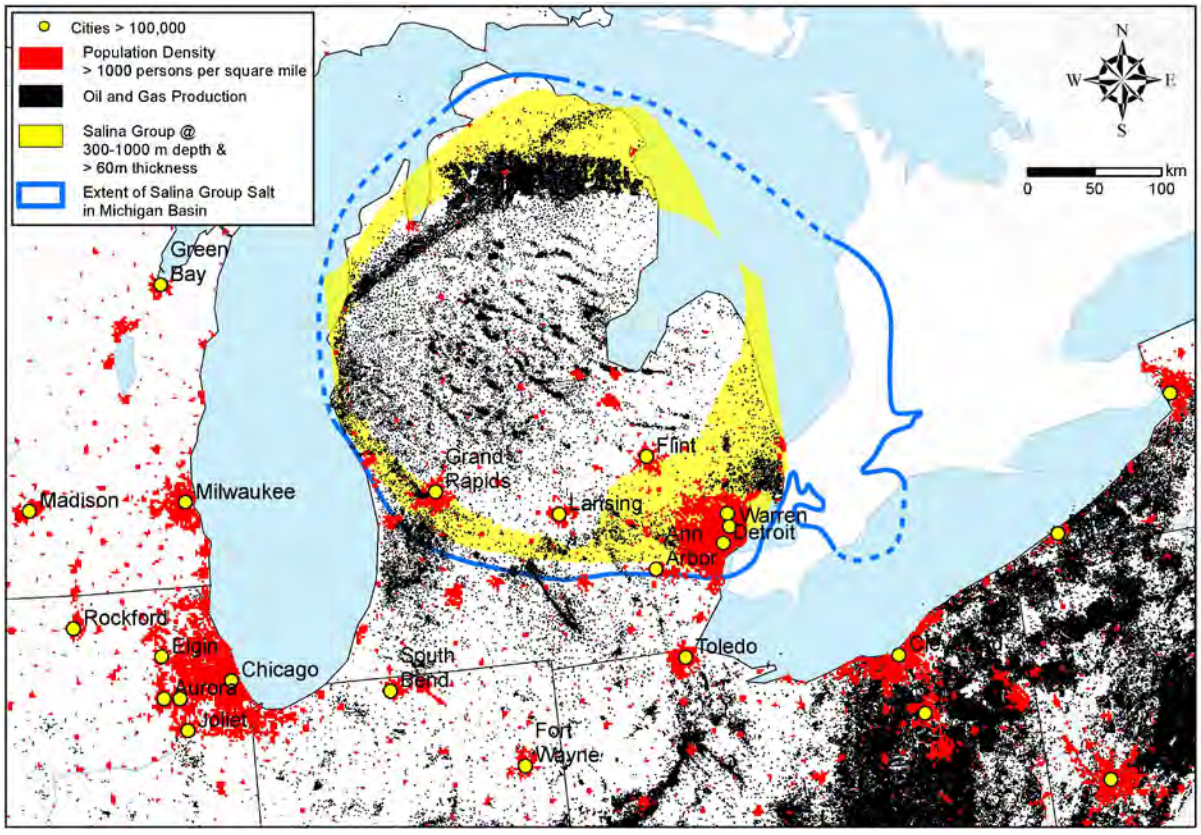

Figure 6-19. The Salina Group in the Michigan basin. Area shown in yellow is the portion of the salt between a depth of 300 and 1000 meters. Salt lying inside of the yellow area is at a depth greater than 1000 meters. Areas of oil and gas production are shown in black. Areas with population density greater than 1000 persons per square mile are shown in red.

The example for the Michigan Basin also demonstrates how additional information can be included to show the relationship between geology and potential siting guidelines that could inform siting decisions. In this case, population density (areas with density of > 1000 persons per square miles) and oil and gas drilling data are displayed to show their spatial relationship to the Salina Group. Several potential siting issues are thus highlighted in this example, including the proximity to population centers, areas of oil and gas drilling and the proximity to the Great Lakes. As mentioned earlier, high population density and oil and resources were factors in deferring further site screening activities within the Michigan and Appalachian Basin region during the 1980s (DOE, 1986a).

The second example is for the Pierre Shale in the northern Great Plains region (Figure 6-20). This example illustrates the typical relationship between geologic formations of large lateral extent, deep sedimentary basins, and oil and gas drilling activities. A recent issue that has emerged since shale was first considered as a potential repository host rock is the tremendous expansion of horizontal drilling and hydraulic fracturing to recover unconventional oil and natural gas resources. These techniques have been extensively applied in the Williston Basin of Montana and North Dakota in recent years (Figure 6-20). As has historically been the case, oil and gas resources (and therefore drilling) are focused in the deeper portions of basins because of their thermal maturation history. Thus the drilling density within the entire extent of the Pierre Shale varies greatly depending on location (Figure 6-20). In siting scenarios where high drilling density is of concern, areas of the Pierre Shale away from the central parts of major basins offer opportunities for siting where there has been little previous drilling history.

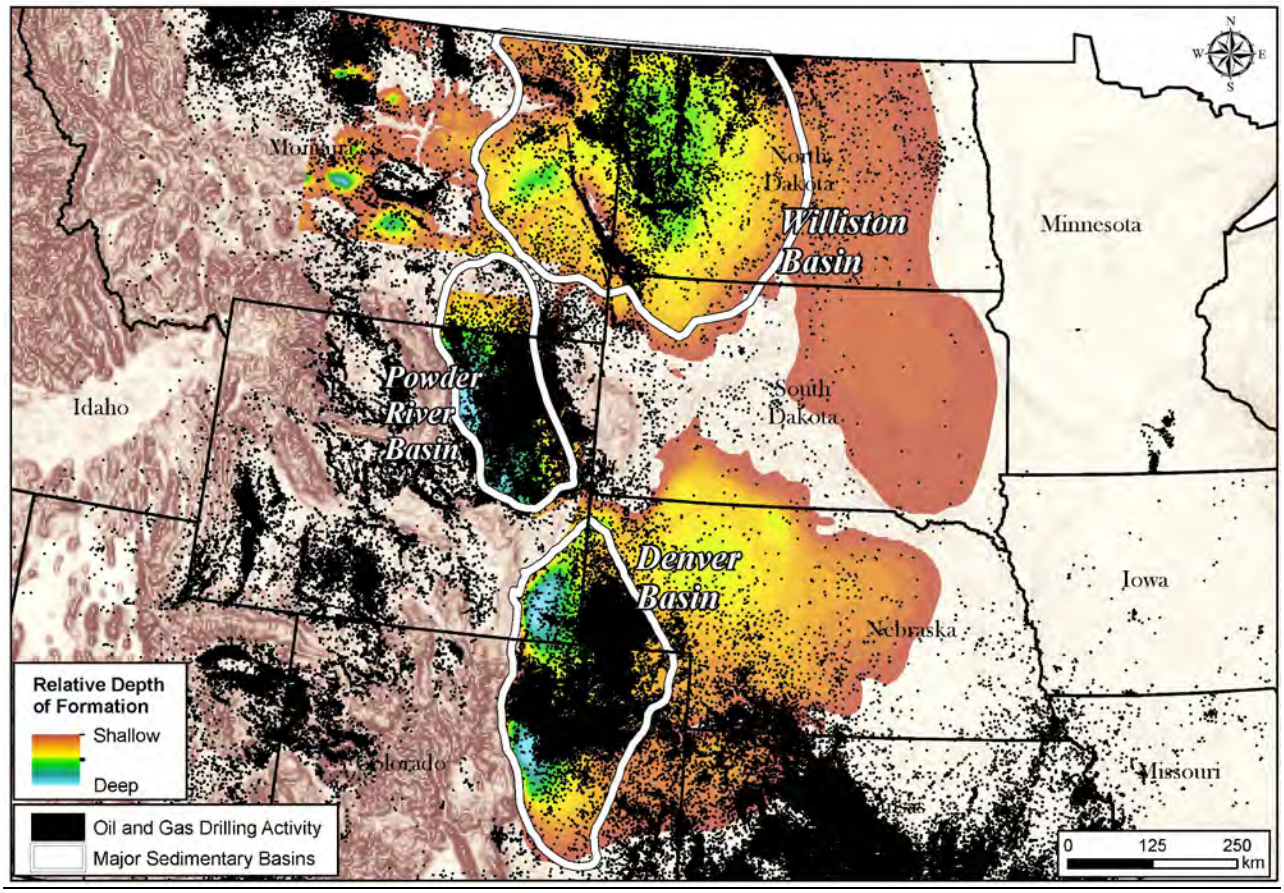

Figure 6-20. The distribution of the Pierre Shale and equivalents in the northern Great Plains region and areas with drilling activity (in black). Cell sizes of oil and gas areas are exaggerated in the figure to increase visibility. The locations of major basin boundaries in the region (Denver, Powder River and Williston Basins) are outlined in white (basin boundary data from Coleman and Cahan, 2012). Areas with high drilling density are also apparent in the intermontane basins to the west of the Pierre Shale. The background of the figure is smoothed topographic slope.

7. Conclusions

Significant progress has been made in populating a GIS database with geologic data at the formation level for crystalline rocks (granite), salt and shale. One goal of this work package is to obtain data that will allow identification of potential rock formations or parts of formations that have suitable depth and thickness to host a mined repository. This goal has been accomplished for salt formations with some work remaining for shale deposits, although a significant number of shale formations are now included as part of the database. A second goal is to acquire data related to potential siting guidelines and to develop methods to evaluate the relationship between potential host geology and potential siting guidelines and issues. Many of these methods have been developed and applied in the examples included in this report.

Although it is not the goal of this work package to develop siting guidelines, we will continue to develop tools that will allow evaluation of the relationships between geology and potential siting guidelines as well as the impacts of potential siting guidelines on a site screening

and site selection process in the US. By doing so, we will be in a better position to anticipate and inform future siting guidelines that will likely be based on recent international siting experiences and past US guidelines. These guidelines are likely to address issues of human intrusion, including exploration for natural resources and proximity to freshwater aquifers, and of constraints imposed by social and cultural features such as population and transportation infrastructure. The database and analysis methods will allow comparison of future regional siting options to anticipate site screening and site selection issues that are inherent to any repository program. The database and analysis tools will also facilitate identification of regions that may not warrant a more detailed evaluation in a future siting framework.

8. Acknowledgements

From Los Alamos National Laboratory, Florie Caporuscio reviewed this report and his feedback is greatly appreciated. We are grateful to Susan Lopez for assisting us with the references.

From Lawrence Berkeley National Laboratory, Curt Oldenburg reviewed this report and his feedback was greatly appreciated. Editorial assistance was also provided by Helen Prieto and Peter Persoff.

Many individuals generously shared their knowledge and data to help populate the GIS database described in Section 4. Maria Richards of the Southern Methodist University Geothermal Laboratory shared GIS data for sediment thickness in the US. Colin Williams, Director of the Geology, Minerals, Energy, and Geophysics Science Center (of the USGS) provided estimates of temperature at depth for the US. Steve Ruppel and Cari Breton of the University of Texas, Bureau of Economic Geology, provided us with their GIS dataset for the Woodford Shale in the Permian Basin. John Bocan, with the West Virginia Geological and Economic Survey, provided us with GIS data for the Utica Shale that had been developed by the Trenton-Black River Research Consortium. Jim McDonald of the Ohio Department of Natural Resources shared with us a regional GIS dataset for the Marcellus Shale. Christopher Korose of the Illinois State Geological Survey provided us with GIS data for the New Albany Shale that was developed by the Illinois Basin Consortium. Jeff Zimmerman of the Susquehanna River Basin Commission provided us with some USGS GIS data for the Utica and Marcellus Shales. David Effert of the Louisiana Department of Natural Resources gave us access to GIS data for the Haynesville Shale. Brian Cardott of the Oklahoma Geological Survey provided us with additional references on the Woodford Shale and Sue Palmer (also of the Oklahoma Geological Survey) provided us with pdf copies of plates depicting the thickness and depth of the Woodford Shale in the Anadarko Basin. Sue Hovorka of the University of Texas, Bureau of Economic Geology, pointed us towards a study conducted by the Gulf Coast Carbon Center, which contains abundant information regarding seals (i.e., shales) in many sedimentary basins in the US. Prof. James Wood (Michigan Tech) provided us with a copy of his digital dataset for the Antrim Shale in the Michigan Basin. Julie LeFever (North Dakota Geological Survey) shared her GIS data for the Bakken Formation. Sam Limerick helped us track down the source files for the EIA shale play maps, and Jack Perrin and Meg Coleman (US EIA) generously provided us with the associated GIS data. Don Sweetkind (USGS) shared the GIS data associated with his reports on the Monterey Formation in the Cuyama and Santa Maria Basins. Many thanks for all of their contributions.

9. References

9.1 Regional Geology and Siting Guidelines (for all sections except Section 5)

Agrawal, A., 2009. A technical and economic study of completion techniques in five emerging U.S. gas shale plays. M.S. thesis, Texas A&M University, 135 p.

Amsden, T.W., 1975. Hunton Group (Late Ordovician, Silurian, and Early Devonian) in the Anadarko Basin of Oklahoma. Oklahoma Geological Survey Bulletin 121, 214 p.

Amsden, T.W., 1980. Hunton Group (Late Ordovician, Silurian, and Early Devonian) in the Arkoma Basin of Oklahoma. Oklahoma Geological Survey Bulletin 129, 136 p.

Anderson, S.B. and Hansen, D.E., 1957. Halite Deposits in North Dakota. North Dakota Geologic Survey, Report of Investigation No. 28, 3 p.

Anna, L.O., 2009. Geologic assessment of undiscovered oil and gas in the Powder River Basin Province: U.S. Geological Survey Digital Data Series DDS–69–U, 93 p.

Arnold, B.W., P.V. Brady, S.J. Bauer, C. Herrick, S. Pye, and J. Finger. 2011. Reference Design and Operations for Deep Borehole Disposal of High-Level Radioactive Waste. SAND2011-6749.Albuquerque, NM: Sandia National Laboratories.

Arnold B.W., Brady, P., Altman, S., Vaughn, P., Nielson, D., Lee, J., Gibb, F., Mariner, P., Travis, K., Halsey, W., Beswick, J., and J. Tillman, 2013. Deep Borehole Disposal Research: Demonstration Site Selection Guidelines, Borehole Seals Design, and RD&D Needs. FCRD-USED-2013-000409.

Bachman, G. O., and Johnson, R. B., 1973. Stability of Salt in the Permian Salt Basin of Kansas, Oklahoma, Texas and New Mexico. USGS, Open-File Report 4339-4, 67 p.

Baltz, E. A., 1957. Distribution and Thickness of Salt in the Paradox Basin of Southwestern Colorado and Southeastern Utah: A Preliminary Report. USGS, Trace Elements Investigations Report 706, 42 p.

Barbeau, D.L., 2003. A flexural model for the Paradox Basin: implications of the tectonics for the Ancestral Rocky Mountains. Department of Geosciences, University of Arizona, Basin Research 15, 97-115, 19 p.

Beckman, J. D.; Williamson, A. K., 1990. Salt-dome locations in the Gulf Coastal Plain, South-Central United States, USGS Water-Resources Investigations Report 90-4060, 44 p.

Biewick, Laura R.H., 2008, Areas of historical oil and gas exploration and production in the United States: U.S. Geological Survey Digital Data Series DDS-69-Q.

Blackford, M.A., 2007. Electrostratigraphy, thickness, and petrophysical evaluation of the Woodford Shale, Arkoma Basin, Oklahoma. Master's thesis, Oklahoma State University, 84 p.

Blackwell, D.D., P. Negraru, and M. Richards, 2007. Assessment of the enhanced geothermal system resource base of the United States, Natural Resources Research, DOI 10:1007/s11053-007-9028-7.

Brady, P.V., Arnold, B.W, Freeze, G.A., Swift, P.N., Bauer, S.J., Kanney, J.L., Rechard, R.J., and J.S. Stein. 2009. Deep Borehole Disposal of High-Level Radioactive Waste. Sandia National Laboratories, SANDIA REPORT SAND2009-4401.

Bristol, H.M., and Buschbach, T.C., 1973. Ordovician Galena Group (Trenton) of Illinois – Structure and oil fields. Illinois State Geological Survey, Illinois Petroleum 99, 38 p.

Broadhead, R.F., 2010. The Woodford Shale in southeastern New Mexico: distribution and source rock characteristics. New Mexico Geology, v. 32, pp. 79-90.

Broadhead, R.F., and Gillard, L., 2007. The Barnett shale in southeastern New Mexico: Distribution, thickness, and source rock characterization. New Mexico Bureau of Geology and Mineral Resources, Open-File Report 502, 56 p.

Bruner, K.R., and Smosna, R., 2011. A comparative study of the Mississippian Barnett Shale, Fort Worth Basin, and Devonian Marcellus Shale, Appalachian Basin. National Energy Technology Laboratory Report, DOE/NETL-2011/1478.

Budnik R., and D. Smith, 1982. Regional Stratigraphic Framework for the Texas Panhandle *in* Gustavson, T.C., and others, Geology and Geohydrology of the Palo Duro Basin, Texas Panhandle: A Report on the Progress of Nuclear Waste Isolation Feasibility Studies (1981). Bureau of Economic Geology, University of Texas at Austin. Prepared for the DOE, Office of Waste Isolation, Contract No. DE-AC97-80ET46615, Annual Report, pp. 38-86.

Cardott, B.J., 2012. Thermal maturity of Woodford Shale gas and oil plays, Oklahoma, USA, International Journal of Coal Geology, doi:10.1016/j.coal.2012.06.004

Cardott, B.J., and Lambert, M.W., 1985. Thermal maturation by vitrinite reflectance of Woodford Shale, Anadarko Basin, Oklahoma. American Association of Petroleum Geologists Bulletin, v. 69, pp. 1982-1998.

Carlson, C.G., 1982. Structure map on top of the Cretaceous Pierre Formation in North Dakota. North Dakota Geological Survey, Miscellaneous Map No. 23.

Catacosinos, P. A., Harrison III, W. B., Reynolds, R. F., Westjohn, D. B. and Wollensak, M. S., 2000. Stratigraphic Nomenclature for Michigan. Michigan Department of Environmental Quality, Geologic Survey Division and Michigan Basin Geological Society, Chart 301468-7, 1 sheet.

Catacosinos, P.A., and Daniels, P.A., Jr., 1991, Stratigraphy of middle Proterozoic to Middle Ordovician formations of the Michigan basin. Geological Society of America Special Paper 256, pp. 53–72.

Catacosinos, P.A., Harrison, W.B., III, and Daniels, P.A., Jr., 1991. Structure, stratigraphy, and petroleum geology of the Michigan Basin, Chapter 30, in Leighton, M.W., Kolata D.R., Oltz, D.F., and Eidel, J.J., eds., Interior cratonic basins: American Association of Petroleum Geologists Memoir 51, pp. 561–601.

Catacosinos, P.A., Harrison, W.B., III, and Daniels, P.A., Jr., 1991. Structure, stratigraphy, and petroleum geology of the Michigan Basin, Chapter 30, in Leighton, M.W., Kolata D.R., Oltz, D.F., and Eidel, J.J., eds., Interior cratonic basins: American Association of Petroleum Geologists Memoir 51, pp. 561–601.

Coleman, J.L., Jr., and Cahan, S.M., 2012. Preliminary catalog of the sedimentary basins of the United States: U.S. Geological Survey Open-File Report 2012–1111, 27 p. (plus 4 figures and 1 table available as separate files) Available online at http://pubs.usgs.gov/of/2012/1111/.

Collinson, C., Sargent, M. L., and Jennings, J. R., 1988, Chapter 14: Illinois Basin region, *in* Sloss, L. L., ed., The Geology of North America, v. D-2, Sedimentary Cover—North American Craton: U.S.: Decade of North American Geology: Geological Society of America, pp. 383–426.

Comer, J.B., 1991. Stratigraphic analysis of the Upper Devonian Woodford Formation Permian Basin West Texas and Southeastern New Mexico. The University of Texas at Austin, Bureau of Economic Geology Report of Investigations No. 201, 63 p.

Condon, S.M., 2000. Stratigraphic framework of Lower and Upper Cretaceous rocks in central and eastern Montana. U.S Geological Survey Digital Data Series DDS-57, 12 p, 23 plates.

Cooper, B. N., 1966. Geology of the salt and gypsum deposits in the Saltville area Smyth and Washington Counties, Virginia. *in* Rau, J. L., ed. Second symposium on salt: Cleveland. Northern Ohio Geol. Soc. v. I, p. 11-34.

Cuadros, J., 2008. Clay as sealing material in nuclear waste repositories. Geology Today, v. 24, p. 99-103.

Culler, F. L., March 17, 1971. Technical Status of the Radioactive Waste Repository. A Demonstration Project for Solid Radioactive Waste Disposal, Testimony to the Joint Committee of Congress, The United States of America. Washington, D.C.

Dechesne, M., Raynolds, R.G., Barkmann, P.E., and Johnson, K.R., 2011. Notes on the Denver Basin geologic maps: Bedrock geology, structure, and isopach maps of the Upper Cretaceous to Paleogene strata between Greeley and Colorado Springs, Colorado. Colorado Geological Survey, 35 p.

Defra (Department for Environment, Food and Rural Affairs, UK). 2008. Managing Radioactive Waste Safely, A Framework for Implementing Geological Disposal: A White Paper by Defra, BERR and the devolved administrations for Wales and Northern Ireland. Her Majesty's Stationery Office. 100 p.

Denson, N.M., Gibson, M.L., and Sims, G.L., 1993a. Geologic and structure map, with contours on top of the Pierre Shale, for the north half of the Powder River Basin, southeastern Montana and northeastern Wyoming. U.S. Geological Survey Miscellaneous Investigations Series Map I-2343-A.

Denson, N.M., Gibson, M.L., and Sims, G.L., 1993b. Geologic and structure map, with contours on top of the Pierre Shale, for the south half of the Powder River Basin, northeastern Wyoming. U.S. Geological Survey Miscellaneous Investigations Series Map I-2343-B.

Denson, N.M., Gibson, M.L., and Sims, G.L., 1993c. Geologic map showing thickness of the Upper Cretaceous Pierre Shale in the north half of the Powder River Basin, southeastern Montana and northeastern Wyoming. U.S. Geological Survey Miscellaneous Investigations Series Map I-2380-A.

Denson, N.M., Gibson, M.L., and Sims, G.L., 1993d. Geologic map showing thickness of the Upper Cretaceous Pierre Shale in the south half of the Powder River Basin, northeastern Wyoming and adjacent areas. U.S. Geological Survey Miscellaneous Investigations Series Map I-2380-B.

Dobson, P.F., 2011. Survey of clay/shale formations in the US. In: FY11 Report on Unsaturated Flow and Transport, FCRD-USED-2011-000296.

Dobson, P.F., 2012. Status of Shale Geology: Information on Extent, Thickness and Depth of Shale Deposits. FCRD-UFD-2012-000296, 34 p.

Dobson, P.F. and J.E. Houseworth, 2013. Inventory of Shale Formations in the US including Geologic, Hydrological, and Mechanical Characteristics. FCRD-UFD-2014-000513, 90 p.

DOE, 1986a. Environmental Assessment, Deaf Smith County Site, Texas. U.S. Department of Energy-Office of Civilian Radioactive Waste Management, DOE/RW-0069, Vol.1, 784 p.

DOE, 1986b. Draft Area Recommendation Report for the Crystalline Repository Project. U.S. Department of Energy, Office of Civilian Radioactive Waste Management, Crystalline Repository Project Office, DOE/CH-15(0).

Dolton, G.L., and Fox, J.E., 1996. Powder River Basin Province (033), in Gautier, D.L., Dolton, G.L., Varnes, K.L., and Takahashi, K.I., eds., 1995 National Assessment of United States Oil and Gas Resources—Results, methodology, and supporting data: U.S. Geological Survey Digital Data Series DDS-30, one CD-ROM, Release 2.

Dubiel, R.F., 2003. Geology, depositional models, and oil and gas assessment of the Green River Total Petroleum System, Uinta-Piceance Province, Eastern Utah and Western Colorado, Chapter 5 of Petroleum systems and geologic assessment of oil and gas in the Uinta-Piceance Province, Utah and Colorado, USGS Uinta-Piceance Assessment Team, U.S. Geological Survey Digital Data Series DDS–69–B. http://pubs.usgs.gov/dds/dds-069/dds-069-b/REPORTS/Chapter_5.pdf

Ege, J. R., 1985. Maps showing Distribution, Thickness and Depth of Salt Deposits of the United States. United States Geologic Survey Open-File Report 85-28, 12 p, 4 Plates.

EIA (Energy Information Administration), 2011. Review of Emerging Resources: U.S. Shale Gas and Shale Oil Plays. www.eia.gov/analysis/studies/usshalegas/pdf/usshaleplays.pdf

Energy Information Administration (EIA), 2010, Eagle Ford Shale Play, Western Gulf Basin, South Texas. Map date May 29, 2010. http://www.eia.gov/oil_gas/rpd/shaleusa9.pdf

Energy Information Administration (EIA), 2011. Review of Emerging Resources: U.S. Shale Gas and Shale Oil Plays. www.eia.gov/analysis/studies/usshalegas/pdf/usshaleplays.pdf

Engelder, T., 2011. Analogue study of shale cap rock barrier integrity. Report for the Nuclear Waste Management Organization, NWMO DGR-TR-2011-23, 108 p.

EPRI, 2010. *EPRI review of geologic disposal for used fuel and high-level radioactive waste. Volume III—review of national repository programs, final report, December 2010*. Palo Alto, CA: Electrical Power Research Institute.

Erenpreiss, M.S., Wickstrom, L.H., Perry C.J., Riley, R.A., Martin, D.R., and others, 2011. Regional organic-thickness map of the Marcellus Shale with additional organic-rich shale beds in the Hamilton Group included for New York, Pennsylvania, and West Virginia. Ohio Department of Natural Resources, Division of Geological Survey, scale 1 inch equals 52 miles.

Ettensohn, F.R., 2008. The Appalachian foreland basin in Eastern United States. In: Miall, A.D. (ed.) The Sedimentary Basins of the United States and Canada, Vol. 5, Sedimentary Basins of the World. Elsevier, Amsterdam, p. 105-179

Faulds, J. E., Schreiber, B. C., Reynolds, S. J., Gonzales, L. A. and D. Okaya, 1997. Origin and Paleogeography of an Immense, Nonmarine Miocene Salt Deposit in the Basin and Range (Western USA). The Journal of Geology, Vol. 105, No. 1, pp. 19-36.

Gale, J.F.W., and Holder, J., 2010. Natural fractures in some US shales and their importance for gas production. In: Vining, B.A., and Pickering, S.C., eds., Petroleum Geology: From Mature Basins to New Frontiers. Proceedings of the 7th Petroleum Geology Conference, pp. 1131-1140.

Gallen, S. F., Wegmann, K. W., and Bohenstiehl, D. R., 2013, Miocene rejuvenation of topographic relief in the southern Appalachians: GSA Today, 23, doi:10.1130/GSATG163A.1.

GAO, 1979. The nation's nuclear waste - proposals for organization and siting. EMD-79-77, Washington, DC: Government Accountability Office. Comptroller General of the United States. 34 pp.

Garrity and Soller, 2009. Database of the Geologic Map of North America; adapted from the map by J.C. Reed, Jr. and others (2005). U.S. Geological Survey Data Series 424.

Gerhard, L.C., Anderson, S.B., LeFever, J.A. and Carlson, C.G., 1982. Geological development, origin, and energy mineral resources of Williston Basin, North Dakota. American Association of Petroleum Geologists Bulletin v. 66, p. 989-1020.

Gonzales, S., and Johnson, K.S., 1985. Shale and other argillaceous strata in the United States. Oak Ridge National Laboratory report 84-64794, 594 p.

Gray, J.D., Struble, R.A., Carlton, R.W., Hodges, D.A., Honeycutt, F.M., Kingsbury, R.H., Knapp, N.F., Majchszak, F.L., and Stith, D.A., 1982. An integrated study of the Devonian-age black shales in eastern Ohio. Technical Information Center, US Department of Energy, DOE/ET/12131-1399.

Hammes, U., Hamlin, H.S., and Ewing, T.E., 2011. Geologic analysis of the Upper Jurassic Haynesville Shale in east Texas and west Louisiana. AAPG Bulletin, v. 95, no. 10, pp. 1643–1666.

Hammond, W.C., Blewitt, G., Li, Z., Plag, H.-P., Kreemer, C., 2012. Contemporary uplift of the Sierra Nevada, western United States, from GPS and InSAR measurements. Geology, 40 (7), p. 667–670.

Handford, C.R. 1980. Lower Permian facies of the Palo Duro Basin, Texas: depositional systems, shelf-margin evolution, paleogeography, and petroleum potential: The University of Texas at Austin, Bureau of Economic Geology Report of Investigations No. 102, 31 p.

Harbor, R.L., 2011. Facies characterization and stratigraphic architecture of organic-rich Mudrocks, Upper Cretaceous Eagle Ford Formation, South Texas. M.S. Thesis, University of Texas, Austin, 184 p.

Hasenmueller, N.R., and Comer, J.B., eds., 1994. Gas potential of the New Albany Shale (Devonian and Mississippian) in the Illinois Basin**,** Gas Research Institute Technical Report GRI-92/0391.

Hasenmueller, N.R., and Comer, J.B., eds., 2000. GIS compilation of gas potential of the New Albany Shale in the Illinois Basin, Gas Research Institute Technical Report GRI-00/0068.

Heidbach, O., Tingay, M., Barth, A., Reinecker, J., Kurfeß, D. and Müller, B., 2008. The World Stress Map database release 2008 doi:10.1594/GFZ.WSM.Rel2008. http://dc-app3-14.gfz-potsdam.de/pub/introduction/introduction_frame.html

Heidbach, O., Tingay, M., Barth, A., Reinecker, J., Kurfeß, D., Müller, B., 2009. The World Stress Map based on the database release 2008, equatorial scale 1:46,000,000, Commission for the Geological Map of the World, Paris, doi:10.1594/GFZ.WSM.Map2009.

Higley, D.K. and Cox, D.O., 2007. Oil and gas exploration and development along the front range in the Denver Basin of Colorado, Nebraska, and Wyoming, in Higley, D.K., compiler, Petroleum systems and assessment of undiscovered oil and gas in the Denver Basin Province, Colorado, Kansas, Nebraska, South Dakota, and Wyoming—USGS Province 39: U.S. Geological Survey Digital Data Series DDS–69–P, Ch. 2, 41 p. http://pubs.usgs.gov/dds/dds-069/dds-069-p/REPORTS/69_P_CH_2.pdf

Higley, D.K., Pollastro, R.M., and Clayton, J.L., 1996. Denver Basin Province (039), *in* Gautier, D. L., Dolton, G.L., Takahashi, K.I., and Varnes, K.L., eds., 1995 National Assessment of United States oil and gas resources; Results, methodology, and supporting data: U.S. Geological Survey Digital Data Series DDS-30, Release 2, one CD-ROM. http://certmapper.cr.usgs.gov/data/noga95/prov39/text/prov39.pdf

Hosford Scheirer, A., 2013. The three-dimensional geologic model used for the 2003 National Oil and Gas Assessment of the San Joaquin Basin Province, California: Chapter 7 in Petroleum systems and geologic assessment of oil and gas in the San Joaquin Basin Province, California, U.S. Geological Survey Professional Paper 1713-7, 81 p.

Hovorka, S.D. 1998. Characterization of Bedded Salt for Storage Caverns—A Case Study from the Midland Basin. The University of Texas at Austin Bureau of Economic Geology. Prepared for National Petroleum Technology Center, U. S. Department of Energy, Bartlesville, Oklahoma, Contract No. DE-AF26-97BC15030.

Hovorka, S.D., Romero, M.L., Warne, A.G., Ambrose, W.A., Tremblay, T.A., Treviño, R.H., and Sasson, D., 2003. Technical summary: Optimal geological environments for carbon dioxide disposal in brine formations (saline aquifers) in the United States. Gulf Coast Carbon Center, University of Texas, Bureau of Economic Geology, http://www.beg.utexas.edu/gccc/finalreport.pdf

Johnson, E.A., 2003. Geologic assessment of the Phosphoria Total Petroleum System, Uinta-Piceance Province, Utah and Colorado, Chapter 9 of Petroleum systems and geologic assessment of oil and gas in the Uinta-Piceance Province, Utah and Colorado, USGS Uinta-Piceance Assessment Team, U.S. Geological Survey Digital Data Series DDS–69–B, http://pubs.usgs.gov/dds/dds-069/dds-069-b/REPORTS/Chapter_9.pdf

Johnson, K. S. and S. Gonzales, 1978. Salt deposits in the United States and regional geologic characteristics important for storage of radioactive waste. Prepared for the Office of Waste Isolation, Union Carbide Corporation, Nuclear Division. Y/OWI/SUB—7414/1.NAS, 1957.

Johnson, R.C., Mercier, T.J., Brownfield, M.E. and Self, J.G., 2010. Assessment of in-place oil shale resources in the Eocene Green River Formation, Uinta Basin, Utah and Colorado: U.S. Geological Survey Digital Data Series DDS–69–BB, Ch. 1, 153 p. http://pubs.usgs.gov/dds/dds-069/dds-069-bb/REPORTS/69_BB_CH_1.pdf

Kent, D.M., and J.E. Christopher, 1994. Geological history of the Peace River Arch; in Geological Atlas of the Western Canada Sedimentary Basin, G.D. Mossop and I. Shetsen (comp.), Canadian Society of Petroleum Geologists and Alberta Research Council, http://www.ags.gov.ab.ca/publications/wcsb_atlas/atlas.html, December, 2012.

King, P.B., 1948. Geology of the Southern Guadalupe Mountains, Texas. USGS Professional Paper, 215, 138 pp.

Kolata, D.R., and Noger, M.C., 1990. Chapter 5: Tippecanoe I Subsequence Middle and Upper Ordovician Series. In: Interior Cratonic Basins, M.W. Leighton, D.R. Kolata, D.F. Oltz, and J.J. Eider., eds. American Association of Petroleum Geologists Memoir 51, pp. 89–99.

Lagoe, M.B., 1982. Stratigraphy and paleoenvironments of the Monterey Formation and associated rocks, Cuyama Basin, California. Ph.D. thesis, Stanford University, 216 p.

Lagoe, M.B., 1984. Paleogeography of Monterey Formation, Cuyama Basin, California. American Association of Petroleum Geologists Bulletin, v. 68, pp. 610–627.

Landes, K. K., 1951. Detroit River Group in the Michigan Basin. United States Geological Survey, Circular 133, 27 p

LandScan (2010. High Resolution global Population Data Set copyrighted by UT-Battelle, LLC, operator of Oak Ridge National Laboratory under Contract No. DE-AC05-00OR22725 with the United States Department of Energy. The United States Government has certain rights in this Data Set. Neither UT-BATTELLE, LLC NOR THE UNITED STATES DEPARTMENT OF ENERGY, NOR ANY OF THEIR EMPLOYEES, MAKES ANY WARRANTY, EXPRESS OR IMPLIED, OR ASSUMES ANY LEGAL LIABILITY OR RESPONSIBILITY FOR THE ACCURACY, COMPLETENESS, OR USEFULNESS OF THE DATA SET.

Lash, G.G., and Engelder, T., 2011. Thickness trends and sequence stratigraphy of the Middle Devonian Marcellus Formation, Appalachian Basin: Implications for Acadian foreland basin evolution. American Association of Petroleum Geologists Bulletin v. 95, pp. 61–103.

LeFever, J.A., 2008. Structural contour and isopach maps of the Bakken Formation in North Dakota. North Dakota Geological Survey Geologic Investigations No. 59, 5 sheets.

LeFever, J.A., LeFever, R.D., and Nordeng, S.H., 2012. Extending the Bakken. Williston Basin Petroleum Conference.

Lewis, B.D., and Hotchkiss, W.R., 1981. Thickness, percent sand, and configuration of shallow hydrogeologic units in the Powder River Basin, Montana and Wyoming. U.S. Geological Survey Miscellaneous Investigations Series, Map I-1317.

Li, P., Ratchford, M.E., and Jarvie, D.M., 2010. Geochemistry and thermal maturation analysis of the Fayetteville Shale and Chattanooga Shale in the western Arkoma Basin of Arkansas. Arkansas Geological Survey Information Circular 40, 191 p.

Lomenick, T. F., 1963. The Geology of a Portion of the Hutchinson Salt Member of the Wellington Formation in the Mine of the Carey Salt Company, Lyons, Kansas. Oak Ridge National Laboratory, ORNL-TM-597, 18 p.

Lomenick, T. F., 1996. The Siting Record: An Account of the Programs of Federal Agencies and Events that have Led to the Selection of a Potential Site for a Geologic Repository for High-Level Radioactive Waste, ORNL/TM-12940; Oak Ridge, Tenn.: Oak Ridge National Lab.

Macfarlane, P.A., Combes, J., Turbek, S., and Kirshen, D., 1993. Shallow subsurface bedrock geology and hydrostratigraphy of southwestern Kansas. Kansas Geological Survey, Open-File Report 93-1a. (plates updated in 2010 by J.J. Woods).

Magoon, L.B., Lillis, P.G., and Peters, K.E., 2009. Petroleum systems used to determine the assessment units in the San Joaquin Basin Province, California: Chapter 8 in Petroleum systems and geologic

assessment of oil and gas in the San Joaquin Basin Province, California, U.S. Geological Survey Professional Paper 1713-8, 65 p.

McCormick, K., 2010. Precambrian Basement Terrane of South Dakota, Bulletin 41, Department of Environmental and Natural Resources, University of South Dakota.

McKee, Jacob J., Rose, Amy N., Bright, Eddie, & Huynh, Timmy (2014, Under Review). A Locally-Adaptive, Spatially-Explicit Projection of U.S. Population for 2030 and 2050. *Proceedings of the National Academy of Sciences*.

Meijer Drees, N.C., 1994. Devonian Elk Point Group of the Western Canada Sedimentary Basin; in Geological Atlas of the Western Canada Sedimentary Basin, G.D. Mossop and I. Shetsen (comp.), Canadian Society of Petroleum Geologists and Alberta Research Council, http://www.ags.gov.ab.ca/publications/wcsb_atlas/atlas.html, December, 2012.

Mercier, T.J., Gunther, G.L., and Skinner, C.C., 2010a. The GIS project for the geologic assessment of in-place oil shale resources of the Eocene Green River Formation, Greater Green River Basin, Wyoming, Colorado, and Utah, U.S. Geological Survey Oil Shale Assessment Team, U.S. Geological Survey Digital Data Series DDS–69–DD, http://pubs.usgs.gov/dds/dds-069/dds-069-dd/REPORTS/69_DD_CH_3.pdf

Mercier, T.J., Gunther, G.L., and Skinner, C.C., 2010b. The GIS project for the geologic assessment of in-place oil shale resources of the Piceance Basin, Colorado. In: Oil shale and nahcolite resources of the Piceance Basin, Colorado, U.S. Geological Survey Oil Shale Assessment Team, U.S. Geological Survey Digital Data Series DDS–69–Y, http://pubs.usgs.gov/dds/dds-069/dds-069-y/REPORTS/69_Y_CH_4.pdf

Mercier, T.J., Gunther, G.L., and Skinner, C.C., 2010c. The GIS project for the geologic assessment of in-place oil shale resources of the Uinta Basin, Utah and Colorado. In: Oil shale resources of the Uinta Basin, Utah and Colorado, U.S. Geological Survey Oil Shale Assessment Team, U.S. Geological Survey Digital Data Series DDS–69–BB, http://pubs.usgs.gov/dds/dds-069/dds-069-bb/REPORTS/69_BB_CH_4.pdf

Mercier, T.J., and Johnson, R.C., 2012. Isopach and isoresource maps for oil shale deposits in the Eocene Green River Formation for the combined Uinta and Piceance Basins, Utah and Colorado: U.S. Geological Survey Scientific Investigations Report 2012–5076, 85 p., 1 pl., http://pubs.usgs.gov/sir/2012/5076/SIR12-5076.pdf

Merewether, E.A., Sharps, J.A., Gill, J.R., and Cooley, M.E., 1973. Shale, mudstone, and claystone as potential host rocks for underground emplacement of waste. U.S. Geological Survey Open-File Report 73-184, 44 p.

Merriam, D. F., 1963. The geologic history of Kansas: Kansas Geological Survey, Bulletin 162, 317 p.

MIT. 2006. The Future of Geothermal Energy. Cambridge, MA, MIT.

Montgomery, D. R. and Brandon, M. T., 2002. Topographic controls on erosion rates in tectonically active mountain ranges. Earth and Planetary Science Letters, 201, p. 481–489.

National Atlas of the United States, 2005, Federal and Indian Lands (December 2005). http://nationalatlas.gov

NOAA, National Geophysical Data Center, 2006. *2-minute Gridded Global Relief Data (ETOPO2v2)* http://www.ngdc.noaa.gov/mgg/fliers/06mgg01.html

Nordeng, S.H., 2009. Salt as Candidates for Air Storage in the Williston Basin, ND. North Dakota Geologic Survey, Geologic Investigation, No. 78, 13 p.

Nutt, M. 2011. Used Fuel Disposition Campaign Disposal Research and Development Roadmap, FCR&D-USED-2011-000065, Rev 0.

NWMO. 2010. Moving Forward Together: Process for Selecting a Site for Canada's Deep Geological Repository for Used Nuclear Fuel. Toronto: Nuclear Waste Management Organization. 52 p.

Oldham, D.W., 1996. Permian salt in the northern Denver Basin; controls on occurrence and relationship to oil and gas production from Cretaceous reservoirs, in Longman, M.W., and Sonnenfeld, M.D., eds., Paleozoic Systems of the Rocky Mountain Region: Denver, Society for Sedimentary Geology (SEPM), Rocky Mountain Section, p. 335–354.

Party, J.M., Wipf, R.A., Byl, J.M., Lawton, J., and Hill, J.M., 2008. Woodford Shale, Ardmore Basin, Oklahoma: A developing shale play. Oklahoma Geological Survey, Gas Shales Workshop, 51 slides. http://www.ogs.ou.edu/pdf/GSPartyS.pdf.

Pashin, J.C., 2008. Gas shale potential of Alabama. 2008 International Coalbed and Shale Gas Symposium, Paper 808.

Patchen, D.G., Hickman, J.B., Harris, D.C., Drahovzal, J.A., Lake, P.D., Smith, L.B., Nyahay, R., Schulze, R., Riley, R.A., Baranoski, M.T., Wickstrom, L.H., Laughrey, C.D., Kostelnik, J., Harper, J.A., Avary, K.L., Bocan, J., Hohn, M.E., and McDowell, R., 2006. A Geologic play book for Trenton-Black River Appalachian Basin exploration. DOE Award DE-FC26-03NT41856, http://www.wvgs.wvnet.edu/www/tbr/docs/41856R06.pdf

Pawlewicz, M.J. and Hatch, J.R., 2007. Petroleum assessment of the Chattanooga Shale/Floyd Shale - Paleozoic Total Petroleum System, Black Warrior Basin, Alabama and Mississippi, in Hatch, J.R., and Pawlewicz, J.J., compilers, Geologic assessment of undiscovered oil and gas resources of the Black Warrior Basin Province, Alabama and Mississippi. U.S. Geological Survey Digital Data Series DDS-69-I, chap. 3, 23 p. http://pubs.usgs.gov/dds/dds-069/dds-069-i/REPORTS/69_I_CH_3.pdf

Perry, F., Kelley, R., and Woldegabriel, G., 2011. Regional geology and tectonic hazards – FY 2011 Status Report. FCRD-USED-2012-000002.

Perry, F.V., Kelley, R., and Dobson, P., 2012. Regional geology: Distribution of alternative host rock formations and description of siting factors that potentially influence siting and site characterization. FCRD-USED-2012-27013. 78 p.

Perry, F.V., Dobson, P.F., and Kelley, R.E., 2013a. Assessment of alternative host-rock distribution in the U.S. using GIS. Proceedings, International High-Level Waste Management Conference 2013, Albuquerque, N.M., April 28-May 2, 2013, American Nuclear Society, pp. 85–93.

Perry, F.V., Dobson, P.F., and Kelley, R.E., 2013b. Evaluation of geologic options for disposal of high-level radioactive waste using a GIS database. Geological Society of America *Abstracts with Programs.* Vol. 45, No. 7, p.219.

Petersen, M.D., Frankel, A.D., Harmsen, S.C., Mueller, C.S., Haller, K.M., Wheeler, R.L., Wesson, R.L., Zeng, Yuehua, Boyd, O.S., Perkins, D.M., Luco, Nicolas, Field, E.H., Wills, C.J., and Rukstales, K.S., 2011, Seismic-Hazard Maps for the Conterminous United States, 2008: U.S. Geological Survey Scientific Investigations Map 3195, 6 sheets, scale 1: 7,000,000. GIS data accessed from http://pubs.usgs.gov/sim/3195/contents/datafiles/.

Peterson, J.A., 1984. Geology and hydrology of the Madison Limestone and associated rocks in parts of Montana, Nebraska, North Dakota, South Dakota, and Wyoming. U.S. Geological Survey Professional Paper 1273A, 34 p.

Pierce, W. G. and Rich, E. I. 1962. Summary of rock salt deposits in the United States as possible storage sites for radioactive waste materials. U.S. Geol. Survey Bull. 1148. 91 p.

Pitman, J.K., 2008. Reservoirs and Petroleum Systems of the Gulf Coast. AAPG Datapages GIS Open-File website. http://www.datapages.com/AssociatedWebsites/GISOpenFiles/ReservoirsandPetroleumSystemsoftheGulfCoast.aspx

Pollastro, R.M., Jarvie, D.M., Hill, R.J., and Adams, C.W., 2007. Geologic framework of the Mississippian Barnett Shale, Barnett-Paleozoic total petroleum system, Bend Arch–Fort Worth Basin, Texas. American Association of Petroleum Geologists Bulletin v. 91, pp. 405–436.

Pollastro, R.M., Roberts, L.N.R., Cook, T.A. and Lewan, M.D., 2008. Assessment of undiscovered technically recoverable oil and gas resources of the Bakken Formation, Williston Basin, Montana and North Dakota, 2008: U.S. Geological Survey Open-File Report 2008–1353, 3 sheets.

Powers, D.W. and Richardson, R.G, 2004a. Basic Data Report for Drillhole SNL-3(C-2949), Waste Isolation Pilot Plant. DOE/WIPP, Data Report, DOE/WIPP 03-3294, p. 96.

Powers D.W., and Richardson, R.G., 2004b. Basic Data Report for Drillhole SNL-12(C-2954), Waste Isolation Pilot Plant. DOE/WIPP, Data Report, DOE/WIPP 03-3295, p. 114.

Presley, M.W., 1981. San Andres Salt Stratigraphy and Salt Purity in Gustavson, T.C., and others, *in* Geology and Geohydrology of the Palo Duro Basin, Texas Panhandle: A Report on the Progress of Nuclear Waste Isolation Feasibility Studies (1980). Bureau of Economic Geology, University of Texas at Austin. Prepared for the DOE, Office of Waste Isolation, Contract No. DE-AC97-80ET46615, Annual Report, pp. 33-40.

Ratchford, M.E., Bridges, L.C., Jordan, D., Dow, W.G., Colbert, A., and Jarvie, D.M., 2006. Organic geochemistry and thermal maturation analysis within the Fayetteville Shale study area – Eastern Arkoma Basin and Mississippi embayment regions, Arkansas. Arkansas Geological Survey Information Circular 37, DFF-OG-FS-EAB/ME 008, 12 p.

Raup, O. B. and Hite, R. J., 1992. Lithology of Evaporite Cycles and Cycle Boundaries in the Upper Part of the Paradox Formation of the Hermosa Group of Pennsylvanian Age in the Paradox Basin, Utah and Colorado. United States Geological Survey, Bulletin 2000-B, 37 p.

Rauzi, S. L., 2000. Arizona Has Salt. Arizona Geological Survey, Circular 30, 36 p.

Rauzi, S. L., 2000. Permian Salt in the Holbrook Basin, Arizona. Arizona Geological Survey, Open-File Report 00-03, 21 p.

Rechard, R.P., Perry, F.V., and Cotton, T.A., 2011a. Site selection, characterization, and research and development for spent nuclear fuel and high-level waste disposal. International High-Level Radioactive Waste Management Conference 2001, Albuquerque, NM, April 10-14, 2011, American Nuclear Society, 174-181

Rechard. R.P., Goldstein, B., Harris Greenburg, H., James A. Blink, J., Halsey, W.G., Sutton, M., Perry, F.V., Levy, S., Cotton, T.A., Carter, J.T., and A. O'Neal Delly. 2011b. System-Wide Integration and Site Selection Concepts for Future Disposition Options for UNF and HLW. FCRD-USED-2011-000335, Rev 0.

Ridgley, J.L., Condon, S.M., and Hatch, J.R., 2013. Geology and oil and gas assessment of the Mancos-Menefee Composite Total Petroleum System, San Juan Basin, New Mexico and Colorado, chap. 4 *of* U.S. Geological Survey San Juan Basin Assessment Team, Total petroleum systems and geologic assessment of undiscovered oil and gas resources in the San Juan Basin Province, exclusive of Paleozoic rocks, New Mexico and Colorado. U.S. Geological Survey Digital Data Series 69–F, p. 1–97.

Rottmann, K., 2000. Isopach map of Woodford Shale in Oklahoma and Texas Panhandle. In: Hunton play in Oklahoma (including northeast Texas panhandle): Oklahoma Geological Survey Special Publication 2000-2, plate 2.

Ruppel, S.C., Jones, R.H., Breton, C.L, and Kane, J.A., 2005. Preparation of maps depicting geothermal gradient and Precambrian structure in the Permian Basin: unpublished contract report prepared for the U. S. Geological Survey, 21 p. plus data CD.

Ryder, R.T., Burruss, R.C. and Hatch, J.R., 1998. Black shale source rocks and oil generation in the Cambrian and Ordovician of the central Appalachian Basin, USA. AAPG Bulletin 82, pp. 412-441.

Ryder, R.T., Trippi, M.H., Swezey, C.S. Crangle, R.D., Jr., Hope, R.S., Rowan, E.L., and Lentz, E.E., 2012, Geologic cross section C–C' through the Appalachian basin from Erie County, north-central Ohio, to the Valley and Ridge province, Bedford County, south-central Pennsylvania: U.S. Geological Survey Scientific Investigations Map 3172, 2 sheets, 70-p. pamphlet. (Also available at http://pubs.usgs.gov/sim/3172/.

Sandberg, C.A., 1962. Geology of the Williston Basin, North Dakota, Montana and South Dakota, with Reference to Subsurface Disposal of Radioactive Wastes. USGS Open-File Report: 62-115, 151 p.

Self, J.G., Ryder, R.T., Johnson, R.C., Brownfield, M.E., and Mercier, T.J., 2011. Stratigraphic cross sections of the Eocene Green River Formation in the Green River Basin, southwestern Wyoming, northwestern Colorado, and northeastern Utah, in U.S. Geological Survey Oil Shale Assessment Team, ed., Oil shale resources in the Eocene Green River Formation, Greater Green River Basin, Wyoming, Colorado, and Utah. U.S. Geological Survey Digital Data Series DDS–69–DD, chap. 5, 7 p., 24 plates.

Shurr, G.W., 1977. The Pierre Shale, Northern Great Plains; A potential isolation medium for radioactive waste. U.S. Geological Survey Open File Report 77-776, 27 p.

Sims, P.K., K. Lund, and E. Anderson, 2005. Precambrian Crystalline Basement Map of Idaho—An Interpretation Of Aeromagnetic Anomalies. Scientific Investigations Map 2884, U.S. Geological Survey.

Sims, P.K., R.W. Saltus, and E.D. Anderson, 2008. Precambrian Basement Structure Map of the Continental United States – An Interpretation of Geologic and Aeromagnetic Data. Scientific Investigations Map 3012, U.S. Geological Survey.

Smith, L.N., 1999. Structure contour map on the top of the Upper Cretaceous Pierre (Bearpaw) Shale, east-central Montana. Montana Bureau of Mines and Geology, Montana Ground-Water Assessment Open-File Report 13, Revision 1.1.

Surles, M.A., Jr., 1987. Stratigraphy of the Eagle Ford Group (Upper Cretaceous) and its source-rock potential in the East Texas Basin. Baylor Geological Studies Bulletin No. 45, 57 p.

Sweetkind, D.S., Bova, S.C., Langenheim, V.E., Shumaker, L.E., and Scheirer, D.S., 2013. Digital tabulation of stratigraphic data from oil and gas wells in Cuyama Valley and surrounding areas, central California. U.S. Geological Survey Open-File Report 2013-1084, 44 p.

Sweetkind, D.S., Tennyson, M.E., Langenheim, V.E., and Shumaker, L.E., 2010. Digital tabulation of stratigraphic data from oil and gas wells in the Santa Maria Basin and surrounding areas, central California coast. U.S. Geological Survey Open-File Report 2010-1129, 11 p.

Swezey, C.S, 2002. Regional Stratigraphy and Petroleum Systems of the Appalachian Basin, North America. U.S Geological Survey Scientific Investigations Map 2978, 1 sheet.

Swezey, C.S., 2008. Regional stratigraphy and petroleum systems of the Michigan Basin, North America. U.S. Geological Survey Scientific Investigations Map 2978, 1 sheet. http://pubs.usgs.gov/sim/2978/sim2978MichChart.pdf

Swezey, C.S., 2009. Regional Stratigraphy and Petroleum Systems of the Illinois Basin, U.S.A. U.S. Geological Survey Scientific Investigations Map 3068, 1 sheet. http://pubs.usgs.gov/sim/3068/illinoisbasin.pdf

Swift, P.N. and Corbet, T.F., 2000. The Geologic and Hydrogeologic Setting of the Waste Isolation Pilot Plant. Reliability Engineering and System Safety, 69, p. 47–58

Thomas, W.A., 1988. The Black Warrior Basin. In: Sloss, L.L., ed., The Geology of North America, v. D-2, Sedimentary Cover—North American Craton: U.S.: Decade of North American Geology: Geological Society of America, pp. 471–492.

Trudgill, B. D., 2011. Evolution of salt structures in the northern Paradox Basin: controls on evaporite deposition, salt wall growth and supra-salt stratigraphic architecture. Basin Research (2011) 23, 208-238, doi: 10.1111/j.1365-2117.2010.00478.x, 31 p.

Trudgill, B. D., and Arbuckle, W. C., 2009. Reservoir Characterization Of Clastic Cycle Sequences in the Paradox Formation of the Hermosa Group, Paradox Basin, Utah. Utah Geological Survey Open-File Report 543, 95 p.

USGS Southwestern Wyoming Province Assessment Team, 2005. The Southwestern Wyoming Province — Introduction to a geologic assessment of undiscovered oil and gas resources, U.S. Geological Survey Digital Data Series DDS–69–D, Chapter 2, 34 p. http://pubs.usgs.gov/dds/dds-069/dds-069-d/REPORTS/69_D_CH_2.pdf

USGS Uinta-Piceance Assessment Team, 2003. Petroleum systems and geologic assessment of oil and gas in the Uinta-Piceance Province, Utah and Colorado: U.S. Geological Survey Digital Data Series DDS–69–B, Ch. 2. http://pubs.usgs.gov/dds/dds-069/dds-069-b/REPORTS/Chapter_2.pdf

USGS, 2006. Quaternary fault and fold database for the United States, accessed January 2014 from USGS web site: http//earthquakes.usgs.gov/regional/qfaults/.

Williams, L.A., 1982. Lithology of the Monterey Formation (Miocene) in the San Joaquin Valley of California. In: Williams, L.A., and Graham, S.A., eds., Monterey Formation and associated coarse clastic rocks, central San Joaquin Basin, California. Pacific Section, Society of Economic Paleontologists and Mineralogists Annual Field Trip Guidebook, pp. 17-35.

Willman, H.B., Atherton, W., Buschbach, T.C., Collinson, C., Frye, J.C., Hopkins, M.E., and Lineback, J.A., 1975. Handbook of Illinois stratigraphy, Illinois Geological Survey Bulletin 95, 261 p.

Wylie, A.S., Jr., and Wood, J.R., 2004. Map views of the producing formations in Michigan, the Michigan Basin, U.S. American Association of Petroleum Geologists Eastern Section Meeting, Columbus, OH, Oct. 3-6, 2004.

Wylie, A.S., and Wood, J.R., 2005. Historical production trends suggest remaining upside for E&D in Michigan. Oil and Gas Journal, vol. 103, issue 23.

Zambito, J. J., Benison, K. C., Foster, T. M., Soreghan, G. S., Soreghan, M. J. and Kane, M., 2012. Lithostratigraphy of Permian Red Beds and Evaporites in the Rebecca K. Bounds Core, Greeley County, Kansas. Kansas Geological Survey Open-File Report 2012-15, 45 p.

9.2 Rock Properties and In-Situ Conditions for Shale Estimated from Sonic Velocity Measurements (Section 5 of this report)

Baeyens, B., Bradbury, M.H. (1994). Physico-Chemical Characterisation and Calculated In Situ Porewater Chemistries for a Low Permeability Palfris Marl Sample from Wellenberg, Nagra Technical Report 94-22.

Bastiaens, W., Bernier, F., Li, X.L. (2007). SELFRAC: Experiments and conclusions on fracturing, self-healing and self-sealing processes in clays, Physics and Chemistry of the Earth, 32, 600–615.

Bock, H. (2001). RA Experiment Rock Mechanics Analyses and Synthesis: Data Report on Rock Mechanics, Mont Terri Project, Technical Report 2000-02.

Bock, H. (2009). RA Experiment: Updated Review of the Rock Mechanics Properties of the Opalinus Clay of the Mont Terri URL based on Laboratory and Field Testing, Mont Terri Project, Technical Report 2008-04.

Boisson, J.-Y. (2005). Clay Club Catalogue of Characteristics of Argillaceous Rocks, Nuclear Energy Agency, Organisation for Economic Co-Operation and Development.

Bruner,K.R. and R. Smosna 2011. A Comparative Study of the Mississippian Barnett Shale, Fort Worth Basin, and Devonian Marcellus Shale, Appalachian Basin, DOE/NETL-2011/1478.

Burland, J.B., Longworth, T.I., Moore, J.F.A. (1977). A study of ground movement and progressive failure caused by a deep excavation in Oxford Clay, Géotechnique 27, No. 4,557-591.

Charlier, R., Collin, F., Pardoen, B., Talandier, J., Radu, J.-P., Gerard, P. (2013). An unsaturated hydro-mechanical modelling of two in-situ experiments in Callovo-Oxfordian argillite, Engineering Geology, http://dx.doi.org/10.1016/j.enggeo.2013.05.021.

CNX/GTI (2008). New Albany Shale RVSP, New Albany Shale Gas Project, RVSP Seismic Project Report.

Dehandschutter, B., Gaviglio, P., Sizun, J.P., Sintubin, M., Vandycke, S., Vandenberghe, N., Wouters, L., (2005a). Volumetric matrix strain related to intraformational faulting in argillaceous sediments, Journal of the Geological Society, London, Vol. 162, 2005, pp. 801–813.

Dehandschutter, B, Vandycke, S., Sintubina, M., Vandenberghe, N., Wouters, L. (2005b). Brittle fractures and ductile shear bands in argillaceous sediments:inferences from Oligocene Boom Clay (Belgium), Journal of Structural Geology 27, 1095–1112.

EAEC (European Atomic Energy Community) (1984). Nuclear Science and Technology - Research Project for the Determination of the Suitability of the Mine 'Konrad' as a Final Repository for Radioactive Waste Products, Final report 1978-80, EUR 8984 EN.

EIA (Energy Information Administration) (2011). http://www.eia.gov/pub/oil_gas/natural_gas/analysis_publications/maps/maps.htm

Fedor, F., Hámos, G., Jobbik, A., Máthé, Z., Somodi, G., Sz}ucs, I. (2008). Laboratory pressure pulse decay permeability measurement of Boda Claystone, Mecsek Mts., SW Hungary, Physics and Chemistry of the Earth 33, S45–S53.

Geosites in Denmark (2013). Retrieved November 13, 2013, from http://geosites.dk/lokaliteter/jylland/hanklit.html.

Ghorbani, A., Cosenza, Ph., Revil, A., Zamora, M., Schmutz, M., Florsch, N., Jougnot, D. (2009). Non-invasive monitoring of water content and textural changes in clay-rocks using spectral induced polarization: A laboratory investigation, Applied Clay Science, 43, 493–502.

Giraud, A., Huynh, Q.V., Hoxha, D., Kondo, D. (2007). Application of results on Eshelby tensor to the determination of effective poroelastic properties of anisotropic rocks-like composites, International Journal of Solids and Structures, 44, 3756–3772.

Han, D.-H., Nur,A, Morgan, D. (1986). Effects of porosity and clay content on wave velocities in sandstones, Geophysics, Vol. 51. No. II; P. 2093-2107.

Hardage, B.A., Alkin, E., Backus, M.W., DeAngelo, M.V., Sava, D., Wagner, D., Graebner, R.J. (2013). Evaluation of Fracture Systems and Stress Fields Within the Marcellus Shale and Utica Shale and Characterization of Associated Water-Disposal Reservoirs: Appalachian Basin, Final Report to RPSEA, RPSEA Subcontract: 08122-55.

Horseman, S. T., McCann, D. M., McEwen, T. J., Brightman, M. A. (1986). Determination of the geotechnical properties of mudrocks .from geophysical logging of the Harwell boreholes. Report, Fluid Processes Research Group, British Geological Survey, FLPU 84-14.

Horsrud, P. (2001). Estimating Mechanical Properties of Shale From Empirical Correlations, SPE Drilling & Completion.

Ingram, G.W., Urai, J.L. (1999). Top-seal leakage through faults and fractures: the role of mudrock properties, from." Aplin, A. C., Fleet, A. J., Macquaker, J. H. S. (eds) Muds and Mudstones: Physical and Fluid Flow Properties. Geological Society, London, Special Publications, 158, 125-135.

Johnston, J.E., Christensen, N.I. (1995). Seismic anisotropy of shales, Journal Of Geophysical Research, Vol. 100, No. B4, pp. 5991-6003.

Jougnot, D., Revil, A., Lu, N., Wayllace, A. (2010). Transport properties of the Callovo-Oxfordian clay rock under partially saturated conditions, Water Resources Research, Vol. 46, W08514, doi:10.1029/2009WR008552.

Kerner, C., Dyer, B., Worthington, M. (1989). Wave propagation in a vertical transversely isotropic medium: field experiment and model study, Geophysical Journal, 7, 295-309.

Kutschke, W.G, Vallejo, L.E. (2012). Investigation of Lateral Stress Relief Using Finite Elements and Fracture Mechanics: Case History Study of the Saxon Pit, J. Geotech. Geoenviron. Eng., 138:1277-1283.

Lima, A., Romero, E., Piña, Y., Gens, A., Li, X. (2012). Water Retention Properties of Two Deep Belgian Clay Formations, in: Unsaturated Soils: Research and Applications 1, Mancuso, C., Jommi, C., D'Onza, F. (eds), Springer-Verlag, Berlin Heidelberg.

Liu, X. (1994). Nonlinear Elasticity, Seismic Anisotropy, and Petrophysical Properties of Reservoir Rocks, Ph.D. thesis, Stanford University.

Liu, E. (1997). Crosshole Channel Wave Analysis from Antrim Shale Gas Play, Michigan Basin, EAGE Conference and Technical Exhibition, 59th annual meeting 1997, European Association of Petroleum Geoscientists.

Lomenick, T.F. 1996. The Siting Record: An Account of the Programs of Federal Agencies and Events That Have Led to the Selection of a Potential Site for a Geologic Repository for High-Level Radioactive Waste. ORNLTM-12940. Oak Ridge, TN: Oak Ridge National Laboratory.

Matray, J.M., Savoye, S., Cabrera, J. (2007). Desaturation and structure relationships around drifts excavated in the well-compacted Tournemire's argillite (Aveyron, France), Engineering Geology 90, 1–16.

McDonal, F.J., Angona, F.A., Mills, R.I., Sengbush, R.L., Van Nostrand, R.G., White, J.E. (1958). Attenuation Of Shear And Compressional Waves In Pierre Shale, Geophysics, Vol. XXIII, No. 3, pp. 421-439.

Midttømme, K., Roaldset, E., Aagaard, P. (1998). Thermal conductivity claystones and mudstones of selected from England, Clay Minerals (1998) 33, 131-145.

Millard, A., Rejeb, A. (2008). Simulation of Short Term and Long Term Responses of the Tournemire Argillite in a Mine-by-test Experiment, The 12th International Conference of International Association for Computer Methods and Advances in Geomechanics (IACMAG) 1-6 October, 2008 Goa, India.

Montaut, A. 2012. Detection and Quantification of Rock Physics Properties for Improved Hydraulic Fracturing in Hydrocarbon-Bearing Shales, Master of Science in Engineering Thesis, The University of Texas at Austin.

Neuzil, C.E. (1993). Low Fluid Pressure Within the Pierre Shale: A Transient Response to Erosion, Water Resources Research, Vol. 29, No. 7, pp. 2007-2020.

Neuzil, C.E. (1994). How permeable are clays and shales? Water Resources Research, Vol. 30, No. 2, pp. 145-15.

Niandou, H., Shao, J.F., Henry, J.P., Fourmaintraux, D. (1997). Laboratory Investigation of the Behaviour of Tournemire Shale, Int. J. Rock Mech. Min. Sci. Vol. 34, No, 1, pp. 3-16.

Nichols, T.C. (1992). Rebound in the Pierre Shale of South Dakota and Colorado Field and laboratory evidence of physical conditions related to processes of shale rebound, U.S.G.S. Open-File Report 92-440.

Nunn, J.A. 2012. Burial and Thermal History of the Haynesville Shale: Implications for Overpressure, Gas Generation, and Natural Hydrofracture, GCAGS Journal, v. 1 (2012), p. 81–96.

Nygård, R., Gutierrez, M., Bratli, R.K., Høeg, K. (2006). Brittle–ductile transition, shear failure and leakage in shales and mudrocks, Marine and Petroleum Geology, 23, 201–212.

Parshall, J. (2008). Barnett Shale Showcases Tight-Gas Development, Journal of Petroleum Technology, Vol. 60, No. 9.

Piña-Diaz, Y.E. (2011). Thermo-Hydro-Mechanical Behaviour of Ypresian Clay, Dept. de Enginyeria del Terreny, Cartogràfica i Geofisica E.T.S. Enginyers de Camins, Canals i Ports, Universitat Politècnica de Catalunya.

Pope, C.D., Palisch, T.T., Lolon, E.P, Dzubin, B.A., Chapman, M.A. (2010). Improving Stimulation Effectiveness: Field Results in the Haynesville Shale, Society of Petroleum Engineers, Conference Paper 134165-MS, SPE Annual Technical Conference and Exhibition, 19-22 September 2010, Florence, Italy.

Shaw, R. (2010). Review of Boom Clay and Opalinus Clay parameters, FORGE Report D4.6 – VER 1.0. Euratom 7th Framework Programme Project.

Sondhi, N. (2011). Petrophysical Characterization of Eagle Ford Shale, M.S. Thesis, University of Oklahoma.

Tosaya, C.A. (1982). Acoustical Properties of Clay-Bearing Rocks, Ph.D. Dissertation, Standford University.

USGS (United States Geological Survey) (2013). http://mrdata.usgs.gov/geology/state/sgmc-lith.php?code=2.1.1

Verma, S., Mutlu, O., Marfurt, K.J. (2013). Seismic modeling evaluation of fault illumination in the Woodford Shale, SEG Houston 2013 Annual Meeting.

Volckaert, G., Bernier, F., Sillen, X., Van Geet, M., Mayor, J.-C., Göbel, I., Blümling, P., Frieg, B., Su, K. (2004). Similarities and Differences in the Behaviour of Plastic and Indurated Clays, http://cordis.europa.eu/fp6-euratom/ev_euradwaste04_proceedings.htm, The Sixth European Commission Conference on 'The Management and Disposal of Radioactive Waste: Euradwaste '04', held on 29-31 March 2004 in Luxembourg.

Wang, F.P., Hammes, U. (2010). Effects of petrophysical factors on Haynesville fluid flow and production, World Oil, June 2010.

Wenk, H.-R., Voltolini, M., Mazurek, M., Van Loon, L.R., Vinsot, A. (2008). Preferred Orientations and Anisotropy in Shales: Callovo-Oxfordian Shale (France) and Opalinus Clay (Switzerland), Clays and Clay Minerals, Vol. 56, No. 3, 285–306.

Wong, S.-W., Kenter, C.J. (1993). Optimising Shale Drilling in the Northern North Sea: Borehole Stability Considerations, SPE 26736, Offshore European Conference, Aberdeen, Scotland, 7-10 September 1993.

Wyllie, M.R.J., Gregory,A.R., Gardner, L.W. (1956). Elastic Wave Velocities in Heterogeneous and Porous Media, Geophysics, Vol. XXI, No. 1. pp. 41-70.

Wyllie, M.J.R., Gregory, A.R., Gardner, G.H.F. (1958). An Experimental Investigation of Factors Affecting Elastic Wave Velocities in Porous Media, Geophysics, Vol. XXIII, No. 3, pp. 459-493.

Yang, Y., Aplin, A.C. (2004). Definition and practical application of mudstone porosity–effective stress relationships, Petroleum Geoscience, Vol. 10, pp. 153–162.

Yang, Y., Aplin, A.C. (2010). A permeability–porosity relationship for mudstones, Marine and Petroleum Geology, 27, 1692–1697.

Zinszner, B., Meynier, P., Cabrera, J., Volant, P. (2002). Vitesse des ondes ultrasonores, soniques et sismiques dans les argilites du tunnel de Tournemire. Effet de l'anisotropie et de la fracturation naturelle, Oil & Gas Science and Technology – Rev. IFP, Vol. 57, No. 4, pp. 341-353.